A Modular Design Approach For Programmable Cyber-Fluidic Systems

Tanev, Georgi Plamenov

Publication date:
2021

Document Version
Publisher's PDF, also known as Version of record

A Modular Design Approach For Programmable Cyber-Fluidic Systems

Georgi Tanev

Kongens Lyngby 2020

Technical University of Denmark
Department of Applied Mathematics and Computer Science
Richard Petersens Plads, building 324,
2800 Kongens Lyngby, Denmark
Phone +45 4525 3031
compute@compute.dtu.dk
www.compute.dtu.dk

Summary (English)

Digital microfluidic biochips have emerged as a technology for miniaturizing and automating the traditional biochemical laboratory processes. The technology allows for direct programmatic control of droplets without the need for pumps, valves, or defined channels, which makes the digital microfluidic biochips highly programmable and reconfigurable devices. Although the technology has already been in the research spotlight for over two decades, the digital microfluidic biochips face significant difficulties in achieving wide-adoption and living up to the expectations for extensive miniaturization and automation of biomedical applications. Among the most significant challenges is that digital microfluidics is an interdisciplinary field where the research is often focused on technology and component level rather than on a complete future proof system.

Taking the digital microfluidics past the step of technology demonstrators required bridging the gap between digital biochips presented in the context of application-specific short term research goals and a programmable application-agnostic digital microfluidics system. Hence, inspired by the heavily standardized microelectronics industry and modern computer architectures, this dissertation embarked on the journey to efficiently connect the fluidic and control domains into a vision for a modular and reconfigurable cyber-fluidic architecture. The proposed architecture is based on the analysis of an extensive survey of existing technologies and systems, which confirmed that achieving the envisioned cyber-fluidic architecture requires the design, fabrication, and operational aspects to be considered in symbiosis.

The proposed cyber-fluidic architecture is split into three loosely coupled parts; fluidic, instrumentation, and virtual, where each part is deliberately designed in the context of its intrinsic relationships with the rest of the system. The cyber-fluidic architecture was developed into a modular platform-based design, which allowed addressing the spectrum of accompanying challenges on a conceptual and technological level. The engineering research of the fluidic system led to the development of a digital biochip with a large array of individually addressable electrodes, a novel design of reconfigurable embedded heaters, and an innovative low-cost coating method. This dissertation also discusses the design and implementation of the modular instrumentation system that embraces reconfigurability to provide an evolvable and scalable model for digital biochip instrumentation. We also conceptualized a software stack for programmable microfluidics, including a fluidic instruction set architecture, text and graphical-based programming methods, and an execution model.

The capabilities of the proposed cyber-fluidic architecture and the constructed platform are demonstrated with several real-life protocols, namely performing a gene amplification by a polymerase chain reaction and magnetic beads-based enzymatic immunoassays targeting the detection of MRSA and SARS-CoV-2 spiked protein.

Summary (Danish)

Digitale mikrofluidiske biochips er en teknologi til miniaturisering og automatisering af traditionelle biokemiske laboratorieprocesser. Teknologien muliggør direkte programmeringskontrol af dråber uden behov for pumper, ventiler eller veldefinerede kanaler, hvilket gør de digitale mikrofluidiske biochips til programmerbare og rekonfigurerbare enheder. Selvom teknologien allerede har været i forskningens rampelys i over to årtier, er der betydelige udfordringer med at opnå bred anvendelse og at leve op til de forventninger der er ved en omfattende miniaturisering og automatisering af biomedicinske anvendelser. En af de væsentligste udfordringer er at området er et stærkt tværfagligt område, men hvor forskningen ofte fokuserer på teknologi og komponentniveau, snarere end på et holistisk systemniveau.

At løfte digital mikrofluid fra et niveau som teknologisk demonstrator, kræver at der bygges bro mellem den specifikke anvendelses-orienterede forskning og den mere langsigtede forskning med fokus på en generel anvendelsesuafhængig programmerbar cyber-fluidisk arkitektur. Med inspiration fra den højt standardiserede mikroelektronikindustri og moderne computerarkitekturer, var målet med dette forskningsarbejde derfor at koble det fluidiskedomæne med et kontroldomæne til en modulær og rekonfigurerbar cyber-fluidisk arkitektur. Den foreslåede arkitektur er baseret på analyser af en omfattende undersøgelse af eksisterende teknologier og systemer. Analysen bekræftede, at en sådan cyber-fluidisk arkitektur ville kræve at design, fabrikation og operationelle aspekter bliver betragtet i symbiose.

Den foreslåede cyber-fluidiske arkitektur er opdelt i tre løst koblede dele; fluidisk, instrumentering og virtuel, hvor hver del er designet ud fra dens relation

til resten af systemet. Den cyber-fluidiske arkitektur blev udviklet som et modulært platformsbaseret design, som tillod at udfordringer kunne adresseres på et konceptuelt og teknologisk niveau. Forskningen i relation til det fluidiske system førte til udviklingen af en digital biochip med en lang række individuelt adresserbare elektroder, et nyt design af rekonfigurerbare integrerede varmelegemer og en innovativ og billig coating-metode. Denne afhandling diskuterer også design og implementering af det modulære instrumenteringssystem, der udnytter rekonfigurerbarhed til at opnå en udviklings- og skalerbar model for digital biochip instrumentering. Desuden konceptualiseres en software-stack til programmerbar mikrofluid, som omfatter et fluidisk instruktionssæt, tekst og grafiskbaseret programmeringsmetoder og en eksekveringsmodel.

Anvendelsespotentialet af den foreslåede cyber-fluidiske arkitektur og den udviklede platform demonstreres gennem realisering og afvikling af flere virkelige biokemiske protokoller. Udførelse af en protokol til genforstærkning ved polymerasekædereaktion (PCR), samt anvendelse af magnetiske beads-baserede enzymatiske immunoanalyser målrettet påvisning af henholdsvis MRSA og SARS-CoV-2 protein.

Preface

This thesis was prepared as a joint effort between the Department of Applied Mathematics and Computer Science (DTU Compute) and the Department of Biotechnology and Biomedicine (DTU Bioengineering) at the Technical University of Denmark. The work was conducted in fulfilment of the requirements for acquiring a Ph.D. degree in engineering.

This dissertation explores the interdisciplinary field of digital microfluidics, focusing on developing a modular cyber-fluidic microfluidics platform for life science.

The research work presented in this thesis was supervised by Professor Jan Madsen and Professor Winnie Svendsen.

Lyngby, 30-October-2020

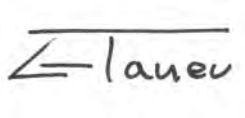

Georgi Tanev

Acknowledgements

Working on this thesis has been a privilege, and I would like to express gratitude to my supervisors, Professor Jan Madsen and Professor Winnie Svendsen, for allowing me to pursue this research endeavor. I would like to thank Jan for his valuable guidance, comprehensive feedback, and immense patience over the last three years. I would like to thank Winnie for her unconditional support, boundless creativity, and for facilitating the unique research environment that made this PhD project possible. Thank you both for your respectful, inspiring, and pragmatic mentorship. This research would not have been possible without your visionary, supportive, and open mindset towards bold or even preposterous ideas.

I would like to thank all of the Embedded Systems Engineering (ESE) section members and the IT Support staff at DTU Compute for the outstanding work environment and generous support. Special thanks to Luca Pezzarossa for embarking on the microfluidics research journey, the countless discussions, and for being a committed member of the Bioware Systems team. I am particularly grateful to Karin Tunder for her tremendous help with administrative and organizational matters and Jørgen Wassmann for his assistance with countless logistics challenges.

I would like to thank everyone at the Nano-Bio Integrated Systems (NaBIS) group at DTU Bioengineering for the accommodating work environment, inspiring discussions, valuable input, and active support. Special thanks go to Jens Hemmingsen for his enabling work on the gene amplification experiment. I want to thank Susan Ibi Preus for the instrumental help, constructive discussions, and extensive assistance with performing the enzymatic assays experiments part of

this thesis work.

I further acknowledge the collaboration with the Yeast Metabolic Engineering group at DTU Biosustain, namely Iben Møller-Hansen and Professor Irina Borodina, as being the nucleus of the MagicBox project. Working with you on the quest to automate reprogramming living cells is an interdisciplinary effort I never envisioned undertaking.

This project is partially funded by the Copenhagen Center for Health Technology, CACHET - a strategic partnership between the Capital Region of Denmark, the City of Copenhagen, the Faculty of Health and Medical Sciences at the University of Copenhagen, and the Technical University of Denmark.

Special thanks to my girlfriend, Galina, for being an inexhaustible source of motivation to keep pushing forward and for tolerating the long work hours and my absence whenever I was busy managing hard deadlines or chasing project goals. Thank you for your understanding, comfort, and encouragement!

And finally, my gratitude goes out to my friends and family for their patience in enduring countless technical monologues. I would like to thank my parents Stoyanka and Plamen, and my sister Elena for their genuine support and never-ending encouragement. Grandpa, you are the best!

Contents

Acronyms list

ADC Analog to Digital Converter

API Application Programming Interface

CAD Computer Aided Design

CNC Computer Numerical Control

CPU Central Processing Unit

CU Computation Unit

DAC Digital to Analog Converter

DNA Deoxyribonucleic Acid

EWOD Electrowetting on Dielectric

FSM Finite State Machine

FSMD Finite State Machine with Datapath

FSMF Finite State Machine with a Fluidic path

GFP Green Fluorescent Protein

I2C Inter-Integrated Circuit

IO Input/Output

ISA Instruction Set Architecture

ITO Indium Tin Oxide

LDPE Low-Density Polyethylene

MCU Micro Controller Unit

MSRA Methicillin-Resistant Staphylococcus Aureus

MVVM Model-View-ViewModel

NaBIS Nano-Bio Integrated Systems

NoC Network-on-chip

NTC Negative Temperature Coefficient

PCB Printed Circuit Board

PCR Polymerase Chain Reaction

PDA Personal digital Assistant

PET Polyethylene Terephthalate

PID Proportional-Integral-Derivative

PMT Photomultiplier Tube

PMMA Poly-methyl Methacrylate

PTFE Polytetrafluoroethylene

PWM Pulse Width Modulation

RNA Ribonucleic Acid

SARS-CoV-2 Severe Acute Respiratory Syndrome Coronavirus 2

SoC System-on-chip

SPI Serial Peripheral Interface

TEG Thermoelectric Generator

UART Universal Asynchronous Receiver-Transmitter

UI User Interface

Chapter 1

Background and Motivation

Microfluidics is a rapidly expanding scientific discipline studying the microscale behavior and controlled manipulation of small volumes of fluids. When the surface tension and fluid resistance become predominant governing forces of the behavior of a fluidic system, unusual and often counter-intuitive fluidic properties appear. Fluidic flow becomes laminar rather than turbulent, mixing takes place exclusively through diffusion, and surface tension counteracts mass and viscosity, thus allowing droplet formation. These small scale liquid qualities are particularly valuable when constructing systems designed to handle low volumes of fluids in the quest to achieve fundamentally new capabilities of controlling fluid molecular space and time concentrations.

1.1 Why digital microfluidics?

The first microfluidic droplet generation experiments date back to 1833, where observation was made on the uniformity of water droplets delivered from a narrow opening. Later, the fluidic dynamics were mathematically modeled in 1878, thus taking the first steps towards theoretical fluid dynamics. In the 1950s, the commercial potential of the microfluidics technology was recognized as the droplet-on-demand generation, leading to the invention of ubiquitous

inkjet printing technology [1]. It took over two decades of collective research effort to develop a controlled and reliable method to move picoliter sized ink droplets out of a nozzle. Nevertheless, this effort materialized as the vast commercialization of the first microfluidic system - the ubiquitous inkjet printers were brought to market in the 1980s. Throughout the 1970s and 1980s, microfluidics was mainly used to enhance the functionality of the developing field of micro-electro-mechanical systems. Nonetheless, this only helped the microfluidic technology to be recognized as a capable platform for miniaturizing and automating fluidic handling for experimental laboratory purposes.

In the 1990s, the concept of miniaturized total chemical systems (μTAS) was first theoretically introduced [2] and quickly started to gain traction. The idea of scaling down the traditional wet laboratory processes to a chip-scale device capable of sample preparation, processing, and sensing led to an explosion in microfluidics discoveries and developments. One of the reasons for this fast progress was the shift from cleanroom fabricated silicon-based devices to more affordable polymer-based lithographic processes and micro-milling fabrication. The adoption of these new fabrication techniques effectively lowered the microfluidics entry barrier and allowed researchers from different research fields to start exploring possible applications. Research domains began to blend with microfluidics chasing the opportunity to do things differently and more efficiently. Scientists from various backgrounds began to work together with the common goal to scale down the traditional lab processes to highly integrated and efficient chip-scale devices. The blending of research domains allowed microfluidics to become an underlying technology for lab-on-a-chip applications (LoC).

A truly self-contained LoC should allow for fluid dispensing, transport, mixing, splitting, incubation, detection, and waste disposal to be handled on-chip without or with little assistance from off-chip instrumentation systems. LoC systems can generally be categorized as continuous flow (channel-based) or planar (channel-less) systems manipulating discrete droplets. As the name implies, channel-based systems operate with continuous-flow fluids physically confined in a fixed channels network fabricated on a substrate in two-and-a-half or three-dimensional space. The transport mechanism is typically based on pressure pushing the fluidic stream forward. The pressure source is usually an external pump, and valves control the fluidic flow [3] [4] [5]. Another approach to the channel-based systems utilizes electrokinetic or centrifugal forces as a propulsion method. Nevertheless, the channels-based microfluidics paradigm has constrained versatility due to the fixed and often one-way channel structure.

In contrast, the discrete droplet-based systems are constructed as a substrate patterned with an insulated array of control electrodes without any physically defined channels. Droplets are formed by the fluid surface tension force, and actuation is achieved by controlling the droplet contact angle with the substrate

by applying voltage potential on control electrodes. Droplets can be individually controlled through driving the control electrodes, thus effectively providing a first-order digital fluidic control. The technology is known as digital microfluidics, and the LoC devices based on it are referred to as digital biochips (see Chapter 2).

Both technologies have strengths and weaknesses based on fabrication methods, control schemes, cost, size, robustness, integration level, comparability with existing equipment, etc. Nevertheless, digital microfluidics excels in automation capability, reconfigurability, and device construction simplicity. Furthermore, traditional benchtop protocols are generally executed on discrete volumes of reagents, much similar to the operation performed on digital biochips, making protocol translation a matter of volume scaling and optimization. Due to the individual droplet manipulation, digital microfluidics fare better than their continuous flow rival in regards to dead volume and fluidic management. The lack of bulky external instrumentation with moving parts is also a clear advantage of the digital microfluidics. The direct use of voltage potential to actuate fluids is more efficient and straightforward compared to an electromechanical pneumatic system where energy crosses multiple domains. Due to the listed advantages, the digital microfluidics shows a clear competitive edge when high reconfigurability, ease of programmability, simple fabrication, and operation are considered as top priorities.

1.2 Current applications

Digital biochips operate with individually addressable droplets, where each droplet is not only a discrete vessel, but it can also serve the purpose of a reaction chamber. Droplets can be precisely dispensed from reservoirs, moved, merged, mixed (reacted), incubated, heated, or cooled, thus allowing complex biochemical protocols to be performed on a digital biochip. These devices usually operate with lower reagent volumes compared to the traditional benchtop protocols, have flexible and reconfigurable architecture, can be highly automated, and require only compact and simple external instrumentation. Because of these unique characteristics, digital biochips have been a subject of significant research interest, and a broad range of applications in the life science field have already been demonstrated in various laboratory setups.

Digital microfluidic applications can be divided into five main categories [6]: chemical and enzymatic assays, immunoassays, clinical diagnostics, nucleic-acid based, and cell-based applications. This categorization is not inclusive since there is a variety of niche research projects; nevertheless, it provides a repre-

sentative state-of-the-art outline of the most established research topics. There is also an overlap between the different categories since a given technology is applicable in multiple settings.

A colorimetric enzymatic assay for measuring glucose [7] was one of the earliest application demonstrated on an oil-filled digital biochip. In-line absorbance measurement of the color development reaction was monitored with an integrated pair of a light source and photodetector. The method allowed for analysis time lower than a minute with comparable accuracy to already established measuring techniques. On the other hand, immunoassays are a classical and effective approach to detect analyte presence based on an antibody-antigen interaction. These assays have high sensitivity and specificity, but they require multistep repetitive protocols. Antibodies can be either functionalized on a hydrophilic spot on the biochip [8] or on coated magnetic particles [9]. The measurable output signal is produced as a response of an antibody-antigen binding, where either one of the two is labeled with a detection marker. The output signal can be in the form of fluorescence, color change, or radiation.

Clinical diagnostics is a significant part of the modern healthcare sector, which relies on symptom evaluation, medical record, and laboratory testing to recognize and evaluate a medical condition. Sample preparation and analytical processes have been implemented and proven to be feasible on a digital biochip [10]. The reduced size, cost, and processing time allow for testing to be shifted out from the centralized testing facilities and brought closer to the patient side, for instance, at the general practician's office, paramedical emergency vehicle, or even at home. The point-of-care testing on digital biochips offers optimized performance on multiple levels, including the faster assessment of health status, logistics and reagents cost, and portability, hence providing medical testing access when laboratory infrastructure is non-existent.

A major application area of digital microfluidics is related to the manipulation and characterization of nucleic acids, such as deoxyribonucleic acid (DNA) and ribonucleic acid (RNA). DNA and RNA are a biological storage medium extensively used in the fields of genomics and medical diagnostics. Working with nucleic acids frequently involves assembling sequences, amplifying, or modifying DNA fragments. A widespread method for DNA manipulation is the polymerase chain reaction (PCR) used to make many copies of a DNA region. The PCR is an amplification process that allows the amplified product to be used for other purposes such as sequencing, to be visualized by gel electrophoresis, or cloned into a plasmid. An example of using DNA amplification for diagnostic purposes is the digital microfluidics platform for detecting microbial DNA in clinical specimens [11]. This device showed faster processing time and reduced reagent volumes with performance comparable to the conventional techniques. Another notable application is the cell-free cloning [12] shown on a digital biochip. This

application is particularly exciting since it provides the ability to engineer biological code and directly reprogram living cells. Streamlined digital biochips can automate the otherwise laborious PCR sample handling and replace expensive and complex equipment such as pipetting robots, specialized thermal cyclers, and measuring instruments.

Digital biochips are also used to automate multistep cell-based processes providing an alternative to the high initial and operation costs of the robotic liquid handlers. After the feasibility of moving living cells on a digital biochip for hours [13] has been demonstrated, several techniques for suspended, two-dimensional (cells adhered to the surface), and three-dimensional (e.g., in hydrogel) have been developed [14]. Optical and electrical forces have been used to perform cell sorting to separate and encapsulate labeled droplets for further processing. Another cell-based application is related to toxicity testing performing viability assays with newly developed drugs or different compounds on living cells. The ability to analyze cell behavior in an artificial environment allows for better studies of the complexity of nature.

Digital microfluidics is an enabling technology for the field of synthetic biology. Engineering segments of DNA, genes to reprogram living cells [15], and biological computing [16] [17] are among the emerging applications driven by the progress of synthetic biology. The programmatic fluidic handling of digital microfluidics, in conjunction with the small operational volumes, is a gateway towards lowering the entry barrier to the synthetic biology field and promoting the development of new applications.

1.3 Present challenges

Despite the exciting and promising applications and the fact that digital biochips are equipped with sampling, processing, and analytical detection capabilities, the vision for laboratory shelves being stocked with digital biochips designed to perform a wide range of applications has not been delivered yet! It is counter-intuitive for such a capable technology to stay commercially undeveloped. One may ask, what is the cause? Is it due to the technology not being robust and mature enough? Probably not, since at least two companies are using digital microfluidics in medical-grade diagnostics equipment already available on the market [18] [19] [20]. What about a prohibitive cost that might hinder the commercialization? Definitely not, since low-cost fabrication techniques and materials such as standard printed circuit boards (PCB) [21], inkjet printed plastic [22], or even inkjet printing on paper [10] [23] digital biochips were demonstrated to be feasible fabrication techniques. What about integration challenges, then?

Integration is certainly lacking behind, but it has been shown that a range of solutions such as low-cost paper-based replaceable electrochemical sensors [10] or sensors integrated directly on the chips' surface [8] can address the integration challenges. Is it a scalable technology? Yes, digital microfluidics can scale, based on its relatively simple control technique, device fabrication, and many technological paradigms similar to the traditional micro-fabrication [24] [25]. Are there methods for programming and controlling these devices? Undoubtedly, there are some challenges finding a convenient and user-friendly approach to capture the semantics of a lab protocol and compile them to a program that can run on a biochip, but yet capable domain-specific programming languages have already been proposed [26].

Navigating the digital microfluidics field appears to be a complex task. Nonetheless, what is the reason for not fulfilling the promised years ago microfluidics revolution [27] [28]? Why digital biochips still remain mainly prototyping devices in a laboratory research context? Probably one of the significant obstacles, indeed, is the fact that digital biochips are often designed and used in the context of achieving precise short-term research goals. This results in application-specific, proof-of-concept prototypes which have limited application to a small subset of problems. Nonetheless, the development effort for such an experimental setup can not be easily undermined since it usually costs hundreds if not even thousands of man-hours. Furthermore, developing a digital microfluidics system is a truly multidisciplinary endeavor requiring experiences spanning across multiple disciplines such as physics, material science, fluid dynamics, chemistry, biology, fabrication, electronics, and computer science. Assembling and managing a team with these competencies is generally not a trivial task, which results in many research groups focusing only on a niche and domain-specific topics.

Lack of standardization and thus, compatibility on multiple levels is also considered to be a significant burden on the digital microfluidics progress. A few open-source platforms and digital biochips have been developed in the past decade [29] [30] [31], but cross-compatibility of devices and software is questionable. Furthermore, notable efforts for modularity on design and implementation levels are not evident, which significantly hinders the reconfigurability and reusability of the subsystems. The lack of standardization in the digital microfluidics field has been seriously overlooked for years, and this substantially affects the development and adoption pace. How cumbersome would it be to work in a wet research lab without the standardized well plates, Petri dishes, pipet tips, microscope slides, and all associated instruments?

Even though the scientific community is continuously making incremental efforts for improving the design, programming, and operation of digital biochips, a common software framework is virtually non-existent. Regardless of the developed domain-specific programming languages [32] [26] and compilers [33] [34] [35],

manually drawn device layouts, applications mapped to electrode activation sequences, and device operation carried out as executing the activation sequence as a simple script are still widely used. This is mainly due to the lack of established intermediate data exchange formats between the tools, lack of a common digital biochip representation, and a universal instrumentation interface.

Some of the most exciting digital microfluidics applications are in the fields of public health and environmental monitoring, medical diagnostics in developing countries, biological computing, and synthetic biology. Cost becomes a crucial factor in applications such as diagnostics in developing countries where large volumes and low prices are a decisive factor. On the other hand, research-based applications tend to be less cost-sensitive. The combination of royalties associated with intellectual property, the price of a single digital biochip, and potentially marginal profits are probably among the factors influencing the lack of commercial adoption of this technology.

Intellectual property is also an essential factor in the technology transition process from the research laboratory to commercialization. In the past two decades, the field of digital microfluidics has been heavily patented (see Appendix A). Although some of the initial patents are due to expire soon, there are still a number of new being filed each year, which makes navigating through the field ever so difficult. Infringing patents in research and non-commercial settings is not an issue, but it can be a significant obstacle to product commercialization.

The importance of the application is often overlooked [36] since researchers tend to focus more on the device itself rather than on what problem it can solve. Finding a "killer application" is one of the prerequisites for successfully pushing a promising technology beyond the proof of concept phase. From a user perspective, a simple and streamlined operation process is more valuable than a capable but yet complex and difficult to operate device. For those who are not involved in research, the benefits of using microfluidics will become evident only when microfluidics start solving routine problems. Like the inkjet printer where the internal working mechanisms are abstracted for the user, digital biochips and the corresponding instrumentation need to develop and integrate to the stage where the required user interaction is on the level of "loading paper in the tray" and pressing the "print" button.

1.4 Motivation and perspective

Digital microfluidics is a fascinating droplet manipulation technology spanning across multiple research domains. As contributions are being made from differ-

ent scientific fields, unrealistic assumptions will likely appear due to the limited scope of the research area. The field of computer science is no exception to that. Often artificial problems are being solved or optimized without considering the physical limitations and architecture of a digital biochip. Undoubtedly this is an excellent academic exercise, but it does not necessarily deliver the promised results in the context of digital microfluidics. One example of this is when algorithms for placing, routing, and scheduling are tested in virtual simulators under the false assumption that merging two or more droplets results in a droplet with the same unit size volume or assuming absolute droplet movement fidelity. A "simulation is doomed to succeed"; therefore, assumptions and constraints must be established with caution. However, building and testing is the only way to verify the established concepts when related to physical properties. Therefore, the main research objective of this project was to apply a holistic approach to the field of digital microfluidics and investigate the feasibility of the construction of a programmable cyber-fluidic platform that can adapt and transform with the application needs. A guiding norm in this process was to achieve user-level operation simplicity and scalability regardless of the hidden system complexity. This is achieved by design modularity on every aspect, starting from the high-level user interface and going down to the technology-related details of the digital biochip constructs. A notable example of a modular platform where usability is more important than the system complexity is the personal computer. The personal computer allows users to run user-level applications seamlessly, such as internet browsers, word processors, graphic editors, and even a microfluidic-enabled device such as the home inkjet printer.

The microfluidic technology has been used for decades under the hood of the inkjet printer, thus serving the purpose of a standard periphery output device. Text or graphics mapped to pixels get seemingly deposited as microscopic ink droplets on a piece of paper, hence creating a physical representation of a virtual object. Likewise, allowing digital biochips to become an integrated part of a highly reconfigurable cyber-fluidic system adopting the programming and operation model of modern computing holds the potential to disrupt the fields of life and computer science. The vision was to develop a cyber-fluidic processor manipulating not only digital data bits but also a broad range of chemical species, thus performing computations, chemical and enzymatic reactions, immunoassays protocols, manipulating nucleic-acids, or even interfacing with living cells. The future is digital, and the goal of this work is to bring digital microfluidics along or at least move the field a step forward.

1.5 Research contribution

The main contributions of this thesis work are within the interdisciplinary field of the cyber-fluidic system. We propose a modular, reconfigurable, and programmable cyber-fluidic architecture that scales and adapts to the fluidic experimental needs. We have applied a holistic system approach and developed the proposed architecture into a cyber-fluidics platform consisting of fluidic, instrumentation, and virtual systems. The conceptual design and engineering research of the fluidic system yielded innovative scalable and low-cost digital biochip fabrication methods. The proposed modular instrumentation system contributes to the microfluidic field with its unique reconfigurability providing application and digital biochip agnostic instrumentation.

Another notable contribution of this thesis work is identifying the need and conceptualizing a software stack for programmable cyber-fluidic systems. We argue the need for a common fluidic instruction set architecture, text and graphical-based programming methods, and an execution model, as necessary next steps towards developing a cyber-fluidic bioprocessor.

We supplement our contributions with a demonstration of the constructed platform with several real-life protocols, namely performing a gene amplification by a polymerase chain reaction (PCR) and magnetic beads-based enzymatic immunoassays targeting the detection of MRSA and SARS-CoV-2 spiked protein.

1.6 Thesis overview

This dissertation presents a holistic approach to architecting, designing, implementing, programming, and operating cyber-fluidic systems. The following list of chapters presents a detailed outline of the endeavor:

Chapter 1 serves the purpose of introducing digital microfluidics as a fluid manipulation technology for LoC devices. The chapter continues with a discussion about the typical digital biochip applications and the current technology development challenges. The motivation for carrying out this research work is laid out along with the main contributions of this research project.

Chapter 2 provides an overview of the origin, operation principles, and technological development of the digital microfluidics and the digital biochips as LoC devices.

Chapter 3 reviews some of the notable digital microfluidic platforms and briefly analyses their construction, features, and capabilities. This study serves the purpose of a brief state of the art review, and it also sets a departure point for the design of the cyber-fluidic platform subject of this dissertation.

Chapter 4 is about the advantages and characteristics of using a platform-based design in the context of digital microfluidics. Modularity and abstraction levels regarding the protocol, fluidic, instrumentation, and programming models are discussed. This analysis sets the foundation of the holistic modular designing philosophy and sets a set of loose requirements for the cyber-fluidic platform.

Chapter 5 outlines the essential aspects of applying the holistic system engineering approach to the architecting and developing the cyber-fluidics platform. The chapter is split into three parts, each addressing the fluidic, instrumentation, and virtual aspects of the platform. This chapter also outlines the significant contributions of this thesis work to the microfluidics field.

Chapter 6 is split into two parts. The first part presents the testing and integration challenges associated with the cyber-fluidic platform. The second part focuses on putting the digital microfluidics at work and using the cyber-fluidic platform to conduct a PCR and two enzymatic immunoassays. The chapter includes an outline of the elaborate PCR debugging process and preliminary experimental data on detecting an MRSA and SARS-CoV-2 proteins.

Chapter 7 discusses the innovative, creative, and inspiring engineering accomplishments. The chapter also acknowledges a range of pending obstacles identified but yet not addressed in the scope of this thesis work.

Chapter 8 concludes this dissertation by summarizing the contributions of this thesis work and outlining possible future directions.

Appendix A contains a short patent report prepared as part of a special course in "Topics in advanced lab-on-a-chip systems." The report serves to supplement state of the art presented in Chapter 3 and manifests the complexity of the patent landscape.

Appendix B contains details on a predecessor system used as a concept validation for the cyber-fluidic instrumentation system subject of this dissertation.

Appendix C contains experimental details on fabrication of paper-based digital biochips.

1.7 Research Dissemination

The research work carried out through this project was disseminated in the following forms and venues:

Book chapter

- Biolabs as Computing Components. Tanev G., Svendsen W., Madsen J. (2020) In: Bhattacharyya S., Potkonjak M., Velipasalar S. (eds) Embedded, Cyber-Physical, and IoT Systems. Springer, Cham

Journals

- Paper-based sensors for rapid detection of virulence factor produced by Pseudomonas aeruginosa. Alatraktchi, Fatima AlZahra'a; Noori, Jafar Safaa; Tanev, Georgi Plamenov; Mortensen, John; Dimaki, Maria; Johansen, Helle Krogh; Madsen, Jan; Molin, Søren; Svendsen, Winnie Edith. In: P L o S One, Vol. 13, No. 3, e0194157, 2018.

Conferences

- A modular reconfigurable digital microfluidics platform. Tanev, Georgi Plamenov; Svendsen, Winnie Edith; Madsen, Jan. Proceedings of the 2018 Symposium on Design, Test, Integration and Packaging of MEMS and MOEMS (DTIP). IEEE, 2018.
- A Reconfigurable Digital Microfluidics Platform.Tanev, Georgi Plamenov; Svendsen, Winnie Edith; Madsen, Jan. Proceedings of the 11th International Workshop on Bio-Design Automation 2019

Presentations and Demonstrations

- Presentation: Biolab: Computer Aided Sample Preparation - DTU High Tech Summit 2017
- Presentation: Digital microfluidics at work - DTU High Tech Summit 2019
- Demo: Computer-Aided Sample Preparation - DTU High Tech Summit 2018

- Demo: DATE2019 University Booth
- Demo: A Reconfigurable Digital Biolab - DTU PhD bazaar. Won the best showcase award.

Inventions

At the time of submitting this dissertation, three invention reports were submitted to the DTU patent administration. Due to undergoing evaluation, the content of the invention reports is not fully disclosed in this dissertation. Nonetheless, the inventions are titled and dealing with:

- **NoI 1:** Methods for coating electrowetting driven actuators
- **NoI 2:** Method for temperature control of electrowetting-driven actuators
- **NoI 3:** Linear electrowetting-based actuator

Prior enabling work

The contributions listed below contain work carried out prior to the beginning of the PhD period, but yet they are considered relevant to the project:

- Affordable fabrication of conductive electrodes and dielectric films for a paper-based digital microfluidic chip. Soum, Veasna and Kim, Yunpyo and Park, Sooyong and Chuong, Mary and Ryu, Soo Ryeon and Lee, Sang Ho and Tanev, Georgi and Madsen, Jan and Kwon, Oh Sun and Shin, Kwanwoo. In: Micromachines 2019
- A Correct-by-Construction Design and Programming Approach for Open Paper-Based Digital Microfluidics. Tanev, Georgi and Madsen, Jan. Proceedings of the 2017 Symposium on Design, Test, Integration and Packaging of MEMS and MOEMS (DTIP). IEEE, 2017.
- Paper-Based Digital Microfluidic Chip for Multiple Electrochemical Assay Operated by a Wireless Portable Control System. Ruecha, Nipapan and Lee, Jumi and Chae, Heedo and Cheong, Haena and Soum, Veasna and Preechakasedkit, Pattarachaya and Chailapakul, Orawon and Tanev, Georgi and Madsen, Jan and Rodthongkum, Nadnudda and Kwon, Oh-Sun and Shin, Kwanwoo. In: Advanced Materials Technologies 2017

Chapter 2

Digital Microfluidics

Droplet-based digital microfluidics emerged in the early 2000s as an alternative liquid handling technology to the traditional continuous flow channel based microfluidics. Instead of using pressure as a propulsion force, digital microfluidics is based on a principle known as electrowetting on a dielectric (EWOD), which allows small volumes of liquids to be moved on a two-dimensional array of electrodes using electrical potential. This chapter looks into the origin of the electrowetting effect and provides an overview of the development stages of the electrowetting technology.

2.1 The origin of electrowetting

The electrowetting effect is based on the fundamental electrocapillarity phenomenon, first observed in the early 1800s, and later investigated in detail by Gabriel Lippmann in 1875 [37]. The electrocapillarity effect was recognized as the variations in the surface energy of a droplet of mercury in an electrolytic solution under applied voltage potential. This early work presented a theoretical explanation of the electrocapillary effect and also developed several practical applications such as highly sensitive electrometer and electrocapillary motor [38]. The operating principle of these devices was explained as changing the capillary

constant under the influence of an electrical polarization on the interfaced surface, as shown in Figure 2.1a. A notable characteristic of the metal-electrolyte interface is the fact that no electrical current flows between the materials if the potential is kept under several tens of volts. This effect is caused by the formation of a double layer of charged ions acting as an isolator at the surface interface. The properties of the double layer formation were later studied in detail in 1947, which laid the foundation for the electrowetting effect discovery [39].

In the early electrocapillarity studies, a voltage potential was directly applied to the metal-electrolyte interface, resulting in the formation of a double layer acting as an insulator and hence preventing ohmic current from flowing. However, this is also a limiting factor for using the electrocapillarity effect for water-based solutions since applying voltage potential higher than a few hundred millivolts causes an electrolytic decomposition of aqueous solutions. This was the case until 1993, when the use of a thin insulating layer was introduced by Bruno Berge [40] to serve as electrical insulation between the conductive electrode and the liquid, thus preventing electrolysis. The added dielectric layer has a thickness in the range of hundreds of nanometers to several micrometers and provides reliable insulation between the liquid and the solid phase. Reducing the surface energy by making the insulation layer hydrophobic allows for controlling the contact angle of an aqueous droplet placed on the surface as a function of applied electrical potential. This effect is known as electrowetting on dielectric (EWOD), and it is an essential part of the digital microfluidics technology.

2.2 Electrowetting on dielectric

The electrocapillary and electrowetting setups are shown in Figure 2.1. The main difference between the two is that the electrocapillary effect relies on forming a double layer on the metal-electrolyte interface instead of a dedicated dielectric layer used in the EWOD setup. The basic EWOD experimental setup consists of a solid conductive electrode, a hydrophobic dielectric layer completely covering the electrode, and an electrolyte droplet, as shown in Figure 2.1b. Without voltage being applied to the liquid-to-solid interface, the system is in its equilibrium state. This state is defined by the hydrophobicity of the isolator and the surface tension of the electrolyte. However, if the droplet gets exposed to an external electric field, the distribution of charge carriers over the surface of the droplet changes and, this forces the droplet geometry to adjust and reach a new equilibrium state. The pulling forces on the edge of the liquid-to-solid interface govern the new droplet geometry. Furthermore, the solid-to-liquid interface forms a capacitor between the metal electrode and the conductive liquid. The surface charge of the so formed capacitor changes

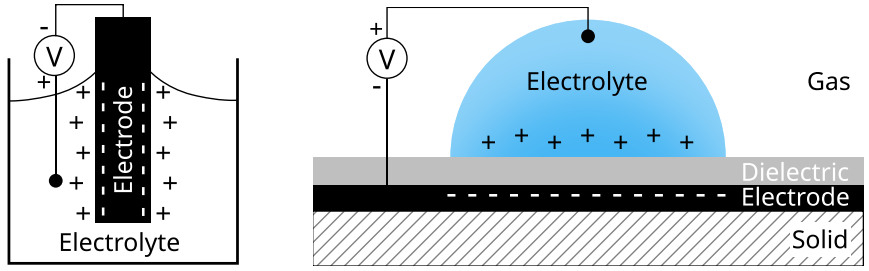

(a) Electrocapillarity setup

(b) EWOD setup

Figure 2.1: Illustration of the classic electrocapillarity and the EWOD set-up. The charge separation for the electrocapillary setup is around 1 nm in contrast with the electrowetting set-up where the additional dielectric layer is with thickens in the range of 0.5-10 µm. Redrawn from [41].

and tends to pull the droplet down, reducing the contact angle and increasing the contact area. Based on these two mechanisms, the droplet contact angle is varied as a function of applied voltage potential.

The electrocapillary phenomenon observed at the mercury-electrolyte interface is virtually identical to the EWOD, with one difference - the magnitude of the formed capacitor. In the classical electrocapillary case, the double layer isolation barrier is in the order of nanometers, which results in capacitance in the range of microfarads per square centimeter. In the case of EWOD, the isolation layer is usually in the range of micrometers, which results in capacitance in the range of picofarads. The thicker isolation layer allows for higher voltage potential to be applied between the droplet and the electrode without the risk of dielectric breakdown. The higher voltage potential translates in higher wetting force and droplet movement [40]. The investigation of the variation of the contact angle, contour instability, and charge injection of a water droplet on a polyethylene terephthalate (PET) films [42] [43] laid the foundation for the EWOD as a droplet propulsion technology for digital microfluidics.

2.3 EWOD as a droplet propulsion technology

The adhesive and cohesive intermolecular forces govern how well a droplet spreads on a solid surface. The adhesive forces appear between the liquid-solid interface and favor the droplet spreading over the solid surface. On the

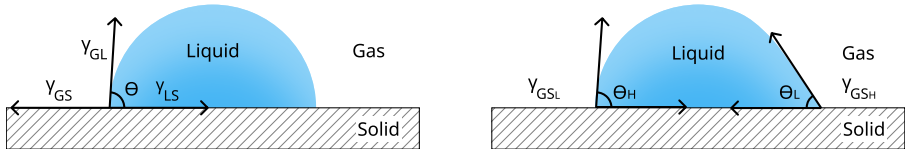

(a) (b)

Figure 2.2: Forces acting on a droplet placed on a flat surface where γ_{GS}, γ_{GL}, and γ_{LS} are respectively the gas-solid, gas-liquid and liquid-solid energies. *(a)* Droplet in equilibrium state. γ_{GS}, γ_{GL}, and γ_{LS} shown only on one side of the interface cross-section. *(b)* Droplet on a surface with an energy gradient $\gamma_{\mathrm{GS_H}} > \gamma_{\mathrm{GS_L}}$.

contrary, the cohesive forces pull the droplet away from the contact surface towards a spherical shape. The two counteracting forces are a consequence of the surface energies on the gas-liquid-solid interface, as shown in Figure 2.2a. The balance between the molecular interactions at the three interfaces determines the contact angle where the liquid-vapor interface meets the solid surface. Perfect wetting is considered when the contact angle θ approaches a value close to zero, which means that the solid-liquid molecular force is dominant, and the droplet fully spreads out on the surface. The contact angle decreases together with the tendency of a droplet to spread over the surface. The effect of gravity force pulling down the droplet is insignificant, and it can be neglected [37].

In regards to aqueous fluids, surfaces can be generally divided into two types - hydrophilic when the wettability is high, and the contact angle in the range $0^{\circ} < \theta < 90^{\circ}$, and hydrophobic when the surface wettability is low, and the contact angle is in the range $90^{\circ} < \theta < 180^{\circ}$. Hydrophobic surfaces such as fluoropolymers exhibit low surface energy and allow contact angle as high as 120°. The low surface energy combined with the high contact angle reduces the liquid-solid interface area and thus lowers the friction between the droplet and the solid substrate.

When a droplet resting on a surface is exposed to variation in the surface energies, the droplet tries to achieve a new equilibrium state by adjusting its shape correspondingly. This effect is shown in Figure 2.2b where the gas-solid energy on the left side of the droplet is lower than the corresponding energy on the right interface edge ($\gamma_{\mathrm{GS_L}} < \gamma_{\mathrm{GS_H}}$). This causes the droplet to be effectively pulled towards the higher surface energy area in the effort of wetting it. As a consequence, the surface tension gradients can produce flow in liquid films or droplets [44] if certain surface characteristics such as flatness, roughness, and heterogeneity are met. Therefore, active control of one of the interfacial energies can translate into droplet movement.

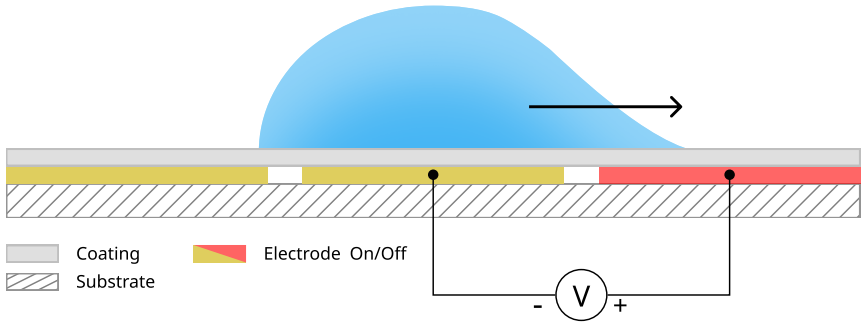

(a) Open configuration.

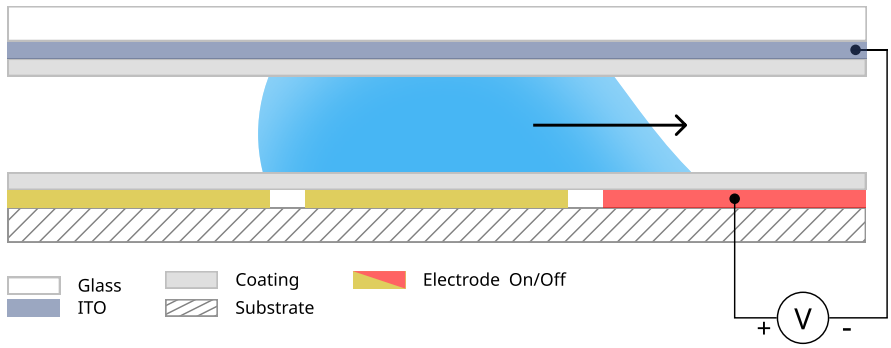

(b) Closed configuration.

Figure 2.3: Side-view of open and closed digital microfluidic droplet actuators.

To achieve controlled and reversible droplet actuation, the mean of controlling the surface energy needs to be connected to a physical variable that is relatively easy to alter. The surface energy of the solid-gas or solid-liquid interface can easily be changed with voltage potential, as it was previously discussed in Section 2.2. The classical electrowetting setup, shown in Figure 2.1b, controls the potential between a solid electrode embedded in the substrate and the liquid droplet. The footprint of the droplet entirely fits inside of the area of the electrode, and hence the whole droplet is exposed to the same change in surface energy. As a consequence, the droplet contact angle remains uniform along the peripheral of the liquid-solid-gas interface, and the droplet can be flattened on the surface. However, asymmetrical surface energization can be achieved by dividing the planar electrode into an array of individually addressable electrodes, as shown in Figure 2.3. Consequently, applying a voltage potential between neighboring electrodes creates a surface energy gradient that changes the contact angle and transports the droplet towards the energized electrode.

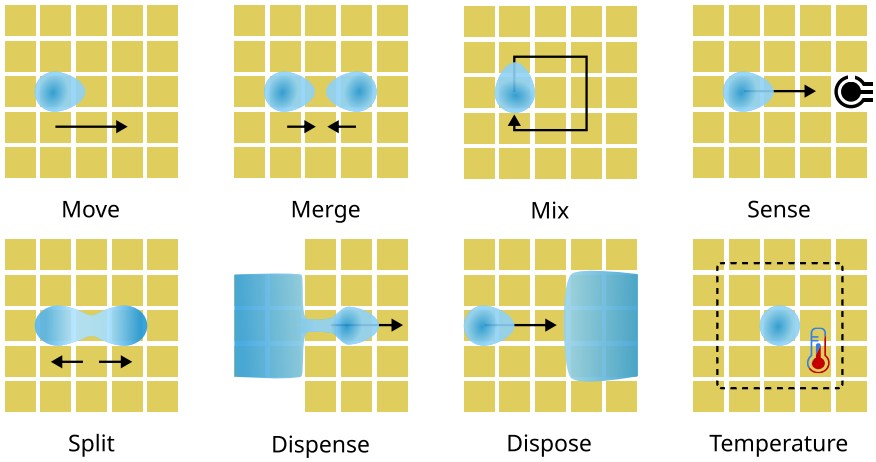

Figure 2.4: Fluidic droplet operations.

A single plate open digital microfluidic droplet actuator is shown in Figure 2.3a. The device consists of a solid flat substrate patterned with conductive electrodes and a hydrophobic dielectric layer. A conductive polar droplet is placed on the top of the electrodes array, with a volume that allows for overlapping with the neighboring electrodes. When all electrodes are at the same potential, the hydrophobic layer ensures a high contact angle and low interfacial energy. When a voltage potential is applied to two neighboring electrodes beneath the droplet, the surface energy gradient drives the droplet towards the area with higher potential, as shown in Figure 2.3a. Sequential activation of the electrodes creates moving high surface energy regions that pull the droplet along the actuation path. This allows for droplets to be moved, merged, and mixed on the surface of the device, as shown in Figure 2.4.

The closed digital microfluidic configuration is shown in Figure 2.3b, and it inherits most of the structure of the open design. As the name implies, the closed design adds a second top plate, which also has a conductive planar electrode covered with hydrophobic layer. The top electrode serves the purpose of the second wire in the traditional electrocapillary setup (see Figure 2.1a), and it provides an uninterrupted connection to a low voltage potential. The droplet is sandwiched between the top and the bottom plate, and often, the cavity between the top and the bottom plate is filled with an immiscible inert nonpolar fluid such as silicone oil. The filler fluid prevents droplet evaporation and also serves as a lubrication medium for droplet transport. The device operation is similar to the open design, with the only difference that the top plate always remains connected to low potential. When an electrode beneath the droplet is connected

to a higher potential referenced to the top plate, the droplet moves towards the region with higher surface energy aligning itself with the plates of the locally formed capacitor.

The closed system also allows droplets to be split and dispensed from reservoirs, as shown in Figure 2.4. Droplet splitting on an open system has been reported as well [45], but it is unprecise and unreliable, and therefore not suitable for real-life applications. The integration of the digital microfluidics with miniaturized sensors and actuators allows for operations, such as sense and temperature control, to be implemented on both open and closed systems, as shown in Figure 2.4. This integration effectively promotes the digital microfluidic droplet actuator to a capable digital biochip equipped to carry out full sample-to-answer processes.

2.4 Digital biochips

The digital biochips can be traced back to 1998 when the first concept for a "droplet reactor" emerged in a publication presenting the novel idea of transporting small liquid volumes on an array of electrodes [46]. The droplet reactor concept is shown in Figure 2.5a, and although the actuation technology was not recognized as EWOD, the demonstrated device had the characteristic construction of an electrowetting droplet actuator. The device was constructed as an electrode array covered by a hydrophobic insulation layer, as shown in Figure 2.5b. A particular implementation characteristic is the droplet guiding grooves, which were used to prevent the droplets from accidentally drifting away from the electrode lines. The device falls into the open digital microfluidics configuration, although the author stated the use of a top plate, which was only preventing contamination, i.e., the top plate was not touching the droplets. The operations possible on this device were limited to transport, merging, mixing, and sorting. Nevertheless, splitting droplets on an open system is particularly challenging. Without droplet splitting and dispensing, the digital biochip functionality is somewhat limited and suitable only for carrying out simple protocols.

In the early 2000s, the EWOD was reported as an actuation method not only to change the contact angle of a liquid-to-solid interface but also to move droplets on a planar surface [47]. The demonstrated device was rather simple, consisting of a linear array of interdigitated electrodes. Nevertheless, the authors envisioned the potential of extending the electrode array to a two-dimensional matrix of electrodes, which would allow for arbitrary two-dimensional droplet actuation. A few years later, this vision was proven valid when the first integrated sample-to-answer closed digital biochip was reported [48]. The device is

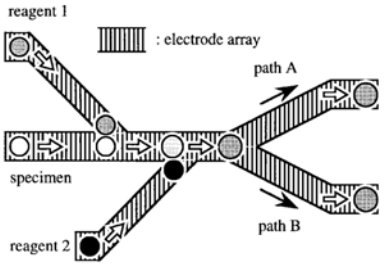

(a) Concept of a "droplet reactor".

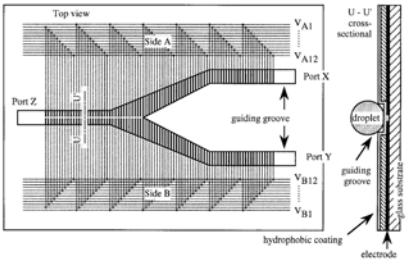

(b) A droplet reactor device for transport, sorting, and mixing of droplets.

Figure 2.5: Early digital biochip prototypes from circa 1998. Reprinted from [46].

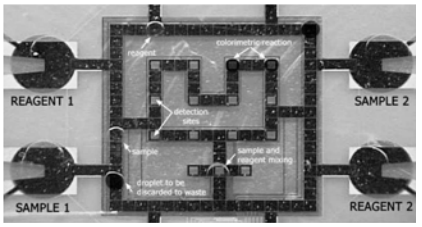

(a) Digital biochip top view.

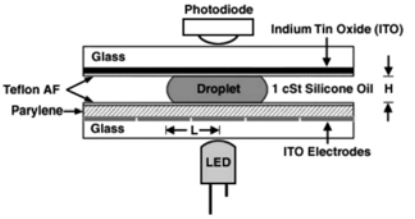

(b) A cross-section of the electrowetting setup with an optical absorbance measurement setup.

Figure 2.6: The first sample-to-answer digital biochip. Reprinted from [49].

shown in Figure 2.6, and it consisted of a two-dimensional array of electrodes, reservoirs, liquid ports, and an optical detector. The electrowetting was acknowledged as capable fluidic handling, and the digital biochips were set on a fast development trajectory.

2.4.1 Materials and fabrication techniques

Early digital biochips were fabricated using photolithography processes directly adopted from the well-established field of semiconductor fabrication [50]. As the technology developed, alternative cost-effective materials and processes were explored and proven feasible for digital biochip fabrication. Besides the structural substrates, three types of materials are essential in the construction of a digital biochip: an electrically conductive material to form the electrodes, an insulation

material to provide reliable and pinhole-free separation between the droplet and the electrodes, and a hydrophobic material to coat the insulator and provide low surface energy surface with high contact angle.

Digital biochips require a flat and smooth substrate to serve as a base for the array of conductive electrodes. Glass and silicon have been used due to their matching mechanical properties and compatibility with the cleanroom photolithographic processes required to form the device conductive electrodes and insulation layer. Using the printed circuit board (PCB) technology has also been shown as a capable method for digital biochip fabrication [51] [52]. Another significant development was the introduction of low-cost substrate materials such as paper [53] [54] or plastic [22]. Even though the cost of glass, silicone, and PCB substrate can be relatively low, the paper and plastic-based digital biochip are better suited for single-use disposable applications. Electrodes on the paper and plastic-based substrates were fabricated with ink-jet printing [10] (yet, another microfluidic technology), screen printing, and plotting [23].

The materials used to fabricate the conductive electrodes on glass and silicon substrates are adopted from the established cleanroom processes for depositing and patterning chromium, silver, and gold. The PCB based digital biochips use laminated copper sheets and lithography to etch the conductive patters. The copper traces can also be gold-plated for a better surface finish and chemical resistance. The top plate of the closed system is usually made of an indium tin oxide (ITO) coated glass or polyethylene terephthalate (PET) sheets. The ITO coated transparent materials are a popular choice since the ITO layer provides good electrical conductivity for the top electrode, and it allows for light to pass through. The translucent top plate allows for the actuated droplets to be visually monitored. Various carbon and silver-based conductive inks [55] have been used in the fabrication of printed electrodes. Conductive inks are usually compatible with a variety of paper and plastic substrates and allow for low-cost and rapid prototyping by using ink-jet printing and plotting [23].

While the material used for substrates and conductive electrodes permit wide variations, the qualities of the insulation and hydrophobic layers are essential for the proper operation of the digital biochips. For proper operation, the insulation layer should have a dielectric constant in the range of 2 to 4, sub- 10 µm thickens, and to be able to produce a uniform pinhole-free layer. The ratio between the dielectric constant and the layer thickness determines the minimum droplet actuation voltage. The higher dielectric constant or thinner layer usually result in lower actuation voltage due to the reduced system capacitance. The uniformity of the insulation layer prevents electrical breakdown at high energy levels and prolonged operation time. Good adhesion to the substrate and the electrodes is essential for long-term stability when the device operates at elevated temperatures, such as those required for the PCR reactions. A broad range of materi-

als had been demonstrated to be suitable as an insulation layer in an EWOD setup [14], among which are Polytetrafluoroethylene (PTFE), ParyleneC, low-density polyethylene (LDPE), silicon dioxide (Si02), SU8, etc. Each of these materials has specific use characteristics and a particular application process.

The hydrophobic layer is usually a fluoropolymer-based material such as Teflon, Cytop [56], or FloroPel [57]. These substances have good adhesion to the previously mentioned insulation materials, ensure and provide contact angle with aqueous solutions higher than 100°. The fabrication procedures include spin coating, spraying, and dip coating, typically followed by annealing at elevated temperatures. Ideally, only one material can be used to provide both insulation and hydrophobic surface since that would reduce the number of fabrication steps and allow for lower actuation voltage due to the thinner structure.

2.4.2 Fluidic operations and control techniques

Droplet transport

Droplet transport is achieved by sequentially energizing electrodes beneath the actuated droplet, thus creating a moving surface energy gradient that correspondingly moves the droplet along the actuation path. Nevertheless, due to imperfections in the interfacing surfaces, a digital biochip can experience different failures. For instance, droplet motion can get obstructed by either surface imperfections leaving hydrophilic regions or foreign particles that have contaminated the system. Dielectric breakdown is a destructive failure caused by either surface nonuniformity, microscopic cracks, pinholes, dielectric breakdown due to excessively high voltages, or other mechanical defects. The result of dielectric breakdown is a failure that usually results in ohmic current flowing through the droplet, causing electrolysis, thus destroying both the liquid sample and the involved electrodes. Another common issue is related to droplets with high protein content. The proteins tend to stick to the hydrophobic surface and prevent the droplet from moving. This effect is known as biofouling, and even though there are countermeasures such as the use of surfactants [58], it requires extra attention to ensure normal operation and prevention of cross-contamination.

Splitting and droplet monitoring

Droplets splitting and dispensing from reservoirs are critical fluidic operations directly related to on-chip sample volume management. On-chip volume metering can be accomplished with either image-based methods or electrical mea-

surements. A computer vision algorithm and a suitable camera configuration can perform droplet detection, velocity measuring, and droplet geometry detection [59] to monitor droplet movement and calculate the corresponding volume. The optical approach requires computational power, optically transparent top surfaces, and potentially expensive camera equipment and extra illumination. In contrast, the electrical methods rely on detecting a change in the capacitance between the droplet and overlapping electrodes. Direct capacitance measurement was demonstrated [60] as a part of a precise reservoir dispensing technique. Nevertheless, this method requires electrical multiplexing of each electrode to a measuring circuit, which can significantly complicate the instrumentation circuitry. An alternative approach is known as impedance sensing, and it monitors the capacitive coupling between the bottom control electrodes and the top reference plate [29] [61] [62]. These techniques allow for real-time droplet actuation monitoring, thus ensuring actuation fidelity.

The device geometries are also known to be an essential design consideration with regards to the fluidic operations. For instance, the challenges associated with reliable and accurate dispensing and splitting were identified in one of the earlier studies of the fundamental microfluidic operations [63], where the general conclusion was that smaller electrode spacing, larger droplet size, and larger contact angle change make droplet cutting and splitting easier. Further studies focused on closed-loop monitoring, and proportional integral derivative (PID) control of the splitting process by using on-chip capacitive sensing and reaching droplet dispensing accuracy in the order of $\pm 2\,\%$ [64] and later improved to $\pm 1\,\%$ [65] for droplets in the range of 200- 250 nl. Another instance for closed-loop controlled splitting was presented in [62], where the authors claim the use of pulse width modulation (PWM) together with a PID controller to achieve precise droplet volume measurement and splitting. The closed-loop control can be used as well for achieving non-symmetric splitting with micro-volume adjustment in the range of $\pm 10\,\%$.

The closed digital biochips typically operate with volumes close to or lower than 1 µL. At 250 µL the Eppendorf®Research plus 0.1-2.5 µL variable pipet has $\pm 48\,\%$ systematic error and $\pm 12\,\%$ random error. At working volumes of 1.25 µl the systematic error is reduced to $\pm 42.5\,\%$ and the random error to $\pm 1.5\,\%$. The reported splitting and dispensing accuracy of digital biochips are well within the volume metering error of a common pipetting device even without considering the variations introduced by the pipetting technique.

Mixing

Droplet transport and merging can be seen as discrete operations since they are performed in a single electrode actuation step. However, when two droplets are merged, they do not immediately become homogeneously mixed. At this microscopic scale, mixing is mainly based on diffusion due to the predominant effect of the laminar flow. Mixing by diffusion is a slow, inefficient, and temperature-dependent process. Furthermore, this process is also affected by flow reversibility when the droplet changes its actuation direction. Therefore, the merged droplets need to be moved further to achieve efficient and homogeneous mixing. Different actuation paths exhibit distinct mixing properties [66], where one of the most effective schemes is to move the droplet in a rectangular pattern over an array of two by four electrodes.

Temperature control

Methods for on-chip temperature control are required for a variety of applications. Prolonged on-chip reagents' storage might need low temperatures, or sample incubation might require raised reaction temperature. An elevated and stable temperature control is required for performing PCR reactions where two or three independent temperature zones are needed. The temperature amplitude spans from close to 0°C for reagent storage to nearly 100°C for the PCR denaturalization step. Two methods are widely used for implementing temperature control on digital biochips: Joule heating, which relies on producing thermal energy from electrical current passing through a conductor, and thermoelectric heating or cooling based on the Peltier effect. Joule heating is useful only to elevate the device temperature to temperatures higher than ambient. This heating approach utilized external resistive heaters [11] [67] [68], and it can be used to create localized heating regions. The thermoelectric temperature control is achieved by creating a heat flux at the junction of two solid materials (temperature can be transferred between the two materials), thus allowing for creating a temperature region that can go below or above the ambient temperature. Temperature can be "pumped" between the hot and the cold side of a Peltier element with typical efficiency lower than 10 %. The low efficiency forces the need for external thermal management in the form of heatsinking, which complicates the system. Nevertheless, such a temperature regulation approach has been proven to be feasible in the context of digital biochips [69].

Sensing

Biosensing is an essential part of the sample-to-answer functionality of digital biochips. Biosensors are transducers converting a signal from a biological recognition element into another more straightforward to measure physical quantity such as electrical signal, change in optical properties, or mass transfer. Based on the transducing mechanism, biosensors can be electrochemical, optical, piezoelectric, and magnetic. The electrochemical biosensors are usually constructed of two to four planar electrodes on a flat rigid substrate. The electrodes can be used as a reactive component, or they can additionally be functionalized with an enzyme, antibodies, or proteins. A biochemical event occurring on the surface of the electrodes gets transduced to change in an electrical signal such as current, voltage, or impedance. The electrochemical biosensors are well suited for integration with the digital biochips due to the similarities in the fabrication processes [70] [10] [71]. The optical-based biosensing is often characterized by change of color, optical density [72], or by biochemical fluorescence [73] [9]. However, the mass transfer piezoelectric and the magnetic biosensors have not seen comprehensive integration to the digital biochips due to their specific construction and operation mechanics.

2.4.3 Biochemical compatibility

Electrowetting actuation is compatible with distilled water, salt buffers, solutions with biomolecules such as DNA, different proteins, and even human physiological fluids [74] [75]. Furthermore, EWOD has been successfully demonstrated to be capable of handling droplets containing suspended cell cultures [14]. Nevertheless, biofouling is a potential issue that manifests as reduced droplet mobility due to non-specific protein binding on the device's surface. This contamination disrupts the hydrophobicity and results in a significant increase in surface friction and contact angle hysteresis. Biofouling can be minimized by filling the device with an inert immiscible fluid such as silicone oil, thus encapsulating the droplet and reducing the risk of droplet-surface interaction. Another established techniques to counteract the surface contamination process employs antifouling agents such as Tween 20 or Pluronic variations [76]. Other important factors influencing the ability of a fluid to be compatible with electrowetting actuation is the viscosity (suitable range from 1cSt to 30-40cSt) and the droplet surface tension.

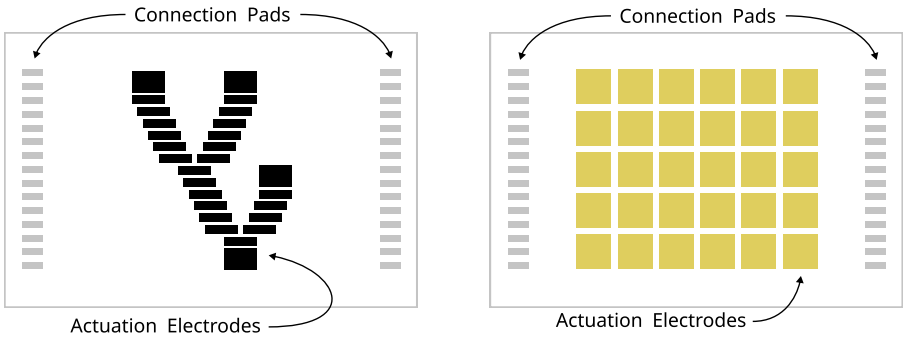

(a) Application-specific layout. **(b)** Reconfigurable layout.

Figure 2.7: Digital biochip layout types and components.

2.4.4 Digital biochip layouts

The conductive elements of an electrowetting droplet actuator consist of *actuation electrodes*, *connection pads* to interface with the external driving circuitry, and *routing tracks* connecting the actuation electrodes with the connection pads. Based on the electrode layout, the digital biochips can be categorized as application-specific and reconfigurable, as shown in Figure 2.7. The application-specific digital biochips have a predefined electrode pattern which can carry out a limited sequence of fluidic operations. This enables the use of low-cost fabrication techniques such as printing, which poses constraints due to the limited resolution and a single functional layer [10]. The reprogrammable digital biochips consist of a two-dimensional array of addressable electrodes that can route droplets anywhere on the array's surface. This effectively allows for programmable droplet routing, thus reconfiguring the digital biochip for different purposes. A distinctive characteristic of the array-based design is that if any of the array dimensions is greater than two (in some cases three [22]) stacked electrodes, more than one routing layer is required for routing tracks between the actuation electrodes and the connection pads. Multilayer routing can be achieved with a cleanroom photolithographic process, traditional PCB fabrication techniques, and recently, it has been demonstrated on a paper substrate as well [77].

2.4.5 Digital biochip automation

With the growing number of control electrodes, sensors, and actuators, the need for automation becomes apparent. A software toolchain for protocol capturing, programming, and controlling the digital biochip through an instrumentation system becomes mandatory with the increased device complexity. This need has already been recognized, and universal microfluidic programming languages and architectures [26] [32] [78] along with instrumentation systems [79] [30] have been proposed. Nevertheless, a closer look shows that digital biochip programming is still largely a manual process carried out by simple scripting of electrode actuation sequences.

The lack of adoption of the higher-level programming tools is mainly due to the difficulties originating in the discrepancies between the virtual models and the actual microfluidic systems. For instance, a significant challenge poses the delicacy of the electrowetting actuation, e.g, the small actuation forces can be easily defeated by defects and contaminants, thus resulting in droplet miss-actuation. Models for error correction have been developed as fault-tolerant compilation and synthesis algorithms [35], but applying them to a physical system remains mostly unexplored. Solving the digital microfluidics automation challenge appears to require not only programming tools developed under the right assumptions but also an execution model that accounts for the physical characteristics of the system.

2.5 Alternative droplet propulsion technologies

There are alternative techniques to actuate discrete droplets on a planar surface using temperature gradient, magnetic fields, or focused light. Although some of these techniques are impractical for wide adoption, they are still interesting to discuss as alternative droplet propulsion methods.

Thermocapillary droplet actuation on surfaces is based on modulating the droplet surface tension by varying the substrate temperature. A thermal gradient induces a shear flow, which also contributes to the droplet propulsion. The thermocapillary effect allows for two-dimensional droplet routing, merging, and splitting, as demonstrated in [80]. Surface modification such as lubricant-impregnation allows for droplet actuation speed to reach 6.5mm/s with a temperature gradient of several K/mm as demonstrated in [81]. Nevertheless, thermocapillary droplet actuation is a highly energy-demanding process that furthermore exposes the actuated droplets to elevated temperatures.

Two-dimensional magnetic droplet actuation has been reported in [82]. The device was constructed from a PCB substrate with embedded copper coils, external permanent magnets, and a reservoir filled with silicon oil covering the active area. Aqueous droplets containing magnetic microparticles were suspended in the silicone oil reservoir. Actuating the build-in coils allows for forming magnetic channels and thus actuating the droplets.

Optical actuation of a droplet, known as optoelectrowetting, has been published in [83] [84]. Discrete, stepwise, and continuous droplet actuation were reported using light from a projector, a display matrix, or a laser beam. In both examples, an externally generated electrical field is routed on the device substrate using photosensitive materials that change conductivity when illuminated.

Dielectrophoresis droplet actuation [85] [86] is another alternative for single droplet manipulation. This actuation method is governed by a fluid's translational motion when exposed to a non-uniform electric field. Droplets are floated in a filler fluid, such as silicone oil, such that they do not get in contact with the bottom substrate. A controlled electric field is then generated by an array of control electrodes on the bottom substrate, which causes droplets to move from a low to a high field potential.

2.6 Summary

The electrocapillary phenomenon was first observed nearly two centuries ago. Empirical and fundamental studies resulted in incremental developments in understanding and idea generation, which led to the discovery of the EWOD as a droplet propulsion technology. Acknowledging the time it took for the electrocapillary phenomenon to be understood and employed in EWOD, digital microfluidics has come a long way since it was first introduced in the early 2000s. New, low-cost fabrication methods have been shown to supplement or even entirely replace the traditional cleanroom processes. Materials such as plastic, paper, various conductive inks, and fluoropolymers have been successfully tested as an alternative to the glass substrates with deposited rear metal electrodes. Sensors and actuators have been successfully integrated, demonstrating applications in medical diagnostics and life science.

A significant challenge remain the integration, automation, and usability concerns related to the delicate nature of the fluidic actuators. Ensuring reliable operation and robust interfacing to the outside world has been gaining more traction since digital microfluidics has proven to be capable in a research setting, and technology transfer is slowly becoming a reality.

Chapter 3

Digital Microfluidics Systems and Platforms

Digital biochips have been developed from a bottom-up perspective by integrating various fluidic components, sensors, and actuators on the course of achieving specific functionality. Similar to the microelectronics field, where the component-level design, integration, and standardization led to an exponential growth following Moore's law, the microfluidics community has been slowly developing and adopting computer-aided design tools and automation techniques to support the research. Various unique fluidic and control systems have already been demonstrated on the course of achieving short-term research goals, but namely, the uniqueness of these designs is both helping and hindering the design-build-test cycle. Reusing already available design components remains somehow limited outside of a given research group instead of "seeing further" by stepping "upon the shoulders of giants" [87]. Of course, such an endeavour would require reaching a level of abstraction and unification where hardware components, e.g., interfacing and control hardware, can be easily reused with corresponding software tools for design and programming. As the first step of undertaking the effort of designing and implementing a universal digital microfluidics platform, we will outline several of the already existing digital microfluidics and discuss their unique characteristics.

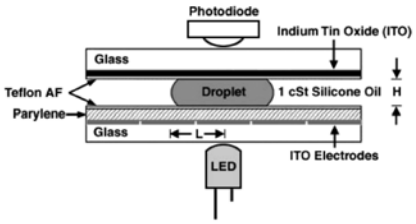

(a) Cross-section of the electrowetting setup with an integrated optical absorbance measurement.

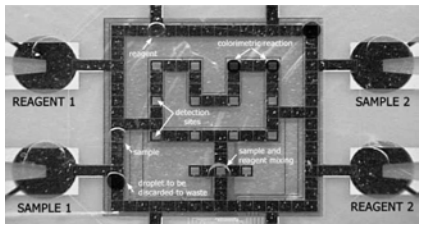

(b) A digital microfluidic lab-on-a-chip.

Figure 3.1: The first sample-to-answer digital biochip introduced in early 2000s. Images from [49].

3.1 On the quest for digital biochip automation

One of the earliest prototypes of electrowetting digital microfluidics biochips was published as a brief letter report in 2000 by a research group from the Duke University [47] followed by a full detailed article two years later [88]. Digital microfluidic was demonstrated to be a capable fluidic handling technology with several advantages compared to the continuous flow, such as discrete volume operation, reduced reagent size, virtual lack of dead volumes, simplistic fabrication, elegant control, and versatility. The demonstrated transport, merging, splitting, mixing, and dispensing of discrete nano- and micro- litter droplets closely resemble the manual operations performed as a part of the traditional bench-top wet chemistry laboratory work. Full lab-on-a-chip functionality was demonstrated two years later in 2004, where a digital biochip was integrated with optical detection [49], thus allowing for full sample-to-answer functionality on a single digital biochip. This device is shown in Figure 3.1, and it was demonstrated to be compatible with human body fluids such as blood, sweat, tears, serum, plasma, urine, and saliva. A proof of concept glucose assay was demonstrated on the biochip, with performance comparable to the standard analytical techniques. The chip consisted of pathways, mixing regions, and an optical detections side forming an integrated and reconfigurable digital biochip. The potential for scaling, automation, and close translation from the traditional lab protocols was soon recognized and attracted scientists from different research domains to start working on the various aspects of the design, fabrication, and operation of these devices, just a few years after the first use of EWOD as a liquid handling method. This has led to significant development in the materials, interaction, and instrumentation, further broadening the horizon of possible applications.

The EWOD provides a first-order electrical-to-liquid propulsion interface. This fluid actuation scheme is excellent for interfacing with computerized control systems, thus creating programmable autonomous digital biochips. The need for digital biochip control and automation poses a variety of unique challenges in the fields of electronics and computing. For instance, an immediate challenge lies in the electronics domain related to the large number of electrodes that need to be interfaced and controlled with a relatively high voltage in the range from several tens to hundreds of volts. This is, in fact, a two-fold problem, where, first, the control electrodes need to be electrically connected to the driving circuitry, and second the electrode drivers need to be capable to withstand the high control voltage and possible failure modes while maintaining a small footprint and efficiency. Equally important to address are some of the computationally related problems such as protocol capture, translation, fluidic scheduling, place, and routing.

Custom made input/output (IO) cards attached to a computer running commercial or custom control software were used [89] [7] in the early stage of development. Building a control system from commercially available laboratory instruments is cumbersome, challenging, and costly. This is mainly because lab instruments are constructed as application-specific high-performance tools. A basic system for controlling the electrodes of a digital biochip would require a high-voltage power supply, signal generator, high-voltage amplifier, switching box for controlling the electrodes, and a programmable controller to produce a correct actuation sequence and timing. The operation complexity, footprint, cost, and flexibility of a system built from generic laboratory instruments is substantial compared to a purposely built instrumentation system for digital biochips.

Creating the first custom-built and truly portable digital biochip control systems has started just a few years after the appearance of the first digital biochips. The earliest example is probably the system shown in Figure 3.2. The author [90] presents a novel concept for a cross-reference droplet actuation scheme that relies on a single linear array of electrodes on both the top and the bottom plate of a digital biochip. The electrode arrays are placed orthogonally, thus creating a virtual two-dimensional array of driving and reference electrodes. This cross-reference driving scheme simplifies the digital biochip design and reduces the number of electrode drivers but poses limitations on moving multiple droplets independently on such an array. A notable design feature of the presented prototype is the reusable conductive elastomer interfacing between the control systems and the digital biochip. This promotes modularity and simplifies the operation of the device. Another important visionary concept introduced in this work is the recognition of the personal digital assistant (PDA) (the predecessor of the modern portable smart devices) as a portable controller and user interface. Unfortunately, there is no clear evidence of the extent of the system developed

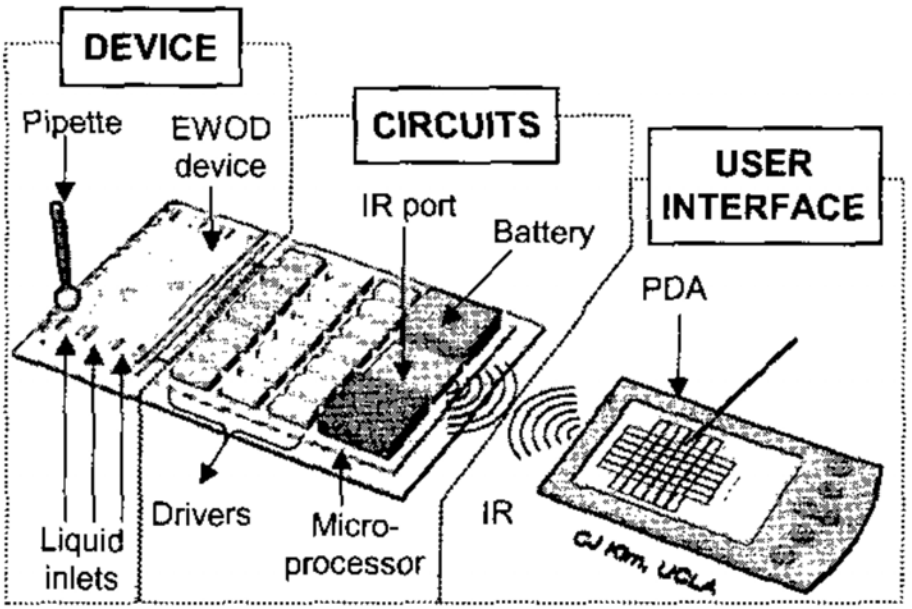

Figure 3.2: An early prototype of a portable digital microfluidics system. Reprinted from [90].

and the further evolution.

Several digital microfluidic prototypes, platforms, and commercial instruments have emerged since the introduction of the digital biochips. Research groups worldwide have been building instrumentation systems based on their current application needs and technical expertise, leading to innovative, interesting, and impactful designs. The most notable systems are discussed throughout the rest of this chapter and include both open source projects and commercial medical grade equipment.

3.1.1 DropBot

The DropBot is an open-source digital microfluidics control system first introduced in 2013 [79]. The system is shown in Figure 3.3, and it was designed to provide a controlled and reproducible droplet driving force by compensating for the parasitic capacitance introduced by the electrode connection lines and fabrication process variations. The compensation is achieved through monitoring the loading effect on the high voltage control lines and correspondingly regulat-

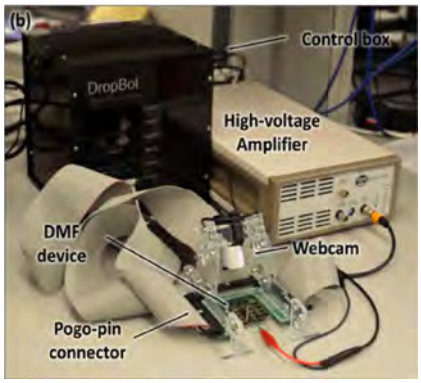

(a) DropBot early prototype circa 2013.

(b) Drop bot current prototype.

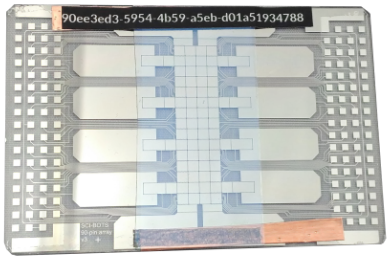

(c) Drop bot current prototype.

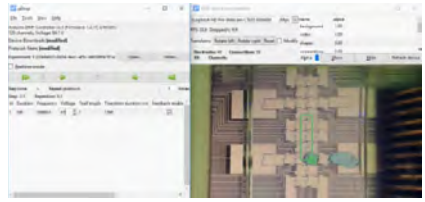

(d) DropBot control software.

Figure 3.3: DropBot digital microfluidics system. Source [29] [92].

ing the actuation voltage. This allows not only for precise droplet actuation but also for detecting failures on the digital biochip. The system has a modular construction and consists of several custom developed electronic boards responsible for signal generation, switching, impedance measurement, and control. The displayed prototype can have up to 120 electrodes connected to the driving boards through custom spring-loaded connectors. A custom Python-based control software employing the graphical GTK toolkit is used to manage the DropBot over a USB connection. The system allows for studying the droplet velocity under different actuation voltages, determining the saturation voltage and the optimal driving potential, so the risk of dielectric breakdown is reduced [91].

The DropBot control system functionality has been demonstrated in the context of several applications. A digital biochip with an integrated electrochemical sensor [71] has been shown to perform standard dilution and measure acetaminophen concentration with comparable performance to the commercial techniques. Another application instance is the use of a DropBot based instru-

Figure 3.4: OpenDrop V4. Image source [93].

ment for serological surveys [9]. The device included a photomultiplier tube (PMT), a magnetic stage, and a web-camera to monitor the test assay. Furthermore, the DropBot has been used as a tool to study and characterize the velocity saturation phenomenon as a function of applied voltage [91]. Determining the optimal control voltage allows for a safe force window to be found for different types of liquids and negate the effect of compromising the device hydrophobicity, dielectric breakdown, and satellite droplet formation.

Due to the open-source design, OpenDrop has been replicated and put into use in several research laboratories around the world. This device and the collaborative effort deserve recognition not only because they lower the entry barrier to the digital microfluidics research field but also as an enabling platform for developing and adapting biochemical applications to the digital microfluidic technology. A spin-out company called Sci-bots [92] appears to be supporting and continuing the development of the DropBot platform.

3.1.2 OpenDrop

Reducing complexity and the initial investment is a proven method to lower the entry barrier and expand the user base of a given technology. GaudiLabs [94] addressed these challenges by designing a simple but yet capable integrated open-source digital microfluidic device. The device is called OpenDrop [30] [93], and it consists of a do-it-yourself digital biochip and a graphical software application. The early hardware versions were built as a single PCB that integrates an array of 128 control electrodes, electrode drivers, a high voltage power supply, a microcontroller, and a simplistic user interface. OpenDrop V4 has introduced a replaceable cartridge with actuation electrodes. The design focuses on low-cost materials, reliable but straightforward digital biochip fabrication procedures, and a user-friendly control interface. The project is still under active development by its originators and as well as hobbyists, makers, (bio)hackers, and research groups. The latest official version of the OpenDrop is shown in Figure 3.4.

3.1.3 NeoPrep

Advanced Liquid Logic was founded in 2004 by Richard Fair, Vamsee Pamula, and Michael Pollack, who have established and pioneered the digital microfluidics field in the early 2000s. Illumina acquired Advanced Liquid Logic in 2013 [95] and utilized digital microfluidics as the backbone of the NeoPrep - a sequencing library preparation instrument launched in 2015 [96]. The device is shown in Figure 3.5, and it was targeted towards mid-sized laboratories promising reduced hands-on time. Unfortunately, only two years later, in 2017, Illumina discontinued the NeoPrep without a clear statement. Unofficially, reliability issues were pointed out as a possible reason for the early discontinuation [97]. Fortunately, the Advanced Liquid Logic decades of experiences and knowledge were not lost, but they were channeled into a new company focusing on newborn screening.

3.1.4 Baebies

The Baebies company was founded in 2014, shortly after Illumina acquired the Advanced Liquid Logic in 2013 [95]. The company created SEEKER, a laboratory instrument for newborn screening and pediatric testing. The instrument employs digital microfluidics as sample handling technology in the screening workflows, and it is capable of performing a range of tests with minimal hands-

(a) Instrument.

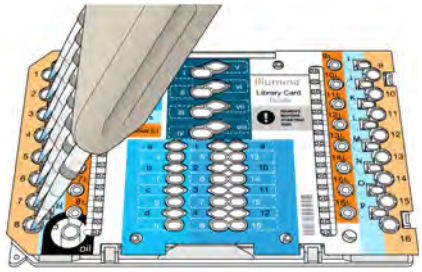

(b) NeoPrep library card.

Figure 3.5: Baebies SEEKER. Images source [96].

(a) Instrument.

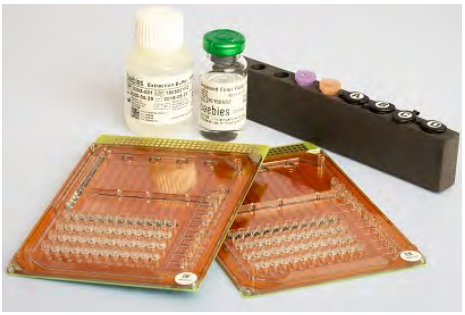

(b) Consumables.

Figure 3.6: Baebies SEEKER. Images source [18].

on preparation time per run. Two machines are capable of running up to 960 tests per day, and a single run cycle is less than 3 hours. Replaceable cartridges are used to load and process the reagents. The instrument is commercially available, and it has received clearance for commercial use.

3.1.5 GenMark ePlex

GenMarkDx ePlex is a complete sample-to-answer system that combines digital microfluidics sample handling with an electronic sensor (eSensor) for DNA detection to streamline the diagnostics workflow. The microfluidic technology was licensed from Advanced Liquid [95] [98] while the eSensor is proprietary. The ePlex system is a modular instrument that consists of a main control module, which can be expanded with add-on towers and hence vary the instrument's capacity from 3 to 24 test bays, as shown in Figure 3.7a and Figure 3.7b. The

(a) ePlex 3 test bay configuration.

(b) ePlex 24 test bay configuration.

(c) Respiratory Pathogen (RP) Panel.

(d) Blood Culture Identification (BCID) Panels.

Figure 3.7: GenMarkDx ePlex diagnostic system and test cartridges. Image source [19].

throughput of the system ranges from 36 to 288 samples for 24 hours, depending on the tower configuration. The actual sample processing takes place in plug-in multiplexed cartridges called panels. Currently, there are two classes of multiplexed diagnostic panels: respiratory pathogens [99], which test for 17 viral and bacterial targets; and three blood culture identification panels [100] that can check for a broad range of bacteria causing sepsis and their resisting genes. Hands-on time is reduced to the sample loading onto a test panel. The readout is based on a proprietary eSensor technology that combines competitive DNA hybridization and highly specific electrochemical detection. The ePlex system also supports integration with existing laboratory systems allowing for better resource utilization.

3.1.6 VolTRAX

VolTRAX is a portable library preparation digital microfluidics device developed by Oxford Nanopore Technologies, which uses digital microfluidics as a propulsion technology for moving, mixing, separation, and incubation on the

Figure 3.8: VolTRAX library preparation device. Image source [20].

chip [20]. It is constructed from a base that contains all of the control electronics and a fluid handling cartridge with reagent loading ports. The cartridge is designed to be sent back for recycling after being used. The VolTRAX has integrated heaters, a thermoelectric cooler, four magnets to handle magnetic beads, and a cooling fan embedded into the instrument's base. These features allow for extraction, reverse transcription, amplification, florescent DNA or RNA quantification, and magnetic beads clean up to be performed on the device. When the preparation is completed, the processed sample can be pipetted out and passed to other instruments for further processing. For instance, a biological sample in its raw form can be loaded and processed to a stage where it is ready for passing to a nanopore sequencing device [101]. Oxford Nanopore offers a unique workflow of automated library preparation based on digital microfluidics, real-time direct DNA or RNA sequencing, and data analysis tools. The tools are still under active development, and with a price tag over 7000€ for a starter pack and a single carriage price over 200€ for a quantity of 50, the operational cost remains somewhat prohibitive. Nevertheless, VolTRAX holds the potential to deliver a thoroughly portable and user-friendly sequencing solution. A proof for its versatility is that the device has already been used for end-to-end identification and full genome sequencing of multiple microbial populations, even onboard the international space station [102].

Figure 3.9: DigiBio microfluidics platform. Image source [103].

3.1.7 DigiBio

Another digital microfluidics platform was introduced in 2017 by a company called DigiBio [103]. The device is shown in Figure 3.9, and it consists of a hardware instrument, replaceable microfluidic cartages, and cloud-based software. The microfluidic cartridges are showing rather interesting and unique actuation electrode patterns. The vision for the platform is to support temperature control, perform purification with magnetic beads, and to have a built-in camera for optical detection. It appears that the DigiBio platform supports automated programmable liquid handling through a graphical web-based interface, including functionality for dispensing from a reservoir and on-chip incubation. The platform is targeting general lab automation as well as synthetic biology applications such as isothermal cloning. The company's website indicates that the platform is currently in a beta testing stage in collaboration with third parties.

3.1.8 Miro Canvas

Miroculus is a start-up company founded in 2012, focusing on digital microfluidics [104] and developing a platform for next-generation sequencing library preparation, synthetic biology, and combinatorial chemistry. The platform is

called Miro Canvas, and only scarce information is available on the company's newsletter bulletin and social media handles. Nevertheless, the company has a track record of several patents concerning the digital microfluidics field. The first patents are dating back to 2010, which potentially indicates more than a decade of development of their digital microfluidics platform.

3.2 The motivation for a new system

In this chapter, we reviewed some of the most distinguished digital microfluidic systems. The first observation worth mentioning is the separation between systems built for the research field and for commercial use. The research devices are DropBot and OpenDrop, where the focus is on functionality and evolvability rather than ease of use. These two systems can be programmed by basic scripting of the electrode actuation sequences, and a variable level of modularity is evident in their implementation. With the do-it-yourself open-source designs, DropBot and OpenDrop are responsible for lowering the entry barrier of the digital microfluidics field and used widely as a research tool.

The commercially targeted systems, NeoPrep, SEEKER, ePlex, VolTRAX, DigiBio, and Miro Canvas, focus on streamlined operation and user-friendly interface. They are built as laboratory instruments rather than research platforms and target a particular set of use cases. It appears that they have a variable degree of user programmability and reconfigurability. While these systems are a remarkable engineering feat, we believe that the digital microfluidic technology has a higher potential than only being used as a liquid handling technology for application-specific biochemical protocols.

Drawing parallels between the computer processor and the digital biochip shows similarities that are not immediately apparent. For instance, the computer processor works with virtual data bits, and likewise, the digital biochip operates with droplets. Virtual data bits are binary representations of logical low or high level, and when grouped, bits start to represent numbers, data structures, or machine instructions. Even though a liquid droplet is often seen as a unit, it has volume, mass, viscosity, temperature, and distinct chemical composition. Similar to how numbers or data structures can be processed to yield a result, droplets can be manipulated, i.e., split, merged, or heated, thus producing volume, color, or chemical composition change. Unlike the virtual data bits, which, unless manipulated, remain static, when two droplets are merged, the newly formed droplet acts as a reactor chamber in which chemical processes can take place.

A modern personal computer operates with virtual data by retrieving it from memory, processing the data by a central processing unit (CPU) or other peripheral modules, and saving the data back in memory. Likewise, droplets can be dispensed, processed, reacted, sensed, and disposed on a digital biochip. Despite the similarities between the data and droplet handling models, the computers are ubiquitous while the utilization of the digital biochips remains limited. An immediate cause for this division is the fact that personal computers are multipurpose machines intended to be used directly by an untrained end-user. An unlimited number of user-level application software can be run due to an extensive programming model and modular architecture. In contrast, digital biochips are often treated as purposely built devices rather than a capable general-purpose lab-on-a-chip. With limited programming infrastructures and the purposely built as application-specific devices, the digital biochips remain largely unexplored in conjunction with modern computation.

A few aspects of the design and operation principles of digital biochips need to be changed to allow for a paradigm shift from application-specific to a general-purpose fluidic handling approach. The first aspect relates to the scalability of the digital biochips. The systems presented in this chapter offer a limited number of control electrodes in the range of 100-300, except VolTRAX, which has an extensive array of thin-film transistor-based electrodes. However, the cost of the VolTRAX consumables makes it suitable only for low-volume high impact applications. The integration of sensors and actuators has mainly been explored in an application-specific context, which does not necessarily map to reprogrammable application-agnostic digital biochips.

The application-specific design of the digital biochips also reflects in the instrumentation system architecture. Regardless of the evidence of modularity in the two research platforms, the hardware level of implementation is far from the usual level of modularity present in modern computers and microelectronics. The lack of modularity presents a two-fold problem. First, it naturally results in digital microfluidics systems designed as monolithic instruments rather than flexible and platform-based machines, and second, the monolithic design projects high redesign cost and thus hinders the system evolution.

The digital biochip programming tools appear to remain mostly an academic exercise rather than a practical automation approach for digital microfluidics. Scripting of actuation sequences is de facto a standard practice for digital biochip automation. However, the basic scripting usually does not implement flow control constructs, which does not allow for runtime adaptation to changing an environment, such as sensor input signals. A high-level programming language, a compiler accounting for the physical model of the system, and a runtime environment are needed to implement a practical programming environment that does not depend on hard-coded actuation sequences and gracefully handles the

uncertainties in the fluidic path.

Addressing the scalability and programmability challenges is what pushed modern electronics and computers forward in the early 1970s. Design automation tools, standardized components, defined interfaces, and programming models supported by Moore's law resulted in remarkable downscaling and integration while keeping complexity at a manageable level. Modern computer functionality has been steadily growing, where each new generation of software and hardware is based on a predecessor system or acquired knowledge. Design reusability and standardization are recognized as crucial components in the development path of modern computers. In contrast, the digital microfluidic field lacks standardization, which correspondingly hinders scalability, design automation, and programmability.

We base the motivation for a new system on the reasons given above and argue for the need for a cyber-fluidic architecture that can address the scalability, adaptability, and programmability issues. Based on the commonalities between digital biochips and microelectronics, we recognize adopting and adapting the fundamental concept of design reusability through modularity, defined interfaces, microarchitecture, and a clear programming model be the way forward for fully realizing the computational potential of digital biochips. Throughout this thesis, we will focus on creating a scalable digital microfluidics architecture, building and testing a cyber-fluidic system prototype, and conceptualizing the systems programming model.

Chapter 4

Approach to Cyber-fluidic System Engineering

Specifying, designing, and building complex cyber-fluid systems lie beyond the limits of a single engineering discipline. Domain expertise in the fields of software engineering, embedded systems, mechanical design, or fluid dynamics suffices for addressing particular technical aspects but lacks the scope to aid the full cyber-fluidic system design. Concept definition and subsequential phases of system architecture development call for the holistic interdisciplinary approach of *system engineering*.

4.1 Engineering challenges

The engineering of a complex system usually begins with detailing the expectations for the final design and outlining how these expectations can be met by either existing technologies or recognizing the need for innovation. In the context of an experimental cyber-fluidic system for research purposes, it is challenging to establish full system specifications due to the unforeseen functional demands and correspondingly emerged requirements. Nevertheless, understanding the system's magnitude and complexity aids the identification of the system's primary functions, components, and design constraints early in the design process.

Furthermore, knowledge about the system as a whole benefits the recognition of the areas where existing technologies are not sufficient and innovation is needed. When a system requires multidisciplinary expertise to develop the different components, especially when these components have intricate relationships, bridging the traditional engineering disciplines becomes crucial. The complete system architecture becomes essential for the system lifecycle, particularly for the concept, development, production, and operation phases.

A cyber-fluidic system is composed of three main parts, namely, software stack, instrumentation system, and fluidic path. This fundamental separation needs to be considered when deciding on a monolithic, modular, or mixed system architecture. The separation naturally calls for a modular system design, which comes on the cost of increased complexity but also allows for greater flexibility throughout the system lifecycle. Nevertheless, monolithic or mixed design can yield a more straightforward and cost-effective architecture suitable for the entire system or different subsystems. Identifying the different parts of the system and their interactions in conjunction with the system requirements need to be accounted for the overall system architecture.

The software stack for cyber-fluidic systems is falling behind compared to the capabilities of the modern computer systems. The reason for that has at least three dimensions related to: first, domain-specific languages for protocol capture; second, the physical nature and dimensions of the fluidic operations; third, the execution model of the system. The challenges associated with developing a capable but intuitive domain-specific programming language originate from the fact that lab protocols are usually captured in natural language. They often include ambiguous details that only an experienced operator can successfully interpret [32] [26]. The lack of precise and explicit description poses the risk of erroneous protocol translation into a sequence of fluidic operations, regardless of the otherwise human-readable description. Apart from a few domain-specific languages [26] [78], cyber-fluidic systems are controlled with custom scripting languages with a lack of flow control constructs. Omitting the flow control limits the system automation to executing a linear set of instructions, which makes virtually impossible handling runtime uncertainty in the fluidic path. Implementing flow control opens up for truly programmable cyber-fluidic systems where the next step of the executed protocol depends not only on the previous state but also on sensory input from the fluidic system (Mealy type logic). The programmability aspects are further discussed in Section 5.5.

The second challenge comes from the nature of the fluidic operations. For instance, the merging of two droplets can be seen as simple addition operation - droplet *d1* is added to droplet *d2*. The product is a new droplet *d3*, which in the fluidic domain experiences physical changes such as volume, occupied area, chemical composition, temperature, etc. Handling these physical characteris-

tics in matching virtual representations requires building a programming and simulation model based on realistic assumptions. This further extends to the challenge of designing a software execution model that can gracefully bridge the gap between the cyber and the physical part of the system.

While the software stack (including firmware) materializes as virtual "data bits," the hardware part of the system, fluidics, mechanics, and electronics, are formed from physical materials. Hardware designs are directed by architectural decisions made early in the process, and once built, they are, in general, difficult to "refactor." This causes engineering of the physical parts of a cyber-fluidic system to be a tedious process, with long design-build-test cycles following the waterfall model. In contrast, the software can evolve through the system lifecycle by new releases or re-writing existing logic, thus improving performance and adding new features. The significant discrepancies between software and hardware/fluidics development challenge the traditional sequential engineering practices. Although the cyber and the physical parts of the system are intertwined on the operational level, they can be decoupled entirely in the design and development phases, thus allowing them to advance at a different pace. Nevertheless, integration and functional testing require both parts of the system to be present and functional.

The fluidic part of cyber-fluidic systems presents a particular risk due to its delicate operation conditions. Although digital microfluidics has been under active research for more than two decades, fabrication and operation of even basic electrowetting droplet actuators require not only domain-specific knowledge, specialized equipment, and processes but also substantial practical experience. Designing from scratch and optimizing the fluidic path's performance is considered a non-trivial task even for those skilled in the art of digital microfluidics. Considering the state-of-the-art presented earlier in this work, the droplet actuator assembly is an area where innovation is likely to be needed in order to advance the field of cyber-fluidic systems. A high level of risk and uncertainties is recognized to be associated with this task. Therefore special attention needs to be paid with respect to risk management.

From an engineering perspective, there is no ultimate design. Nevertheless, under loose time and budgetary constraints, the traditional engineering disciplines strive to excel in all system aspects. This often leads to conflicting demands such as high performance as opposed to limited form factor and power budget or robustness versus development time and cost. The conflicting demands cause a system to be a result of deliberate design decisions and compromises made on the course to obtain sufficient performance to meet the design constraints and requirements. Therefore, another particularly challenging task is to strike a complexity and performance balance throughout the system as an entity rather than allowing certain aspects to be over-engineered at the cost of other under-

developed parts. Achieving this balance in the context of cyber-fluidic systems is a difficult endeavor due to the variables associated with the fluidic path.

The considerations listed above are a subset of the anticipated challenges associated with the design, implementation, and operation of an experimental cyber-fluidic system. A detailed analysis can potentially try to capture the full engineering design space, but modeling the complete system, including the uncertainties associated with the fluidic path, appear to be a particularly difficult task. It becomes evident that ensuring a coherent system development requires methods for splitting, navigating, and managing the complexity of the engineering space, the risks associated with the fluidic system, and the functionality of the cyber-fluidic system as an entity. The field of *system engineering* provides a methodical approach for coping with complexity and assists in avoiding unrealistic design assumptions even in the context of conflicting constraints. System engineering practices can be used to bridge the gap between different engineering disciplines, manage risk, and support the system lifecycle.

4.2 Engineering complex systems

The term system engineering likely originated in the Bell Telephone Laboratories back in the 1940s [105], and its prime objective is "to guide the engineering of complex systems" [106]. Utilizing a framework for managing the complexity aids the process of passing the period of uncertainty and confusion associated with the early stages of system development. When a system is composed of different components, meeting the requirements at the component level does not necessarily result in a functional system assembly. In fact, the complexity of the system imposes the need for a structured system design process in order to meet the requirements not only on a component level but also on a system level.

System engineering is an approach rather than a firm set of methods. A variety of frameworks have been established, often tailored to the internal institutional structure or influenced by the system's context. Nevertheless, the different frameworks can usually be mapped to the traditional system life cycle model [106], as shown in Figure 4.1. The three primary stages cover the *concept development*, *engineering development*, and *post-development*, and they are further subdivided into eight phases reflecting different parts of the system lifecycle.

The *concept development* stage starts with *needs analysis*. As the name implies, this phase aims to identify the demand for the envisioned system by evaluating whether the current or future needs can be met by physical, functional, or

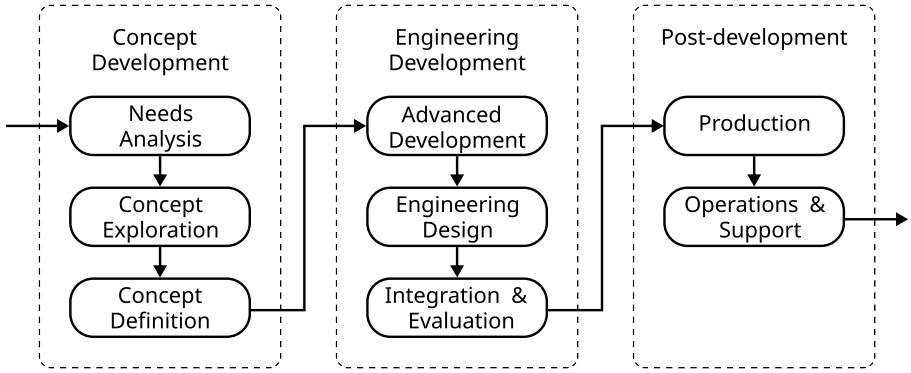

Figure 4.1: Classical system engineering life cycle. Inspired from [106].

technological modifications of an already existing system. Formal, subjective, and experimental assessments can be carried out as a part of the *needs analysis*. In the case of positive identification of the need for a new system, the outcome of this phase is summarized in an initial capabilities description.

The second step of the *concept development* is the *concept exploration* stage, which investigates the feasibility and potential cost of the envisioned system. This phase aims to derive a set of capabilities and corresponding performance measures, along with possibly more than one system concept. In the case of more than one system candidates, the *concept definition* phase takes a role in evaluating the key characteristics of the possible systems and deciding on the optimal concept. Measuring characteristics can be individually adapted to the project constraints and can include functionality, risk, cost, etc. A high-level system architecture can be added to capture the concept perspective in an unambiguous manner. It is worth mentioning that the three phases of the *concept development* can be combined into a large pre-project concept study [107]. Nevertheless, regarding the organization of the *needs analysis*, *concept exploration*, and *definition*, the objective of *concept development* is to explore a spectrum of ideas, determine feasibility, draft functional requirements, identify potential technologies, estimate cost, and possibly deliver a preliminary system architecture.

Choosing a feasible system concept, producing high-level system architecture, and risk evaluation are also associated with reaching a considerable understanding of the operational environment. This understanding serves as the base for transitioning into the *advanced development* phase, and the beginning of the *engineering development* stage. This phase refines and elaborates further on the selected system concept and decomposes the system into components. Ex-

perimental models and simulations are often used to validate different aspects of the subsystems, extending the knowledge, reducing the unknown factors, and thus reducing the associated risk.

The *engineering design* phase focuses on the detailed design and implementation of the envisioned system, where component specifications are transformed into component designs by the different engineering disciplines. At this development phase, rigorous control is required to maintain compatibility on the requirement, interface, and function level. Physical and virtual functional prototypes of the subsystems or the full system, models, and simulations are considered as outcomes at the end of this phase. However, the extent of the produced artifact is dictated by the type, scale, and complexity of the system.

Integration and evaluation is the last step of the *engineering and development* phase. This step assists the process of integrating the engineered components into a complete system. The system undergoes an integration testing where interfaces and components should not only meet their individual specifications, but they have to operate together and deliver the envisioned system functionality as well. This phase is expected to produce a functioning system prototype fulfilling the requirements of the stakeholders. The magnitude of the integration process should not be underestimated since it might require the construction of test structures and simulators. Furthermore, compatibility or performance issues can become evident first in this stage, regardless of the comprehensive planning and execution processes. Identifying problems at this stage might cause unforeseen delays and overhead.

The *post-development* stage starts with the *production phase* which is focused on establishing and managing the manufacturing process. Resolving unforeseen problems, assuring quality control, and meeting the schedule are important parts of this phase. Once the system is deployed, it enters the final, *operation and support* phase, where the role of system engineering is to provide logistics support, training programs for both operators and maintenance personnel, field updates, bug fixes, etc. This is the final phase of the system lifecycle beyond which lies only the system decommissioning.

The system engineering lifecycle, as shown in Figure 4.1, presents the system development as a continuous linear process. Nevertheless, the *concept development* and *engineering development* stages often involve iterative and incremental strategies that reflect better the explorative nature of conceptual and engineering development phases. The exact dynamics of each phase can vary and can be dependent on the technical management processes used throughout the project. Namely, the fact that system engineering aims to increase the holistic system awareness by allowing methods and tools to be assembled to fit the organizational or project needs allows system engineering to be employed at different

breadth and depth, but yet still benefiting from the holistic system approach. The flexibility and decoupled processes allow for tools and concepts to be applied even on the small scale of this thesis work without causing overhead but still guiding the research process.

4.3 Cyber-fluidic system engineering

It is seldom the case where the concept development starts from a completely blank canvas. Usually, at least some artifacts from similar ideas and technologies can be found and analyzed as starting points of new system design. Moreover, it is common practice to base the design of a new system on common or acquired knowledge from a predecessor system that cannot meet the new requirement due to unresolvable design deficiencies. Using the predecessor systems as a departure point to the new system accelerates the concept development phase and allows for an earlier focus shift to the essential aspects of the new design.

4.3.1 The predecessor systems

The journey that led to this thesis started in the autumn of 2015 as a special lab course on digital microfluidics. The study was motivated by the emerging at that time, printable paper-based digital biochips [54] [53] as a low-cost point-of-care diagnostics platform. The simple and cost-effective fabrication, ease of disposal, and the ability of the paper-based digital biochips to be integrated with printable biosensors called for an equally cost-effective and straightforward control and instrumentation scheme. Therefore, the challenge to develop equally simple and elegant control and instrumentation schemes was undertaken. The subject of the course was set to explore the digital microfluidics field, acquire a basic understanding of the EWOD actuation principle, and investigate the technical feasibility of creating a low-cost battery-powered portable instrumentation system. The outcome of this project work was two-fold: first, the feasibility of a truly portable digital-microfluidics control system was proven and demonstrated with a functioning prototype, which is shown in Figure 4.2; and second, design and fabrication of digital biochips was recognized to be a particularly difficult subject.

The block diagram of the developed system is shown in Figure 4.2a, and it consists of a smartphone used as a control device and a simple prototype of an instrumentation device. The system served the purpose of a proof-of-concept, and it had eight electrode driving channels controlled manually from toggle

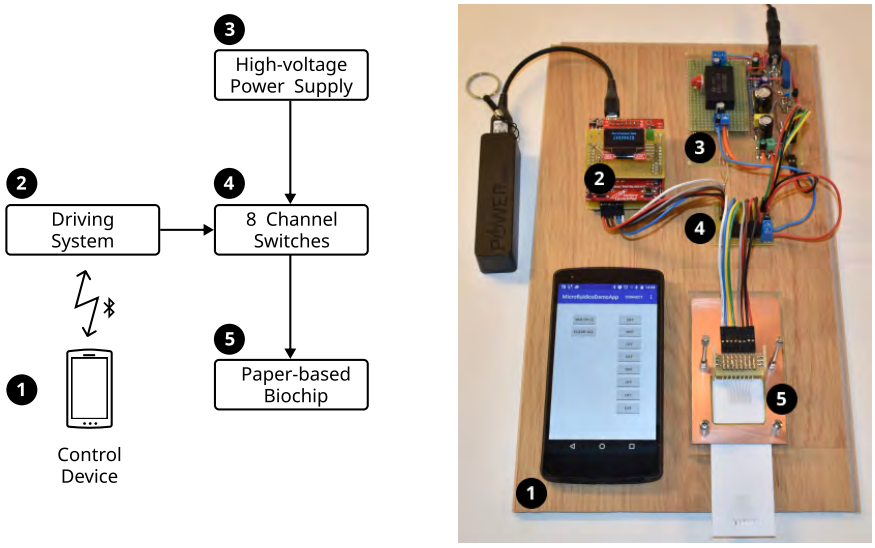

(a) Block diagram. (b) Prototype.

Figure 4.2: Proof of concept portable digital microfluidics system. The system has been developed as a part of a special course in autumn 2015.

buttons within a custom app running on the smartphone controller. Although the insufficient number of control channels and manual operation limited the system's usability, it nevertheless proved the technological feasibility [23] and set a departure point for further developing the concept.

The second iteration of needs analysis and concept exploration followed in the spring of 2016 as a master's project. The project was focused on addressing the usability issues, namely the design, simulation, automation, and fault tolerance in the aspect of a portable digital microfluidics instrumentation system. The outcome of this study was a modular correct-by-construction design and programming approach [108] for application-specific paper-based digital biochips. Additionally, the instrumentation and control systems were developed into a considerably more capable device with 32 driving channels, software adjustable actuation voltage, scripting language, and automated script execution. The prototype of the system is snown in Figure 4.3, and it has been used as a research tool [10] at the Biological Interface Group at Sogang University in Seoul, Korea [109] [110].An interesting fact is that the prototype also appeared on Korean national broadcast television [111]. The new prototype replaced a large, cumbersome system built of a personal computer, multi-channel relay boards, and a laboratory power supply. Furthermore, the new prototype offered the ability to autonomously execute a sequence of commands as in contrast with the manual

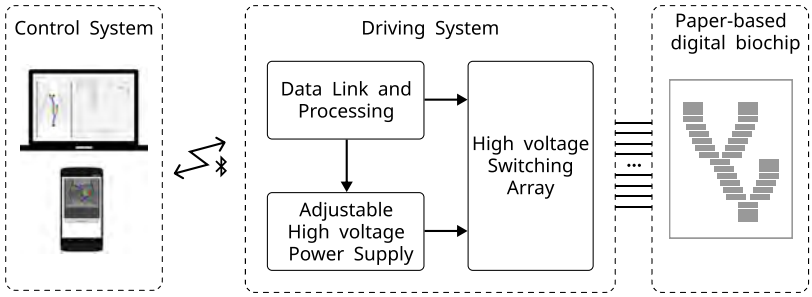

(a) Block diagram.

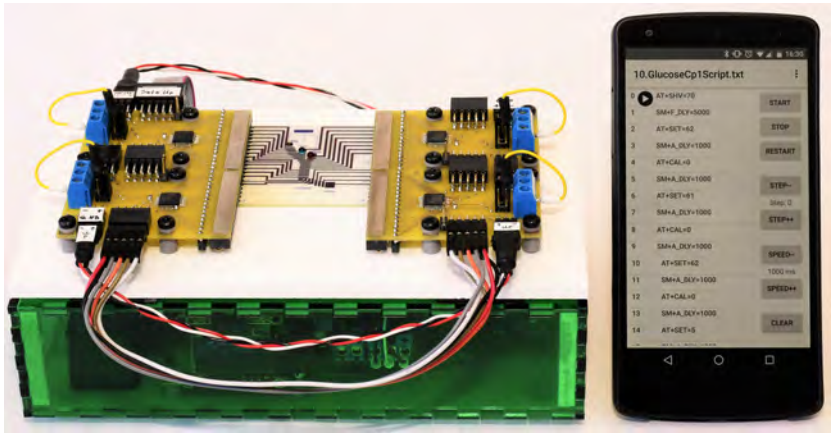

(b) Prototype.

Figure 4.3: The second iteration of the portable digital microfluidics system, developed as a part of a master's project in spring 2016.

control of the former system. The automated setup streamlined the operation process, reduced the variability, and eliminated the human factor errors.

Retrospectively, the two predecessor systems were intended and carried out as independent projects. Even though system engineering methods were not formally applied, the projects naturally followed the design-build-test-learn cycle. However, the focus was more on the concept and technology exploration rather than the needs analysis of the stakeholders. Needless to say that those two projects have laid the foundation for this thesis work by creating practical experience, gaining an understanding of the wet lab work, and studying the immense amount of research published in the past twenty years. The knowledge gained from working on the predecessor systems led to the concepts explored in this thesis work, namely the possibility to create an application-agnostic cyber-fluidic

architecture that gracefully blends the cyber and the fluidic domains.

4.3.2 Cyber-fluidic system needs analysis

The vision for a universal cyber-fluidic architecture was fueled by the fact that the fluidic experimental conditions and needs vary significantly between different applications. These variations often force the need for full or partial system redesign, which is recognized as a deficiency in the approach of the current system, as discussed in 3.2. A primary objective is to explore the possibility of designing a cyber-fluidic architecture that accommodates not only the widespread use cases (see Section 1.2) but also helps bridging the gap between the fluidic and traditional computation.

Shaping the objectives for the new cyber-fluidic system was based on the knowledge acquired from the predecessor projects (Section 4.3.1), studying state of the art (Chapter 1 & 2), a patent survey (Appendix A), and analysis of the already available systems (Chapter 3). Regardless of the knowledge accumulated so far, we hesitate to define final system requirements due to technological challenges and the clear need for innovation for the fluidic path. Considering the project's research nature, system requirements at this stage will be closer to a conditional approximation rather than firm system specifications. Therefore the therm *objectives* is used instead of *requirements* in order to capture the abstract definition of the envisioned system. Below is the summary of the operational, functional, and physical objectives used as design guidelines for initiating the new cyber-fluidic system design.

Operational objectives

- Accommodate for cyber-fluidic system evolution:
  - Allow plug-and-play functionality.
  - Allow for minimum system configuration, e.g., system functionality is matched to experimental needs.
  - Provide interface(s) for adding new functionality to the system.
- Support exchangeable fluidic path, e.g., the digital biochip should be replaceable.
- Provide biocompatibility throughout the fluidic path and digital biochip.
- Provide chemically inert fluidic path and digital biochip.

- Allow for biosensor integration, e.g., electrochemical, impedance, colorimetric.
- Provide a flexible programming model.
- Provide user friendly control interface and operation model.
- Provide an interface for external controller(s).

Functional objectives

- The cyber-system should provide a cyber-fluidic interface with a digital biochip where:
  - Programmatic droplet dispensing, transport, merging, splitting should be supported.
  - The digital biochip should provide a large array of individually addressable electrodes.
  - The digital biochip should be replaceable.
  - The digital biochip should be able to accommodate or interface with different biosensing methods.
  - The digital biochip should be able to support temperature controlled reaction(s).
- The cyber-fluidic system should implement a self-contained instrumentation subsystem.
- The system should provide an interface for external controller(s)
- The user should be able to manually control the cyber-fluidic system.
- The user should be able to program the cyber fluidic system.
- Low-cost processes and material should be used throughout the cyber-fluidic system.

Physical objectives

- The system should be portable, e.g., fit on a standard desktop.
- The system should be easy to transport, i.e. the weight and the physical dimensions of the system should be within the handling capabilities of a single operator.

- The system should be capable to run on batteries, e.g., compact form factor and design optimized for battery power. The battery should not compromise the portability of the system.
- The system should preferably incorporate components with standardized physical dimensions, e.g., standard for factor for fluidic path components, the digital biochip, instrumentation system(s) and modules.

Non-functional objectives

- Extensibility - the cyber-fluidic architecture should allow for adding new functionality to the system without the need of architectural changes.
- Simplicity - the cyber-fluidic architecture should focus on user-orientated simplicity.
- Flexibility - the cyber-fluidic architecture should be able to adapt and respond to internal or external operational changes.
- Reliability - the cyber-fluidic system architecture should accommodate for fault isolation, e.g, a faulty component should not directly affect and cause failures in other parts of the system. The cyber-fluidic system should implement means for self diagnostics and monitoring.
- Robustness - the cyber-fluidic architecture and system should adopt methods and design practices for robust operation, e.g., coping with system and user level introduced errors.
- Maintainability - the cyber-fluidic system designed should allow for efficient repairs.
- Initial cost - the cyber-fluidic system should apply cost-effective engineering practices.
- Operational cost - the consumables for the fluidic path should be preferably designed to be cost-effective.

4.3.3 Concept exploration and definition

The early concept exploration phase was based on the predecessor systems outlined in Section 4.3.1. They mainly explored concepts and the feasibility of paper-based digital biochips, the use of external system controllers, partial system modularity, system portability, etc. Naturally, a variety of alternative functional concepts were considered and tested in the limited scope of the projects,

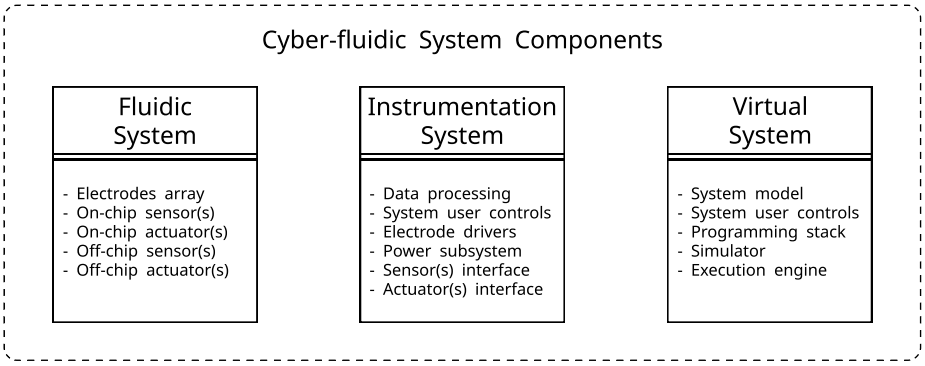

Figure 4.4: First level of cyber-fluidic system decomposition. A cyber-fluidic system typically consists of a virtual system, hardware instrumentation, fluidics and digital biochip.

such as different fabrication techniques for the paper-based chips or the use of a mobile device or a personal computer as a system controller. Similar concept explorations were evident throughout the digital microfluidic systems discussed in Chapter 3. What appears to be a common characteristic for all of the discussed microfluidic systems is the clear separation between the cyber, the instrumentation, and the fluidic part of the system. This clear separation is the foundation for the majority of functional and non-functional objectives discussed in Section 4.3.2 since it enables a cyber-fluidic system to be universally decomposed into three distinctive parts shown in Figure 4.4.

The *fluidic system* is likely the most challenging to define at this stage since digital biochips can be fabricated with different materials and methods, have various form factors, generic or application-specific layout, and incorporate different sensors and actuators. Moreover, the field is still under active development, which is steadily increasing the number of possible fabrication methods, materials, and applications. For instance, paper-based digital microfluidics was introduced only in recent years allowing for highly-cost sensitive applications. To a great extent, the digital biochip construction is dictated by the target application, including performance, cost requirements, and available fabrication technologies. Application-specific high-volume and low-cost diagnostic applications can benefit from the recent introduction of paper-based digital biochips, while the glass, silicon, and PCB based devices present great flexibility at a moderate cost. Nevertheless, a distinguishable characteristic of the digital biochips is the array of control electrodes, but apart from that, the different technologies exhibit unique integration with sensors and actuators. This not only poses challenges to defining a standard physical interface between the *instrumentation system* and the *fluidic system* but also extends the functional requirements to

the instrumentation system.

The *instrumentation system* is bridging the virtual with the fluidic domain, and it is usually composed of one or many embedded devices. The main functionality is to instrument the fluidic components by providing essential functions such as a high voltage power supply, actuation electrodes driver, sensors interfacing, etc. Moreover, advanced features such as capacitive position sensing, interfacing with biosensors, and different actuators such as heaters, coolers, loading pumps, etc. can be implemented to meet the fluidic system instrumentation needs.

The operation of the *virtual system* is based on an emulation of the physical characteristics of the fluidic and instrumentation components. The virtual system provides a framework of software modules for control, protocol capture, programming, simulation, and execution of protocols on the physical device. While each of the software modules targets a specific need, their integration plays a vital role in the overall performance, flexibility, and scalability of the system. Establishing a universal framework for control and programming for cyber-fluidic systems is recognized as a critical step towards standardizing the microfluidics field and promoting growth.

4.3.4 Modularity and platform-based design

The system architecture determines the capabilities of a system to evolve through its lifecycle. There are two major types of system architectures: monolithic, where the system is built as tightly coupled and dependable integrated devices; and modular, where defined interfaces ensure interoperability between loosely coupled subsystems. The choice of the monolithic system design is often motivated by cost-effectiveness, a precise definition of the stakeholder requirements, and specific performance or self-containment needs. A typical design lifecycle characteristic of these systems is that they have an expected lifespan and remain static after development, e.g., performance-orientated systems found in healthcare, instrumentation, telecommunication, transportation, commercial electronics, etc. Updating and modernizing monolithically designed systems is impractical or, in many cases, even impossible due to computational, interfacing, and often physical lack of resources.

As the name implies, the modular system architecture is based on modules as building blocks. A set of modules with different features and defined interfaces assemble a system. The platform-based design approach employs the concept of modularity and allows for variations of systems to be efficiently built from a library of existing modules. This points to two of the main characteristics of the platform-based design: the *platform architecture* and the *platform*

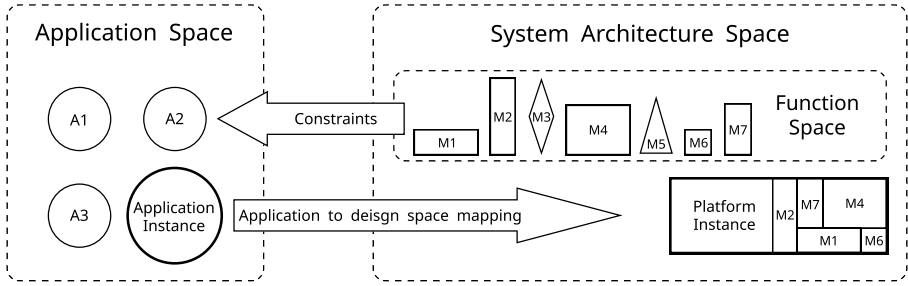

Figure 4.5: Application space to platform instance mapping. The platform instance is composed of a library of available modules. Inspired from [112].

instance [112]. The *platform architecture* presents an abstract interface constrained architecture, enabling interactions between strictly defined microarchitectures. An example of a platform architecture is the personal computer (e.g., the x86 family), where a defined instruction set architecture (ISA), set of established interfaces, and input/output (IO) devices allow the composition of a *platform instance*. A platform instance is a purposely built system that matches a set of requirements, as shown in Figure 4.5. The loosely coupled architecture of the platform-based design allows subsystems to be effectively replaced and updated without the need for major system changes. This allows new functionality to be added throughout the system lifecycle, thus allowing the platform instance to evolve and adjust to a changing environment and requirements.

Another important characteristic of the platform-based design is the relation between the platform *function space* and the *application space*, as shown in Figure 4.5. An application instance is possible in a given platform framework as long as the required functionality is available. The function space needs to expand in order to accommodate for changing application requirements.

The platform-based design approach shows its advantages in the context of cyber-fluidic systems, particularly when accounting for the digital biochip's instrumentation uncertainties. For instance, high voltage power supplies and electrode drivers can be reused to control the actuation electrodes of different digital biochip architectures. The platform's function space can be expanded with biosensors or a heater instrumentation module to match the needs of a particular experiment. Nevertheless, considering the development of the modern embedded systems, the platform's function space is likely to be composed of integrated embedded systems, allowing for even greater flexibility and re-programmability. This concept promotes the use of an application programming interface (API) at the module subsystem level. The API interface allows functionality to be built

from defined software function calls, thus mapping the machine's structural design view to a set of API calls abstracting the low-level operation details. The API is also recognized as a programming model, and it allows for advanced functionality to be built by utilizing the platform's programming model.

4.3.5 Concept selection

Navigating the design space of cyber-fluidic systems and originating a new platform-based design is not a trivial task. Important design choices will inevitably be made under various levels of uncertainty due to lack of information, understanding, or the need for innovation. To reduce the impact of potentially sub-optimal decisions, we see the use of a loosely coupled platform-based modular cyber-fluidic architecture as the path towards originating a truly reconfigurable and evolvable digital microfluidics system. An essential factor for choosing such a system design is its capability to maintain maximal operational performance through the subsystem lifecycle, by software and hardware updates and upgrades. The modular design enables the platform capabilities to be developed on a continuous basis under a manageable schedule and cost. The modular design also reduces the technical uncertainties associated with the fluidic path by decoupling it from the rest of the system as a separate part.

Nevertheless, the modular design comes at the cost of increased design complexity, e.g., the decomposition of the potentially monolithic system into a number of interconnected subsystems. This requires establishing interfaces, bringing integration challenges, adding layers to the system's testing process, and inevitably increasing its initial costs and implementation time. However, the platform-based design provides unmatched design reusability and flexibility benefits throughout the system life cycle, potentially minimizing the overall system development and maintenance effort.

4.3.6 Concept validation

The concept of a modular platform-based cyber-fluidic system was validated by first prototyping a pilot system, which is discussed in Appendix B. The pilot system went through a complete design-build-test cycle serving the purpose of cyber-fluidic architecture evaluation, a testbed for technical methods and components, and technological feasibility exploration of the fluidic path.

4.3.7 System design and architecting

The concept development phase targets to produce heterogeneous system architecture views such as operational, logical, and physical. Since the architecting, engineering and innovation activities related to the cyber-fluidic platform are considered to be part of the essential contributions of this thesis work, they will be discussed in detail throughout Chapter 5. Blending the discussion of architecting on the platform and module-level, together with the engineering of the different components, allows for motivating design decisions on both conceptual and practical levels.

4.4 Summary

The interdisciplinary nature of cyber-fluidic systems presents a wide range of challenges calling for both innovative and advanced engineering solutions. Navigating the design space requires establishing fundamental understanding and processes to handle the complexity and uncertainty throughout the decision-making process. This chapter discussed aspects covering the concept development phase of our vision for a highly reconfigurable cyber-fluidic system. Originating from the holistic approach of system engineering, the operational and technological challenges of the cyber-fluidic system were addressed based on prior experience with digital microfluidics. A set of design objectives for the envisioned reconfigurable cyber-fluidic system were presented, and it was argued in favor of the modular, platform-based design as rational system architecture.

Chapter 5

Cyber-fluidic platform design

This chapter presents the architecting, engineering, and innovation activities involved in creating a reconfigurable cyber-fluidic platform. The chapter begins with establishing the cyber-fluidic platform architecture and continues with an iterative bottom-up description of the system's fluidic, instrumentation, and virtual domains. The reader is guided through the system development process by discussions for the central design objectives. Due to the technical nature of the discussion, the reader is expected to be familiar with the digital microfluidics operation principles explained in Chapter 2, and to have an essential understanding of computational systems and electronics. The chapter contains mainly original work, unless otherwise stated, and it is considered to be a central part of this thesis.

5.1 Cyber-fluidic platform architecture

The motivation for a platform-based cyber-fluidic system is based on the operational, functional, non-functional, and physical system objectives outlined in Section 4.3.2. Key considerations are the system's programming model, the ability to evolve and accommodate changing functional requirements, and the

ease of use from the end-user perspective. Throughout the concept development phase, we have argued in favor of modular platform-based design as a framework for maximizing the system's operational performance and accommodating for the uncertainties associated with the system's fluidic path. At the first level of system decomposition, as shown in Figure 4.4, we have identified three main categories of cyber-fluidic system components, namely the fluidic, instrumentation, and the virtual parts. The fluidic system consists of a digital biochip and all related sensors, actuators, and devices. For example, a digital biochip can have an integrated biosensor, off-chip color sensor, and off-chip pump and waste reservoir. Regardless of calling the sensor and pump reservoirs to be off-chip, it only clarifies that they are not an integral part of the digital biochip, but they still remain part of the fluidic system. Moreover, we can consider the fluidic system to take the central position in the overall system design since it is responsible for manipulating the reagents and carrying out the experimental work. We consider the fluidic system to be the most delicate and technologically constrained of the three parts, and therefore the modularity and functional mapping of the instrumentation and virtual parts of the platform are governed by the constraints imposed from the fluidic system.

The instrumentation needs of the fluidic system can be split into three main categories based on their functionality, namely *control*, *feedback*, and *supply* [113]. The *control category* manages devices and resources to the digital biochip, such as multiplexing a high-voltage source to the array of control electrodes or controlling heating elements. The *feedback category* groups functionality that requires instrumentation for extracting data from the fluid path, such as an electrochemical biosensor or a temperature sensor. The *supply category* carries out the auxiliary functionalities such as providing an electrical power source for actuation electrodes or vacuum/pressure sources for interfacing the digital biochip with external reservoirs or systems. The fluidic system is discussed in details in Section 5.3.

The control, feedback, and supply functionality model is projected onto the modular decomposition of the instrumentation system, as shown in Figure 5.1. This yields a one-to-one functionality mapping, e.g., an instrumentation need of the fluidic system is met from a module in the instrumentation system. A set of control, feedback, and supply modules create an instrumentation system instance matching particular experimental needs. The instrumentation modules are connected through plug-and-play bus interfaces to the processing and control subsystem, as shown in Figure 5.1. The instrumentation system also implements modules to add auxiliary functionality such as power management, communication, and user interface subsystems. This instrumentation subsystem is further discussed in Section 5.4.

The virtual system consists of software tools to control, program, and simulate

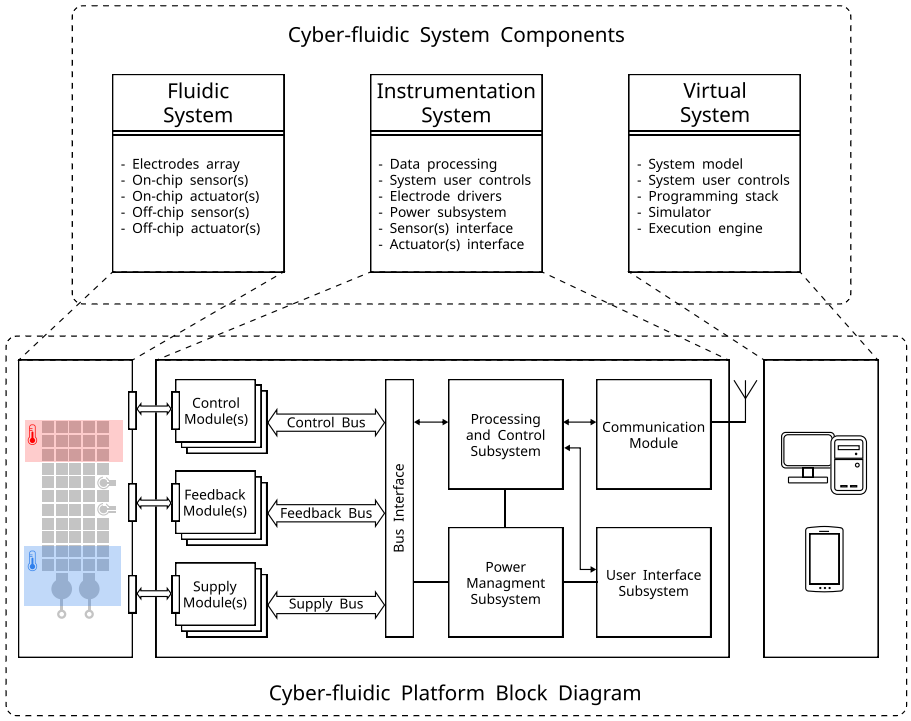

Figure 5.1: Cyber-fluidic platform architecture.

the instrumentation and fluidic components. The software stack holds a model of the physical and functional characteristics of the physical system so they can be mapped to a virtual representation. This allows for effective manual control of the system and provides the programming toolchain with relevant device-specific architectural and features context. The software framework captures details from the full depth of the system and abstracts them to a visual or textual programming paradigm. An example of the interaction depth can be recognized even in the most basic operations such as driving of a control electrode on the digital biochip - a software command needs to be propagated through multiple layers and interfaces until reaching the digital biochip. This shows the link between the two interaction points with the system: the fluidic interface, e.g., loading or extracting reagents of the digital biochip; and the system's control and programming interface. These two interaction points, fluidic and virtual, can be considered the external boundaries of the cyber-fluidic system, and the software framework should capture a significant level of semantics to allow for efficient operations. Nevertheless, proper design and implementation hold the potential for seamless integration of the fluidic subsystem with a traditional

computation, thus allowing for performing computation not only with virtual data but also with fluidic reagents. Section 5.5 is dedicated to discussing the virtual system and developing the idea of the digital biochips as computational components [114].

5.2 Modularity considerations

The concept of modularity is essential to the entire cyber-fluidic system and is frequently discussed throughout this chapter. Important design goals are to achieve modularity on fluidic, mechanical, electrical, and virtual levels, not only on the module but also on the subassembly level.

The modular design approach divides a system into smaller independent parts. This approach allows modules to encapsulate specific functions that can be independently developed and tested outside of the boundaries of the whole system. Modules interconnect through defined interfaces on the physical, electrical, and protocol level. The physical level deals with how the connection between two compatible interfaces is established, e.g., the used connection type and signal layout. The electrical level ensures that input and output signals between the interconnected modules are compatible. The protocol level is responsible for establishing the signaling and data exchange procedure between the interconnected system. While the protocol level can be software-defined to a great extent, the physical and electrical characteristics of the interfaces and the modules must be established early in the design process. Therefore, before we continue with the detailed design of the platform-based cyber-fluidic system, we will discuss the modularity guiding principle utilized later in the system design.

5.2.1 Physical level

An instance of the fluidic system requires matching interfacing capabilities from the instrumentation system. This is achieved by assembling an instrumentation instance from the necessary functional modules. Each of these modules is designed as a stand-alone embedded system built with materials and processes available to the electronic fabrication industry, such as PCBs, through-hole, and surface mount components. To streamline the module design and subsequent system assembly, we enforce unit size-constrained dimensioning on each module's length and width, as shown in Figure 5.2. One unit is 25 mm, and each module's physical footprint has to comply with the increments of the unit size. The recommended space for positioning mounting holes is 5 mm from the edge

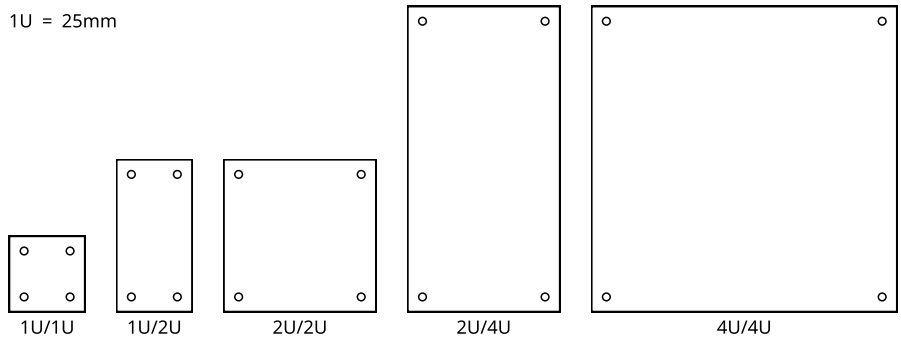

Figure 5.2: Module unit size. A *unit* is denoted with U and is equal to 25mm. The mounting holes are positioned 5mm from the module edges. The drawing is not to scale.

of the PCB, preferably aligned with increments of the 1U/1U module, as shown in Figure 5.2. Even though these physical design constraints can lead to less space-efficient modules, adhering to the unit size and mounting holes placement allows modules to be easily stacked vertically and horizontally. However, to potentially reduce component placement constraints, the mounting holes can be partially or completely avoided since other PCB features such as edges or connectors can be used as attachment points. The concept of physical modularity is further illustrated throughout Section 5.3, Section 5.4, and the rest of this thesis.

Another critical aspect of modularity is the data interface and power delivery system. Although wireless communication and stand-alone battery operation are feasible from a technical standpoint, at this stage, we consider it impractical from the perspective of the envisioned cyber-fluidic system. Therefore, physical connections are used for data transfer and power delivery throughout the instrumentation system. Important considerations for the system interconnects are the physical size, convenience, rigidity, safety, and power rating. A guiding principle when deciding on a family and type of connectors is minimizing the risk of misuse, e.g., using the same type of connector for more than one purpose. Therefore, we adopted the policy of using a unique connector for a single purpose. This protects from mishandling the system and streamlines its operation.

The modularity on the electronic circuit level allows for design reusability, thus reducing the development cycle and providing streamlined design solutions. For instance, an embedded system consists of several recurring circuit design patterns, such as communicational interfaces, clock domains, power subsystems,

etc. Establishing a platform-wide approach for implementing the repetitive design patterns resonates with the overall modular concept and simplifies the development process. An example of that is the unit sized microcontroller module presented in Section 5.4.7, which is utilized as a building component for each instrumentation system.

5.2.2 Virtual level

Modularity on the software occurs both on an application and framework level. Modular software design practices strive to achieve functionality encapsulation, thus promoting independent and interchangeable software modules. Interfaces between components are decoupling the different software modules allowing streamlined application development. On the framework level, the different applications are decoupled through either file-based techniques or service orientated designs. Even though the virtual modularity is inherently easier to develop than the physical, it has a significant role in meeting the functional and non-functional operational objectives outlined in Section 4.3.2. The discussion about the envisioned software framework continues in Section 5.5.

5.3 The fluidic system

The fluidic system consists of a digital biochip and any associated auxiliary sensors and actuators. For example, an instance of the fluidic system can include a digital biochip, off-chip reservoirs and pumps, a magnetic stage, and a photomultiplier tube (PMT). The mentioned components are considered a part of the fluidic system since they interact with the used reagents. In this thesis, we focus on developing the core technology for the digital biochip while accounting for overall flexibility in the fluidic system.

The discussion throughout Section 5.3 outlines the motivation and the design objectives for creating what can easily be dismissed as "yet another digital biochip design." However, we believe that we have managed to push the digital biochip fabrication envelope in three different directions. First, we established a scalable method for building larger individually addressable PCB-based arrays of control electrodes. To the best of our knowledge, we report the largest PCB-based removable digital biochip with 640 individually addressable electrodes and the capacity for efficiently scaling the electrode count by a factor of two or even four without significant design cost. The second unique contribution is the use of PCB embedded heaters, which serve the dual purpose of heating and tem-

perature sensing elements. This allows for heating capabilities to be added to the digital biochip at virtually zero cost and with minimum external interfacing and instrumentation. The third significant contribution is the conceptualization and development of removable foil-based frames used as a dielectric and hydrophobic coating method. Even though the concept of using foils for digital biochip coating purposes have been demonstrated before, the use for real application remains somehow limited. Our claim to the foil-based techniques is thus threefold. First, we have developed a streamlined, efficient, and reproducible foil application process by the use of prefabricated plastic frames. Second, to the best of our knowledge, we claimed to be the first to demonstrate the use of 5 µm thick foils, including the novel use of PTFE foil. And third, we report the first demonstration of PCR and full ELISA performed on a foil-coated digital biochip, consequently addressing the biofouling and sustainability issues associated with these reactions, i.e., only the foil coating is replaced rather than the whole digital biochip. The experimental aspects of the reported innovations are further discussed in Chapter 6.

5.3.1 Design objectives

The size of the actuation array is proportional to the number of parallel operations that can be carried out on a digital biochip. A large number of individually addressable electrodes suggests a multicolumn-multirow electrode organization so that droplets can be freely routed between any two points on the array. Furthermore, each electrode can be considered not only as an actuation device but also as a storage location when the droplet remains stationary. Comparing a droplet to a data type, and an actuation electrode to a memory cell, we can draw parallels with the memory found in modern computers, where larger memory allows for more data storage and computations. Therefore one of the design goals for the digital biochip is to maximize the number of individually addressable electrodes. A large number of control electrodes will enable multiple operations to be carried out on a single device as well as for place and routing flexibility.

A typical characteristic of the electrowetting droplet actuators is the unit droplet size, i.e., the droplet volume required to cover a single electrode. A minimum droplet volume is needed so that droplet can be effectively transported from one electrode to another. The droplet unit size is determined by the electrode area, the contact angle, and whether the digital biochip is open or closed. For practical reasons such as ease of handling and practical reagents volume, we aim to design a digital droplet actuator capable of operating with droplet unit size in the range of 1-3 µL in the closed configuration, and 10-20 µL in an open configuration.

Lowering the recurring operational cost is a key factor for increasing the widespread of a given technology. Without considering the non-recurring cost of research and development, the value of a digital biochip can be estimated as the sum of the used materials plus the fabrication cost. Another approach to reducing the operational cost and favor sustainability is to design a fully or partially reusable biochip. We consider the cost and environmental aspects, and we aim to develop a cost-effective and sustainable digital biochip lifecycle.

The digital biochip should follow the overall modularity concept of the cyber-fluidic system. This means complying with the introduced module unit size, establishing reusable electrical and fluidic interfaces, and allowing for functional extensions. Furthermore, to truly test the modularity concept, we plan to use the first design of the digital biochip not only as a technology demonstrator but also as a lab-on-a-chip capable of running relevant lab protocols. Therefore, we aim to design and test the cyber-fluidic system's capability to perform enzymatic reactions and DNA amplification by PCR.

An overview of the-high level design objectives for the digital biochip are listed below:

- A large array of individually addressable electrodes.
- Unit droplet size in the range of 1-3 µL in a closed configuration and 10-20 µL in an open configuration.
- Cost-effective and sustainable digital biochip lifecycle.
- Adopt modularity and reconfigurability concepts.
- Equipped for proof of concept PCR and enzymatic reactions.

5.3.2 Fabrication technology

A variety of digital biochip fabrication techniques have been discussed in Section 2.4.1. The most popular practices gravitate towards using glass or silicon wafers as a substrate patterned with cleanroom fabricated conductive electrodes. Common processes for insulation coating utilize deposition processes (Parylene C, SiO2) or spin-coated polymers (SU8). A widely adopted technique for fabricating the hydrophobic layer is spin-coating a PTFE or other fluoropolymer solution on the top of the insulation layer. Although glass and silicon substrates are suitable for manufacturing multiple conductive layers, their use has not been adopted to fabricate digital biochips. A single conductive layer limits the driving electrodes pattern by forcing the control electrodes and the corresponding

connecting tracks to be placed on the same layer. A single conductive layer makes laying out and routing an array of 3×3 individually addressable driving electrodes impossible since escape routing the center electrode requires at least one extra conductive layer. Multiple conductive layers and via interconnects are required to allow for routing an individually addressable multirow and multicolumn array of control electrodes.

Multilayer PCB boards have been demonstrated as an alternative to the glass and silicon-based chips, as discussed in Chapter 2. The modern PCB fabrication capabilities offer track width and spacing of 50 µm (2/2 mil), minimum hole size of 150 µm, and are widely produced with more than 16 conductive layers. The fast development of the electronics industry made it possible for 1 dm^2 of 6 layered PCB to come at the cost of less than 2 USD for small quantities. The features size, layer count, and affordable price, along with the well-developed service orientated marked, make the commercial PCB technology a fit candidate for fabricating digital biochips with a large array of individually addressable electrodes.

The PCB technology has one significant disadvantage when it comes to direct application for fabricating droplet actuators - the surface of the control electrodes array is not flat. The top copper layer usually has a thickness of 17.5 µm or 35 µm (0.5oz or 1oz), which combined with the substantive manufacturing process results in trenches with the height of the copper layer between the electrodes. The uneven patterned area renders the surface of the chip incompatible with the conventional spin coating, and therefore the space between the electrodes needs to undergo a leveling procedure such as multistep coating and polishing [115]. Alternatively, a foil layer can be applied to the array, serving the purpose of an insulation layer and covering the trenches between the actuation electrodes.

Compared with the glass or silicone-based digital biochips, the commercial PCB technology offers a cost-effective process for developing and testing digital biochip designs. The spatial resolution of 50 µm is on the level required for reliable droplet actuation, and the ease of implementing multilayer structures opens for advanced electrode patterns. Furthermore, it has already been demonstrated as a feasible technology, as discussed throughout Chapter 3. Nevertheless, the PCB-based digital biochips pose challenges to the traditional coating techniques, which we address in Section 5.3.4.

5.3.3 Digital biochip design

The digital biochip design process aims to map the design objectives (see Section 5.3.1) into the PCB technological capabilities and identify the potential need for innovation. An iterative exploration of the design space has led to the development of a custom digital biochip, and the discussion below motivates the primary design intents related to the electrode sizing, physical dimensions, and expected features set. We call this digital biochip design TC008, where the TC008 acronym stands from Test Chip, and the three following digits indicate the specific design number. Each design, fabricated or not, is assigned a unique identifier that can be recognized by the instrumentation system, as discussed in Section 5.3.3.4. The TC008 design presented here is the product of an extensive exploration process carried out as part of this thesis work. Besides the outsourced manufacturing of the TC008 PCB and unless otherwise stated, we claim the authorship of conceptualization, innovation, design, fabrication, and testing and consider these activities as essential parts of this thesis work.

5.3.3.1 Actuation electrode array

The first design consideration is related to the relationship between the control electrode size and the unit droplet size. In a closed system, the unit droplet size is directly related to the ratio between the electrode area and the gap height. Furthermore, to allow for controlled droplet splitting, the aspect ratio between electrode pitch and gap height is recommended to be in the range of 2-7 [60]. An electrode size of 2 mm×2 mm and a gap height of 0.3-0.8 µm allows for unit droplet volume of 1-2.5 µL and aspect ratio in the range of 2.5 to 7.

Another tradeoff is the control electrode array size to the digital biochip outline dimensions. In order to fit with the platform's physical modularity, the digital biochip dimensions must comply with the module unit size as outlined in Section 5.2.1. In general, the digital biochip needs to accommodate the main electrode array, on-chip reservoirs, connection interface to the electrode drivers, and for a mechanical attachment method. A compact form factor can be achieved by aiming for 25-50% utilization of core fluidic functionality, i.e., the control electrode array and on-chip reservoirs. To provide sufficient room for routing and allow for a large array of control electrodes while still maintaining a compact physical form factor, the TC008 is designed to fit the 4U/4U size, resulting in outline dimensions of 100 mm×100 mm. Considering a single electrode area of 4 mm^2 and worst-case chip utilization of 25%, the selected 4U/4U chip size still allows for at least 625 control electrodes to be fitted.

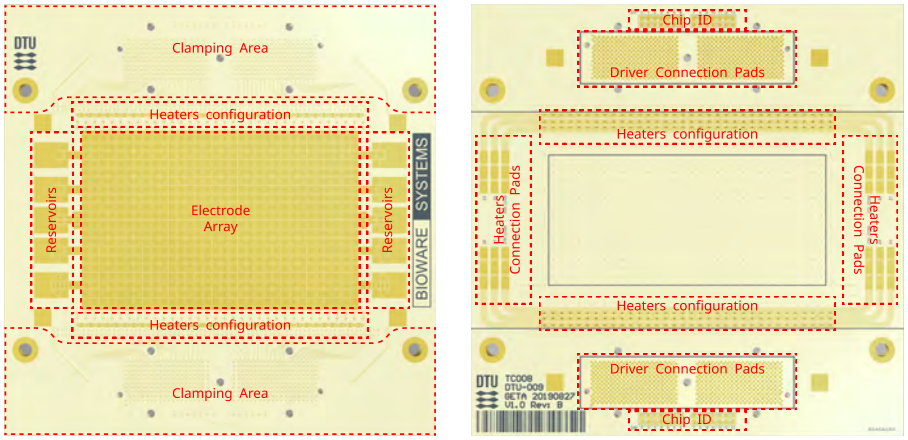

(a) TC008 Top. **(b)** TC008 Bottom.

Figure 5.3: Model of the TC008 digital biochip. The digital biochip fits 4U/4U, and it has outside dimensions of 100mm × 100mm. The different functional areas are marked and annotated in red. A high-resolution version is available in the digital copy.

The interfacing between the digital biochip and the external electrode drivers poses the unique challenge of reliably and efficiently making hundreds of electrical connections. Traditionally, spring-loaded barrel connectors (also known as "pogo pins"), or computer memory slots have been used to connect the digital biochip and the electrode drivers (see Chapter 3). These approaches do not provide the connection density (number of connections per unit area), reliability, and ease of use of the envisioned over 600 control electrodes. An extensive market search yielded a low profile dual compression connector capable of delivering up to 400 connections in a relatively compact 12 mm×50 mm size [116]. The connector pitch is 1 mm, and the contacts are organized in 10 rows and 40 columns. The PCB fabrication capabilities (trace width and spacing) and the small pitch of the connector create routing requirements that affect the number of required layers. A separate PCB layer is needed for escape routing of every two contact rows, thus needing at least five routing layers. This requirement fits with the standard six-layer board stack, which is still suitable for cost-sensitive applications. In comparison, the cost of a 6-layer PCB is roughly 25% more expensive than a 4-layer PCB, and an 8-layer PCB is almost twice as expensive as a 6 layer design.

Considering the physical 4U/4U outline of the chip, connector capabilities, electrode size, and available PCB area, the electrode array was designed in 20 rows and 32 columns, resulting in 640 droplet actuation electrodes. The design of the

TC008 was made in an electronic design automation software, and a visualization of the PCB is shown in Figure 5.3a. The figure also shows the different parts of the digital biochip annotated with red. The electrode array is centered on the TC008, which leaves room for placing on-chip reservoirs to the left and right sides. Routing of the control electrodes to the driving circuitry connectors is made towards the top and the bottom of TC008. The digital biochip is logically split by a horizontal centerline, which allows for balancing the routing paths to the driver connection pads. All electrodes positioned above the horizontal centerline are routed towards the top driver connection pads, and all electrodes below the centerline are routed to the bottom driver connection pads. The two driver connection pad areas are shown in Figure 5.3b.

5.3.3.2 Reservoirs

A reservoir is constructed from a large electrode and a line of smaller unit size electrodes used to extract a droplet. We have designed five different electrode extraction patterns so that different approaches can be tested. The same five reservoir designs are replicated on the left and the right sides of the electrode array, as shown in Figure 5.3a. The reservoir designs differ in the extraction path pattern, e.g., using smaller electrodes, thus aiming to implement a more granular extraction procedure.

The reservoir electrodes also add to the total number of driver channels. The total number of driving lines for the reservoir and main control electrodes should be kept within the 400 connections per connection side. Each reservoir bank consists of 43 electrodes, which added to the 320 electrodes on the main array fit into the connection number per side.

5.3.3.3 Temperature control

Reagents temperature control is an essential part of the wet lab work. Elevated temperature is used to control the speed of a process or to trigger and sustain a reaction in the case of a PCR. Therefore, one of the primary objectives for the digital biochip is to design and implement a mechanism for creating on-chip multiple temperature-controlled regions. For example, the capacity to create three separate high-temperature regions will allow for space domain PCR, i.e., a droplet containing a master mix being transported between annealing, elongation, and melting temperature regions.

Temperature control for digital microfluidic chips has been traditionally im-

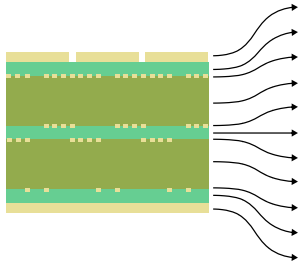

Layer	Material Type	Thickness	Primary Funciton
Top Solder Mask	Solder Mask	127µm	Insulation
Top Layer 1	Copper	35µm	Electrode array
Prepreg	2113*1	100µm	Insulation
Inner Layer 2	Inner Layer 2	175µm	Heaters meander
Core	Core	565µm	Insulation
Inner Layer 3	Inner Layer 3	175µm	Electrode routing
Prepreg	2116*1	127µm	Insulation
Inner Layer 4	Inner Layer 4	175µm	Electrode routing
Core	Core	565µm	Insulation
Inner Layer 5	Inner Layer 5	175µm	Electrode routing
Prepreg	2113*1	100µmm	Insulation
Bottom Layer 6	Bottom Layer 6	35µm	Connections area
Bottom Solder Mask	Solder Mask	127µm	Insulation

Figure 5.4: Digital biochip PCB layer stack.

plemented by Joule heating or solid-state thermoelectric heat pumps. A conventional approach is to attach resistive heater bars to the bottom side of the chip [15] and calibrate for the thermal mass, losses, and variation introduced from the thermal interfacing. An alternative approach where the heater and temperature sensor have been built as a part of an actuation electrode [117] has the advantage of providing local heating tightly coupled with the on-chip droplets. By minimizing the thermal path's length and reducing the thermal mass, this approach claims to deliver outstanding thermal response - achieving PCR melting temperature in 7 seconds. Contact heating and cooling have been realized as well with thermoelectric Peltier modules [52] [118]. The thermoelectric temperature control is associated with big thermal mass, long thermal path, and low efficiency. Non-contact infrared and induction heating have been demonstrated as well [119], but their capabilities and instrumentation are considered suboptimal in the context of a flexible general-purpose application. Nevertheless, the listed approaches are, in general, not suitable for runtime reconfiguration in the context of large actuation electrode arrays due to the fixed heating area. External heaters have confined space and fixed thermal interfacing. The embedded heaters electrode solution [117] appears to be challenging to scale, requires advanced fabrication techniques, and exhibits reduced droplet mobility over the heating electrode.

In the context of a reprogrammable digital biochip, we aimed to achieve a unique heaters' versatility by allowing for multiple individually configurable on-chip heating regions. The simple and effective resistive heating appears to be a suitable approach to be used on a PCB-based digital biochip. The multilayer construction of the digital biochip allows for heating structures to be built on an internal layer positioned close to the actuation electrodes. A cross-section of TC008 and the PCB stack-up is shown in Figure 5.4, where the arrangement of

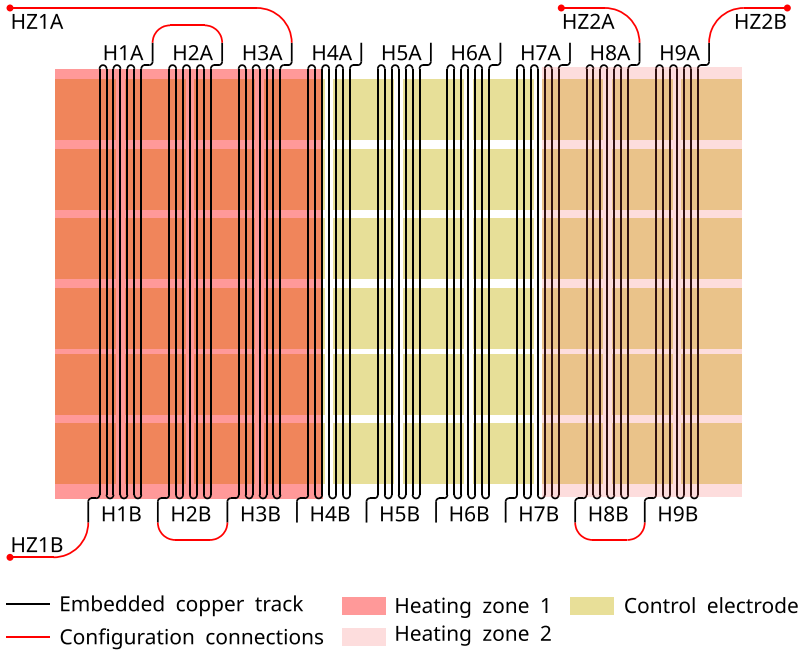

Figure 5.5: Illustration of the embedded heaters structure and configuration options.

the internal copper and insulating layers is shown. The primary function of the top layer is to accommodate the control electrodes array. The second copper layer is separated from the top layer by 100 µm, and it is dedicated to forming meander heater structures. Using inner layer 2 for heating effectively positions the heaters closer to the digital biochip top surface as opposed to mounting an external heating element on the backside of the PCB. The inner layers 3, 4, and 5 are used for routing the electrode array to the driver connection pad area (see Figure 5.3). The bottom layer of the PCB accommodates the driver connection area, the heaters' configuration pads, and the heaters' connection pads, as shown in Figure 5.3b.

The thermal control of TC008 is based on the unique approach of building the heaters on inner layer 2, which has a thickness of 17.5 µm and lies 100 µm below the top electrodes layer. The layer is patterned with meander structures, each positioned between two columns of electrodes, as illustrated in Figure 5.5. The ends of each meander structure are terminated to copper pads on the two outer PCB layers, which allows them to be connected to an external power source and used as resistive heaters. The heating elements can be connected in series

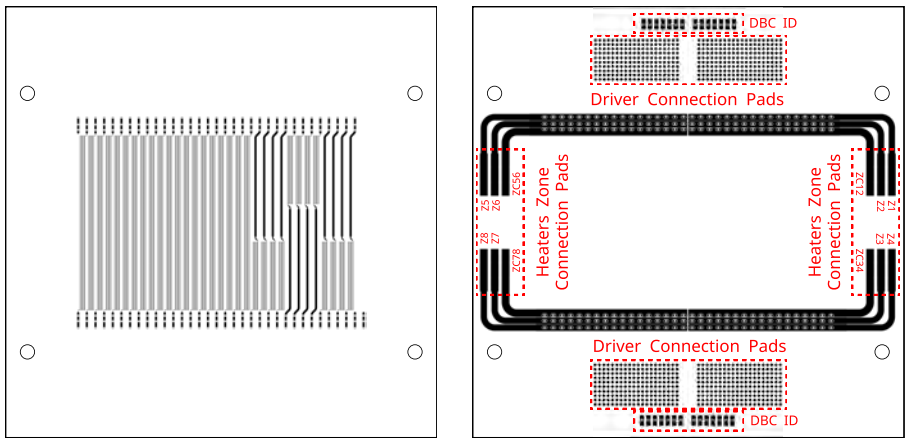

(a) Meander heaters on inner layer 2.

(b) Heater connections on the bottom layer.

Figure 5.6: Heaters layout on TC008. A high-resolution version is available in the digital copy.

(or in parallel) to form a heating region anywhere under the electrode array. For instance, Figure 5.5 illustrates two independent heating zones formed from two and three heating elements. Heating zone 1 is formed from heating elements H1, H2, and H3, by establishing the external connections marked in red, namely connecting H1A to H2A, H2B to H3B and applying the power to H3A and H1B by connecting them to HZ1A and HZ1B. Heating zone 2 is configured in a similar manner, and it is separated from heating zone 1 by three columns of electrodes. Based on the required temperature profile, the heating zones need to be horizontally spaced on the chip in order to manage the effect of thermal leakage.

Configuration of the heaters is achieved by solder bridges on the external top and bottom layers of the digital biochip, and the configuration areas are shown in Figure 5.3. Even though this approach requires the arrangement of the heater to be manually created, we argue that runtime reconfiguration is feasible, and it can be implemented by using solid-state switches. However, to reduce the likelihood of runtime limitations due to fixed heating regions, we have designed the digital biochip to support up to eight individually controllable heating regions. Two different patterns of meander heating elements have been designed - twenty vertical heaters covering the full height of the electrode array and twelve heaters with a height of eight electrodes, as shown in Figure 5.6a.

The meandering heater structure increases the track length and its resistance

(Pouillet's law). A higher heater resistance results in a lower current on the cost of increased voltage for given output power (Ohm's law). The resistance of a single heater was targeted to be in the 1-5 Ω range for simplifying the control circuitry. The heaters' design is discussed further in Section 5.4.11 along with technical analysis for the heater control module.

Temperature control can be achieved without a feedback loop if the thermal system operates in a static environment. Under fixed operation conditions, a system supplied with constant power will reach an equilibrium state, and it will remain stable unless a deviation in the operational conditions is introduced. A more reliable approach is to implement a closed-loop system, where a temperature sensor provides feedback to a control loop. As a result, the power applied to the heater is adjusted to counteract any change in the operation conditions, thus continuously working to minimize the error between the measured temperature and the set point. Different temperature sensors are available and can be added to the digital biochip. Such an approach will require a temperature sensor for each heater in order to preserve the arbitrary configuration of the heating zones. The introduction of an external component, thermal interfacing, and integration cost to the otherwise streamlined digital biochip design is considered undesirable. To address this issue, we report the second unique approach incorporated into the heater's design of TC008, namely, to use the heater itself as a temperature sensor. The meander structure is not only playing the role of a resistive heater, but it is also used as a resistive temperature sensor. Copper has a positive temperature coefficient of 0.00393% per 1 °C, which translates to a linear dependence between the heater resistance and its temperature. This approach allows for monitoring the temperature without adding external temperature sensors to the digital biochip. Furthermore, it enables measuring the temperature of an arbitrary heating zone configuration based only on the heaters' resistance. The control and measuring techniques are further discussed in Section 5.4.11 along with the design of the heaters control module.

5.3.3.4 Digital biochip identification

The TC008 heaters can be configured with different layouts creating up to eight individual heating regions. Furthermore, various digital biochip designs with varying dimensions of the electrodes, number, shape, reservoir layouts, sensor integration, etc., can potentially be developed. To allow for plug-and-play functionality, we have designed a digital biochip identification mechanism based on two 14-bit identifiers, which are hardware configurable through solder bridges on the digital biochip. The configuration zones are positioned adjacent to the driver connection pads area, as shown in Figure 5.3b and Figure 5.6b. The unique identifier allows the instrumentation platform to identify the attached

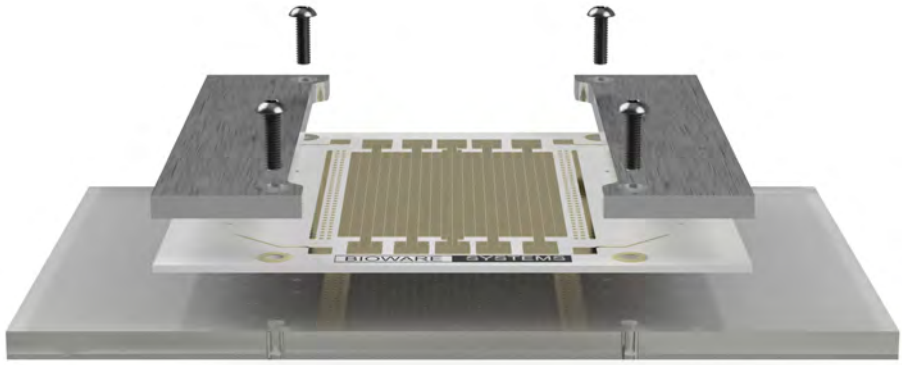

Figure 5.7: TC008 clamping - the two locking plates are bolted to a fixture plate to compress the spring-loaded connections under the digital biochip. A high-resolution version is available in the digital copy.

digital biochip and ensure the proper configuration of the instrumentation subsystem.

5.3.3.5 Digital biochip interfacing

The connection between the digital biochip and the electrode drivers is established through two connectors with 400 spring-loaded contacts [116]. The connector contacts are organized in 10 rows and 40 columns with a 1 mm pitch. Each spring-loaded contact is rated for 30 g of compression force, therefore 12 kg of compressing force per connector is required to secure the electrical connection. The contact pressure is produced from two clamping plates positioned on the top side of the digital biochip bolted to a mechanical fixture, as shown in Figure 5.7.

Interfacing with the heater zones is achieved with individual spring-loaded contacts from the bottom side of the TC008. The eight temperature zones connect with the instrumentation circuitry through 12 groups of 3 pads, namely Z1-Z8 for the individual zones and ZC12, ZC34, ZC56, ZC78 for the common connections, as shown in Figure 5.3b and Figure 5.6b. Each group of 3 pads is designed for the potentially high current demand where two pads are used for power delivery, and the third pad is used for measurement. The use of two power delivery and one sensing pads effectively implements four-terminal sensing by separating the current-carrying and voltage sensing lines in order to eliminate the influence of the wires and contact resistance and achieve more accurate measurements. This technique will be further discussed in Section 5.4.11 along with the design consideration of the heaters control module.

5.3.4 Digital biochip coating

There are two main approaches to create the insulation hydrophobic later for an EWOD droplet actuator. The first and the most conventional approach is based on depositing polymers that bond to the surface of the electrodes and substrate, thus forming a uniform, pinhole-free layer. The deposition techniques include vapor deposition processes, spin or dip coating, as discussed in 2.4.1 and 5.3.2. The planarization issues related to the trenches between the electrodes have been resolved in a scalable manner by at least two companies, DigiBio, and Baebies (former Advanced Liquid Logic, Inc), as outlined in Chapter 3. However, using a digital biochip with high protein content reagents will inevitably lead to surface contamination known as biofouling. This unwanted deposition of proteins or other analytes affects the droplet transport and poses a risk of contamination to any analyte which passes through the fouled area. One approach to try to mitigate the effect of biofouling is by surfactant additives (discussed in the patents review in Appendix A) or with the use of a filler fluid such as silicone oil. These approaches reduce the risk of biofouling, but they can not guarantee a contamination-free surface. Therefore, from a reliability standpoint, digital biochips are often treated as single-use devices. Discarding a PCB-based digital biochip is neither cost-effective nor environmentally friendly, particularly considering the fact that only the surface of the chip might potentially be contaminated.

The second coating approach is based on applying a foil film on top of the electrodes [120] [23] [121]. The most common foil materials are polyethylene, parafilm [122], ethylene tetrafluoroethylene [30] with thickness in the range of 10-17 µm. In some instances, an additional hydrophobic layer is applied to the foil to increase the contact angle. The foil-based coating approach has the benefit of being loosely adhered to, typically by using silicone oil rather than bonded to

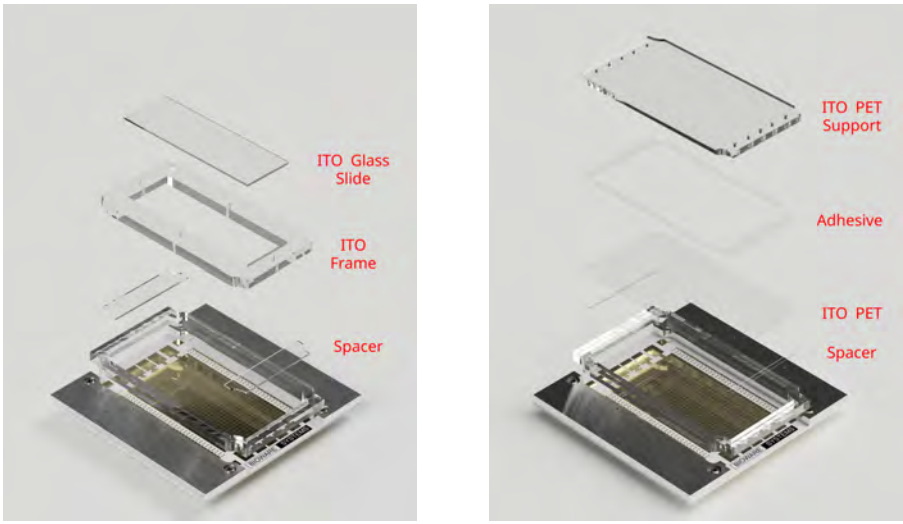

(a) TC008 ITO Glass Slide Assembly. **(b)** TC008 ITO PET Assembly.

Figure 5.8: TC008 foil frame-based coating assemblies. A high-resolution version is available in the digital copy.

the surface of the digital biochip. This allows the foil to be efficiently separated from the digital biochip while the PCB can be reused without risk of contamination. A removable frame-based coating approach has been demonstrated to be a feasible concept in the context of both open and closed systems [30] [23]. Aiming for cost-effective, sustainable, and streamlined operation, we have adopted the frame and foil-based concept as a coating technique for TC008.

The foil-based coating approach provides an elegant solution to the risk of surface contamination and effectively addresses the sustainability concerns, but it also comes with a set of challenges related to the application and operation conditions. Besides the fact that thin foils are generally difficult to stretch and apply to a holder frame, the effect of the heating required for PCR needs to be considered. Foil wrinkling might occur due to thermal expansion. Additionally, the foil might potentially have surface imperfections hindering the droplet actuation. Nevertheless, the foil-based approach holds the potential to provide affordable running costs if optimized and scaled to the array size of TC008. Therefore, we have built upon the currently used materials and techniques and developed a foil-based coating method fitting the digital microfluidics platform modularity concept.

The foil frame-based design approach is shown in Figure 5.8. The frame is made

from 5 mm polymethyl methacrylate (PMMA), also knowns as acrylic, and it is designed to fit with tight tolerance between the clamping brackets. The shape of the clamping plates is used to align and center the acrylic frame on the top of the TC008. The foil is attached to the acrylic frame by pressure-sensitive dual-sided adhesive tape. We have managed to push the envelope and reduce the foil thickness from the previously reported 10-17 µm to the use of foils with a thickness of only 5 µm, thus allowing for actuation voltage in the 120-140V range. Furthermore, to the best of our knowledge, we claim to be the first to demonstrate the use of 5 µm and 8 µm PTFE foil as a coating material. We also recognize as a major contribution to be the first to demonstrate PCR and full ELISA being performed on a foil-coated digital biochip. The experimental aspects of the reported novelties are further discussed in Chapter 6.

The TC008 foil frame is designed as a modification for the 2U/4U to fit the modified 1U/4U curved profile of the clamping plates. The deviation from the rectangular unit size module is intended to guide and center the foil frame when applied on the top of the electrode array.

The foil frame coating is suitable for both open and closed digital microfluidics systems. For the open system, the foil-frame coating allows for streamlined testing of droplet actuation on different foil materials, as discussed above. For closed system operation, the top plate can be fabricated from ITO glass or ITO coated PET plastic sheets treated with a hydrophobic coating. The modular approach of the foil frame allows for variations in the top plate configuration, as shown in Figure 5.8. The used materials and techniques are discussed in detail in Chapter 6.

5.3.5 Sensor integration

The foil-based coating approach has the potential to serve as a substrate for fabricating screen-printable biosensors. In the early stage of the concept development phase of the project, we developed and characterized a printable paper-based electrochemical biosensor [123]. Furthermore, electrochemical biosensors have been demonstrated as stand-alone devices that can be integrated with an open digital biochip [10]. Another compelling approach is the on-chip biosensor reconfiguration [70], which aligns with the overall modular and reconfiguration concept of our digital microfluidic platform. However, investigating the sensor integration in detail remains out of the scope of this thesis work.

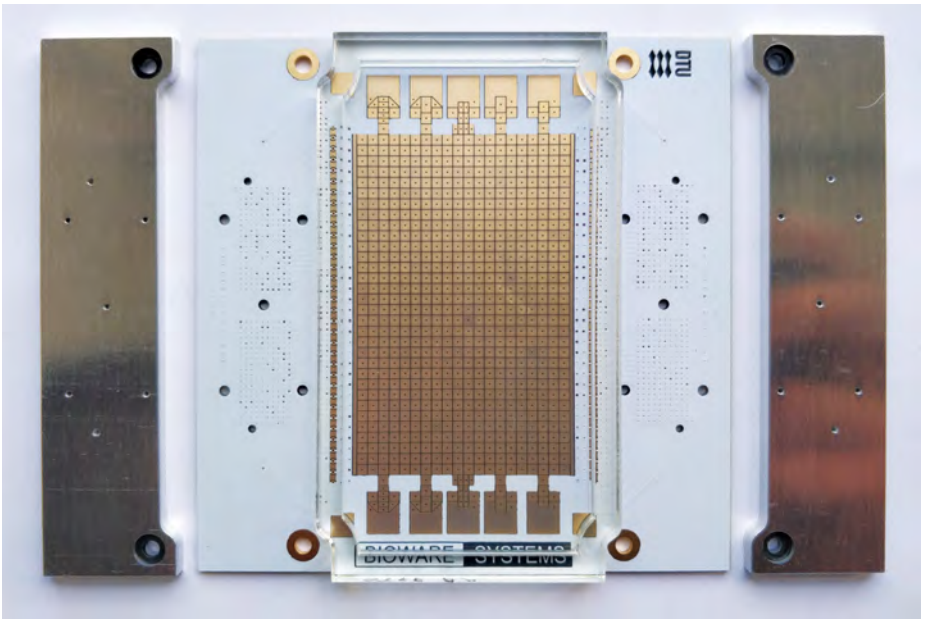

Figure 5.9: Fabricated TC008, clamping plates, and a foil-frame.

5.3.6 Fabrication

A variety of computer-aided design (CAD) packages for 2D and 3D modeling have been used to design the digital biochip and supporting components. The PCB design was made in Altium Designer, and Autodesk Inventor, Fusion 360, and AutoCAD were used for the mechanical modeling. A commercial PCB prototyping service was used to manufacture the TC008 digital biochip. A computer numerical controlled (CNC) milling machine was used to mill the metal clamping plates. The foil frames and the various supporting plastic parts were cut with a CO2 laser cutter from cast acrylic sheets. For reference, the fabricated components are shown in Figure 5.9.

5.3.7 Fluidic system supporting functionality

We designed the digital biochip to be able to interface with external devices as part of a more complex fluidic system. For instance, external pumps can be interfaced with the digital biochip through fluidic ports to carry reagents loading and offloading. Another external functionality is to allow for adding a magnetic

(a) TC008 TEG top view.

(b) TC008 TEG bottom view.

Figure 5.10: TC008 TEG concept assembly. The generated cold region is marked with blue on the electrode array.

stage under the digital biochip to support experiments with functionalized magnetic beads. For that purpose, the area under the main electrode array has been kept free of electrical contacts, so a permanent magnet can be used as discussed in Section 6.5.

On-chip cooling can be achieved by thermally interfacing a thermoelectric generator (TEG) on the backside of the digital biochip. A distinct characteristic of the TEGs is that they operate as heat pumps, i.e., when power is applied, they transfer heat from a cold to a hot side and create a temperature difference. The cold side of a TEG can be coupled to the bottom side of TC008, thus effectively creating a cold temperature region. For efficient operation, the hot side of a TEG needs to be actively cooled. The design of TC008 allows for attaching a thermoelectric generator under the array of electrodes and guiding and dissipating excessive heat from the hot side using an external heatsink, as shown in Figure 5.10.

5.3.8 Fluidic sytstem summary

Throughout Section 5.3, we have discussed the design objectives and the key characteristics and the design decisions taken on the course of designing the TC008 digital biochip. The conventional PCB fabrication process was chosen as a fabrication method for the digital biochip due to the multilayer capabilities, features' size, and affordable cost. Considering the physical system modularity and the PCB characteristics, we have presented the design of TC008 with external dimensions of 4U/4U, the main array of 640 control electrode, 2×5 reservoirs, and 36 embedded individual heaters that can be configured in 8 indi-

vidual heating regions. The interfacing and clamping methods were developed and illustrated to support the control electrode and heaters' connections. A replaceable foil frame-based chip coating approach was designed to fit with the modular platform concept. We conclude the fluidic system design with a brief discussion on potential sensor integration and expanding the fluidic system with off-chip cooling capabilities. Testing of the digital biochip is carried out in Chapter 6, where the unique characteristics of the TC008 are demonstrated in the context of practical experiments.

5.4 The instrumentation system

The instrumentation system is the link between the cyber and the fluidic component of the platform, and its primary purpose is to provide a reconfigurable and evolvable approach to digital microfluidics instrumentation. It is designed in a modular manner, and it manages the instrumentation needs of the fluidic system by control, feedback, and supply instrumentation modules. The modular platform-based design approach discussed in Chapter 4.3.4 advocates for a loosely coupled hierarchical embedded system that provides a framework for meeting the reconfigurability and evolvability goals. We further divide the instrumentation system into two parts - a base control system and a reconfigurable instrumentation subsystem, as shown in Figure 5.11. We recognize our main contribution to applying the modularity concepts to the digital microfluidics instrumentation and thus engineering a system capable of adjusting to the uncertainties of the fluidic part. The design objectives and engineering considerations on module and system level are discussed below.

5.4.1 Design objectives

The instrumentation system is the link between the virtual system and the physical environment, and this reflects the design objectives and the overall system architecture. A clear example are the variations and uncertainties of the fluidic system, and how they translate into the reconfiguration and evolvability requirements of the instrumentation system. Namely, from the application standpoint, the TC008 can be used for enzymatic or PCR reactions, and while the enzymatic reactions can be performed at room temperature, the PCR requires multiple heating zones. The needs of the different experimental setups can be satisfied by reconfiguring the instrumentation subsystem, thus built a particular system instance.

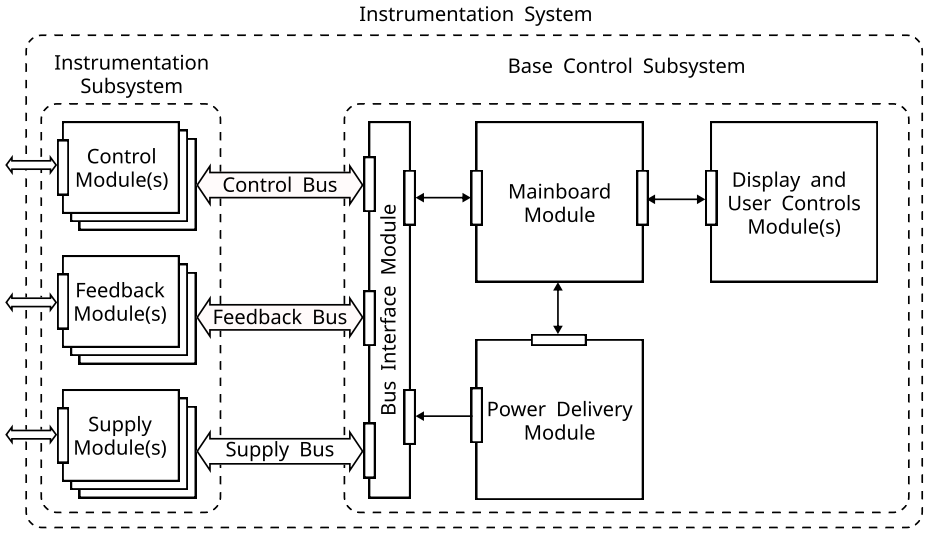

Figure 5.11: Instrumentation system architecture. The instrumentation system is split into a base control subsystem, consisting of a mainboard, bus interface, display and user control modules, and instrumentation subsystem composed of instrumentation modules.

Throughout the instrumentation system, we aim for one-to-one functionality to module mapping. This approach inevitably introduces interfacing overhead, but it provides a clear separation between modules' functionality and favors modularity. Furthermore, the reconfiguration allows for complexity and cost optimization while potentially it avoids conflicting system requirements.

Another primary design objective is related to ease of use, e.g., the modularity should not compromise the user experience by demanding configuration requirements. Therefore, we aim to design for plug-and-play functionality covering the full system chain from the path to the external controller. The instrumentation system should be capable of identifying as many attached fluidic components as possible and provide the information to an external virtual system or controller.

Since the digital biochips are inherently portable due to their dimensions in the centimeter range, preserving the overall system portability is of high importance considering potential operation in a remote setting. The portability design objective also calls for a flexible connection option to a portable system controller, e.g., a smartphone, tablet, or a portable computer.

In summary, the design objectives for the instrumentation system are:

- Reconfigurable and evolvable instrumentation subsystem.
- One-to-one mapping between an instrumentation need and instrumentation module functionality.
- Plug-and-play instrumentation module functionality.
- Ease of operation.
- Portable and battery-powered operation.
- Allow for connection to an external virtual system(s) serving the controller purpose.

5.4.2 Instrumentation system instance

While the base control system functionality is somewhat defined, the instrumentation subsystem functionality is directly affected by the instrumentation needs of the fluidic part. Nevertheless, considering that the cyber-fluidic platform is targeted towards digital microfluidics, we can derive a minimal system instance for both the base and the instrumentation subsystems. For the base system, the minimum configuration will consist of a mainboard, power delivery, bus interface, display and user controls modules, where the names of the modules are indicative of their function (see Figure 5.11). The minimal configuration of the instrumentation subsystem should be able to meet the needs of a basic EWOD droplet actuator, namely to provide control voltage and multiplex it to the control electrodes. Therefore, the minimal configuration of the instrumentation subsystem consists of a high voltage power supply and electrode driver modules. These six modules, namely, a mainboard, power delivery, bus interface, display and user controls, high voltage power supply, and electrode drivers, compose the minimal instrumentation system instance.

Since we aim to demonstrate the capabilities of the instrumentation platform with PCR and enzymatic reactions, we need to be able to create a system instance for each of these applications. The TC008 design presented in Section 5.3.3 already includes embedded heaters for forming the temperature zones required for performing PCR. Nevertheless, for proper operation, we need to create a heaters control module and a temperature calibration system to study the thermal response of the digital biochip as a unit. The enzymatic reactions will be using functionalized magnetic beads, which require a magnetic stage to keep the beads stationary for extraction.

The rest of Section 5.4 presents eight modules of the instrumentation system that were designed, built, and tested throughout this thesis work. Besides those

required by the base control subsystem, the development of the instrumentation modules was prioritized first to meet the needs for a minimal system instance for interfacing with the TC008 digital biochip, and then followed by the function-specific modules required to make the system fit for the two target applications. The following modules will be discussed next:

- The mainboard module performs communicational and processing tasks, and it is discussed in Section 5.4.3.
- The bus interface module serves the purpose of a physical isolation layer between the mainboard and the instrumentation modules, and it is further described in Section 5.4.4
- The power delivery module is responsible for providing the power supply to all system modules, as further described in Section 5.4.5.
- The display and user controls are discussed as part of Section 5.4.3 and 5.4.6.
- The high voltage power supply module is discussed in Section 5.4.8.
- The electrodes driver module interfaces with the digital biochip and provides control signals to the droplet activation electrodes, as described in Section 5.4.9.
- The heaters controller module is responsible for instrumenting the TC008 embedded heaters, and it is outlined in Section 5.4.11.
- The temperature sensors interface module is used as a thermal profiling and calibration tool, and it is discussed in Section 5.4.12.
- The MCU and prototyping modules are two separate PCBs intended to be used as prototyping tools aiding the instrumentation modules development. The modules are further described in Section 5.4.7.

The list of modules will grow together with the instrumentation needs of the fluid system. For instance, if electrochemical or impedance biosensors become integrated on the digital biochip, correspondingly, potentiostatic and impedance measurement systems can be implemented as independent modules. We recognize the architecting of the modular system as a major contribution of this thesis work. Moreover, all system modules have been conceptually developed, engineered, built, and tested in the timeframe of the project. While some modules are considered straightforward engineering work, a certain level of unique design is attributed to the electrodes driver and the high voltage power supply modules, and a degree of innovation (detailed in Section 1.7 NoI 2) for the heaters control and temperature sensor interface modules.

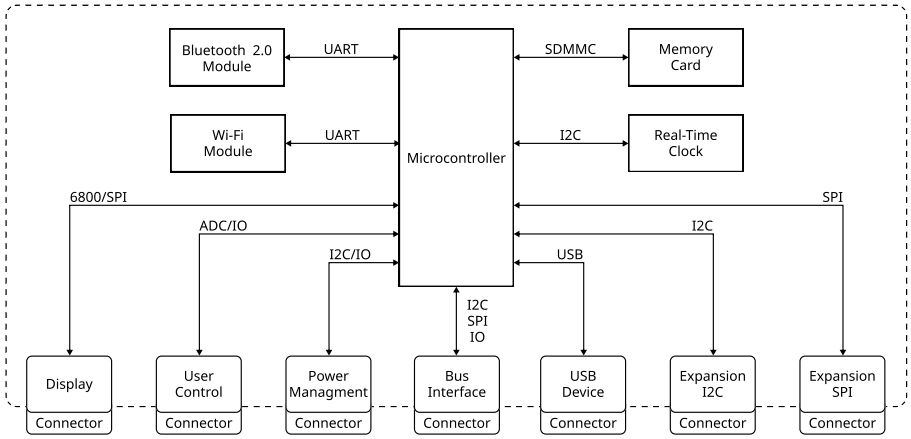

Figure 5.12: Mainboard block diagram. The external device connectors are shown at the bottom part of the diagram.

5.4.3 The mainboard

The mainboard is a central component of the instrumentation system, and it carries the communication between the instrumentation modules and the virtual system. The mainboard is similar to the computer motherboard by containing various subsystems such as communication, computation, storage, user interface, etc., as well as it allows external devices to be connected. In respect to the mainboard, the plugin devices are the instrumentation bus interface, graphical display, user interface controls, external storage memory card, and the power delivery system. The design focuses on striking a balance of a capable, compact, and features-rich, but power-efficient embedded system fitting into the 4U/4U form factor.

A block diagram of the mainboard is shown in Figure 5.12. The design is based on a microcontroller communicating through serial and parallel interfaces with peripheral devices and subsystems. Communication with an external controller can be established through a wireless link such as Bluetooth or Wi-Fi or a wired USB connection. Onboard low-power real-time clock is used for accurate timekeeping, e.g., timestamping data or measuring long time periods. A memory card slot is added to allow long-term data storage to enable the instrumentation system to function autonomously if required.

The bottom part of Figure 5.12 shows the interfaces to external devices that can be connected to the mainboard. From left to right, the first two are related to the instrumentation system local user interface - an interface to a touch screen

graphical display module and hardware user controls. The next connection is to a power delivery module, and it is intended for monitoring and controlling the platform's power distribution. The power delivery module has been partially prototyped, and it is further discussed in Section 5.4.5. The bus interface connector implements a set of signals meant to connect to the bus interface module, which is addressed in Section 5.4.4. The mainboard is designed to work as a USB device for host communication and firmware updates. The last two connectors expose I2C (Inter-Integrated Circuit) and SPI (Serial Peripheral Interface) serial interfaces with the sole purpose of future-proofing the mainboard aiding the potential addition of new functionality.

The onboard peripherals and plugin subsystems are designed to match the initially intended functionality as well as to allow for potential future expansions. Possible limiting factors are the bandwidth of the wireless communication modules, the serial and parallel interfaces, or the microcontroller's computation capabilities. However, the communication interfaces can achieve over 1Mbps, which is considered sufficient for passing commands and data. The effect of communication latency and jitter were deemed to be neglectable based on the experience with the predecessor systems.

The microcontroller capabilities are critical for the overall system performance. A large number of IO pins and communication peripherals are required to connect with onboard devices and plugin subsystems. The use of a display, user controls, and many communication channels naturally calls for a graphical library and embedded real-time operating system. Correspondingly, this increases the program's required footprint and working memory even without considering the application logic. The predecessor systems were based on an ARM Cortex M4 (Tiva TM4C123) microcontroller running at 80MHz and delivering 100 DMIPS, with 64KB program memory and 24KB RAM. Even though the performance was sufficient, there was a lack of IO - the microcontroller offered 43 IO pins, which were not enough to fulfill the interfacing need of the envisioned instrumentation system. Considering the added complexity in comparison with the predecessor system, we have switched to a more powerful ARM Cortex M7 (STM32F767ZIT6) microcontroller running at 216MHz and delivering 462 DMIPS, with 2MB program memory, 512KB RAM, and 114 IO pins. The microcontroller and the associated toolchain were first tested in the pilot system (Appendix B). As a result of this test, the STM32 microcontroller and ecosystem were chosen to be used throughout the microfluidics platform. Deciding factors were the wide range of microcontroller configurations, extensive peripheral libraries, and integrated configuration and development environment.

A Bluetooth 2.0 module (HC-05) and a ESP32 Wi-Fi module (ESP-WROOM-32) are connected to the microcontroller through two independent universal asynchronous receiver-transmitter (UART) together with status signals. The

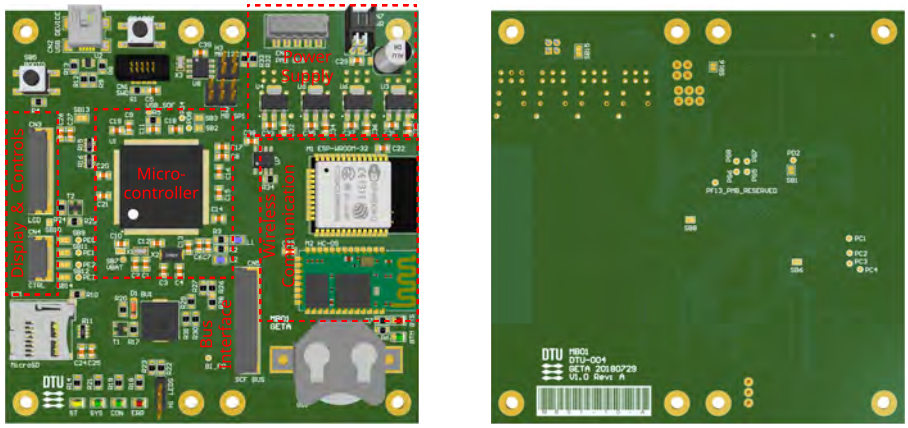

(a) Mainboard top view. **(b)** Mainbaord bottom view.

Figure 5.13: Mainboard design visualization. A high-resolution version is available in the digital copy.

two different wireless communication interfaces allow for external controllers to be connected to the instrumentation system.

From an engineering perspective, the mainboard is an entirely digital design, and it was created as a 4-layer PCB. The board was fabricated by a PCB prototyping service, and it was assembled, tested, and programmed in house. A visualization of the mainboard is shown in Figure 5.13, where the main components are marked with red. The mounting hole pattern allows for stacking with other 2U/4U or 4U/4U boards, and it is demonstrated as an assembled system with the bus interface module, power supply module, and the display module, as discussed in Section 5.4.6. The components and connectors placement was chosen to fit the stacked design.

5.4.4 The bus interface

The bus interface links the mainboard with the instrumentation modules, and it is tailored to the needs of the cyber-fluidic platform. The bus interface module implements the physical layer of the interface, namely to electrically isolate the mainboard from the instrumentation subsystems and to provide power to the attached modules.

The supply, control, and feedback busses are electrically decoupled from each other by the use of digital isolators and isolated power supplies, as shown in

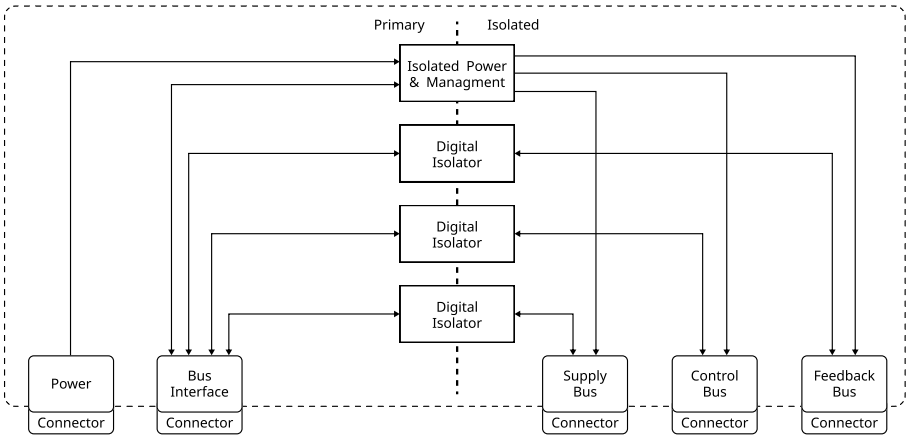

Figure 5.14: Bus interface block diagram.

Figure 5.14. The power supply of each instrumentation bus can be toggled and monitored through individual enable and power good signals, allowing for load control, monitoring, and detecting overload or power failure conditions. Tracking the power delivery is particularly important in the context of plug-and-play instrumentation subsystem since the power budget of each bus can be exceeded by the connected subsystems. Nonetheless, to mitigate the potential risk of power delivery being a limiting factor, an external power injection concept is discussed later in the section.

The bus interface signals with respect to the supply, control, and feedback buses are shown in Figure 5.15. The first column lists the names of all logical and power lines. The "X" signs indicate which signals and power lines are composing the three bus interfaces. The "X" sign also denotes the number of physical wires used for the connection. The use of multiple wires for power delivery is aligned with the estimated power requirements for each bus interface. For instance, the supply and control modules are likely to require more power than the feedback modules, due to the potential use of power-demanding components such as heaters, thermoelectric coolers, electromagnetic pumps, and valves.

The set of signals shown in Figure 5.15 is used for communication between the mainboard and the supply, control, and feedback modules. Each bus consists of an independent set of signals for implementing bus level control and securing the bandwidth. The SDA and SCL signals are a part of the standard I2C protocol, and the MOSI, MISO, and CLK are a part of the conventional SPI communication. The INT signal is an open-drain signal allowing modules to request attention by sending an interrupt request to the mainboard. The BUSY

Signal Name	Signal Type	Supply Bus	Control Bus	Feedback Bus	Description
SDA	In/Out	X	X	X	I2C serial data
SCL	Out	X	X	X	I2c serial clockSCL
INT	In	X	X	X	Bus module interupt request out
BUSY	In	X	X	X	Bus module busy out
SYNC	Out	X	X	X	Bus module synchonize input
HOLD	Out	X	X	X	Bus module hold input
ENUM	In/Out	X	X	X	Bus module enumeration in/out
MOSI	Out			X	SPI master data out
MISO	In			X	SPI master data in
CLK	Out			X	SPI clock
VLOGIC	Power	XXX	XX	X	Bus module 5V power supply
VBUS	Power	XXX	XX	X	Bus module 12V power supply
GND	Power	XXX	XX	XX	Bus module power ground

Figure 5.15: Bus interface signals. The "X" denotes the number of wires used in a bus connector.

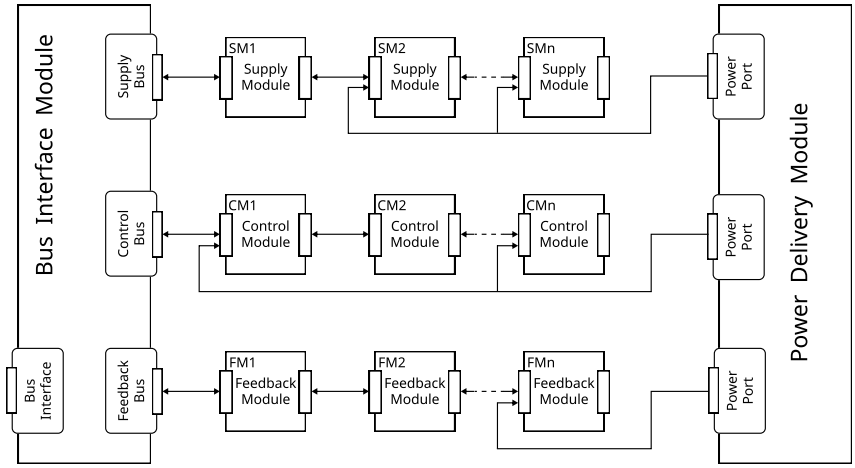

Figure 5.16: Instrumentation module connection and external power delivery.

signal is an open-drain output of each module, and as the name implies this signal indicates whether a module is in a ready or busy state. It is enough for one module to indicate a busy state to halt the bus communication. The SYNC signal is a synchronization output from the mainboard, which allows synchronous operations to be triggered among the instrumentation system. The HOLD functionality is similar to the SYNC since it enables the mainboard to halt all ongoing processes in the attached instrumentation modules. The ENUM

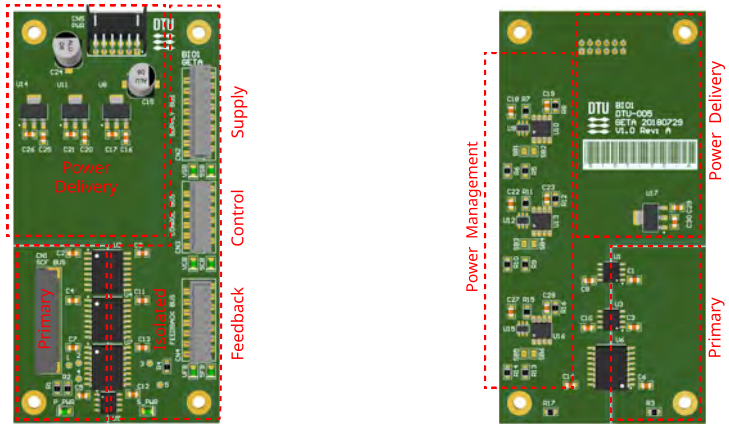

(a) Bus interface top view.

(b) Bus interface bottom view.

Figure 5.17: Bus Interface design visualization. A high-resolution version is available in the digital copy.

is the only daisy-chained signal, and it is used for module initialization and addressing. This signal allows the mainboard to recognize and assign addresses corresponding to the module's location on the corresponding bus.

Instrumentation modules are designed to have input and output connectors, thus allowing daisy-chain connection, which optimizes the number and the length of the used wires. The supply, control, and feedback buses use connectors with correspondingly 16, 12, and 14 contacts, which prevents incorrect attachment. The connection scheme is shown in Figure 5.16 along with a technique to provide auxiliary power supply if the power requirements of the module exceeds the energy budget of the bus. Extra power is delivered from separated ports of the power delivery module only to the modules that require it.

The bus interface module is designed as a 4-layer PCB, and it is shown in Figure 5.17. The module is intended to be mounted on top of the mainboard, thus minimizing the footprint and wiring of the system. The supply, control, and feedback bus connectors are placed on the right edge of the board, allowing for easy access.

5.4.5 The power delivery module

The power delivery module is designed to deliver the multiple power domains required by the mainboard, the bus interface, and the instrumentation modules.

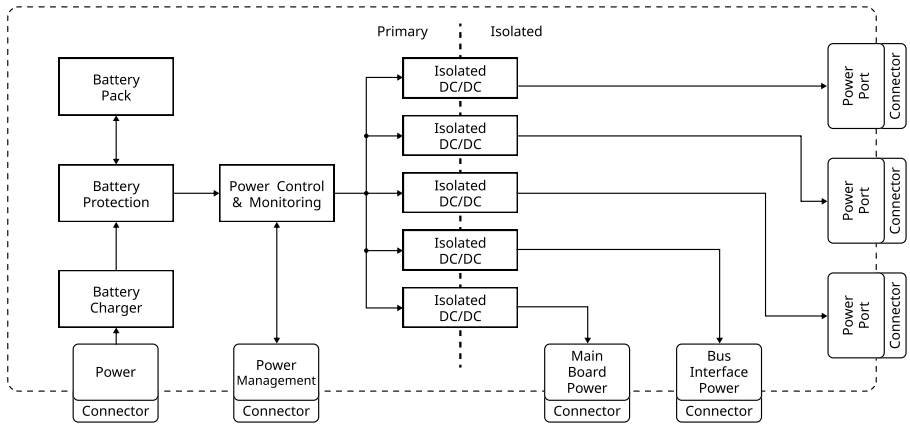

Figure 5.18: Power delivery module block diagram.

To meet the system portability design objective, the module is designed to operate from a battery pack. A block diagram is shown in Figure 5.18, which shows that the module is separated into a primary and secondary isolated part. The battery pack, charger, protection, power control and monitoring are located on the primary side and are responsible for supplying the flyback DC/DC (direct current to direct current) power converters. Each DC/DC power converter provides isolated voltage rails to the mainboard, bus interface module, and to the auxiliary power ports. The mainboard can control and monitor the power distribution through the power management port. This allows functionality such as battery charge level monitoring and power usage optimization.

The power delivery module has been prototyped on a 4U/4U solderable breadboard designed to fit under the mainboard. It is based on three LiIon batteries connecting in series, forming a battery pack with a capacity of 24Wh. Depending on the configuration and operation mode of the system, the current battery pack allows for up to a few hours of autonomous operation for the minimal instrumentation system instance presented in Section 5.4.10. However, the average required power for sustaining the temperature of the three heating zones for the space domain PCR experiment (see Section 6.4.1) was measured to be in the range of 6-8W. However, heaters' power consumption is closely related to the generated temperature profile; hence the system needs to be profiled and the battery capacity adjusted according to the particular application.

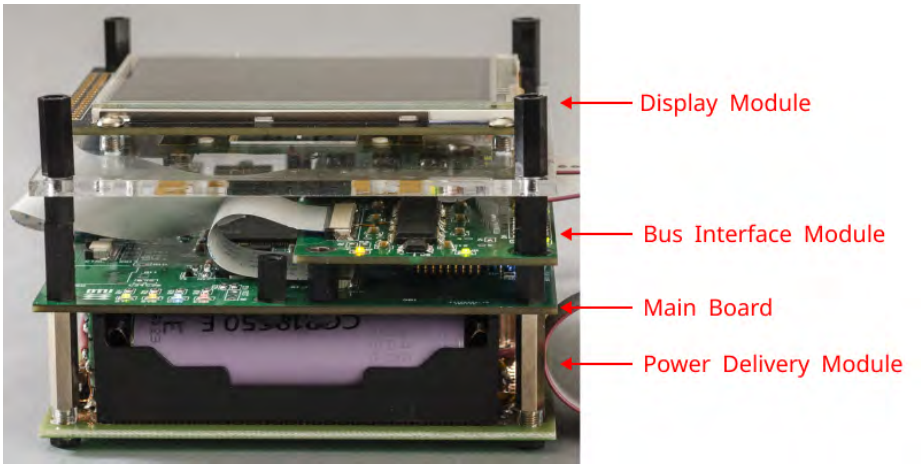

Figure 5.19: The base control subsystem configuration consisting of power delivery, mainboard, bus interface, and optional display modules. The modules are stacked together as they comply with the unit size mounting hole placement.

5.4.6 The base control subsystem

The base control subsystem consists of a mainboard, bus interface module, power delivery module, and an optional display module. This combination of modules does not have any instrumentation capabilities, but it is equipped for communication with an external controller and ready to accept instrumentation modules. The base system assembly is shown in Figure 5.19, where the modules are stacked together to form the subsystem. The mainboard and bus interface modules are built as final devices on professionally fabricated PCB, while the power delivery and the display modules are prototyped on universal boards. Complying with the unit module size allows for the compact assembly shown in the figure.

5.4.7 The MCU and prototyping modules

The supply, control, and feedback instrumentation modules are designed around an ARM Cortex M4 (STM32F405RG) microcontroller running at 168MHz and delivering 210DMIPS, with 1MB program memory, 192KB RAM, and 51 IO pins. This microcontroller is in the same ecosystem as the one used for the mainboard, thus streamlining the development process. The microcontroller

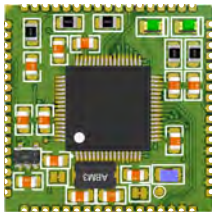

(a) MCU module top view.

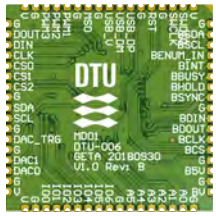

(b) MCU module bottom view.

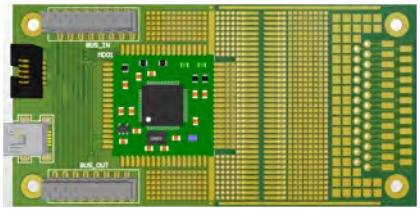

(c) Prototyping board top view.

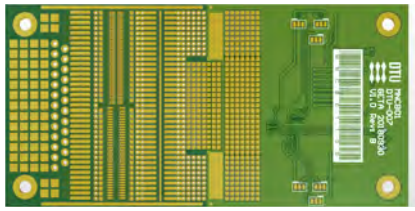

(d) Prototyping board bottom view.

Figure 5.20: MCU module and MCU prototyping board. The MCU module is designed as a 1U/1U universal instrumentation microcontroller board.

has a wide variety of peripherals such: 2.4 MSPS 12-bit analog to digital converters (ADC), 12-bit digital to analog converters (DAC); a number of serial interfaces I2C, SPI, UART; general-purpose direct memory access controllers (DMA); configurable timers, etc. The selected microcontroller is a capable peripheral rich device that provides analog and digital processing capabilities, to facilitate the development of different instrumentation systems.

A 4 layer MCU carrier board with size 1U/1U has been designed to standardize the microcontroller IO layout, contain the power and clock circuitry and streamline the development process. The MCU module is designed to simplify the connection with the bus interfaces, group and reroute the microcontroller interfaces into a consistent layout. The MCU module is shown in Figure 5.20a, and the signal arrangement can be seen in Figure 5.20b as labels on the bottom side of the PCB. The bus interface signals are located on the right side of the design shown in Figure 5.20b, and the other three edges are occupied with three timer outputs (PWM1, PWM2, and PWM3), SPI, I2C, two DAC outputs, seven general-purpose IOs, and six ADC channels.

A prototyping carrier PCB for the MCU module is shown in Figure 5.20c and 5.20d. The board is designed to work with the MCU module and connect the supply, control, or feedback bus based on the soldered connector type. The board is designed on two layers with a 2U/4U size and offers a prototyping area

adapted to fit various surface-mounted component packages. The combination of the MCU module and the prototyping board allows for fast assembling and testing new instrumentation modules, and it has been used heavily throughout the development phase of the instrumentation modules. For instance, the prototyping board was used not only to test subsystems but also to build fully functional prototypes as in the case with the high voltage power supply module presented in the next section or the heaters controller presented in Section 5.4.11.

5.4.8 The high voltage power supply module

Digital microfluidics is associated with electrode control voltages in the range of tens to hundreds of volts depending on the dielectric properties of the coating layer [124] [45]. A commonly used actuation voltage is in the range of 80-200 V on a dielectric layer with a thickness in the range of 5-10 µm [14]. Using an actuation voltage higher than 300 V poses scalability challenges due to the lack of integrated arrays of high-voltage switches capable of withstanding such high voltage potentials. Moreover, it has been demonstrated that an upper limit of 300 V is sufficient for a wide range of isolation layer thicknesses [14].

The high voltage power supply module is designed to take the available battery power and convert it to a sufficiently high voltage to drive the digital biochip control electrode. Since a design objective of the instrumentation platform is to be able to adapt to the needs of the fluidic path, the high-voltage power supply should provide a variable output voltage in a wide range. In general, a variable output voltage is needed to tune the droplet actuation response, based on the thickness of the isolation layer, the surface properties, the composition of the actuated fluid, and other related environmental parameters such as the presence of filler fluid, its viscosity, temperature, etc. Furthermore, the actuation voltage is responsible for the velocity saturation phenomenon characterized by the counterintuitive fact that increasing the actuation voltage leads to decreased droplet actuation fidelity and contact line distortion [79] [91]. Consequently, there is an optimal voltage actuation window correlated with digital biochip construction and operation conditions. The lower value is often found empirically by increasing the actuation voltage until achieving reliable droplet actuation, and the upper limit is marked by the saturation in maximum transport speed.

The design objectives for the high-voltage power supply were set to design a software-controlled isolated boost converter that can operate from input voltage in the range of 3-20 V, and provide regulated output in the range of 30-300 V, have adjustable output current limiting, low output voltage ripple $\leq$100 mV, monitoring of the output voltage and current, and output enable control. Based

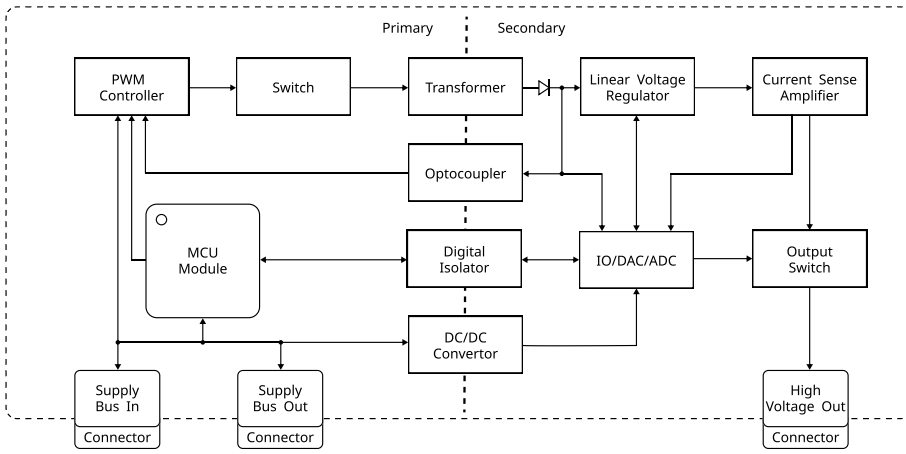

Figure 5.21: Power delivery module block diagram.

on the experience gained from the predecessor systems, designing a boost converter that operates with a wide range of input voltage and produces output with an even greater scale is not a trivial design task especially meeting the low-output ripple requirement. Therefore, a hybrid two-stage power supply, where the first stage is constructed as a flyback converter and followed by a second linear voltage regulator, was chosen as the optimal design approach. This design was inspired by an application note [125] and further developed to match the design objectives for control and monitoring.

The block diagram of the high voltage power supply is shown in Figure 5.21. It is designed to be interfaced with the supply bus, and it is built as an isolated step-up flyback converter. A core component of the flyback converter is a pulse width modulated (PWM) oscillator running at 100kHz and control circuitry to drive a high power semiconductor switch. The control circuit receives a signal for the output voltage from the secondary side through an optocoupler isolator. The secondary output of the transformer is rectified and fed into a linear voltage regulator to minimize the noise and voltage ripple from the flyback converter. To optimize power efficiency, the output of the flyback converter is set to output 15 volts higher than the desired voltage. This allows for sufficient dropout voltage over the linear regulator and prevents excessive power dissipation.

An MCU module at the primary side is connected to the supply bus. The module controls and monitors the secondary side through a digital isolator to the IO, DAC, and ADC channels on the secondary side of the power supply. The output voltage can be set and monitored along with the output current. Observing the output current provides information for the operation of the supplied

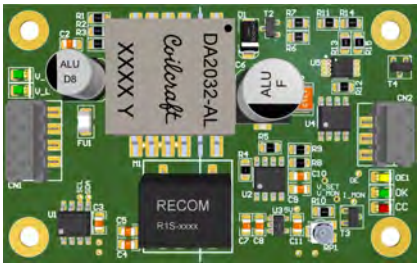

(a) High voltage power supply module top view.

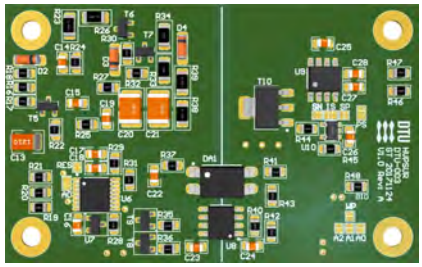

(b) High voltage power supply module bottom view.

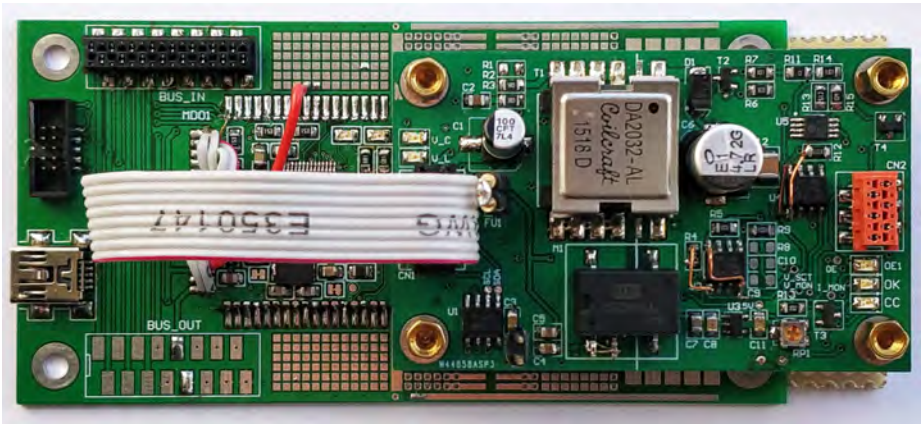

(c) High voltage power supply module prototype top view.

Figure 5.22: High voltage power supply module design and prototype. The prototype is based on the MCU prototyping module described in Section 5.4.7 with the high voltage power supply added on the top of the prototyping area.

system, e.g., allows for the detection of a potential breakdown of the insulation coating of the digital biochip. A current limiting function is implemented, and it protects not only the attached circuitry but also the system operator from an eventual electric shock. The isolation between the primary and secondary sides complicates the design, but in return, it adds another layer of protection and decoupling of the instrumentation system.

The high voltage power supply is a mixed-signal design and the flyback circuitry, the linear output regulator, and the feedback loops have been modeled and simulated using electronic simulation software packages. The power supply design was then partially prototyped to verify the performance of the circuitry

under real operation conditions. After successful testing, a second functional prototype was built on a two-layer PCB as a part of the pilot system testing, as described in Appendix B. The second porotype was only intended as a design evaluation, and therefore, it was not compliant with the unit size form factor and the platform-based bus interfacing, since another redesign was planned. However, regardless of the intention for redesign, due to time and resource constraints, the high voltage power supply board remained in version two, and it was extended on the top of an MCU and prototyping module, as shown in Figure 5.22c.

5.4.9 The electrodes driver module

The electrodes driver module takes the output of the high voltage power supply and delivers it to the actuation electrodes on the digital biochip. One of the design objectives for this module was to implement a large array of individually controlled high voltage switches to provide a one-to-one mapping between the control switches and the TC008 electrodes, e.g., each control electrode is connected to a separate driving channel. Such a mapping scheme delivers the most flexible programmable approach since each control electrode can be individually addressed.

The planning of the electrode drivers was carried out in parallel with the design of TC008 as an iterative process attempting to map the design objectives discussed in Chapter 4.3.2 to a feasible engineering solution. Numerous multi-dimensional considerations including the number of control channels, interfacing between the electrode drivers and the digital biochip, layout and form factor, PCB technology capabilities, mechanical assembly, etc., were evaluated in search of a feasible and balanced design. A significant part of the design process was a subjective evaluation of factors considering the project time frame, available technologies, fabrication capabilities, scalability, future-proof, usability, and reliability aspects.

The block diagram of the electrodes driver module is shown in Figure 5.23a, where it can be seen that the electrode driving circuit is split into two groups, and it is implemented by six high voltage serial-to-parallel converters [126]. Each converter is a separate integrated circuit consisting of a 64-bit logic level shift register connected to an array of output latches. The latching circuit outputs are coupled to 64 push-pull drivers rated for operating with up to 300V. This configuration provides the functionality of a logic level input to a high voltage output shift register suitable for interfacing with the MCU module. The push-pull output configuration of the drivers allows for directly driving control electrodes. Using six of these integrated circuits per module, 384 electrode

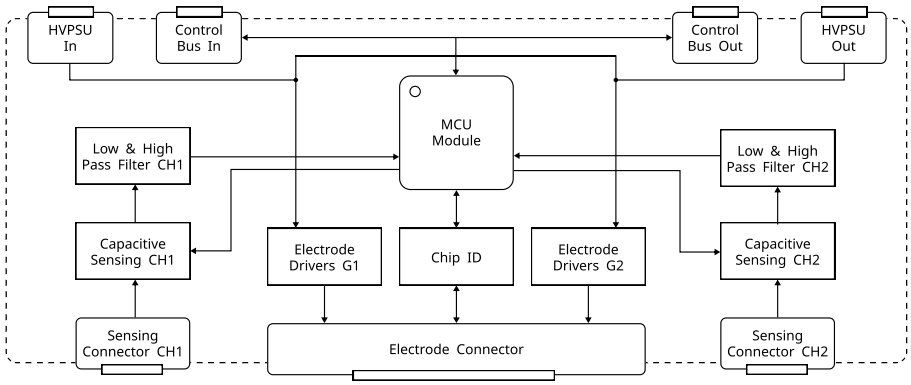

(a) Electrodes driver block diagram.

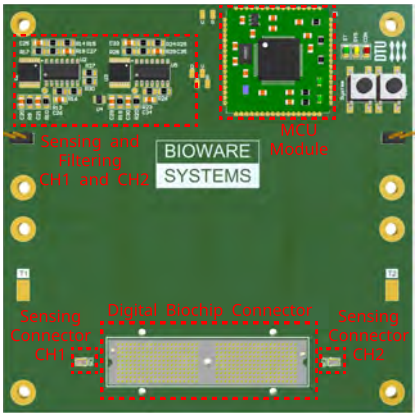

(b) Electrodes driver module top view.

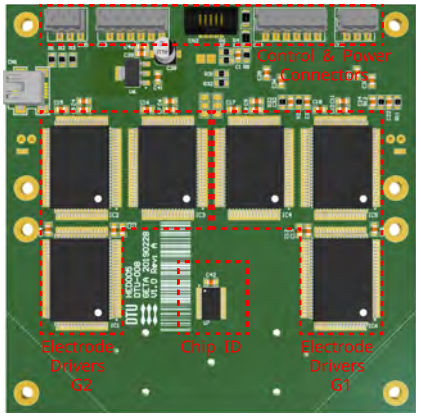

(c) Electrodes driver module bottom view.

Figure 5.23: Electrodes driver module block diagram and design visualization. A high-resolution version is available in the digital copy.

driving channels can be built into a single driver module. A TC008 has two 400 pads connection areas that can interface with electrodes driving modules allowing up to 768 control electrodes.

The electrodes driver module is based on the MCU module, and it connects to the control bus, where the MCU module is responsible for receiving electrode actuation sequence commands from the mainboard, processing them, and sending data to the electrode driver circuits. Data can be clocked to the shift register at 8MHz, which potentially allows for full array updates in the range of 50 µs. The

electrode driver module is also capacitive sensing ready, including two software-configurable trans-impedance amplifiers followed by tunable low and high pass filters. The capacitive sensing implementation was inspired by previously published work [79] [64] [65] [62] and further extended to two channels to provide quicker array scanning. The electrodes control voltage is provided by the high voltage power supply module through a separate power connector.

The electrodes driver module is designed to be daisy-chained, allowing for extending the capabilities of the control subsystem. The module size is 4U/4U, and it is built as a 6 layer PCB board to allow for routing the 400 pin connector to the TC008. Two electrodes driver modules are required to interface with TC008, where the connection between the driver board and the digital biochip is established through 1U wide overlapping and two spring-loaded connectors. A machined aluminum base plate and polycarbonate spacer were fabricated to support the electrode driver boards and the TC008 assembly. An exploded view of the construction is shown in Figure 5.24.

5.4.10 The minimal instrumentation system instance

The minimal instrumentation system instance capable of actuating droplets on a digital biochip is shown in Figure 5.25. The instance consists of the base control subsystem, a high voltage power supply module attached to the supply bus, two daisy-chained electrodes driver modules attached to the control bus, a TC008 digital biochip, and a supporting mechanical fixture. Even though we call this module arrangement a minimal system configuration, it forms a hierarchical embedded system capable of receiving commands from an external controller and actuating droplets on the digital biochip. Droplet transport, merging, mixing, dispensing, and splitting is supported at this system configuration. Furthermore, the digital biochip can be configured in an open or closed configuration allowing for fluidic experimental work to be carried out. For example, this instance of the platform is capable of performing enzymatic reactions.

The PCR requires extending the instrumentation subsystem with an extra module for providing heaters control. The evolvability of the modular design approach becomes evident, not only on a system design level but also from the application perspective. We see the ability to add the heaters control module to the minimal instrumentation system and make the system fit for performing PCR, as a clear demonstration of the flexibility gained from the modular instrumentation design. We recognize the use of modularity in the fluidic and instrumentation parts of the cyber-fluidic architecture as a vital design feature that allows for evolution and effectively extends the system lifecycle.

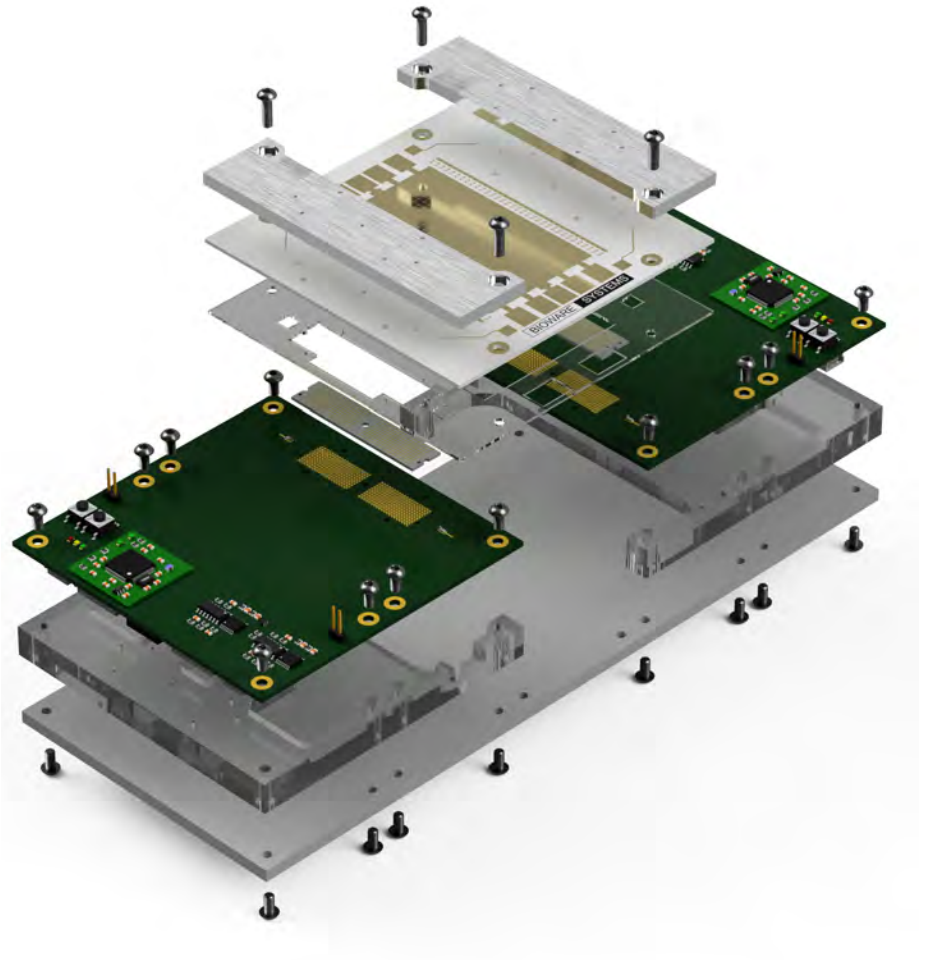

Figure 5.24: An exploded view of two electrode driver modules and TC008 assembly. The assembly consists of a rigid base plate for mounting the electrodes driver module spacers. The driver PCBs are bolted on the top of the spacer and accommodate the spring-loaded connectors. The connectors are aligned and held in place by a spacer plate. TC008 is clamped down on top of the driver boards with the use of the compression plates. The complete assembly is with 4U/10U size and height <1U. A high-resolution version is available in the digital copy.

Figure 5.25: The minimum instrumentation system instance. Droplets can be seen placed on the surface of the open digital biochip.

5.4.11 The heaters controller module

A test use case for the digital microfluidic platform is to perform a PCR that requires elevated temperatures. To accommodate for this use case, TC008 implements an array of embedded reconfigurable meander copper structures, as discussed in Section 5.3.3.3. The copper structures form resistive tracks, which can be used both for heating elements as well as for temperature sensing. Measuring the resistance of a resistive track provides information for the temperature due to the 0.00393% per 1 °C positive temperature coefficient of copper. The temperature coefficient appears to be relatively low, but it can produce significant resistance variation in copper structures with a low-cross section and a considerable length. For instance, a PCB track with 89 µm width, 17.5 µm thickness, and 100 mm length has a resistance of 1.07 Ω at 20 °C. However, the same copper track has a 1.41 Ω resistance at 100 °C which is an increase of 0.34 Ω over the 80 °C span or 4.25 mΩ °C^{-1}.

The power delivery of a resistive heater is governed by the Ohm's Law, where the produced heat is proportional to the current passing through the copper wire. A given power level can be achieved by altering the heater resistance and the applied voltage, e.g., 10 W of dissipated heat can be produced by a 0.1 Ω heater with applied 1 V or by a 10 Ω heater supplied with 10 V. Correspondingly, the current flowing through the 0.1 Ω heater will be 10 A and 1 A for the 10 Ω heater. Although the power remains the same, the current demands are significantly different. Instrumentation challenges quickly escalate in the case of multiple heaters requiring 10 A, particularly the driving electronics, and power delivery to the heaters becomes bulky and difficult to construct. On the contrary, the higher heater resistance requires less current on the cost of increased supply

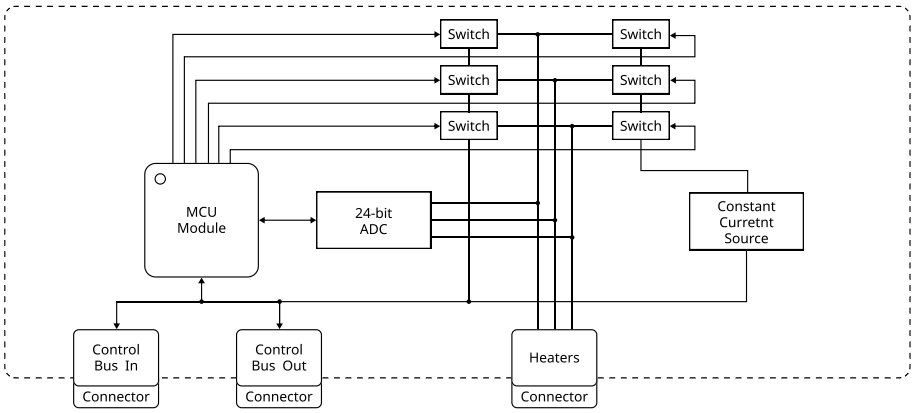

Figure 5.26: Heaters control module block diagram.

voltage, which is, in general, a straightforward engineering task. The higher initial resistance also produces proportionally greater resistance deviation in response to a change of temperature, thus relaxing the requirements to the temperature measuring circuit.

The TC008 heaters are designed as meanders to increase the length of the copper trace, as shown in Figure 5.5. Two different heater designs are present on the device. The first type spans the full height of the electrodes array, and it consists of seven straight 40 mm segments connected with arcs to form a 285 mm copper trace. The PCB fabrication capabilities determine the trace width and spacing to be 89 µm with a thickness of the inner copper layer of 17.5 µm. A single copper trace is forming a heater with a resistance of 3.05 Ω at 20 °C and correspondingly 4.02 Ω at 100 °C. The second heater type is 113.5 mm long with a resistance of 1.21 Ω at 20 °C and 1.6 Ω at 100 °C. The heaters can be connected in series to form a heating region spanning multiple electrode columns.

The heaters controller module is based on the MCU module described earlier, and it is designed to reside on the control bus. The module is intended to control up to three individual temperature zones, which suffice for meeting the thermal requirements for performing a PCR. The heaters' instrumentation circuitry is shown in Figure 5.26, and it consists of three pairs of solid-state switches, a constant current source, and a 24-bit ADC. Each heater group is connected to a pair of switches (power and sensing), allowing the heater group to be connected to power or a constant current source. The MCU module can modulate the energy sent to each heater by pulse width modulation (PWM) signals applied to the power switches. When the power switches are in an off state, the MCU module can close one of the sensing switches, allowing constant current to flow

through the connected heating zone and measure the voltage drop with the 24-bit ADC. The constant current source is set to output 100 A, hence the heating effect of the measuring current is neglectable. The measured voltage drop over the heater is turned to resistance, followed by conversion to temperature.

A four-terminal sensing method is employed to mitigate the effect of the voltage drop over the wires connecting the heaters control module and the TC008. The sensing method is also known as Kelvin sensing, and it relies on two pairs of current-carrying and voltage-sensing wires. The separation of current and voltage components effectively excludes the wire and contact resistance from the measurement, and it presents a significant advantage, particularly for accurate low-resistance measurements. The four-terminal sensing method matched with temperature stable and calibrated current source, and 24-bit ADC allows for accurate milliohm and sub-degree measurement resolution.

The heaters controller module is a mixed-signal design, and parts of the analog circuitry were simulated and optimized. The module was intended to fit the 2U/4U form factor, and it was built as a functional prototype on the MCU module prototyping board, as shown in Figure 5.27a and 5.27b. The contact between the heaters controller module and the TC008 is established through a 2U/4U sized adapter board, shown in Figure 5.27c and 5.27d, where spring-loaded compression contacts are designed to mate with the contact pads on the bottom of TC008. The bottom side of the heaters connection adapter accommodates the connector to the heaters controller module. The adapter board has a cutout area intended for access and forced cooling of the bottom side of the TC008 electrodes array. A custom polycarbonate spacer fitting under the heater connection adapter was fabricated to allow mounting the adapter board to the same height as the electrodes driver boards, as shown in Figure 5.27e.

The additional heater connection adapter board and polycarbonate spacer certainly complicate the overall design, but in return, it truly supports the modularity concept. A clear benefit is the decoupling of the heaters from the electrodes driver interfacing and functionality. The functionality decoupling allows for the instrumentation modules to be developed at a different pace and eventual redesign limited only to the affected subsystem. The decoupling also reduces the potential evolution constraints of the digital biochip design. Another essential characteristic is the maintenance of reconfigurability and evolvability. For example, the electrode adapter board and the polycarbonate spacer can be removed entirely from the assembly, thus providing unobstructed access to the TC008 electrode array's backside or allowing another 2U/4U module to be mounted instead. For example, the new module can utilize thermoelectric generators to implement off-chip heating or cooling.

The MCU module runs a closed control loop measuring the temperature of

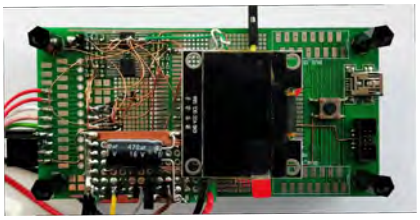

(a) Heaters controller module prototype top view.

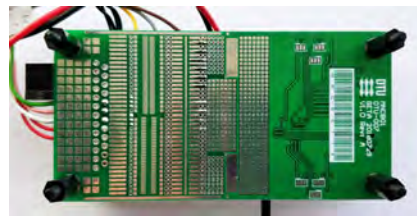

(b) Heaters controller module prototype bottom view.

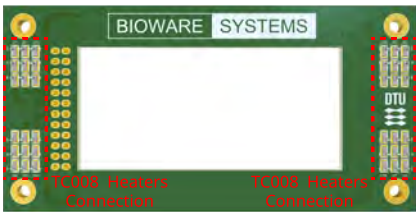

(c) Heaters connection adapter top view.

(d) Heaters connection adapter bottom view.

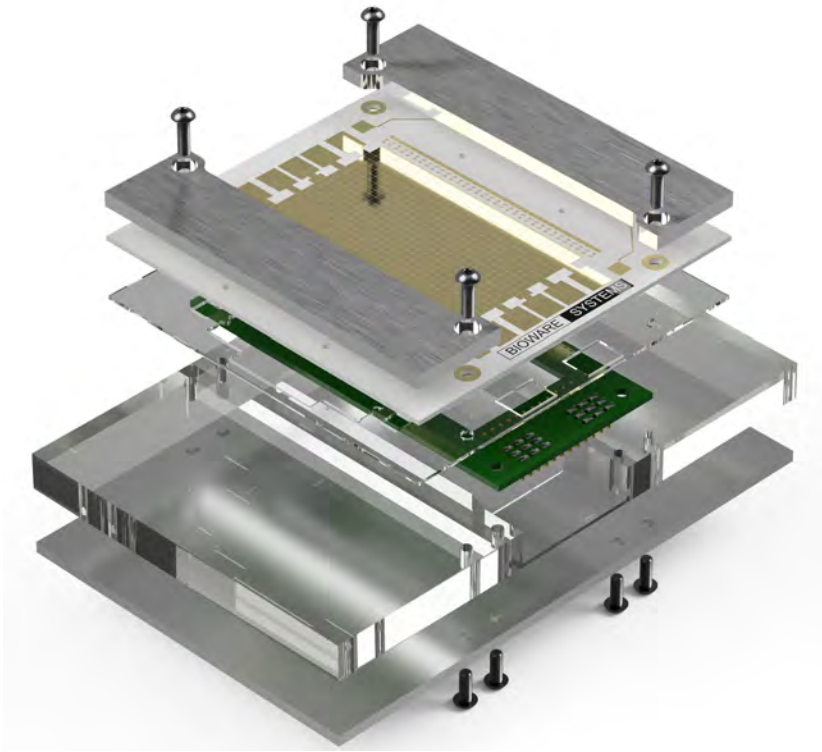

(e) TC008 heaters connection adapter assembly.

Figure 5.27: Heaters controller module prototype, connection adapter board, and exploded view of the adapter board and TC008 assembly. A high-resolution version is available in the digital copy.

each zone, comparing it to a given setpoint, and updating the output PWM signals. The control loop is based on a proportional-integral-derivative (PID) control technique that calculates the error and modulates the output power with a set rate of 50 Hz. An optimally tuned PID controller allows for fast system response and a stable operation. The module is designed to be powered by the control bus. However, if the power delivery limit of the bus is reached due to high thermal losses, the heaters controller can be auxiliary powered using the techniques described in Chapter 5.4.4. An insufficient power supply can lead to a lack of thermal capacity leading to inefficient temperature regulation.

5.4.12 The temperature sensors interface module

The heaters on the TC008 can be configured to form up to eight heating zones under the electrodes array. Although the control of each zone is individual, the temperature profile created on the digital biochip is dependent on the number of zones, their size and location, overall thermal coupling and mass, material type and geometries, environmental conditions, etc. Furthermore, thermoelectric coolers can be attached to the bottom side of the chip to form local cooling zones. This potentially creates high-temperature gradients, which are hard to model and accurately predict. In the case of a PCR experiment that requires on-chip cold storage of reagents, the digital biochip can be exposed to temperature gradients larger than 90 °C. Therefore, ensuring the intended temperature profiles on the chip requires a measuring technique resembling the actual operation configuration of the digital biochip closely.

The temperature sensors interface module is intended to serve the purpose of temperature measurement, profiling, and calibration tool. The measuring setup consists of the temperature sensors interface module and a plugin temperature sensor array. The block diagram of the module is shown in Figure 5.28, it is based on the MCU module, and it is designed to reside on the feedback bus. The temperature sensor interface module has four identical input circuits, each designed to handle up to 10 resistive negative temperature coefficient (NTC) sensors. The input configuration allows up to 40 temperature sensors to be connected and provide multi-channel temperature measurement. To reduce the design complexity, the sensors are multiplexed and measured in groups of five by the 12-bit ADC built into the MCU module or by an external 24-bit ADC. The full array can be scanned with a rate of 100 Hz, which is considered sufficient when accounting for the thermal mass and response of the TC008.

The temperature sensors array is intended to measure the temperature profile of a closed digital biochip, which poses a limit on the maximum sensor thickness to be in the range of 200-500 µm. The thickness requirement is based on the fact

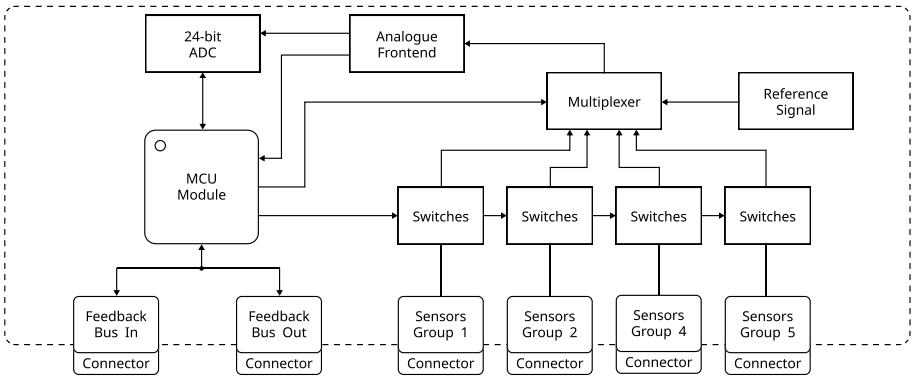

Figure 5.28: Temperature sensors interface block diagram.

that the sensors array needs to fit into the confined space between the top and the bottom plate of a digital biochip. Resistive NTC sensors with surface mount 0402 packages measuring 300×300×500 µm are readily available and appear to be a perfect match for the application. The sensors' array is designed as a flexible 130 µm thick PCB with 40 cutouts to mount the temperature sensors. This construction is shown in Figure 5.29c and 5.29d. The sensors are fit into the cutouts and soldered to symmetrically protrude on the top and bottom side of the PCB. The sensors are equally spaced and cover the full area of the TC008 electrode array, as shown in Figure 5.29e. The figure also shows that the sensors' array is designed to plug into the interface module.

The flexible sensors PCB can be used in conjunction with the foil frame coating approach presented in Chapter 5.3.4. The sensors array can be fit between the bottom foil frame, and the ITO top plate while maintaining 300 µm gap height. This setup places the sensors in close conditions to what a droplet would experience, thus providing a measurement of the actual operating environment. The multisensor configuration allows simultaneous sampling of 40 temperature points of the array and building an accurate two-dimensional heatmap in real-time.

The temperature sensors interface module was designed as a 2U/4U module on a 4-layer PCB board. The temperature array was designed as a 2-layer flexible polyimide core board with 100\100 µm track width and spacing and 17.5 µm thickness. The tracks connecting the sensors were designed to run parallel to the embedded heaters in order to minimize the effect of thermal bridging. The boards were fabricated by a commercial PCB service, and they were assembled, programmed, and tested in house. The custom design and the decoupling of the measuring circuitry from the sensors' array allow for easy system reconfiguration

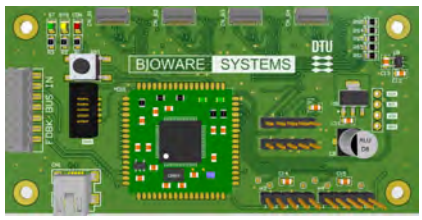

(a) Temperature sensors interface module top view.

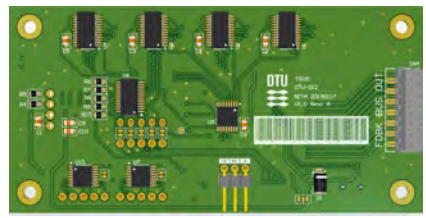

(b) Temperature sensors interface bottom view.

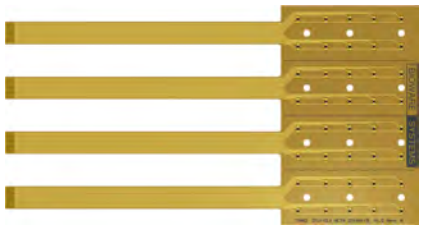

(c) Temperature sensors array top view.

(d) Temperature sensors array close up.

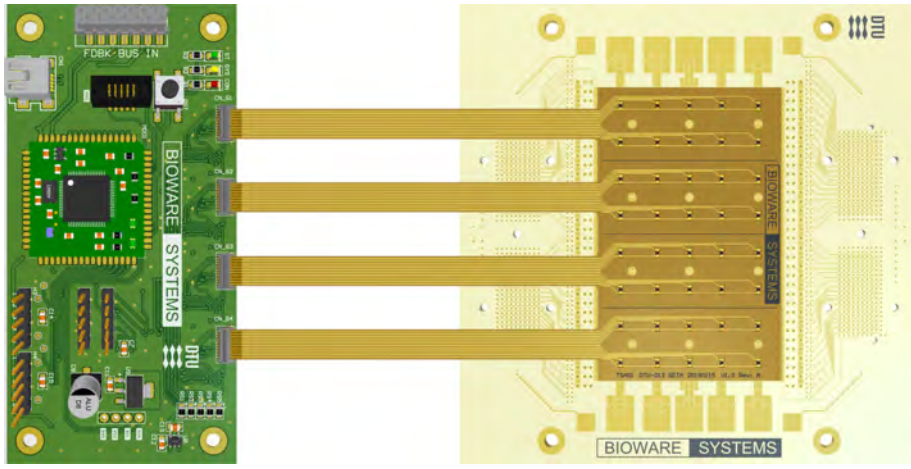

(e) Temperature sensors assembly.

Figure 5.29: Heaters controller module, and TC008 heaters connection adapter assembly. A high-resolution version is available in the digital copy.

by redesigning the sensors array if needed.

5.4.13 Instrumentation system summary

The instrumentation system design goal is to provide a modular, reconfigurable, and evolvable instrumentation approach for digital microfluidics. Throughout Section 5.4, we discussed the design objectives and elaborated on the essential aspects of the system architecting process. We presented eight functional modules: the mainboard, bus interface, power delivery, high voltage power supply, electrodes driver, heaters controller, and temperature sensor array. Additionally, we argued about the development of a prototyping module supporting the development process.

The modular design approach was demonstrated on the physical level when assembling the base control subsystem, as discussed in Section 5.4.6, and the minimal instrumentation system, as explained in Section 5.4.10. With the modules and the system assembly presented in this section, the system was developed to a state where it can provide the functionality needed for the planned PCR and enzymatic test cases.

Developing the system to this stage is a significant milestone in the quest to establish a truly application-agnostic cyber-fluidic architecture. We attribute the successful development of the instrumentation system to the holistic system approach discussed in Chapter 4 and the modularity principles vigorously applied throughout the architecting, designing, and building process of the instrumentation system. The chapter will continue with a discussion of the virtual system in Section 5.5 followed by unit and system-level testing of the complete cyber-fluid platform in Chapter 6.

5.5 The virtual system

The virtual system is the top control layer of the cyber-fluidic platform, and it is comprised of software tools covering the manual and automated instrumentation system control, protocol capture, translation, and execution on the digital biochip, as shown in 5.30. The vision for the virtual system is to provide a versatile and user-friendly software stack addressing all aspects of the design and operation of the cyber-fluidic platform.

Although several digital microfluidic platforms have already been developed (see

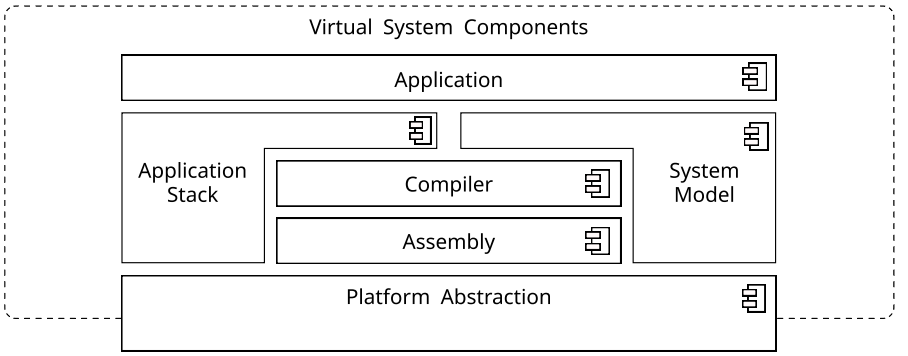

Figure 5.30: Virtual system components.

Chapter 3), unified operation and programming models are virtually nonexistent, leaving the control of the digital biochips to manually scripted electrode actuation sequences [79] [30]. The programming model of the commercial systems [96] [19] remains undisclosed, but considering their application-specific nature, they likely present a fixed user interface. The notion for programmable fluidic architecture [78] along with methods for structured biology protocol capture [32] [127] have been previously explored, but their adoption remains somehow limited. Application-specific programming languages and droplet routing algorithms [26] [35] have also been demonstrated, but they lack behind their computer counterparts, mainly due to the lack of overall toolchain integration and a realistic execution model.

The cyber-fluidic platform architecture discussed throughout Chapter 5 advocates for adopting the loosely coupled modular approach in the design of the virtual system. To holistically address this challenge and fully close the gap between the fluidic and the virtual domain, Section 5.5 discusses the design aspects of a minimalistic platform controller and conceptualizes the abstraction levels required to achieve full platform programmability.

5.5.1 Design objectives

The virtual system is envisioned as a collection of software modules and standardized data exchange mechanisms, allowing for abstract and scalable operation. The software module function assignment is governed by task separation such that modules perform logically decoupled functions. Any cyclic cross-module dependency should be encapsulated in a single module since it is an indicator of suboptimal task separation. The interaction between the differ-

ent software modules is established through standard input/output interfaces such as real-time data streams or file operations. The goal is to design the virtual system as a hierarchical toolchain where dependency is decreased when approaching the lowest-level modules.

Inspired from the agile development method and its iterative approach, the task of building the virtual system was split into two parts, specifically, developing a simplistic but yet practical instrumentation system controller and conceptualizing the programming and execution model of the full system. The design objectives for the instrumentation system controller target addressing the basic control need of the digital biochip, such as manual and automated electrode actuation, manual control of the high voltage power supply, and the heaters controller module. Graphical and command-line interfaces are anticipated as a foundation towards a fully programmable cyber-fluidic system. Modern established programming languages and utilization of design patterns are a necessity for maintaining future scalability. The instrumentation system controller is targeted to play the role of a shell of any future software extensions.

Laboratory protocols are often ambiguous and incomplete, making them difficult to replicate. Moreover, the ambiguity poses significant challenges to their automation. Obscure descriptions such as "incubate overnight" and "keep at room temperature" do not communicate specific process parameters but instead leave their interpretation to the operator. Structuring the protocol steps into a formalized programming language holds the potential to eliminate the ambiguity and provide a foundation for protocol translation and automation. Modern programming paradigms cover virtually any level of abstraction and programmer's skillset - the engaging visual block-based programming languages [128], the enhanced readability and simplicity of interpreted high-level languages [129], the complexity of the object-oriented concurrent programming [130], and the variety of efficient low-level assembly languages. The order of the aforementioned programming paradigms presents a decreasing abstraction level but increasing complexity. The graphical programming methods are the easiest and thus provide an interface for novice users. The object-oriented and low-level assembly programming methods are the most efficient and cumbersome, hence require vast user expertise. However, regardless of the abstraction level, the program intent is decomposed to the low-level assembly language in order to be executed on a computer processor.

An important design objective of this thesis was to address the complexity of protocol capture and execution on a conceptual level. Adhering to the modular approach and gaining inspiration from the traditional compilation pipelines, we envision the need for a high-level descriptive and user-friendly syntax, low-level fluidic-specific instruction set architecture, and a virtual machine responsible for runtime execution. Naturally, a compilation toolchain is required to translate

the high-level program into a low-level assembly suitable for execution. Considering the full software stack, even only at the conceptual level, supports the holistic system approach, and aids architectural decisions.

While the concept of protocol capture and programming make a periodical reappearance in the microfluidics field, the need for a runtime environment has been somehow neglected. The digital biochips have often been treated as devices without feedback capabilities and, consequently, protocols being executed in a monolithic imperative fashion without the use of flow control. However, to fully realize the automation potential offered by the digital microfluidics, the digital biochips need to integrate arrays of sensors, thus allowing for flow-control and runtime decisions. While the sensor integration mainly presents challenges in the physical domain, their integration with the virtual system needs to be achieved through interfacing to the envisioned runtime environment.

5.5.2 The platform controller

The platform controller is a software program serving the purpose of a user interface to the instrumentation system. The program is named the "DMF Toolbox" since it is intended not only to provide manual control but also to acts as a shell for future software functionality extensions. The need for basic droplet and instrumentation modules control was recognized early in the development process, mainly for testing and debugging purposes. The initial functionality of the DMF Toolbox was targeted to provide minimalistic manual control functionality to facilitate the testing of the fluidic and instrumentation subsystems.

The first part of the design phase of the platform controller focused on establishing a loosely coupled modular software architecture providing a scalable framework that can facilitate future modular expansions. Architecture choices are often made considering the used programming language, existing software modules, and established programming models. The modern general-purpose programming language C was chosen due to the state-of-the-art features set, comprehensive user-interface building capabilities, extensive third-party codebase, and the user-friendly integrated development environment. The application was based on the Model-View-ViewModel (MVVM) design pattern that efficiently structures and separates the business from the presentation logic. The design pattern leverages some of the core mechanisms of the Windows Presentation Foundation (WPF) graphical subsystem, namely, data binding, data templates, commands, and notifications. The general MVVM class organization and interaction are shown in Figure 5.31. The View classes encapsulate the user interface (UI) and the code behind logic. The View model is responsible for

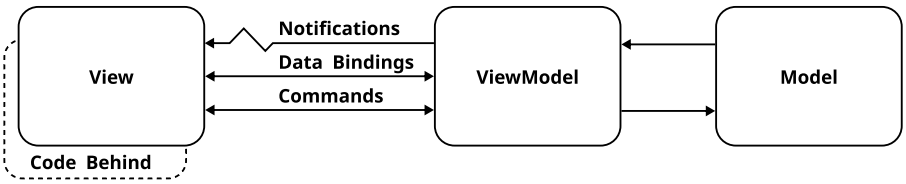

Figure 5.31: The MVVM pattern class separation. Inspired from [131].

presentation logic and preserving the state, and the Model classes implement the business logic of the application. The clear separation of presentation, presentation logic, and business logic are a prerequisite for building scalable and maintainable applications.

The DMF Toolbox is based on the open-source Prism framework [132] that includes the MVVM pattern, dependency injection, EventAggregator, and a ViewModelLocator. The dependency injection effectively separates a client from a service class through an interface, which implies that only the functionality of the client needs to be fixed. From a practical perspective, this allows loosely coupled implementation where service providers can be easily replaced. The EventAggregator is another mechanism that promotes modularity by implementing a multicast publish/subscribe event-based communication across the application components. Different application modules can register and deregister at runtime, allowing system reconfiguration. Another notable feature offered by the Prism framework deals with developing composite UI applications, e.g., when an application consists of different UI components. The technique is referred to as Prism regions and allows module-based views to be dynamically replaced within the main application window. The mentioned features of the Prims framework are aligned with the overall modularity concept, and although they appear to be primarily UI focused, the overall modularity, decoupling, and ease of use are considered an important asset.

The layout of the DMF Toolbox is shown in Figure 5.32, where in this instance, the three application regions are populated with the "Platform Modules", "Chip Controller", and the "Script Controler" modules. The first region is the "Platform Modules," and contains all user controls of the particular instrumentation system instance. A separate control interface represents each instrumentation module, and only the modules' part of the current instrumentation instance are presented to the user. The second region is the "Chip controller," and as the name implies, it contains a virtual representation and manual controls for the digital biochip. The third region is the "Script controller," displaying the currently loaded electrode actuation sequence, and it also manages the execution of the script. Each application region represents a separate View from the MVVM

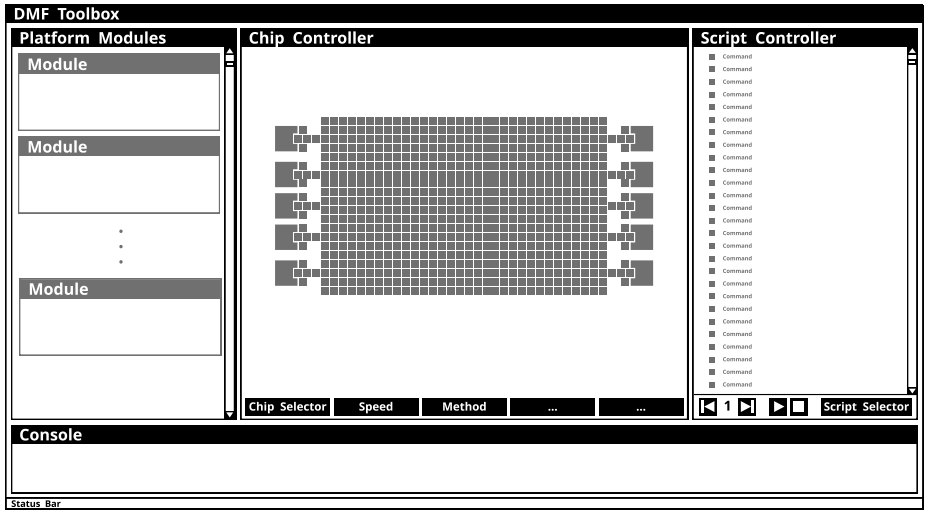

Figure 5.32: DMF Toolbox wireframe layout.

pattern, as illustrated in Figure 5.31. Correspondingly, a ViewModel class is allocated to each view. The business logic is implemented in the corresponding Model classes, seen as module controllers.

The platform modules are represented as separate controller classes derived from a base supply, control, or a feedback class. The communication between the platform module controller classes and the rest of the application is based on a publish/subscribe event mechanism over the Prims event aggregator service. The events are typed, which allows for compile-time checking and easy creation of event groups. Publishers and subscribers can be added or removed at runtime, without direct reference and dependency, thus providing runtime reconfiguration based on the loosely coupled communication mechanism.

The chip controller model implements two-fold functionality. First, it visualizes the state of the electrode array of the digital biochip, i.e., electrodes connected to the actuation voltage are marked with blue color, while the electrodes connected to ground potential are colored in yellow. The array visualization also serves the function of a simplistic simulator that can be used to visualize scripted electrode actuation sequences. The second function of the chip controller is to implement a manual droplet control for tests and debugging purposes. The chip controller implements two manual droplet control strategies and two semi-automatic point-to-point routing schemes. The manual modes are called "Single" and "Multiple," where, as the names imply, the "Single" mode allows only one droplet to be moved on the array, and the "Multiple" mode simultaneously

applies the control input to all active electrodes. Electrodes can be activated or deactivated with left and right mouse click, and the keyboard arrow keys can be used to move all active electrodes to the keyed direction. The semi-automatic modes can route a single droplet between two points on the chip by following a horizontal- or vertical-first approach. The start and endpoints are selected with left and right mouse click, and a middle mouse click activates the routing. These four manual droplet controls and the direct mouse control are considered essential assets for the initial system, such as debugging, fluidic system testing, and manual assay execution.

The script controller is responsible for parsing and executing a hard-coded electrode actuation sequence. Functionality for stepping through an automated time-based execution is considered useful for scripting experiments, demonstration purposes, and system endurance testing. Moreover, the capability of running a hard-coded sequence of commands positions the automation control capabilities of the cyber-fluidic platform on par with several of the already available systems, as discussed in Chapter 3.

Implementing the platform controller classes and the script controller is straightforward from a software engineering perspective since the functionality is limited to sending commands to the instrumentation platform, parsing received status messages, and keeping state. However, the chip controller model presents interesting design tasks, among which the most significant on is considered the virtual representation of the digital biochip. Capturing the physical characteristic and the intrinsic relationship between the different components of the fluidic system in a structured scalable model is viewed as an essential step in achieving complete modularity and ensuring scalability.

A simplified class diagram of the digital biochip model is shown in Figure 5.33. The digital biochip model comprises several physical layers, where each layer is represented as a class and reflects a set of components from the fluidic system. The most obvious example is the electrodes layer representing the planar actuation electrode array and the reservoirs. The "ElecotodeLayer" is constructed from "Electrodes," and each electrode is mapped to an "ElectrodeShape" object representing the physical shape of the electrode. Capturing the electrode layout organization into a virtual model is achieved by treating each electrode as a separate object, with its spatial attributes. Correspondingly, the "ElectrodeLayer", "Electrode", and the "ElectrodeShape" classes have a range of parameters such as physical dimensions, location, and associated functionality.

The "MechanicalLayer" defines the digital biochip physical footprint, device thickness, mounting holes, and any other cutout or dimensional characteristics. The "MechanicalLayer" sets the base dimensional reference and height offsets for any additional layer. As the name implies, a "RoutingLayer" is composed

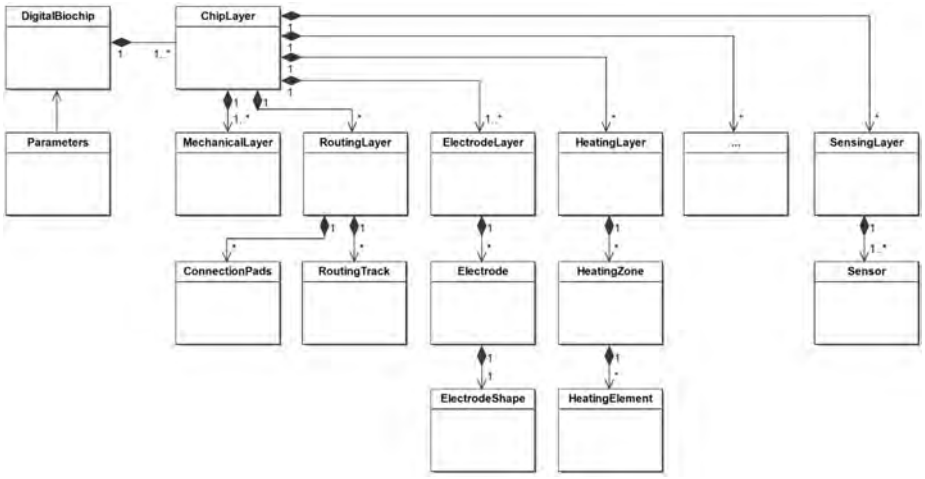

Figure 5.33: Simplified chip model class structure. A high-resolution version is available in the digital copy.

of PCB routing tracks. While the routing layers are essential for the digital biochip, they might not be relevant for the model and hence excluded from the implementation. However, the "ElectrodeLayer" is of crucial importance since it represents the most distinct element of the digital biochips, namely the actuation electrodes.

Other functional digital biochip specific layers are the heating and the sensing layers. In the case of TC008, the heating layer is composed of embedded wire structures that can be configured in a heating zone. However, heating and cooling can also be implemented by components placed beneath the digital biochip or on the top plate for a closed digital biochip. The layered approach allows for capturing the different compositions by adding corresponding dimensions and height offset hence integrating them into a unified model. The integration of sensing elements can be reproduced by the corresponding "SensingLayer" capturing the particular implementation details.

The layered approach provides a scalable modeling method since the model can grow in complexity along with the increasing digital biochip capabilities. The simplified example model presented in Figure 5.33 does not show essential non-functional layers such as the hydrophobic insulation layer and the top plate of a closed system. However, if these layers become essential for simulation or visualization purposes, the digital biochip model can be extended to accommodate for the new system demands.

5.5.3 The cyber-fluidic processor

Modern computers are built as loosely coupled hierarchical systems, where carefully designed abstraction levels promote standardization and module reusability. The loosely coupled model often allows an application-level computer program to operate without knowledge about the underlying operating system, instruction set architecture (ISA), and the actual hardware. The detachment from the underlying hardware-specific details allows a programmer to capture the application functionality into a structured code and then enables an extensive toolchain to compile the program into platform-agnostic or a machine-specific code.

An overview of the distinctive components of a computer system and their location in the hierarchy is shown in Figure 5.34. Drawing parallels between the computer system architecture and the cyber-fluidic platform, it becomes evident that the two systems have a range of similarities, especially on the hardware level. The smallest logical entity of a computer processor is the transistor, and likewise, the digital biochips are built from actuation electrodes. While the fundamental physics effects reaching beyond the logical entities are complex and significantly different from each other, the function of the transistor and the actuation electrode can be reduced to representing and manipulating data. Devices such as logic gates and registers are composed of transistors, and likewise, electrodes are grouped to form reservoirs or create actuation pats. A register stores data, so does an electrode, although the data is in the form of the chemical composition of the droplet.

Moving up in the abstraction levels shown in Figure 5.34, the computer processors handle data in a datapath consisting of different logic units, registers, multiplexers, and buses. The control path is the hardware that manages how data travels through and is processed by the datapath. A similar concept can be applied to the digital biochip, where the fluidic path is composed of the actuation electrodes and the physical boundaries of the device, and different external controls, such as temperature control, can be applied to alter the state of the transported droplets. The data and fluidic path correspondingly assemble micro- and fluidic architecture. The microarchitecture is the hardware implementation of an ISA, and namely, the abstract model of ISA is recognized as one of the significant advancements that enabled standardization of the computer architectures. The ISA is the layer that decouples the software from the hardware functionality, e.i., a machine code compiled for a particular ISA can run on different hardware implementations.

From a bottom-up perspective, the ISA level is where the discrepancies start to grow between the modern computer system and the existing digital microflu-

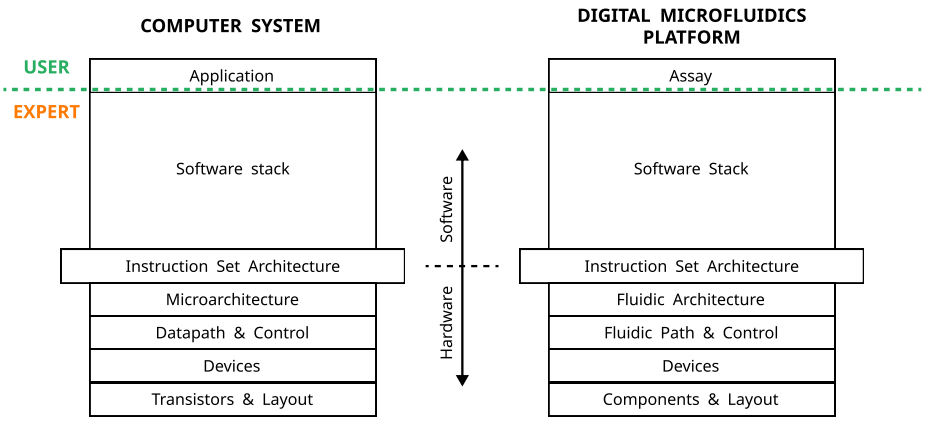

Figure 5.34: Comparison between the hardware abstraction layers of the traditional computer and the digital microfluidics platform.

idic platforms. The lack of standardization and holistic system engineering approach resulted in scientists and engineers developing their research or commercial system without any apparent effort of establishing a common design and automation framework. While developing unique instrumentation systems and digital biochips makes sense in both the research and commercial domain, the lack of a standard ISA is entirely unjustified. A common programming model will reduce the development overhead and allow more effort to be channeled to perfecting the digital biochip, refining existing applications, and adapting new assays.

Although many reasons can be argued for the lack of a standard ISA, subjectively, the most likely causes are the complexity of the endeavor from a technical and logistic perspective and the deceptive impression that digital biochips have not reached a complexity level where such automation tools are required. Nevertheless, as discussed in Chapter 2 and 3, the digital biochips have grown in complexity, and not only the number of control electrodes has increased but sensors and actuators have become integrated and have provided new dimensions of fluidic control and sensing. The digital biochips have often been recognized as solely actuation devices, e.g., not being part of an active feedback loop. However, considering the increasing number of actuation electrodes, e.g., currently the TC008 implements an array of 640 electrodes, but we claim that it can easily be scaled by a factor of two or even four; together with the growing sensor integration, scripting actuation sequences quickly become a tedious and error-prone task. Moreover, the widely adopted execution of hardcoded scripts hardly scales to incorporate flow control based on signals measured from the integrated sensors.

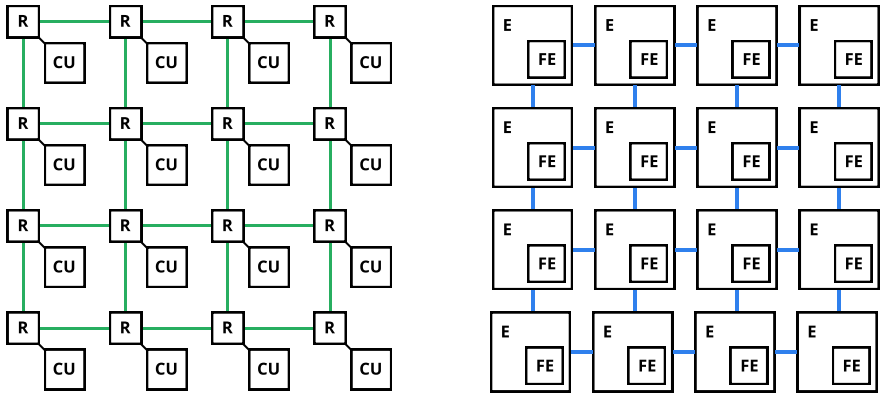

(a) Traditional NoC architecture. **(b)** Digital biochip as a NoC.

Figure 5.35: Similarities between the NoC architecture and the digital biochip. *R* stands for Router, *CU* for Computational Unit, *E* for Electrode, and *FE* for functional element. The green lines show dataflow and the blue lines show fluidic flow.

Before exploring the software abstraction layers described in Section 5.5.4, we will discuss the hardware part using the already established layered model. This iteration establishes a fluidic dataflow model inspired by the network-on-chip (NoC) communication system, typically used to connect semiconductor cores on system-on-chip (SoC) devices [114]. The composition of the traditional NoC is shown in Figure 5.35a, and it consists of packet routers with associated computation units (CU). A NoC utilizes the packet switching routers to pass data throughout the different nodes or to the CU. Among the benefits of the NoC compared to bus communication is the increased data throughput and computational flexibility. Likewise, if a single actuation electrode is considered to be a droplet router and electrodes are organized in a two-dimensional array, this configuration allows for flexible droplet routing between any two electrodes on the digital biochip. Considering a droplet as a data packet and its chemical composition representing data, a single droplet serves the purpose of a fluid carrier of a chemical payload. By associating a functional element (FE) to each electrode, a droplet becomes the equivalent of a data packet that can be transported through the network and processed by a FE, as shown in Figure 5.35b. An example of a FE can be a heating element, biochemical sensor, color sensor, or even using the electrode itself for capacitive sensing.

A NoC router serves the purpose of passing data to its neighboring nodes, but it can also implement packet buffering. Likewise, an electrode can draw a droplet from its neighboring electrodes, and it can also act as a storage by keeping the

droplet on its surface. All fluidic operations, namely, transport, merging, mixing, and splitting, are performed based on this pass-and-store mechanism, and the electrodes play the role of droplet routers implementing a reconfigurable fluidic path. However, the routing logic must come from a separate control path that manages the electrode sequence and interfaces with the FEs. The parallels on the hardware level aid adapting the traditional computer system model to the digital microfluidics platform, namely establishing the equivalent of a microarchitecture and ISA. Since the microarchitecture is the actual implementation of a particular ISA, the modular instrumentation system can be seen as the implementation of an envisioned fluidic ISA.

Considering the need for control of the data or the fluidic path leads to another relevant abstraction model, namely the finite state machine (FSM), which, as the name implies, is a computation model that, at any given time instance, is in precisely one of a finite set of states. The FSM is suitable for managing repetitive control tasks consisting of a predetermined sequence of actions. Although decoding an actuation script into electrode states appears relevant to the FSM, this control approach has limited use due to the FSM output being restricted to conventional control signals and the absence of a mechanism to process data. However, extending the FSM model with a data handling mechanism adds computational capabilities, and it results in the more capable concept of a finite state machine with a datapath (FSMD). The model of the classical FSMD is shown in Figure 5.36a, where two distinguished parts can be seen - the control path consisting of an FSM and the datapath responsible for data processing. The control path is constructed from sequential next state logic, state register, and output logic. The next state logic determines the subsequent state transition based on the input command, the current state, and an external feedback signal. The multi-input next stage logic allows for decoding and acting upon a command input in conjunction with the current state and external to the FSM signals. The second part of the FSMD is the datapath that consists of sequential routing and processing circuits, as shown in Figure 5.36a. The processing circuits can perform different functions such as addition or multiplication, thus referred to as functional units.

The coupling of the FSM control path with the processing capabilities of the datapath resembles the functionality of a central processing unit (CPU) since feeding the control path with a sequence of instructions results in programmatical manipulation of data. Referring back to the layered computer system model shown in Figure 5.34, the ISA defines how the machine code will be executed on the underlying hardware. Hence, in the FSM context, the ISA defines how commands are decoded from the FSM and their effect on the datapath. Feeding the FSMD concurrently with commands and digital data offers a runtime configurable data processing.

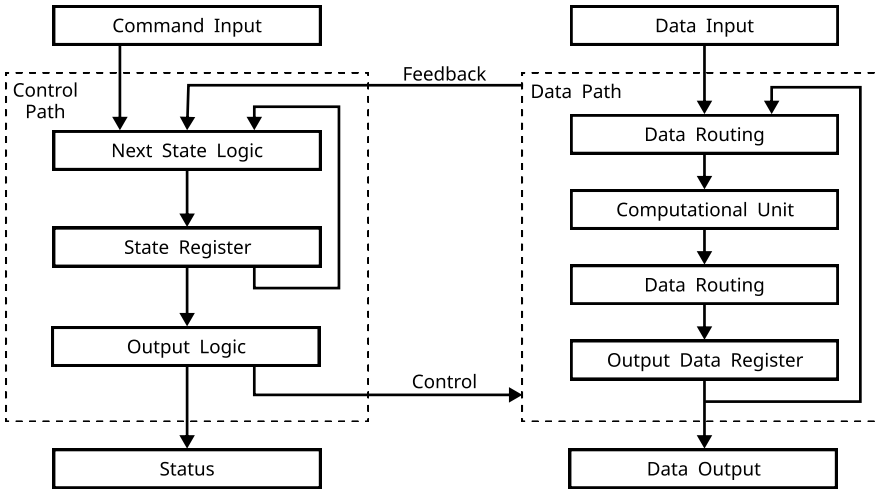

(a) Traditional FSMD.

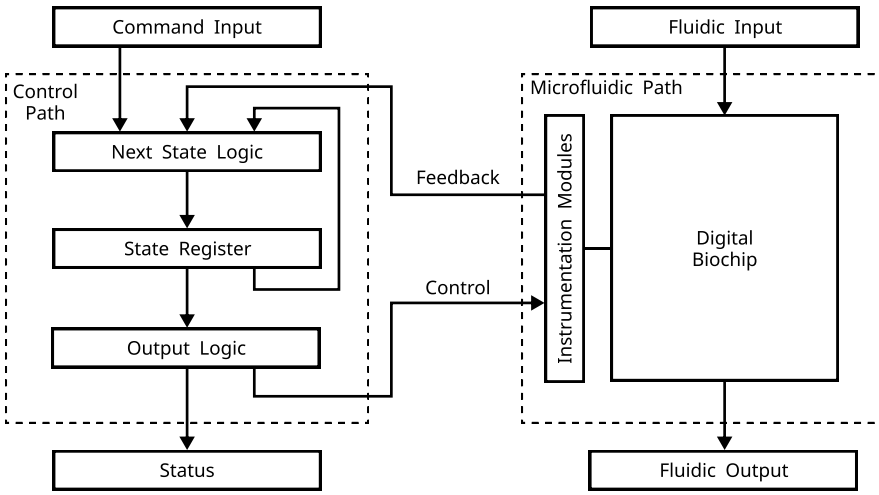

(b) FSM with fluidic path.

Figure 5.36: Finite state machine with data and fluidic paths.

The conventional CPU is fed with data over interface busses, data is manipulated according to the commands sent to the CPU, and then the data is typically transferred to a memory location for further use. Although instructions are often pipelined for boosting performance, the data processing mostly remains a sequential process. Likewise, the digital biochip transports droplets, where

the droplet plays the role of the data packet and the droplet composition is the payload. Similar to how a CPU will proceed to add together two numbers, the digital biochip can merge two droplets adding not only their volumes but also their composition.

The modification of the classical FSMD where a fluidic path substitutes the datapath is shown in Figure 5.36b. The proposed finite state machine with a fluidic path (FSMF) inherits all of the control characteristics of the classical FSMD, but instead of a digital datapath, it implements a fluidic path. The digital-to-fluidic interfacing is established through the instrumentation system, where the instrumentation substems, namely control, feedback, and supply modules, are considered part of the fluidic path, and the control path constitutes the base control substem (see Figure 5.11). Although the instrumentation subsystem and the base control system communicate over the control, feedback, and supply busses, each one of these busses realizes bidirectional communication, which nevertheless matches the model presented in Figure 5.36b. Such implementation details are part of the micro- or the fluidic architecture and usually are not relevant for the layers above the ISA.

Separating the digital and the fluidic domains with ISA allows for establishing a standard microfluidics programming model. The underlying fluidic handling technology does not necessarily need to be EWOD, but it can be any fluidic handling method such as continuous flow or even pipetting robots. However, this poses significant engineering challenges to designing a platform-independent ISA that explicitly defines the memory and addressing model, data types, core and fluidic instructions, peripheral and IO registers. Although the need for a cyber-fluidic ISA has been recognized on the course of this thesis work, the design and implementation have been left out of the scope due to time and resource constraints. Nevertheless, in order to sustain the platform development momentum, Luca Pezzarossa undertook the challenge to fully conceptualize, design, and implement the envisioned cyber-fluidic ISA as a part of a postdoctoral research at DTU Compute. Even though the research project is still ongoing, a parallel synchronous ISA has been designed and implemented into a BioAssembly: a microfluidic specific assembly language executed on a custom virtual machine. Because the BioAssembly ISA has not been publicly announced, further details will be omitted in this thesis work and they will be published in the foreseeable future. Moreover, the contribution of this thesis work in regards to BioAssembly is limited to recognizing the need for a common microfluidics ISA and developing the fluidic and instrumentation systems described in Chapter 5.3 and Chapter 5.4.

A common microfluidic ISA is recognized as the missing link for streamlined cyber-fluidic programming. The programming itself is responsible only for capturing the experimental intent. An extensive toolchain is required to parse,

verify the correctness, type check the variables, and translate the program to assembly. These steps are undertaken by a compiler responsible for taking a generic high-level program input and translating it to low-level assembly targeting a particular platform.

5.5.4 Programmable microfluidics

The early adoption of standardization, design automation, modularity, and reusability strategies fueled the steady development of microelectronics and computer programming in the past half-decade. Computers evolved from slow and unreliable electromechanical machines programmed with jumper cables and paper cards to highly integrated and easily programmable portable devices. Apart from the hardware miniaturization and integration, the variety of programming models and software stacks building from the ISA to a user application level made computers widespread and accessible for a broad user group. The comparison between a classical computer system and the digital microfluidics platform shown in Figure 5.37 reveals similarities both on hardware and software level. The top level of the two systems provides an interface to a non-microfluidics expert user lacking knowledge for the underlying system operation mechanism but yet interested in using the full system as a tool. The green line on the figure marks the boundary between the user and the expert level. Essentially anything below the top application or the assay level is considered to require microfluidics, programming, and electronics domain-specific knowledge beyond the expertise of the typical user.

Building upon an ISA that abstracts the hardware implementation details allow for the digital microfluidics platform software stack to be based on the already proven software architecture of the computer systems. A core concept remains to capture the application or assay logic into a structured program or a protocol and then pass the structured representation through a compilation toolchain. Although the ISA provides a standardized interface, adjustments to the classical computer system model are needed to accommodate the possible variation of the fluidic architecture. While the lack of hardware computation resources can often be circumvented by implementing the required functionality in software, e.g., the absence of hardware floating-point arithmetic unit can be substituted with software emulation, the lack of heating or sensing capabilities on the digital biochip has no software equivalent. Therefore the compilation toolchain requires a model of the targeted biochip in order to allocate and manage the available resources.

Another essential component of the envisioned microfluidics software stack is the virtual machine, which to a great extend, replicates the functionality of an

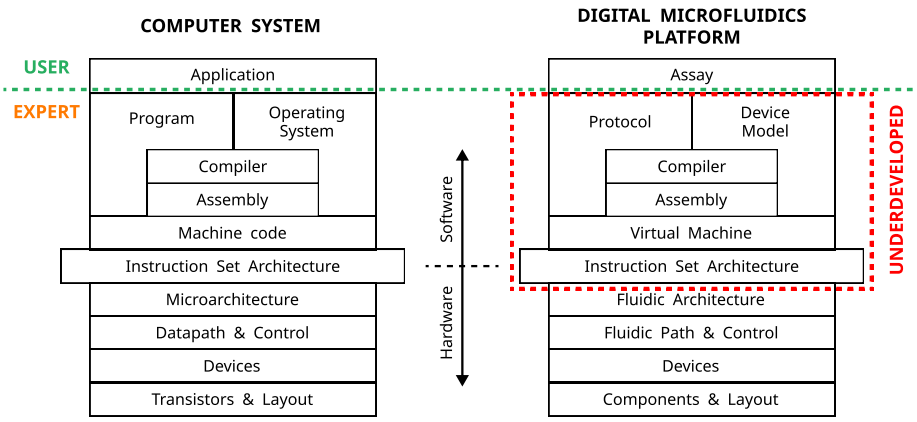

Figure 5.37: Comparison between the full layered stack of the traditional computer and the digital microfluidics platform.

operating system. The virtual machine is responsible for concurrently executing assembly tasks interacting with the instrumentation modules. The virtual machine addresses the runtime handling of the instrumentation and the fluidic systems and provides a mechanism for implementing flow control.

Although efforts for programming languages and compilers periodically appear in the scientific literature (see Section 2.4.5), they remain largely unused, where one of the core reasons for the shortage of adoption is the lack of standard, intermediate data formats. The demand for intermediate formats becomes immediately evident in the case when two software packages need to interact, e.g., different protocol descriptions, device models, or even assembly code. Nevertheless, the software stack comprising the device model, compiler, assembler, virtual machine, and ISA is considered underdeveloped in comparison with the classical computer systems. Namely, the lack of standardization and integration hinders the progress of digital biochips becoming fully-fledged cyber-fluidic processors.

The software stack for the cyber-fluidic platform presents numerous challenges, and from the usability perspective, the most critical one is the actual programming method and interface. Textbase programming is de facto a standard in the computer field, but it appears as a complicated and cumbersome method to users with a lack of prior programming experience. One way to flatten the learning curve and lower the entry barrier to microfluidics programming is to implement a visual symbolic programming language. A key performance metric is the simplicity and readability of the captured protocol. A possible approach is to create a set of intuitive symbols, each representing a particular entity or

operation that can be performed on the digital biochip. A sample symbol set presenting some fluidic operations is shown in Figure 5.38a. The symbols maintain a simple and intuitive design language, aiming to explicitly communicate the fluidic operations. Only the most critical parameter is shown in the symbol, and all additional parameters are left to be accessed through a secondary configuration interface. For example, the symbolic representation of a reagent container resembles an Eppendorf tube, where the color-coded content is used to label the different reagents. A similar intuitive design approach is used for representing mixing with a labeled number of mixing cycles, specified incubation time, heating or cooling temperature, sensing period, a magnetic field for magnetic beads immobilization, and high voltage electroporation.

The correspondence of a graphical and textual representation of a mixing operation and the resulting sequence of fluidic operations is shown in Figure 5.38. The visual description consists of two input reagents, labeled A and B, connected to a mixer module with arrows. The input reagents are the equivalent of droplets on the digital biochip. The mixing operation is initiated by first transporting the two droplets from their current positions to a digital biochip location, where they will merge, as shown in the figure. After merging droplets A and B, they result in a new droplet C, which is the sum of the volume of the two droplets with relatively unmixed chemical content. Next, droplet C is actuated in a 2×4 rectangular mixing pattern for the specified five mixing cycles. An example of an intermediate textual representation of the move and mixed operations is shown under the images. Translating the graphical into a textual representation provides an extra abstraction layer that more experienced users might start using in the quest for more granular low-level control.

A more elaborate example of how the graphical programming approach can be used to describe a widely used lab protocol is shown in Figure 5.39a. The shown sequence of actions describes a PCR, which is discussed in detail in Section 6.4.1. The protocol starts by mixing the five reagents followed by a hot start step at 98 °C for 60s and 30 temperature cycles of 98 °C for 10s, 54 °C for 30s, and 72 °C for 60s. The PCR ends with a final elongation step of 300s at 72 °C followed by moving the reaction product to storage at 72 °C. While the protocol steps are represented with the introduced graphical symbols, the transitions are marked with arrows. A condition that can govern the protocol flow can be associated with each transition arrow.

For comparison, the same PCR protocol is programmed in the microfluidics domain-specific language BioScript [26], and the code is shown in Figure 5.39b. The program starts by declaring all the reagents, followed by a function that implements the PCR protocol. All reagents get dispensed and mixed at the beginning of the *RunPCR()* function, which corresponds to the single mixing operation shown in the graphical representation of the protocol. The *RunPCR()*

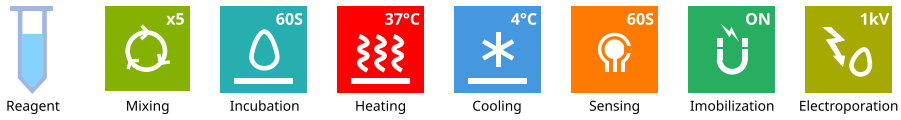

(a) Graphical representaion of generic reagent storage and fluidic operations.

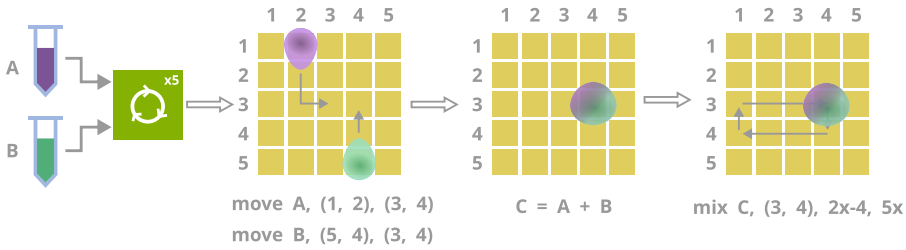

(b) Graphical representaion of a mixing operation and mapping to the digital biochip.

Figure 5.38: Symbols for fluidic operations and an example of mixing of two droplets

function continuous with the hot start followed by a *repeat* statement encapsulating the thermocycling. The function finishes with the final hold at 72 °C for 300s and returning the product of the reaction.

Although the textual representation appears to be more complex, it provides a more granular and structured description of a protocol. In contrast, the graphical representation appears streamlined and intuitive since it purposely omits implementation details. Moreover, the graphical and the textual representations can be coupled together through an intermediate representation that allows for bidirectional translation between the two methods. Such an approach has the benefit of providing an entry point for inexperienced users but not limiting the low-level control through a text-based programming interface.

5.5.5 Virtual system summary

A holistic approach was applied throughout the design and implementation of the virtual system, aiming to match the current control needs and provide a framework for the envisioned software toolchain and programming model. The DMF Toolbox was fully implemented and used extensively in the testing and operation of the instrumentation system. Moreover, the DMF Toolbox was used as a primary platform controller for all biochemical experiments presented in

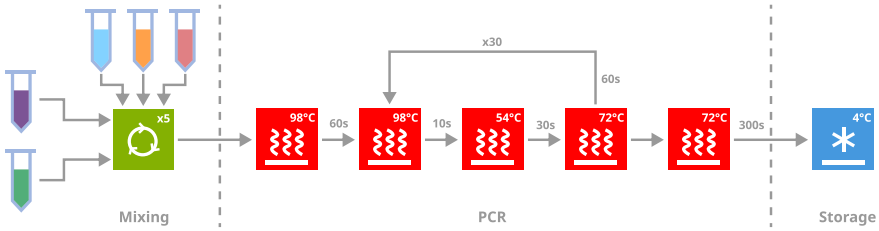

(a) Graphical representaion a PCR protocol.

```
1  // PCR protocol written in
2  // BioScript
3
4  module mod
5
6  manifest PrimerA
7  manifest PrimerB
8  manifest PCRTemplate
9  manifest Water
10 manifest PCRMix
11
12 functions:
13
14 function RunPCR() {
15     pa = dispense PrimerA
16     pb = dispense PrimerB
17     out = mix pa with pb
18     pcrt = dispense PCRTemplate
19     out = mix out with pcrt
20
21     pcrm = dispense PCRMix
22     out = mix out with pcrm
23     w = dispense Water
24     pcrmix = mix out with w
25
26     heat pcrmix at 98c for 60s
27     repeat 30 times
28     {
29         heat pcrmix at 98c for 10s
30         heat pcrmix at 54c for 30s
31         heat pcrmix at 72c for 60s
32     }
33
34     heat pcrmix at 72c for 300s
35     return pcrmix
36 }
37
38 instructions:
39 pcrProduct = RunPCR()
```

(b) The PCR protocol written in BioScript.

Figure 5.39: An example of a PCR protocol represented in graphical and as a BioScript program.

Chapter 6. The modular software design provided a matching virtual model of the physical platform, and throughout preliminary testing, it proved to be capable of integrating with the BioAssembly and the virtual machine developed by Luca Pezzarossa.

Although the concept of a cyber-fluidic processor and programming models were introduced on a visionary level, hence leaving a wide range of engineering changes unaddressed, the notion for a universal fluidic processor and an extensive software toolchain aids the holistic future proof development of the cyber-fluidic platform. However, engaging with the programmability concepts early in the process allows identifying design challenges such as the lack of programmatic volume management, absence of digital biochip resource allocation semantics, and the need for runtime management. The holistic approach helps foresee potential emerging issues on all platform levels and develop the cyber-fluidic platform as a scalable and evolvable architecture.

5.6 Cyber-fluidic platform summary

This chapter took a holistic approach towards the design of the envisioned cyber-fluidics system. The overall platform architecture and the set of modularity considerations were presented, followed by a discussion on the fluidic, instrumentation, and virtual system.

An extensive analysis and design process led to the development of TC008, a digital biochip with 100 mm×100 mm, an array of 640 individually addressable electrodes, 10 reservoirs, and 32 independent heating elements. A complementary foil-frame coating method was developed to extend the modularity and reusability concepts.

The modularity and reusability theme was carried out through the architecting and design of the instrumentation system in the quest for application-agnostic design. Eight instrumentation modules were developed; the mainboard, bus interface, and power delivery modules, comprising the base control system; and the high voltage power supply, electrode drivers, heaters controller, and the temperature sensor interface as a part of the instrumentation subsystem. The modular system approach was illustrated with a series of visualizations, and the instrumentation system was developed to support the targeted functionality for supporting PCR and enzymatic experiments.

The virtual system development was focused on creating a modular loosely coupled application shell, conceptualizing the fluidic system as a universal cyber-fluidic processor accompanied by a full software stack, and discussing a design language for a possible programming interface. The DMF Toolbox was developed as a manual platform controller used through the testing and operation of the cuber-fluidic platform. The cyber-fluidic processor and the proposed programming approach were outlined to support the holistic system approach and establish concepts for future work on the virtual part of the cyber-fluidic platform.

The chapter presented samples of the full spectrum of problems accompanying the design of a complete cyber-fluidic system. Overcoming the obstacles at the conceptual and technological levels allowed the successful realization of a truly modular, scalable, and evolvable cyber-fluidics platform.

Chapter 6

Digital Microfluidics at Work

Beyond implementing the cyber-fluidic concepts onto hardware and software components lies the engaging task of unit, system, and operational level testing. This is the last step of the engineering and development phase and focuses on integration and evaluation of the system as a whole where modules and subsystems should not only meet their specifications, but they should also perform together to provide the envisioned system functionality.

This chapter discusses the practical aspects of building and operating the cyber-fluidic platform, which design was discussed in Chapter 5. The chapter starts with a discussion on the importance of component and system-level testing and continues with the fabrication, characterization, and operation specifics of the TC008 in the context of the cyber-fluidic platform. The chapter concludes by demonstrating the system capabilities by performing a full PCR as the first step of implementing a cell cloning protocol, and two magnetic beads based ELISA assays targeting MRSA and SARS-CoV-2 spiked protein detection.

6.1 Cyber-fluidic platform testing and integration

Testing the complete cyber-fluidic system is a particularly difficult task due to the cross-domain integration challenges, the complexity introduced from the modularity, and the delicacy of the fluidic system. Even though module-level functional testing appears to be a straightforward task, bringing the system together to an operational state requires an extensive integration process. The complexity of the cyber-fluidic system is routed in its cross-disciplinary nature, evident from the range of competence required to fabricate the digital biochip coating, design and produce the droplet actuator, consider the mechanical and electronics aspects of the instrumentation system, originate a programming model, and carry out the extensive firmware and software development tasks.

A list of the primary functional testing and integration tasks are shown in Figure 6.1. Despite the apparent vertical separation, tasks tend to mix horizontally throughout the three system boundaries, namely fluidic, instrumentation, and virtual, creating intricate testing dependencies. An example of that is the essential function of droplet actuation that requires an electrodes driver module to be functional and properly connected to the digital biochip before an actuation command can be sent from the virtual system down to the electrode driver. Purposely built testbeds can be developed and employed throughout the functionality testing process, and although the benefits of this approach are recognized, creating additional test structures will inevitably add overhead to the already challenging timeframe of the project. Despite the more cumbersome debugging process, we ventured into laterally testing the functionality at module, subsystem, and system-level throughout the development, integration, and bring-up processes. The continuous development and integration approach supported growing our expertise and understanding of the functionality of the subsystems in conjunction with the full cyber-fluidic system. Certainly, this approach was more complicated due to the implication of working under multiple assumptions, but it allowed us to quickly advance to a stage where a partially or fully functioning system was present and used to aid the development of the digital biochip.

Testing of the virtual part of the system can mostly be performed in the absence of the physical system. Unit testing of the different software components, followed by integration and functional testing, is sufficient for examining most of the DMF Toolbox functionality. Even though a software simulator can be built to emulate the presence of the physical system, this will only confirm the correct implementation of the assumptions made while designing the simulator.

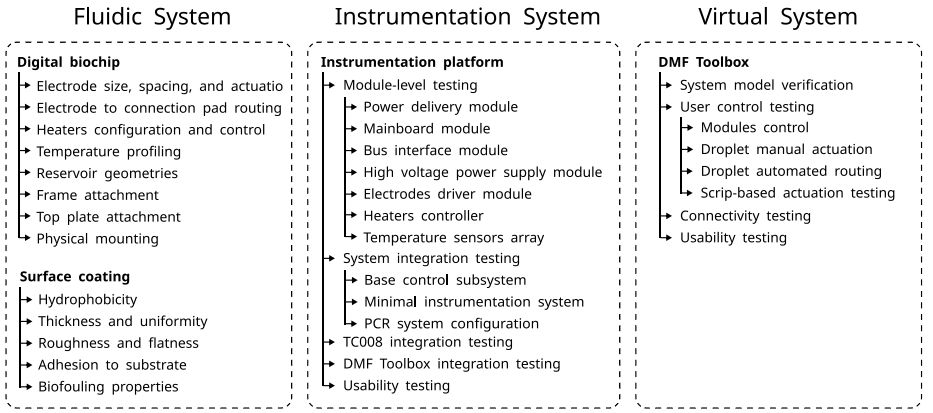

Figure 6.1: Testing consideration and dimensions.

Therefore, the full cyber-fluidic chain is required to verify the envisioned platform functionality, including the mapping of the operation model of the physical system to the virtual domain.

6.1.1 Module level testing

The components of the cyber-fluidic system have undergone functional unit, integration, and system-level testing. The instrumentation system modules have been continuously tested throughout the board bring-up process and the subsequent firmware development phase. The mechanical components have been checked for dimensional accuracy during the fabrication process, followed by assembly fitment with the electrodes drivers module and the TC008 parts. The functionality of the DMF Toolbox software has been continuously tested through the development process with the help of the built-in digital biochip simulator and textual logging.

Functional testing on a module level is a prerequisite for successful system integration. However, the effect of the non-functional properties of a given module on the complete system depends on the particular functionality. For instance, the base control subsystem comprises the power delivery, mainboard, bus interface, and user control modules, as discussed in Section 5.4.6. While the performance of the bus interface and the power delivery module is derived from their hardware design, the functionality of the mainboard is mostly determined by the firmware implementation. This presents the separation between the design and implementation performance properties of the cyber-fluidic system. A

combination of both is seen in the instrumentation modules, where the hardware and firmware implementation define the overall module performance.

Another critical aspect of the non-functional system testing is the boundary between the instrumentation and the fluidic system. While the mainboard carries out mainly virtual transactions, the instrumentation modules interact with the physical environment by monitoring or controlling physical properties. Performance profiling of response time, processing time, and throughput are applicable in the virtual and physical domains. Measurements in the physical domain are considerably more difficult due to the inevitable systematic and random errors induced by the measuring setup. A notable part of the cyber-fluidic system that required extensive testing relates to producing the temperature zones required for the PCR.

While a substantial part of the module, subsystem, and system-level bring-up is considered a trivial engineering effort, several major aspects of the integration and testing have been a central part of the work carried out in this thesis. The digital biochip design, fabrication, and testing are presented next since they are considered a fundamental part of the cyber-fluidic system. Another significant effort was to make the system capable of handling the PCR reagents and implementing the temperature control needed to carry out the reaction successfully. Therefore, the characterization of the thermal performance of the TC008, the heaters controller, and the temperature sensor interface module will be discussed in detail.

6.1.2 Subsystem level testing

A subsystem is considered any assembly of two or more modules performing a collaborative task. An example is the base control subsystem consisting of a mainboard, bus interface module, power delivery module, and an optional display module, as discussed in Section 5.4.6. Each of these modules has a functionality that can be verified through profiling and performance measurements, but that only confirms the proper stand-alone module operation. However, assembled as a part of a subsystem, different interferences can occur and affect the performance on a module and subsystem level. The complexity of the problem only grows with assembling the different subsystems into a full-fledged system. The loosely coupled modular architecture and the particular design of each module target mitigating integration problems already at a design level. Nevertheless, implementation-specific details can affect the overall system functionality, and therefore the subsystem level testing has been continuously performed through the development and implementation cycles.

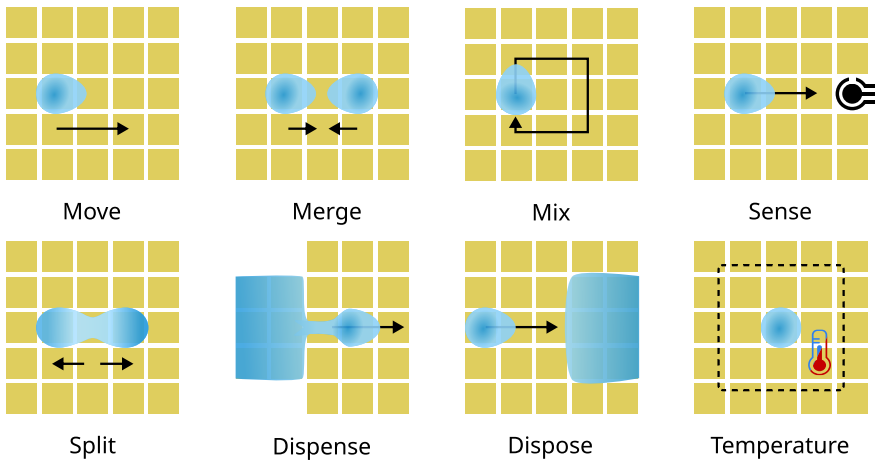

Figure 6.2: Fluidic droplet operations.

6.2 Digital biochip fabrication and characterization

Functional testing of the complete cyber-fluidic system can be performed only in the presence of a properly built digital biochip. A baseline functionality test is whether the platform is capable of performing a partial or the full set of the fluidic operations, as described in Section 2.3. The essential electrowetting droplet operations are move, merge, mix, split, dispense, and dispose, as shown in Figure 6.2. Additional functionality for sensing and temperature control can be integrated to support particular applications, such as the heating required for PCR. We recall from Chapter 2 that there are two types of digital biochips: an open configuration, where a droplet is placed and actuated on a planar array of actuation electrodes, and a closed configuration where the actuated droplet is located between the planar array of actuation electrodes and a top plate. The open configuration is the simplest of the two, but it does not allow for droplet splitting and dispensing. Despite these limitations, it is simpler to build and operate, and therefore it is used as a starting point for the cyber-fluidic platform testing before moving to the more demanding but capable closed system.

The design objectives and fabrication methods for the TC008 were presented at a conceptual level in Section 5.3. The discussion continued in Section 5.4, where the instrumentation system was developed to support the needs of the digital biochip. Due to the six-layer construction and the tight tolerances, the

fabrication of the TC008 was outsourced to a commercial PCB service. Three different batches of TC008 PCB boards were ordered during the period of this thesis work. The batches were based on the same design files and specifications, and for clarity, they will be referred to as B1, B2, and B3. The three batches B1, B2, and B3, were fabricated correspondingly on 1 March 2019, 28 August 2019, and 11 September 2019. As the first step of the testing process, we will characterize the fabricated TC008 PCB by evaluating the geometrical accuracy of the top electrode array and comparing it to the design specifications. The second major test considers characterizing the built-in heaters aiming to identify and quantify any deviations from the design specifications.

6.2.1 Electrodes array characterization

The main electrode array of TC008 consists of 640 electrodes organized in 32 columns and 20 rows, as shown in Figure 6.3a. To meet the 3.5/3.5 mil track width/spacing PCB fabrication capabilities, the pitch of the array was set to be 2 mm, with an electrode size of 1.91 mm×1.91 mm. This results in a gap size of 90 µm, which is larger than the minimum required 3.5mil or 89 µm. The vias in the center of the electrode were designed with the minimal allowed hole size of 0.2 mm in order to maximize the electrode area and decrease the surface disruption.

The physical size of the fabricated electrodes was measured for three PCBs from each batch. High-resolution photographs of the array were taken, and the measurements were carried out by using the image processing program ImageJ [133]. Five electrodes of each chip were measured in order to check and compare the dimensions of the electrodes in the four corners and the center of the array. The spatial resolution was calculated to be 1.1 pixels per 1 µm as the full array was captured in a single photo. The measuring scale was individually calibrated for each image based on a known distance on the PCB, namely the distance between the centers of two vias at the opposite corners of the electrode array. However, the relatively low spatial resolution and the random error introduced from the measurement process cause the performed measurements to provide indicative rather than definitive numbers.

A mean value for the electrode height and width was calculated where the two dimensions were given equal weight. The mean value for electrode height and width for B1, B2, and B3 was estimated to be correspondingly 1.89 mm, 1.885 mm, and 1.875 mm, showing the largest deviation from the designed 1.91 mm in B3. The standard deviation was calculated to be 13 µm, 15 µm, and 22 µm correspondingly for B1, B2, and B3. The maximum measured deviation from the designed electrode size was a maximum of 35 µm. The pitch between the

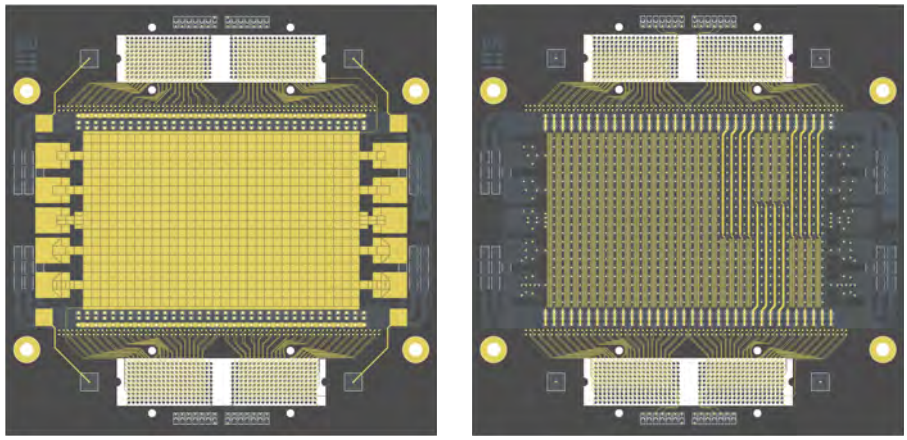

(a) TC008 electrodes array copper layer.

(b) TC008 heaters copper layer reveling the two different heater designs.

Figure 6.3: Exposed copper layers of the electrodes array and heaters layer. The heating structures are positioned between two columns of electrodes on a copper layer 100 µm under the top layer. A high-resolution version is available in the digital copy.

electrodes was measured to match the designed 2 mm. In contrast with the electrodes that are wet etched from a laminated copper sheet, the drilling of the holes for the vias is done with a computer-guided drilling machine, hence the satisfactory accuracy. The wet etching process is typically associated with several variables such as lithographic mask, exposure precision, etching time, etching solution strength, temperature, etc. Furthermore, PCBs are produced on panels with usable area up to 50 cm×60 cm, which can accommodate for up to 30 pieces of TC008. The fact that boards can be fabricated on different panels and on different locations on the panel is considered a contributing factor for the measured variations.

The lower electrode height and width directly translate to an increased gap size between the electrodes. By design, the gap is 89 µm, nonetheless, the gap was measured to be anywhere in the range 95-120 µm, which matches the reduced electrode sizes. Overall the electrode size was estimated to be consistently 15-20 µm less than designed, attributing the difference to variation in the fabrication process. With the increased gap size, it becomes more challenging for a droplet to be actuated from one electrode to another due to the disruption of the surface potential between the electrodes. Moreover, the wider and inconsistent gap potentially affects the accuracy of dispensing and splitting operations, and it is considered a source of random and systematic error. However, these effects

need to be studied further, and the TC008 can be used as a starting point for this evaluation.

6.2.2 Heaters characterization and testing

The TC008 has 32 resistive heaters embedded 100 µm into the PCB under the electrode array. Each heater is built as a copper structure consisting of 7 straight segments and connecting arcs. As previously discussed in Section 5.3.3.3 and Section 5.4.11, there are two different heater designs implemented on the TC008. The first heater type spans the full height of the electrode array, and it is built as 20 meander structures with a length of 285 mm each, as shown in Figure 6.3. The second heater type is organized into three groups of four heating elements, where each heater track is 113.5 mm long and spans eight electrode rows, as shown in Figure 6.3b. The heaters can be organized into eight heating regions by using solder bridges for configuration and connection to the power buses located on the bottom side of the PCB. For clarity, the two heater types are correspondingly referred to as HT1 and HT2.

The first step of the heaters characterization consists of measuring the resistance of each heater on three arbitrary selected PCBs from each batch. The measurements were performed with a 6.5 digit benchtop digital multimeter with a resolution of 1 mΩ. The 32 heaters on each PCB were measured three times in a sequence to reduce the random error introduced from the manual measurement process. The measuring procedure took several hours, and it was carried out at a room temperature of 24±0.5 °C. The results are shown in Figure 6.4, where the variation of the resistance can be compared within and between the three different batches. The first issue that becomes immediately evident is the wide variation of the heater's average resistance within a single batch. The standard deviation for B1, B2, and B3 is correspondingly 0.155 Ω, 0.728 Ω, 0.695 Ω for HT1, and 0.067 Ω, 0.245 Ω, 0.264 Ω for HT2. While B1 shows relatively low variations, B2 and B3 exhibit more than four times higher resistance tolerance than B1. This shows significant inconsistency not only between the different fabrication runs but also within each batch. Furthermore, the theoretical heater resistance at 24 °C is estimated to be correspondingly 3.10 Ω and 1.23 Ω for HT1 and HT2, but the measurements show average heater resistance more than twice the estimated value.

The individual heater resistance for the nine measured TC008 PCBs is shown in Figure 6.5, where for enhancing readability, the two types of heaters are plotted separately. Besides the measured value represented as a data point, the graphs also show the relationship between the heater location on the PCB and its value. While the data for B1 present the lowest standard deviation, from

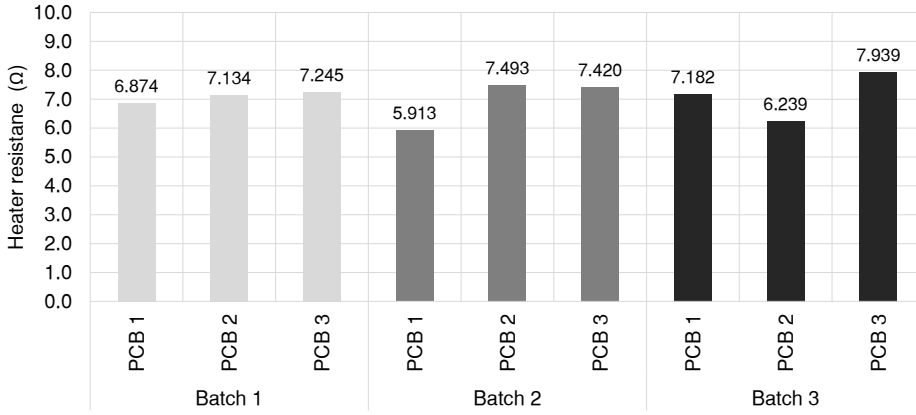

(a) TC008 HT1 L=285 mm

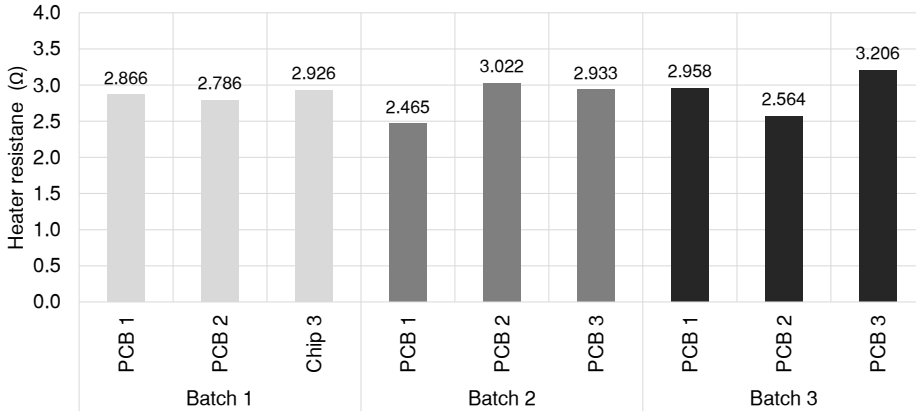

(b) TC008 HT2 L=113.5 mm

Figure 6.4: Average measured resistance for HT1 and HT2 for three PCBs from each batch. The data shows the resistance variation between the PCB from the same and among the batches.

Figure 6.5 becomes evident that the B1 and B2 exhibit the largest fluctuation in the resistance of the heater on a single PCB. However, B2 shows coherency throughout a single PCB, but it also exhibits a larger overall resistance difference between samples from the same batch, as shown in Figure 6.5c and 6.5d. The standard deviation for the PCBs within B1, B2, and B3 is correspondingly, 0.209 Ω, 0.082 Ω, and 0.132 Ω for HT1 and 0.106 Ω, 0.047 Ω, and 0.057 Ω for HT2.

Based on the average heater resistance on a PCB level, B1 appears to be the

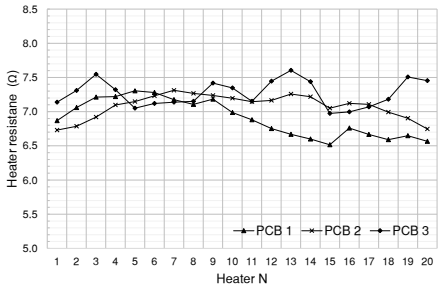

(a) B1 HT1 L=285 mm

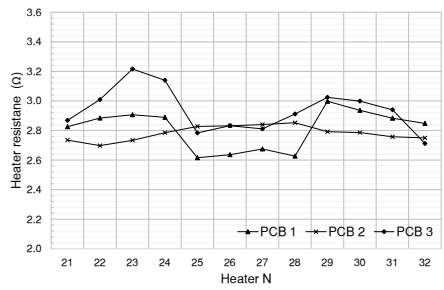

(b) B1 HT2 L=113.5 mm

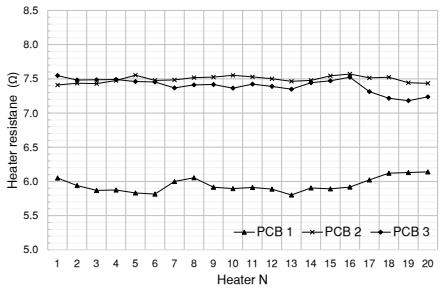

(c) B2 HT1 L=285 mm

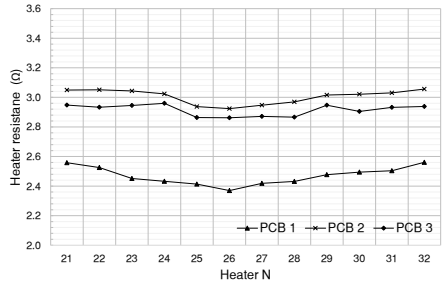

(d) B2 HT2 L=113.5 mm

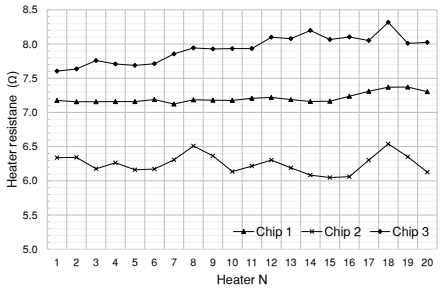

(e) B3 HT1 L=285 mm

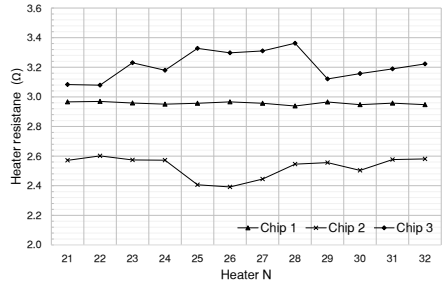

(f) B2 HT2 L=113.5 mm

Figure 6.5: Individual heater resistance for three PCBs from each batch. A high-resolution version is available in the digital copy.

most consistent of the three batches. However, regardless of the 1.58 Ω difference between the lowest and the highest average resistance on a PCB level, B2 shows the lowest standard deviation and thus the highest consistency among the heaters on a single PCB. The largest variability is presented in B3 with 1.70 Ω difference between the average resistance of HT1 on a PCB level.

Thus far, we have identified two types of errors: the deviation of the track resistance from the theoretically estimated value, and the resistance variation on a PCB and batch level. As previously discussed, the source of these errors is routed in the PCB fabrication process, and it relates to inconsistent process parameters. Another potential source of error is the purity of the copper sheets used to fabricate the PCB since impurities in the metal will change the specific electrical resistance of copper and consequently offset the resistance calculation.

The resistance of a conductor is determined by the electrical resistivity of the material that is made of, the cross-section area, and its length. Assuming uniform cross-section, the resistance of a copper heater track can be calculated by using equation 6.1:

$$R = \rho \frac{L}{A} \tag{6.1}$$

where L is the length of the copper segment, A is the cross-section area, and ρ is the electrical resistivity of copper, considered to be $1.68 \times 10^{-8}\,\Omega\,\mathrm{m}$.

The designed dimensions of the copper heaters are 89 µm×17.5 µm, which results in a cross-section are of $1557.5\,\mu\mathrm{m}^2$. The length of the HT1 and TH2 segments is correspondingly 285 mm and 113.5 mm and the estimated resistance for the two heater types is correspondingly $3.10\,\Omega$ and $1.23\,\Omega$ at 24 °C. Since the track length is likely to be a subject of insignificant variations, and the copper resistivity should remain fairly uniform over a single PCB area, we consider the variation in the copper track cross-section area to be the major source of error. Figure 6.6 shows the correlation between the measured heater resistance for HT1 and HT2 and how this resistance translates to the copper wire cross-section if we consider constant copper resistivity of $1.68 \times 10^{-8}\,\Omega\,\mathrm{m}$. By design, the cross-section area is expected to be $1557.5\,\mu\mathrm{m}^2$. Nevertheless, based on the measured resistance, the copper tracks cross-section varies in the range of 595-810 $\mu\mathrm{m}^2$ and thus results in higher resistance. We attribute this difference to variation in the fabrication process.

A known characteristic of the wet etching process is that the final cross-section of the copper track is closer to a trapezoid than a rectangle, as illustrated in Figure 6.7a. It is expected that the difference between the top and the bottom trapezoid bases equals the thickness of the copper layer leading to effectively reducing the track cross-section area by $153.5\,\mu\mathrm{m}^2$. The decrease of the area leads to an increase of the overall resistance, calculated to $3.44\,\Omega$ and $1.37\,\Omega$ at 24 °C. However, even the adjusted values show two times lower resistance than the actual measurement. The etching process can also lead to variation in track width along the copper wire length, as illustrated in Figure 6.7b. The width

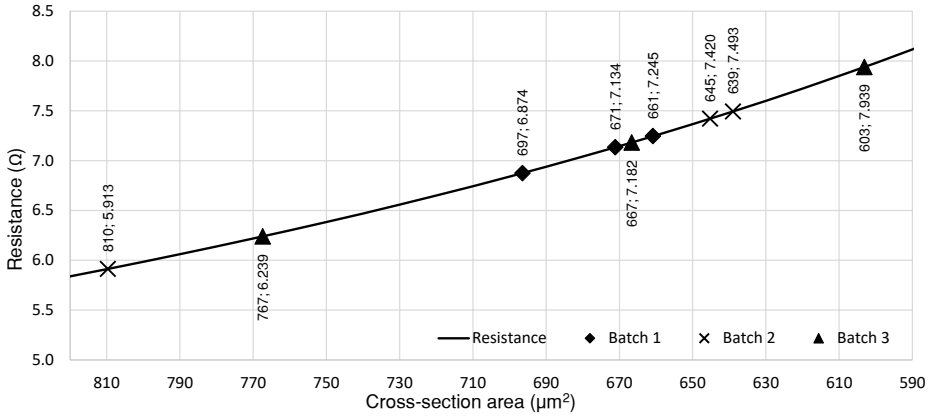

(a) HT1 L=2855 mm

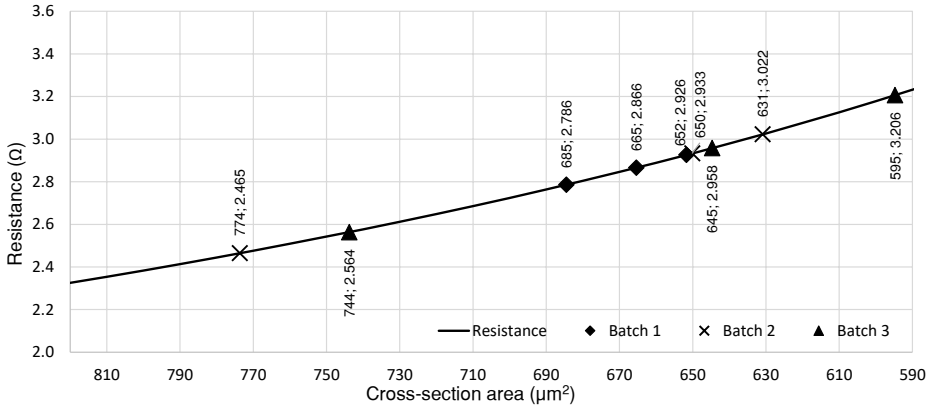

(b) HT2 L=113.5 mm

Figure 6.6: Heater resistance versus copper track cross-section area.

variation leads to a variable resistance along the length of the track due to the formation of local min/max cross-section regions. This irregularity will result in local variations in the produced energy when the copper wire is used as a heater.

To further evaluate the etching irregularities, a TC008 PCB has been cut across the heater tracks, revealing the etched copper profile, as shown in Figure 6.7c. The spacing between the copper segments was measured to be 190 µm, which matches the design specifications. The copper layer thickness measures at 18 µm, which is 0.5 µm thicker than the expected 17.5 µm. However, the track width was measured to be approximately 60 µm, resulting in a cross-section area of

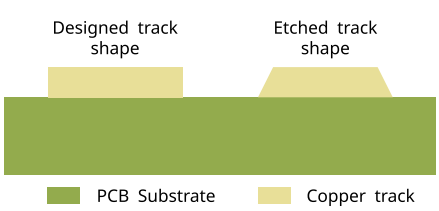

(a) Cross-section showing the designed vs. expected track shape.

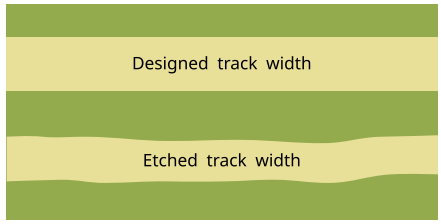

(b) Top view of the designed vs. expected track width.

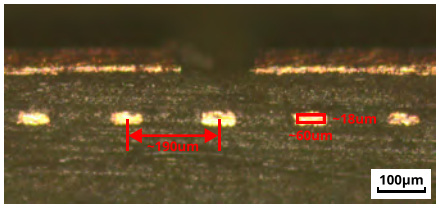

(c) Cross-section of the TC008 PCb showing the size and spacing of the copper heating tracks.

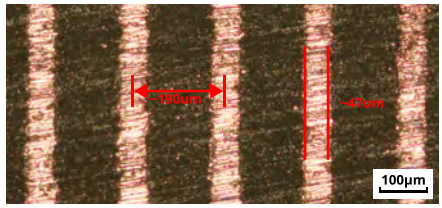

(d) Longitudinal photo of the heater tracks.

Figure 6.7: Designed and fabricated copper track profiles.

1080 µm^2 and estimated resistance of 4.56 Ω for HT1 and 1.82 Ω for HT2. Recalling from Figure 6.6, the estimated copper track cross-section area based on the measured resistance is 595-810 µm^2, and even though the 1080 µm^2 is relatively close, there is still a significant difference between the estimated and measured wire cross-section.

Further inspection of the PCB has led to the longitudinal picture of the resistive tracks, as shown in Figure 6.7d. The image confirms that the spacing between the copper track matches the designed dimensions, but reveals a track width of 47 µm resulting in a wire cross-section of 847 µm^2. This value is significantly closer to the previously estimated range of 595-810 µm^2. The fact that the longitudinal images showed a narrower track than the cross-section might indicate that the cross-section measurement overestimated the height and width of the copper segments. A more accurate method for PCB profiling needs to be found to provide accurate and consistent measurements. Nevertheless, it becomes evident that a better PCB fabrication process is needed to address the lack of consistency of the heater tracks. Impedance controlled PCB is considered as an alternative providing higher track geometrical accuracy.

Regardless of the deviations from the design specifications, the TC008 can serve

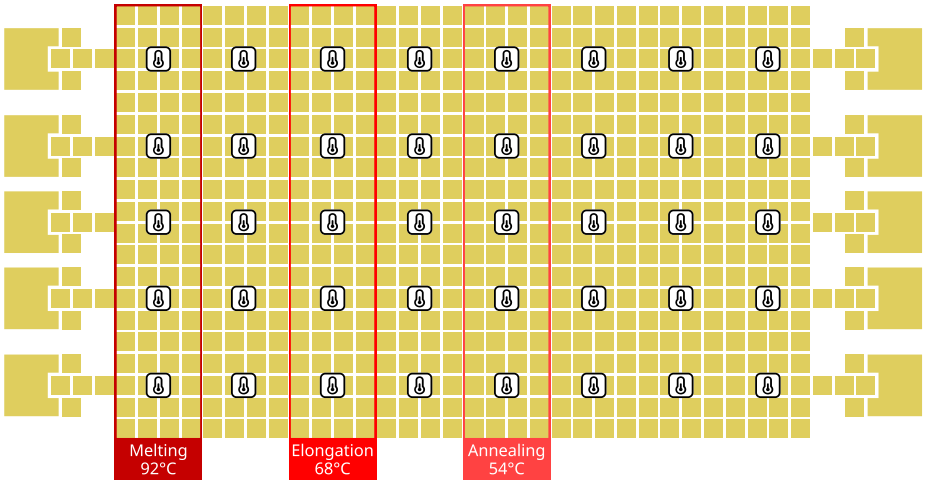

Figure 6.8: Temperature sensors alignment with the TC008 actuation electrode array. The tree temperature zones required for PCR are marked with red.

the purpose of a technology demonstrator. The smaller actuation electrode size might affect the actuated droplet volume, and the increased spacing between the electrodes might result in a higher actuation voltage. However, the heating tracks' resistance variation will require establishing a calibration procedure for every heating region, and it will be discussed next. Moreover, the high thermal conductivity of the copper will likely help mitigate any local temperature deviations resulting in a balanced thermal performance.

6.2.3 Heaters integration and calibration

The individual TC008 heaters can be configured to create up to eight different temperature zones. The heaters controller module presented in Section 5.4.11 is designed to control up to three temperature zones with the goal to fit the needs of the space domain PCR, as described in Section 6.4.4. Although the resistance of a single heater track was measured to be over two times higher than intended, the heaters controller module can function sufficiently with the overall increased heater resistance. However, a calibration step is required due to the presence of a significant resistance variation among the heaters on the same PCB, within a single batch and between the different fabrication iterations. The temperature sensors interface module presented in section 5.4.12 was designed to assist the calibration process and provide a real-time heatmap for the characterization of

the thermal response of the system. The measurement is performed by an array of 5×8 temperature sensors, as shown in Figure 6.8.

The test setup for temperature profiling was based on the minimal instrumentation system instance described in Section 5.4.10, further extended with the heaters controller module (see Section 5.4.11), the temperature sensor interface module complemented by the temperature sensor array (see Section 5.4.12), and an auxiliary fan providing a constant airflow under the digital biochip. A closed digital biochip configuration with 300 µm spacing was used for the calibration process since this particular arrangement was invented for the PCR experiment.

Three temperature zones were configured, and their location relative to the electrode array is marked in Figure 6.8 with red rectangles. Each temperature zone spans the full height of the electrode array, and it is four electrode columns wide. Four electrode columns separate the temperature zones acting as insulation buffer and decrease the thermal leakage. The temperature zones, TZ1, TZ2, and TZ3 correspondingly target to create the temperatures required by the melting, elongation, and annealing steps of the PCR. The temperature sensor array and the measurement interface module were used to measure and calibrate the temperature profile of each zone. A video frame sequence of the temperature ramp-up time is shown in Figure 6.9, where the TC008 is at room temperature of approximately 24 °C when the heating zones get activated. At time point zero (T0), the heat zones are activated, and 20 seconds later (T20), all three zones start warming up. The first zone to reach the set temperature is the annealing zone reaching the setpoint of 54 °C in about 70 seconds. The elongation zone reaches 68.5 °C in about 120 seconds, and the last to reach steady-state operation is the melting zone measuring close to 92 °C 140 seconds after the activation of the heaters.

The temperature registered on the heatmap sequence represents the actual temperature measured between the top and the bottom plate of the digital biochip. A different perspective on the heating process is shown in Figure 6.10, where the data for the ramp-up and the steady-state temperature of each zone is extracted from the heater control module. The first immediate discrepancy is the difference in the temperatures' setpoint - the graph shows a significantly lower steady temperature, especially for the melting zone. This is due to the uncorrected calibration values, i.e., the calculations in the heaters controller module have not been corrected to match the measured temperature. Instead, an offset value from the theoretically calculated temperature is used to establish the setpoint for each temperature zone. While the setpoint for the annealing and melting zones is fairly close to the calculated, the melting zone is offset by approximately 12 °C. The offset has not been addressed at this stage since the actual temperature is verified with the temperature sensor array in the context of the full biochip assembly.

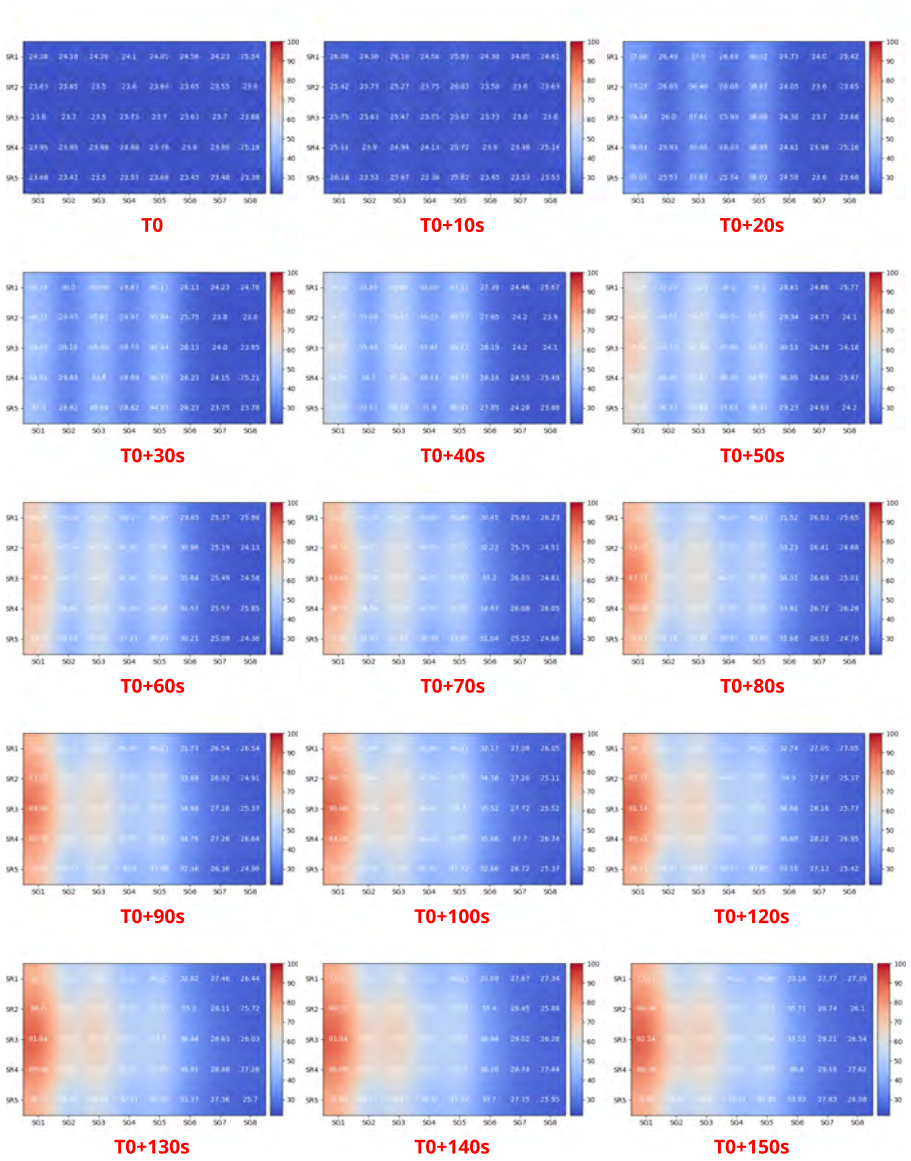

Figure 6.9: Heatmap video frames showing the temperature profile development over the TC008 electrode array. The temperature sensor array is used to simultaneously measure the annotated temperature points. "SR" and "SG" stand for sensor row and group followed by a numeric identifier. A high-resolution version is available in the digital copy.

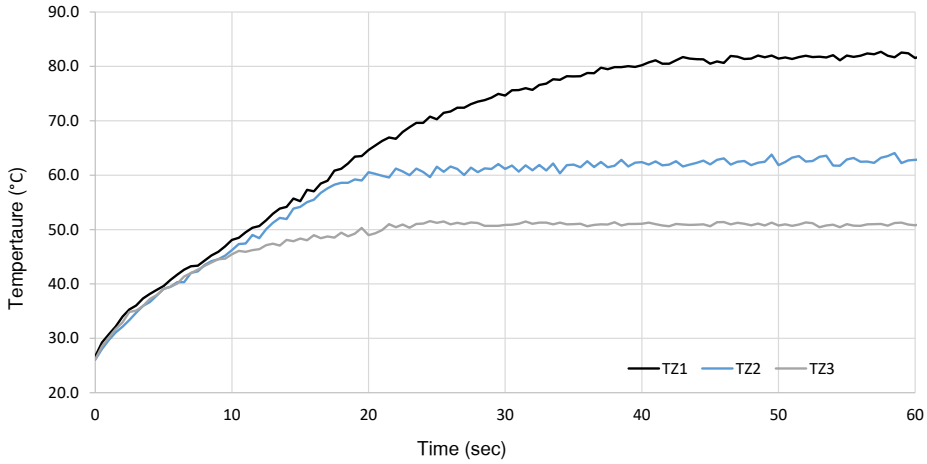

(a) Heating zone temperature ramp-up profile.

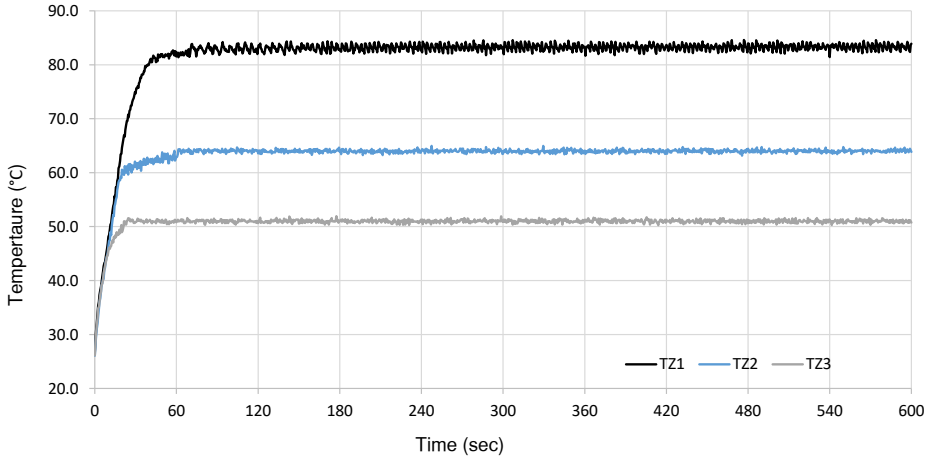

(b) Heating zone steady state temperature.

Figure 6.10: Heating zone temperature ramp-up and steady-state temperature. The graphs show the temperature measured from the heater controller module. There is a setpoint calibration offset between the measured and the actual temperature.

The second immediate deviation from the heatmap sequence is the faster temperature ramp-up shown in Figure 6.10a. According to the heater controller module, the three temperature zones reach their designated temperature in less than 60 seconds as opposed to the previously measured 70, 120, and 140 seconds. This discrepancy comes from the thermal coupling between the heaters and the

rest of the system, as well as the thermal mass and losses associated with each temperature zone. Nevertheless, the more realistic scenario is presented by the heatmap data due to the fact that the sensors on the temperature sensor array are subjected to the operation condition of a droplet actuated in a closed digital biochip. Despite the slower ramp-up time, the steady-state temperature remains within ±0.5 °C, as shown in Figure 6.10b.

The data shown is for a TC008 with three configured temperature zones where the HZ1, HZ2, and HZ3 have resistances of 24.88 Ω, 24.84 Ω, and 24.82 Ω respectively at 24 °C. The heaters controller module was supplied with 12 V for the calibration process. Considering the resistance of the heating zones and the minor power loss in the switching circuits, each heating region was producing approximately 5.5 W of heating power. However, the heaters controller module can be supplied with higher voltage, thus increasing the power delivery and accelerating the thermal response of the system.

The heatmap sequence presented in Figure 6.8 reveals an uneven heat distribution over the temperature zones. The higher the set temperature, the more steep the temperature gradient in the vertical direction. While the vertical temperature gradient over the annealing zones shows roughly 7 °C decline over 16 mm, the melting zone shows a twice higher drop of over 15 °C for the same distance. Using the data provided by this measurement, the temperature of each zone has been adjusted to deliver the set value across the central four rows of electrodes. This approach prevents exceeding the set temperature, and this is particularly important for the melting zone since some of the PCR reagents do not tolerate excessive heating. The effect of overheating the PCR reagents is further discussed in Section 6.4.5.

The uneven heat distribution is due to the extra thermal mass and interfacing in the peripheral area of the digital biochip. For instance, the connection pad area overlaps 25 mm with the electrode drivers assembly (see Section 5.3.3). This overlap creates a thermal interface that moves heat away from the heating zones, outwards to the electrode drivers, and naturally, this is one reason for the uneven temperature profile. This effect can be seen in the thermal images shown in Figure 6.11. Moderating the thermal gradient can be achieved by redesigning the heating structures inside the TC008 to provide a non-linear power delivery, embedding copper polygons helping distribute better the generated heat, or minimizing the thermal interface between the TC008 and the electrode drivers assembly.

The heatmap sequence shown in Figure 6.8 also displays the temperature gradient between the three heating zones. Four electrode columns separate the heating zones, and based on the presented measurements, the temperature between the zones rapidly drops, thus providing sufficient thermal separation. The

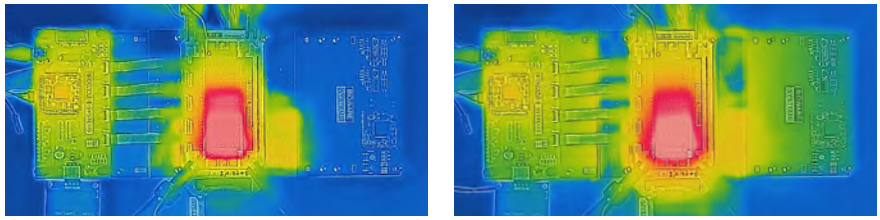

(a) Cooling fan on (b) Cooling fan off

Figure 6.11: The effect of the auxiliary fan on the thermal profile of the TC008 assembly. The blue color corresponds to room temperature of about 24 °C. When the fan is turned off, the temperature of the assembly rises with up to 10 °C above the ambient temperature.

width of four electrodes equals to 8 mm, and a sharp decline of over 15 °C can be seen between the melting and the elongation zone. Cooling the buffer zones is assisted by the auxiliary fan, which provides a constant airflow under the TC008 electrode array. Without the additional airflow, the system still reaches and sustains the designated temperature profiles, but a lower separation is observed between the heating zones. Furthermore, due to the firm mechanical assembly, TC008 has thermal contact with the electrode drivers and the supporting fixtures. This leads to unnecessary thermal leakage from the heating zones to the surrounding modules. The constant airflow produced by the fan has a cooling effect over the whole setup, as it can be seen in Figure 6.11.

Despite the uneven temperature distribution, the current thermal design shows a stable and reproducible performance. After calibration, the central four electrode rows overlapping with the heating regions show a uniform temperature profile that is considered sufficient for performing PCR. The temperature gradient compromises the usable area on the digital biochip, but a refinement of the design of the heater holds the promise to deliver more confined temperature regions. A notable characteristic of the embedded heaters approach is that once the system reaches a steady-state, the control loop manages to keep the temperature within the setpoint limit without overshooting. External disruptions are quickly detected, and the system recovers promptly.

6.2.4 Coating fabrication and testing

The electrowetting droplet actuators require a hydrophobic insulation layer between the actuation electrodes and the controlled droplet. As previously discussed in Section 5.3.4, we have focused on implementing a cost-effective, sus-

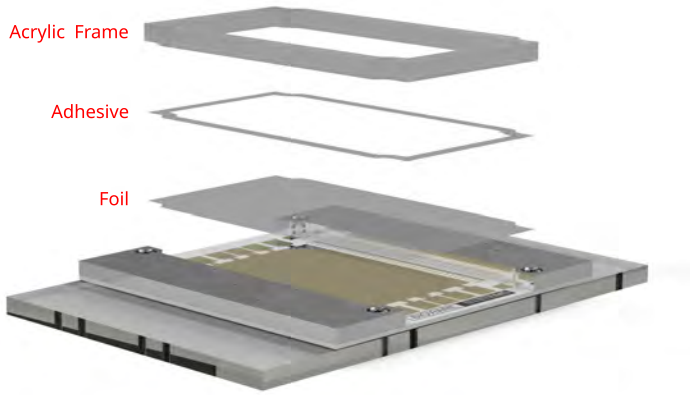

Figure 6.12: Foil-frame assembly.

tainable, and scalable fabrication method for the fluidic system. Therefore, to minimize the amount of disposable waste, we have developed a foil frame-based coating approach, where the TC008 PCB is reused between experiments, and only the foil frame is replaced. The foil coating also provides a planar surface for the droplet actuation by effectively spanning over the trenches between the electrodes. A top plate for the closed system was prototyped from an ITO coated microscopic glass slides, or ITO coated PET.

The construction of a foil frame is shown in Figure 6.12. The main components are a laser-cut acrylic frame, dual-sided pressure-sensitive adhesive, and the foil itself. Three different types of foils were empirically tested throughout this thesis work, namely stretched Parafilm, LDPE, and PTFE. The Parafilm was stretched to 6-8 µm and showed reliable droplet actuation in an open and closed digital biochip configuration. The LDPE foil had thickness of 5 µm, and it was used only for closed configuration digital biochips. Two different thicknesses, 5 µm and 8 µm of the PTFE, were successfully tested in a closed digital biochip configuration. Droplet actuation was achieved with as low as 120 V, and control voltage in the range of 140-200 V was routinely used in the experimental work discussed later in the chapter.

The foil-frame fabrication process consisted of first applying the foil to a holder fixture and then transferring it to the acrylic frame. The purpose of the holder fixture was to ensure uniform pulling tension that keeps the foil tightly stretched before applying it and adhering it to the foil frame.

The top plate fabrication was based on the conventional spin coating of fluoropolymers. Three different materials were tested for the fabrication of the top plate, 2% wt/wt solution of Teflon AF, and the commercially available PFC1101V-FS and PFC1601V-FS. The spin coating profile was set for 30 s at 1000 RPM with 50RPM/s ramp-up speed. After the spin-coating cycle, the top plate was placed for 30 min on a preheated to 160 °C hot plate in the case of ITO glass, and 100 °C in the case of ITO PET.

The spacing between the top and the bottom plate was ensured by the use of spacers made of three types of PCR tape with different thicknesses. It was empirically found that the closed digital biochip configuration operates with gap size in the range of 200-800 µm, where the lower spacing favors dispensing and splitting operations.

The digital biochip was tested in the open configuration on the Parafilm foil and in the closed configuration on all three coating types. The Parafilm coating approach provides a low cost and easy solution for digital biochip fabrication, but it is not suitable for high-temperature applications since the melting point of the Parafilm is close to 60 °C. The Teflon foil is the most temperature and chemically stable of the three, and thus it is the best candidate for digital biochip fabrication for the PCR experiment.

The fluidic manipulation operations shown in Figure 6.2 were tested on the minimal instrumentation system instance (see Section 5.4.10). The tests were performed under manual droplet control and by the use of scripted electrode actuation sequences. Actuation frequencies up to 10Hz were used to transport droplets in an open and closed system configuration successfully. The effective droplet volume for the open configuration was in the range of 10-50 µL and for the closed configuration ranging from 1.5-10 µL. The closed system was successfully tested with and without filler fluid. Silicone oil with viscosity 1cSt or 5cSt was used as a filler fluid.

6.2.5 Platform level testing

Platform level testing spans across the three system domains and exercises the full system integration. The functionality of the DMF Toolbox, the instrumentation, and the fluidic systems were tested and evaluated before proceeding to implement and perform any biochemical assays. Functionality such as adjusting the electrode control voltage, electrode mapping between the virtual and the physical representation of the digital biochip were subject to control measurements and extensive empirical testing. The platform instance used for this test is shown in Figure 6.13, where the top part of the Figure shows the DMF

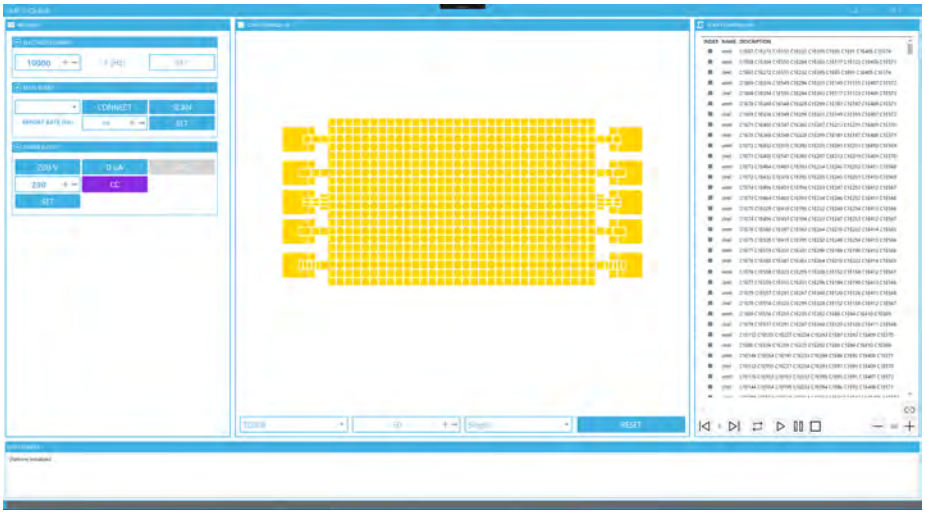

(a) TMF Toolbox

(b) The minimal instrumentataion system instance

Figure 6.13: Heaters controller module, connection adapter board, and exploded view of the adapter board and TC008 assembly.

Toolbox user interface, and the bottom part shows the instrumentation platform with mounted TC008.

Platform-level testing is an iterative process since the functional and integration testing needs to be conducted after the addition of a new module. For example, the heaters control module was not developed at the time of integration testing of the minimal instrumentation system instance. The module was added later in the process when the basic fluidic operations were already established, and the application focus had shifted towards the PCR experiment. The same

applies to the temperature sensor interface module, which was developed for studying the temperature response of the system. Both modules required the development of new control software, firmware, and hardware, which naturally required platform-level integration and testing.

6.3 Application testing

A platform-level application testing was carried out by performing three laboratory assays, namely PCR DNA amplification and two magnetic-beads based enzymatic immunoassays. The experiments were designed and carried out with the primary purpose of demonstrating the fluidic handling capabilities of the modular cyber-fluidic platform developed throughout this thesis work. As it will become evident later in the discussion, experimental conditions were found to be sufficient, although some happen to be suboptimal. Optimization of the experimental conditions is considered to be out of the scope of this thesis work and left for future work. Nevertheless, the three outlined experiments serve the purpose of successful capability demonstrators for the developed cyber-fluidic platform.

The PCR experiment was designed and performed in collaboration with DTU Biosustain and DTU Bioengineering. The experiment is considered the first step in implementing a basic Escherichia coli (E. Coli) cloning procedure on the cyber-fluidic platform and as a part of a larger project called the "Magic Box". The project is supported by the Novo Nordisk Foundation, and it aims to implement an automated strain development by using the cyber-fluidic platform presented in this thesis work. The PCR protocol, reagents, expertise, and consultancy through the design and test phases were provided by Iben Møller-Hansen, Ksenia Chekina, and Irina Borodia from DTU Biosustain. In the final PCR testing stage, Ágnes Kovács Lendvai from DTU Bioengineering contributed to the process with theoretical guidance and practical assistance. The research and development related to making the cyber-fluidic system PCR ready, including the design, fabrication, and operation of the digital biochip, is considered a significant part of this thesis work.

The two enzymatic immunoassays were considered capabilities demonstrators of the developed cyber-fluidic platform, where the platform was reconfigured to accommodate the new experimental requirements. The two assays were part of the regular research activities at the NaBIS group at DTU Bioengineering, and they were designed and prepared by Susan Ibi Preus from DTU Bioengineering. The first assay targets the detection of an MRSA protein, and it is further discussed in Section 6.5.1. The second assay targets the detection of SARS-

CoV-2 protein, and it is addressed in Section 6.5.2. Performing the assays on the digital biochip was supervised and assisted by Susan Ibi Preus. The two assays were successfully adapted from their benchtop equivalent and performed completely on the digital biochip. Demonstrating the enzymatic immunoassays on the platform is considered an important technology demonstrator of the versatility of the digital microfluidic technology and the presented cyber-fluidic platform.

6.4 PCR as a part of a cell cloning protocol

A significant part of the effort through this thesis work was directed towards making the cyber-fluidic platform capable of performing PCR on the digital biochip. Although the PCR is exciting and significant by itself, it was rather considered to be the first step towards achieving full cell cloning on the platform and thus extending the cyber-fluidic capabilities of the platform into the biological domain. The cell cloning, or molecular cloning, is a three-step process: first, assembling a recombinant DNA fragment by using PCR; second, the DNA segment is put into a plasmid serving as a cloning vector; and third, a transformation step where the cloning vector is transformed into a living cell. This three-step process creates genetically modified cell factories, where the cell metabolic processes are altered to produce molecules of interest. We envision the cyber-fluidic platform can be developed to a powerful and easy to use instrument for automated cell programming.

6.4.1 The PCR outline

Polymerase chain reaction (PCR) was invented in 1984, and it has grown into an instrumental method for manipulating DNA samples. The PCR is used to exponentially amplify low-concentration DNA segments, making millions to billions of copies in a matter of hours. In its classical form, the PCR reactants are: forward and reverse single-stranded nucleic-acid fragments called primers, DNA polymerase, DNA nucleotides, and a DNA template. In practice, the DNA polymerase and nucleotides often come as a premix called a master mix (MM), containing all components required by the reaction, except the two primers and the DNA template. The use of a master mix streamlines the PCR preparation process by reducing the hands-on time, risk of contamination, and variation in the final mix. The PCR is performed by thermocycling the final mix through to three elevated temperatures. The technique is robust and routinely used in clinical laboratories and biomedical research.

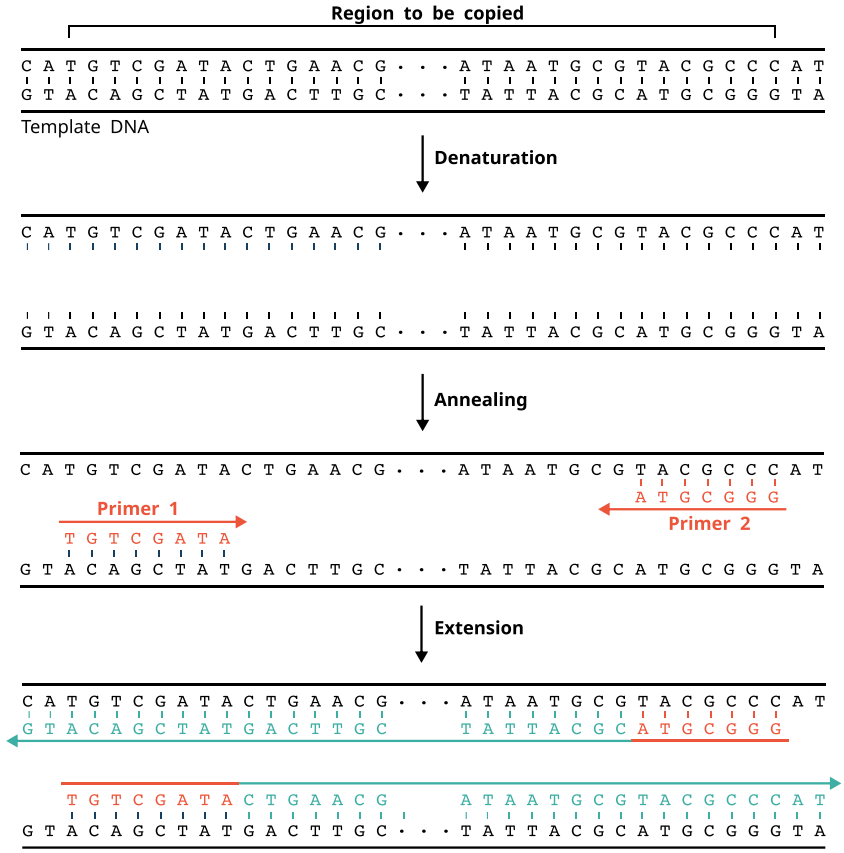

(a) Single PCR cycle. Typically repeated 20-40 times

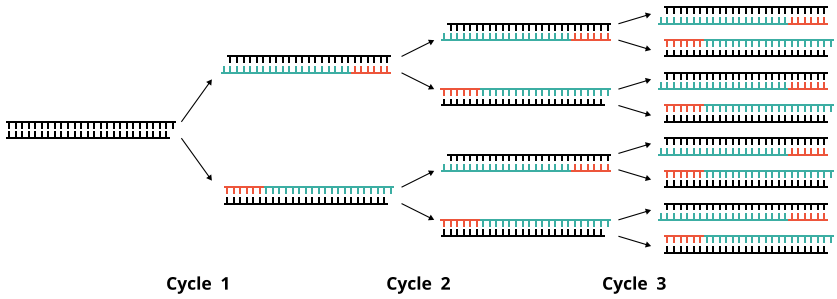

(b) DNA amplification process. The newly created DNA segments are used as templates in the next cycle.

Figure 6.14: Illustration of the PCR DNA amplification. Each amplification cycle doubles the number of DNA segments.

The DNA is composed of four nucleotides called C, G, A, and T, where a base pair can only be formed from an A-T or C-G bond. These four nucleotides and the two possible bonds form the double-stranded DNA used as template DNA for initiating a PCR. The process is illustrated in Figure 6.14a, where the three main steps, namely, denaturation, annealing, and extension, are shown. However, the typical PCR procedure requires two more steps, initialization, which is performed prior to the denaturalization step, and final elongation, performed after the last amplification cycle. Next, we will discuss the practical aspects of each step of the PCR.

Initialization: this step is typically used for heat activation of extremely thermostable polymerases. When this step is included in the PCR procedure, it is usually called a hot-start PCR due to the heating of the sample to 94-98 °C for several minutes before the beginning of the thermocycling. The destructive character of this step serves the purpose of sample preparation for the annealing of the primers.

Denaturation: as the name implies, in this step, the sample is heated to 90-98 °C for 20-30 seconds, which causes breaking the bonds of the double-stranded DNA and producing two single-stranded DNA fragments as shown in Figure 6.14a. This process is also known as DNA melting, and the temperature at which takes place is subject to application-specific optimization.

Annealing: is the step where the forward and reverse primers are annealed to the single-stranded DNA to mark the beginning of the regions to be copied. This process is illustrated in Figure 6.14a, and it typically requires the sample to be kept at 50-65 °C for 20-40 seconds. This step of the process is highly temperature-sensitive, such that proper temperature ensures that the primers will bind specifically to the designated area. A lower temperature might result in an incomplete binding, and contrary, if the temperature is too high, the primers might not bind at all.

Extension: this step is the last one from the typical PCR cycle, and it reconstructs the DNA area from the annealed primer to the end of the single-stranded DNA template. A new complementary strand is synthesized at a temperature of 70-80 °C, and the required time ranges from seconds to several minutes. The used polymerase dictates the exact reaction temperature, and the reaction time is determined based on the used polymerase and the length of the copied segment. Under optimal conditions, the number of copies of the amplified DNA target sequence doubles, leading to an exponentially growing number of copies after each denaturation-annealing-elongation cycle, as shown in Figure 6.14b. After 30 successful PCR cycles and starting with a single DNA template strand, the final number of copies of the replicated region is expected to be over one billion.

Final elongation: this step typically constitutes the end of the PCR cycling program, and it serves the purpose of a prolonged extension cycle, allowing for any remaining single-stranded DNA to be fully reconstructed. The sample temperature is typically kept at 70-75 °C for 5-10 minutes.

A robust and reliable experiment was prepared to serve as a test case to develop the PCR functionality on the cyber-fluidic platform. A green fluorescent protein (GFP) was selected for amplification, and the outcome of the reaction was quantified by gel electrophoresis. The quantification method relies on separating the negatively charged DNA fragments in an agarose gel using an electric current. The shorter fragments travel further in the gel while the longer ones experience more resistance from the pores of the gel. The result of running gel electrophoresis on a DNA sample manifests as grouping the DNA fragments into a ladder-like structure, where each band falls in a particular base-pair length. The outcome of the amplification step is assessed by the intensity and the size of each concentration band. In the case of a successful PCR, only a high-intensity band matching the length of the amplified DNA segment should be present in the gel.

6.4.2 The PCR protocol

The reagents used for the PCR protocol were forward and reverse primers correspondingly PR-24445 and PR-24446, DNA template p1976, and OneTaq®2X. The mixing ratio for 15 µL PCR mix is 6.25 µL H_20, 7.5 µL OneTaq®2X, 0.5 µL PR-24445, 0.5 µL PR-24446, and 0.25 µL p1976.

The initial prescribed temperature program starts with 98 °C for 60 s, followed by 30 cycles of 98 °C for 20 s, 52 °C for 30 s, and 72 °C for 60 s. The PCR finishes with a final elongation step of 72 °C for 5 min. The result of the reaction is evaluated by running the sample through gel electrophoresis.

The materials for the PCR experiments were routinely prepared by Iben Møller-Hansen, and she was responsible for analyzing the PCR by gel electrophoresis. In the final PCR testing stage, reagents preparation was carried out as a part of this thesis work, and Ágnes Kovács Lendvai performed gel electrophoresis.

6.4.3 Space and time-domain PCR

In the early days, the PCR was performed by manually moving the PCR samples between three preheated water baths. Each sample was placed in an open

container that was partially submerged into the preheated liquid, thus resulting in rapid thermal cycling. This approach was used because the initial DNA polymerases were not thermally stable, and the enzymes were virtually destroyed after each melting cycle. This required the laborious and tedious process of adding new enzymes to each PCR sample at the end of each amplification cycle. However, as the research continued, new thermostable DNA polymerases were developed, consequently allowing the PCR reaction to be performed without adding new enzymes after each cycle. The use of a thermostable DNA polymerase simplified the PCR process and led to the wide adoption of the already established thermocyclers. A thermocycler is a machine based on a temperature-controlled metal block to which PCR tubes containing the samples are attached. The machine rises, lowers, or keeps constant the temperature of the block following a preprogrammed sequence, hence performing the PCR thermocycling in an automated manner.

The preheated water bath method and the modern thermocyclers outline two different techniques for performing PCR. The water bath method implements a space domain PCR where the sample is passed between three individual temperature-controlled zones. In this case, the temperature ramping speed depends on the thermal mass of the sample, water baths, and the thermal properties of the container. On the contrary, the thermocycling method implements a time-domain PCR, since the sample is stationary and the temperature changes as a function of time, i.e., the thermal block is heated or cooled. Since the time-domain method is associated with larger thermal mass, e.g., the metal block in comparison with the typical $<100\,\mu L$, this approach, in general, is associated with slower temperature ramps and longer running time. The thermal interface between the metal block and the reaction tube has an impact on the ramping temperature speed inside of the reaction tube as well.

Both time and space domains PCR are feasible in the context of digital microfluidics. However, if conventional Joule heating is used for temperature control, the cooldown cycle will significantly extend the PCR cycle time, unless forced cooling is used. However, the space domain PCR appears to bring the advantage of rapid temperature ramping time, since the thermal mass associated with a typical droplet is relatively low compared to the digital biochip. The space domain PCR method used as a part of this thesis work is shown in Figure 6.15a, and the TC008 is visualized in Figure 6.15b. Three temperature zones are configured on the TC008, where each zone is four columns wide, and there is four column spacing between the zones. The temperature zones are ordered such that a droplet can follow the annealing-extension-melting PCR cycle. The temperature zones are also ordered based on their temperature, where the melting zone is the hottest, and the annealing zone has the lowest temperature of the three. This arrangement helps reduce thermal leakage and supports overall temperature management.

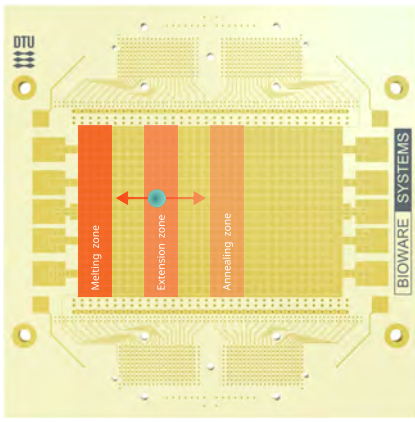

(a) Illustration of space domain PCR on TC008.

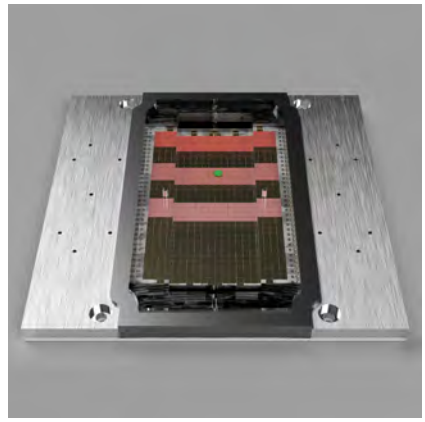

(b) Rendering of TC008 configured for space domain PCR.

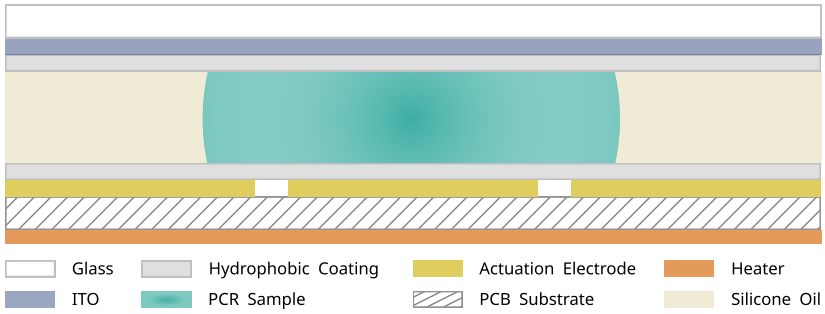

(c) Cross-section of oil filled closed digital biochip.

Figure 6.15: Space domain PCR on TC008.

The PCR uses elevated temperature where the protocol outlined in Section 6.4.2 suggests DNA melting at 98 °C, a temperature very close to the boiling point of water. The high temperature and the relatively long cycles inevitably lead to sample evaporation. The evaporation reduces the amount of the final product and up-concentrates the sample reagents, i.e., the reduction of water content leads to a decreased overall volume and increased concentration. The evaporation effect can be reduced by using a closed digital biochip filled with an immiscible fluid [134]. Silicone oil is often used as a filler fluid between the top and the bottom plates in a closed system, as shown in Figure 6.15c. The oil encapsulates the droplet, thus reducing evaporation. Additionally, the formation of a thin oil layer prevents the droplet from getting in contact with the top and the bottom surface, consequently aiding the actuation and minimizing the effect of biofouling.

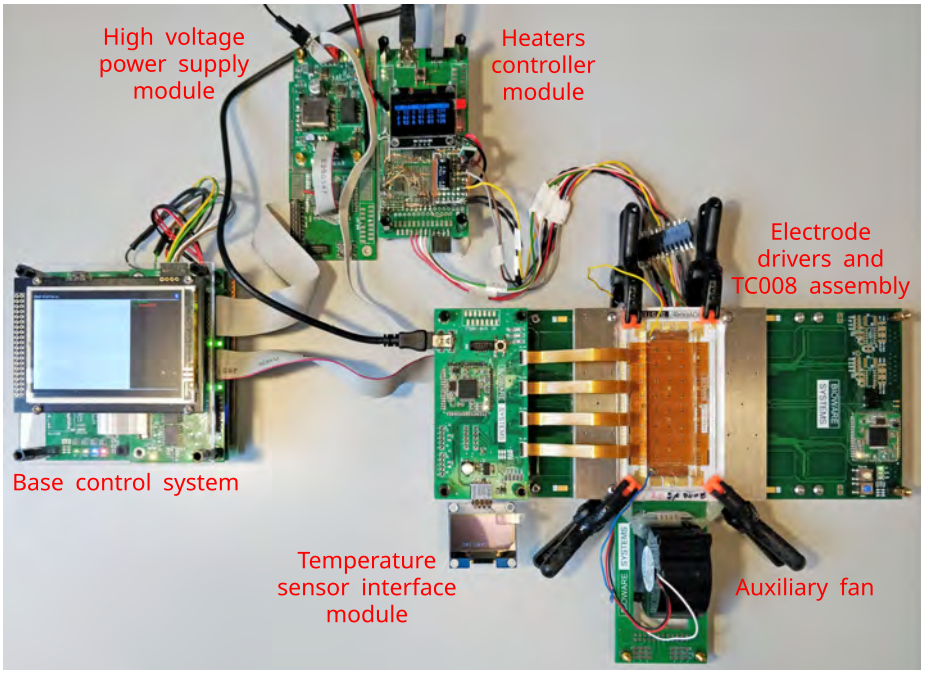

Figure 6.16: Instrumentation system instance for performing PCR. The temperature sensor array and instrumentation modules are mounted as well. The temperature sensor array is removed when performing PCR.

6.4.4 On the digital microfluidics PCR journey

The seemingly straightforward process of running PCR on a digital biochip hides a wide range of challenges. Accurate micrometer-scale temperature measurement, proper thermal design, sample evaporation, bubbles formation, biofouling, and toxicity are among the topmost issues encountered on the journey for performing a successful PCR on our cyber-fluidic platform. Only careful consideration of all of these factors (and likely many others) can lead to a PCR capable digital biochip. Instead of presenting immediate solutions, we will outline the PCR troubleshooting process that has been a significant part of the practical laboratory work carried out as a part of this project. The description of the debugging process is used to emphasize the significant discrepancies between the virtual and the physical domain and underline the practical challenges associated with the otherwise seemingly easy procedure of running PCR on a digital biochip.

The instrumentation system instance used for the PCR experiments is shown in Figure 6.16, and it consists of the minimal instrumentation system instance discussed in Section 5.4.10, with the addition of a heaters controller module and an auxiliary cooling fan. A single premixed droplet of the PCR reagents was loaded on the digital biochip at the beginning of each PCR experiment (see Figure 6.15a). The droplet was loaded in the annealing zone and transported along the digital biochip center line for 30 cycles following the melting, annealing, and elongation cycle. Droplet actuation was controlled manually from the DMF Toolbox through the 30 PCR cycles. The product of each performed PCR was run through gel electrophoresis to evaluate the efficiency of the DNA amplification.

6.4.5 The initial PCR tests

The digital biochip was configured in a closed configuration as described in Section 6.2.4 and shown in Figure 6.15c. The used filler fluid was 5cSt silicone oil. The temperature of the three temperature zones was verified by contact temperature measurement without the top covering plate. The measuring setup is shown in Figure 6.17, and although the measured temperatures were aligned with the expected temperature profiles, the first PCR experiments yield no result. Excessive droplet evaporation was observed, and the initial green color produced by the OneTaq® 2X polymerase changed to light brown color throughout the thermal cycling. Additionally, delamination of the hydrophobic layer of the top ITO cover was observed on a few occasions. The delamination occurred on the top of the melting zone, which is expected to be the most heated area of the digital biochip. The PCR sample discoloration and the hydrophobic layer delamination suggested overheating as the most probable cause of these two irregularities.

Determining the temperature inside the closed digital biochip under normal operating conditions, e.g., the presence of the filler fluid, used materials, spacing, and temperature profile, appeared to be of critical importance. However, temperature measurements inside of the digital biochip appeared to be a challenging task mainly due to the 300 µm spacing between the bottom and top plates. The need for accurate temperature measurement inside the filler fluid where the PCR sample resides triggered the development of the temperature sensor array and the corresponding interfacing module, as outlined in Section 5.4.12. With the in situ measurement method, it was concluded that there is a significant difference between the contact temperature measurement without the presence of the top plate and the temperature profiling carried out inside the channel of the closed digital biochip. While the open system contact temperature measurement showed a melting temperature of 94.1 °C, the in situ measurement

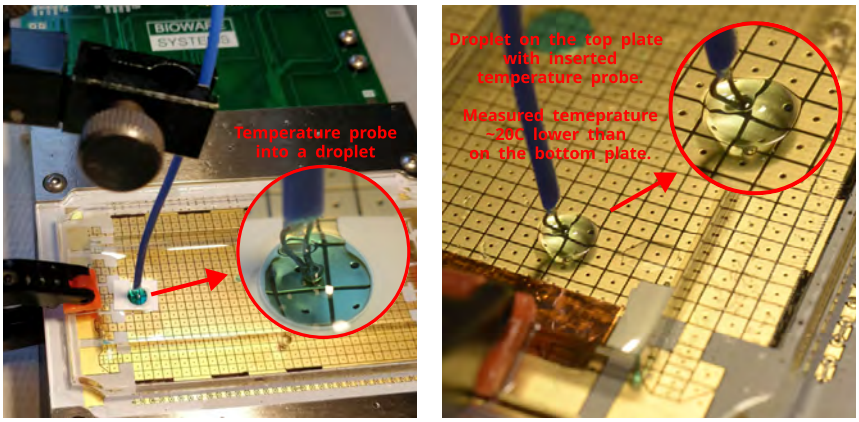

(a) Bottom plate. **(b)** Top plate.

Figure 6.17: Contact temperature measurement. A high-resolution version is available in the digital copy.

registered temperature as high as 101 °C. The overheating in the melting zone was responsible for the excessive sample evaporation, discoloration, hydrophobic layer delamination, and, last but not least, destruction of the polymerase enzyme.

Contact temperature measurement showed that the temperature on the top plate is roughly 20 °C lower than the measured on the bottom plate. The lack of heating of the top plate produces a temperature gradient inside the PCR sample, and although in situ measurement, the temperature can be accurately calibrated, the effect of the temperature gradient inside the droplet remained unknown. Therefore, before performing more PCR tests, the effect of the potential formation of a temperature gradient was evaluated through a series of PCR tests.

6.4.6 The temperature variation test

The effect of temperature variation from the melting, annealing, and elongation setpoints was studied with three PCR experiments performed in a commercial thermocycler. Each of the three PCR tests focused on altering the melting, annealing, and elongation temperature by ±5 °C from the temperature specified in the protocol listed in Section 6.4.2. Eight samples were used for each of the three PCR experiments, where the thermocycler was programmed to deliver a temperature gradient across the samples. The melting temperature gradient

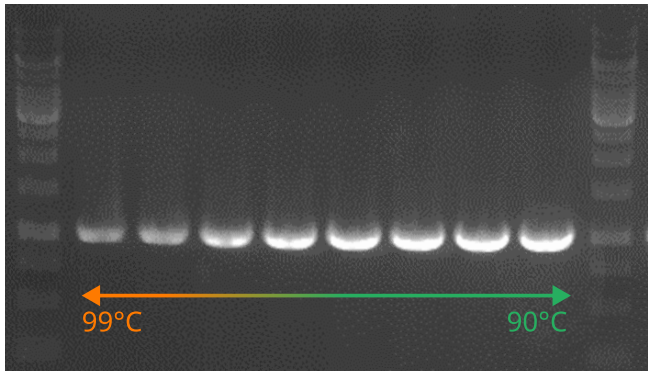

(a) Varying the melting temperature.

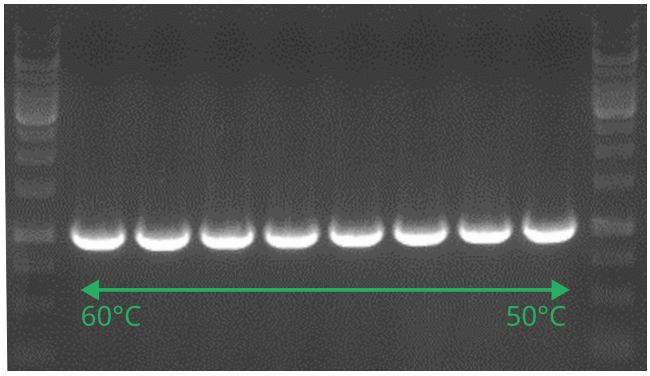

(b) Varying the annealing temperature.

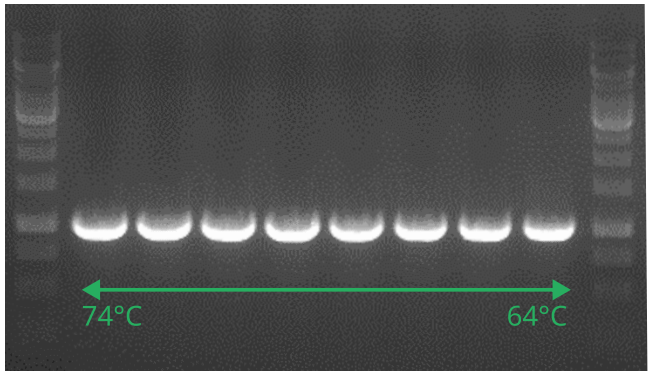

(c) Varying the elongation temperature.

Figure 6.18: The effect of varying the melting, annealing and elongation PCR temperatures.

was set to be in the 90-99 °C to avoid reaching the boiling point of pure water. The annealing temperature gradient was programmed in the 50-60 °C, and the elongation in the 64-74 °C range. Each of the three PCR experiments was programmed to vary only one of the three temperature steps, thus insulating the effect of the other temperature steps.

The amplified PCR product from the three experiments, a total of 24 samples, was run through electrophoresis gel to analyze the efficiency of the reaction. The ladder used as a marker had a concentration of roughly $140\,\mathrm{ng\,\mu L^{-1}}$. The results are shown in Figure 6.18. Varying the melting temperature shows the most significant effect, where temperatures over 96 °C appear to inhibit the PCR, as it becomes evident from Figure 6.18a. This effect is attributed to destroying the polymerizing enzyme when exposed to extreme temperature and the consequent ineffective reconstruction of the newly created DNA copies. Higher temperature will likely result in even more severe inhibition and bring the amplification to a hold.

Varying the annealing and melting temperatures showed no adverse effect on the amount of amplified DNA material. However, this test targetted providing a rough qualitative assessment of the effect of temperature deviation rather than a quantitative measure. Furthermore, it proved the failed initial PCR tests hypothesis, namely that the reaction is inhibited by temperatures higher than 96 °C.

6.4.7 The toxicity investigation

After examining the in situ temperature profile of the system with the use of the temperature sensor array and an interface module, the TC008 was calibrated to ensure proper temperature profile along the centerline of the electrode array. Nonetheless, the followed PCR experiments yielded no results, even though the sample overheating problem was eliminated. The next step of the debugging process was to evaluate whether some of the materials used for building the TC008 and get in contact with the PCR sample are inhibiting the reaction. In order to do that, a series of toxicity tests were carried out, where the material in question was tested for inhibiting the PCR.

The materials in immediate contact with the sample are the bottom foil separating the actuation electrodes from the sample, the top plate hydrophobic coating, and the filler oil. However, considering imperfections in the coating film, the ITO layer om the top plate can potentially contact the PCR sample. Furthermore, for connecting the top plate to ground potential, copper tape was used to establish an electrical connection with the ITO layer. The copper tape

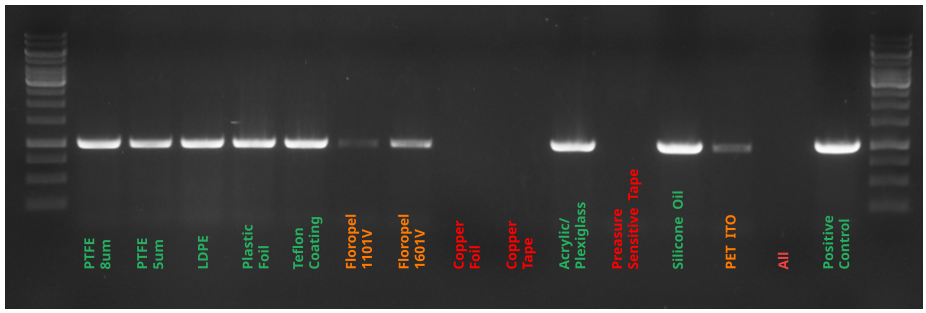

(a) Test group one.

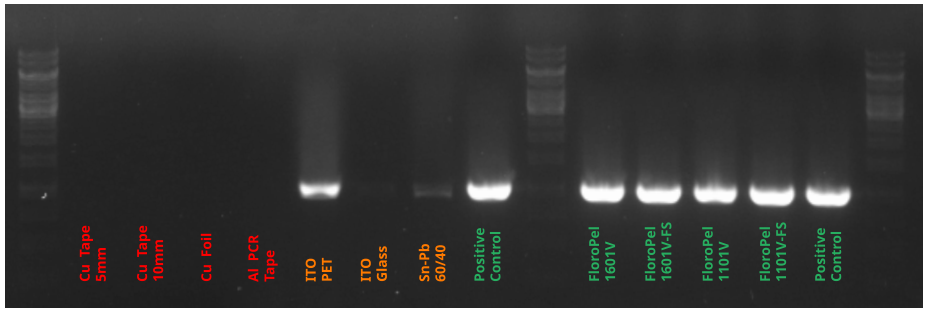

(b) Test group two.

Figure 6.19: Materials toxicity test. The green color indicates a lack of reaction inhibition, orange indicates moderate inhibition, and red indicates severe toxicity.

is submerged in the silicone oil, and in an extreme case, the PCR sample can touch the copper. Leaded solder was used for soldering a wire to the copper tape, and even though a direct contact between the solder joint and the PCR sample was considered unlikely, the solder wire was included in the toxicity test.

Other materials that can get in direct contact with the PCR sample are the acrylic foil frame and the pressure-sensitive dual-sided adhesive used to attach the foil to the acrylic frame. All of the materials mentioned above were tested for PCR inhibition by placing a small sample of the material into a PCR tube, filling the tube with a PCR mix, and running the samples on a commercial thermocycler. The results are shown in Figure 6.19, where the band intensity is used as an indicator for an inhibition effect. A bright and dense line shows a strong amplification where the denser the color, the higher the concentration of the amplified DNA segment. In contrast, a faint band reveals reaction inhibition provoked by the tested material. The results are color-coded with the text used to label the corresponding bands, where the green color indicates a lack

of reaction inhibition, orange indicates moderate inhibition, and red indicates severe toxicity.

Two separate tests were carried out to repeat and increase the number of tested materials. Evaluating the data from Figure 6.19a shows that the PTFE and LDPE foils, as well as the Teflon coating, are inert and have no inhibiting effect on the PCR. The two FoloroPel samples were deposited on ITO PET and then immersed into the PCR mix. The two samples showed interference with the PCR, but the presence of the ITO likely caused the inhibition since the ITO PET sample showed inhibition as well. Therefore, the FloroPel hydrophobic coatings test was repeated, such that the coating was applied on the inner side of the PCR tubes, thus eliminating the potential effect of the ITO. The repeated test data is shown in Figure 6.19b, and it shows no reaction inhibition, hence confirming the hypothesis that the ITO was the source of inhibition in the first test. Another strongly inhibiting material turned out to be the copper tape and the 60/40 solder. However, the inhibition only occurred if the PCR sample was in direct contact with the metal surface. This was tested attempting to contaminate a silicone oil sample by submerging the two metal samples and then checking the toxicity of the oil sample. The test showed negative results meaning that the inert silicone oil did not get contaminated from the contact with the otherwise incapable metals. Our finding of the inhibiting effect of ITO and metals were aligned with previous reports on PCR compatible materials [135].

The acrylic used for the foil frame proved to be inert in contrast with the dual-sided pressure-sensitive adhesive, which showed strong reaction inhibition. However, it was concluded that the inhibition effect is present only when the PCR sample gets in direct contact with the adhesive. Therefore, it was concluded that ensuring a uniform hydrophobic layer on the top ITO plate and careful handling of the PCR sample should ensure suitable conditions for performing PCR on the digital biochip.

6.4.8 Polymerase biofouling

Several unsuccessful PCR experiments were performed following the temperature calibration and the material toxicity study. The outcome of each run was showing a lack of amplified target DNA regardless of the supplementary top plate heating, confirmed temperature profile, and the accurate handling of the sample. However, closer observation of the droplet mobility through the 30 PCR cycles showed that the droplet path in the melting and elongation zone gradually developed a tendency to resist and adhere the PCR sample to the surface. This effect usually became noticeable between the 10-th and the 15-th PCR cycles. The deterioration of the droplet mobility over the actuation path

suggested surface absorption of molecules from the PCR mix. The absorption resulted in decreased hydrophobicity of the top and the bottom surfaces and led to difficult droplet actuation. Moreover, surface absorption also affected the concentration of the different reagents, possibly leading to reaction starvation.

A literature survey pointed to a study about Taq enzyme absorption on different surfaces [136]. The study identified two types of surface absorption - propagating absorption, which continues until all of the absorption material gets bound to the surface, and a contained absorption, where the absorption is time-invariant after the initial material retention. The study addressed various materials, including glass, polyamide, polyethylene, Teflon, and Parafilm. The polymerase absorption effect was considered an inhibiting factor, especially in the context of space domain PCR, where the sample travelled over a considerable area.

Two different tests were designed to evaluate the effect of surface absorption and possible reaction inhibition from the ITO layer. The first test included loading and transporting a 10 µL PCR mix droplet on the digital biochip and the second test covered keeping the droplet stationary with applied electrode actuation voltage for a specified time. Both types of tests were performed in a closed digital biochip configuration at room temperature. The samples were collected and put into a commercial thermocycler to undergo amplification for 30 cycles. The PCR product was then run on gel electrophoresis to evaluate the efficiency of the reaction. Four top plates were used in this experiment - two made of ITO glass and the other two made of PET ITO. Each top plate was coated with FlouroPel 1601-FS, where plates 1 and 3 were coated with a single layer of the hydrophobic material, and plates 2 and 4 were coated with three layers. The bottom foil frame was made of Teflon foil, and it was reused for the four experiments.

The dynamic absorption experiment consisted of loading a PCR mix droplet on the chip and transporting it one time over the digital biochip center line, effectively traveling 128 mm over 64 actuation electrodes. The second dynamic test used another PCR mix droplet, which was transported for 20 full cycles along the digital biochip centerline. The stationary tests were carried out as loading a droplet onto an activated electrode, closing the digital biochip, and allowing the droplet to sit stationary for 15 minutes. Each stationary test was carried out twice at 150 V and 300 V actuation voltage. The test procedure was repeated four times for each new top plate, resulting in 16 PCR samples that were further amplified on a commercial thermocycling machine.

The test results are shown in Figure 6.20, where the first digit of the sample label denotes the top plate number, followed by "C" and the number of cycles, or "S" and the electrode actuation voltage. The data is essentially divided into four groups, and it follows the preparative pattern on a droplet undergone a single

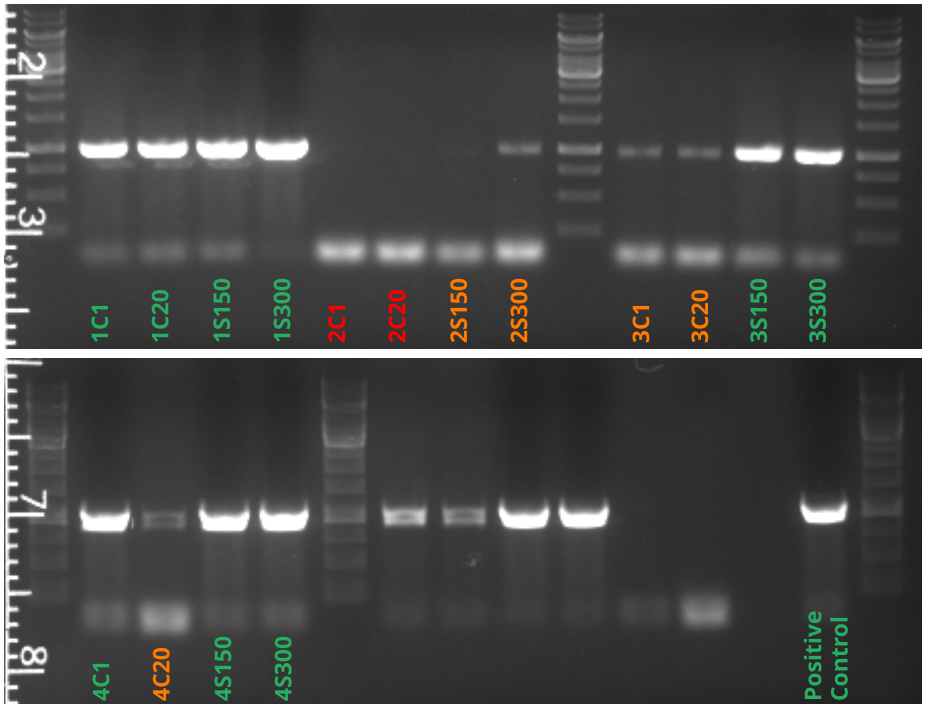

Figure 6.20: OneTaq® 2X polymerase surface absorption test data.

cycle, twenty cycles, 15 minutes stationary at 150 V, and 15 minutes stationary at 300 V. The presented data is somehow counterintuitive and inconclusive, but it clearly indicates an absorption issue. The first four samples show no signs of inhibition, regardless of the expected severe inhibition due to the fact that the bottom foil surface was not exposed to the enzyme yet, and the single-layer coated ITO glass top plate. In contrast, the second four samples show excessive inhibition, although the three layers separate the ITO coating and the sample. The stationary sample at 300 V, namely 2S300, shows a small amount of amplified DNA.

The third test batch shows reaction inhibition in the 3C1 and 3C20 samples, but a fair amount of amplified DNA for the two stationary samples. The similar results for 3C1 and 3C20 are counterintuitive as it was expected that the longer the PCR sample travel on the surface of the digital biochip, the higher the absorption should be. The last batch of four samples reveals mixed results where the 4C20 sample shows reaction inhibition, but the other three samples from the batch display a good concentration of amplified DNA.

The surface absorption test did not lead to conclusive results, and unfortunately, due to the limited timeframe of the project, it was not possible to repeat the experiment. The main argument against the validity of the test is the fact that if ITO has an inhibiting effect on the reaction, the first and the third batch should have exhibited higher inhibition due to the single-layer coated on the top plate. In contrast, bathes two and four used top plates coated with three layers of a hydrophobic material, theoretically providing better encapsulation of the ITO layer and minimizing the inhibition effect. Furthermore, the reuse of the bottom foil and the actuation area for the droplets should have shown a high surface absorption for the first batches, followed by surface saturation and lower absorbance. However, the first batch samples showed a lesser amount of reaction inhibition followed by almost complete inhibition in the second batch and somehow reduced inhibition in the consequential tests.

Another indicator of suboptimal reaction conditions is the presence of primer-dimers, displayed as faint bands aligned with the bottom of the ladder, as it can be seen in Figure 6.20. The primer-dimers are small fragments of DNA, usually shorter than 50 base-pairs, erroneously assembled and amplified. Their formation can lead to exhausting the primers and polymerase, thus inhibiting the amplification of the targeted DNA sequence. The formation of primer-dimers can be due to inaccurate concentration of primers, the PCR master mix components, or the reaction temperature. Although the possibility for inaccurate temperature on the digital biochip exists, the samples were amplified in a commercial thermocycler, thus certainly excluding the temperature as a factor and attributing the formation of primer-dimers to improper concentration caused by surface absorption.

To verify the surface absorption leading to depleting the initial concentrations of reagents in the PCR mix and consequential reaction inhibition, an experiment where concentrated OneTaq®^{2X} polymerase was added throughout the thermocycling. The purpose of the experiment was to test whether the polymerizing enzyme was binding to the surface as it was discussed in prior research [136]. Three PCR runs were performed, namely P20, P21, and P22, with a controlled variation of the experimental setup. The first experiment was carried out on 5 µm LDPE coated with FloroPel 1601V and top plate ITO glass coated with FloroPel 1601V-FS. The second and third experiments were carried out on 5 µm PTFE and top plate ITO glass coated with 1% wt/wt PTFE.

To prevent the potential depletion of the polymerizing enzyme, the PCR sample was systematically spiked with 0.25 µL of OneTaq® 2X. Sample P20 was subjected to 40 cycles, and it was spiked on cycles 7, 17, and 30. Sample P21 was used as a control, and it was subject to 30 cycles without any polymerase spiking. Sample P22 was a subject of 30 amplification cycles with polymerase spiking at cycles 7, 17, and 25. The PCR products of the three samples were run

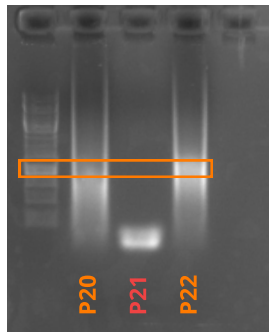

Figure 6.21: PCR sample spiking with Taq enzyme polymerase. The orange rectangle marks the region of interest corresponding to the amplified DNA sequence length.

on gel electrophoresis, and the results are shown in Figure 6.21. The polymerase spiked samples P20 and P22 showed a smear throughout the full height of the ladder while sample P22 revelled no band at all. Notably, the smear showed the highest concentration at the targeted for amplification DNA segment length.

While the results presented in Figure 6.21 does not manifest a properly working PCR, the experiment made evident the problem of surface absorption of the polymerizing enzyme. The two spiked samples showed significant, although unspecific, amplification, in contrast with sample P21, which only produced a significant amount of primer-dimers. The lack of amplification specificity can be attributed to the heavily offset reagent ratios due to the polymerase spiking and the sample evaporation. The comparison between the intensity of the band produced by samples P20 and P22 also suggests that the different materials, FloroPel 1601V and Teflon, can potentially exhibit a different level of biofouling.

The surface absorption can be reduced by surfactant and blocking additives to minimize the contact between the sample and the surface [136]. However, due to the limited scope of the project researching and experimenting with the additive options was considered future work. Moreover, the OneTaq® 2X has green dye additives for producing the distinctive green color, which was hypothesized to be part of the biofouling problem. Furthermore, the property formula of the master mix prevented identifying other potential ingredients that might have an effect on the biofouling properties. Therefore, testing different and possibly simpler master mixes was considered the next step of the PCR debugging process.

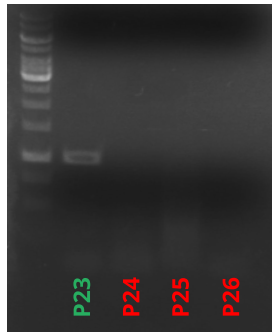

Figure 6.22: Sample P23 presents the successful PCR.

6.4.9 The successful PCR

After eliminating temperature inaccuracies, gaining an understanding of material toxicity, and identifying surface absorption as a strong reaction inhibitor, it was decided to test two other polymerase master mixes, DreamTaq PCR Master Mix 2X and Phusion High-Fidelity DNA Polymer, as a substitution to the OneTaq® 2X. The DreamTaq appears to be designed for high reliability and throughput, while Phusion focused on high fidelity.

Both DreamTaq and Phusion polymerases were tested under identical experimental conditions in four separate PCR runs. The first two experiments were performed with DreamTaq master mix and the second two with Phusion. Experiment one and three were not utilizing top plate heating, while experiment two and four were using top plate heating. The presence and absence of the top plate heating aim to vary the temperature profile and observe for any subsequential effects. All four experiments were performed on 5 µm PTFE foil and Teflon coated ITO glass top plate.

Four PCR reactions were performed on the digital biochip, and the results were studied by processing the PCR products by gel electrophoresis. A picture of the gel is shown in Figure 6.22, where P23 and P25 are DreamTaq samples, and P24 and P25 are Phusion samples. Top plate heating was used for samples P25 and P26. Subjectively, the PCR master mixes with DreamTaq and Phusion polymerase were easier to transport on the digital biochip without significant degradation of the droplet mobility throughout the 30 cycles. The noticeable lack of surface adhesion was considered a positive indicator for reduced surface absorption, which is also supported by the successful amplification of sample P23.

The products of the P23 reaction show nominal DNA concentration and a small number of primer dimers, which is an indication of a successful reaction. The other three samples yielded no results except for sample P25 showing a slight smear towards the bottom of the ladder and thus indicating that even though unsuccessful, some amplification took place and resulted in DNA segments longer than the 30-50 base-pair primer dimers. DreamTaq yielded at least one successful reaction. However, the reason for P26 to produce no result considering the theoretical better temperature profile due to the top plate heating remains unclear. Due to the limited time frame of the project and the partial results, the PCR investigation was not continued further. Although the experimental conditions require further refinement, achieving a successful PCR reaction on the digital biochip was considered a sufficient proof-of-concept for the fluidic handling capabilities of the cyber-fluidic platform.

6.4.10 PCR challenges and discussion

The sections above summarize the debugging process undergone towards achieving a successful PCR on the cyber-fluidics platform. The seemingly straightforward process of loading and moving a droplet of a PCR mix appeared to be associated with a range of unforeseen challenges, namely, achieving proper temperature profiles, materials compatibility, surface absorption, sample evaporation, and bubbles formation.

Achieving precise and repeatable temperature profiles was the first encountered difficulty. It was considered a purely engineering challenge that although presenting the problem of reliably measuring temperature and this microscopic scale, finding a feasible solution was a technicality. Building the temperature sensor array and acquiring two dimensional in situ thermal images in real-time was an instrumental part of calibrating the temperature zones on the TC008. Furthermore, the temperature sensor array allowed for verifying the thermal design, its performance deficiencies, and recognizing the need for reiteration of the design of the heater.

Although no clear distinction between reaction inhibition due to material toxicity and polymerase surface absorption was established, the clear relationship between materials' properties and PCR inhibition was identified. Placing a PCR mix in direct contact with metals and an ITO yielded inhibition, as well as surface adhesion. In Section 6.4.8, we conducted two empirical experiments related to biofouling and listed pointers to previous studies regarding polymerase surface absorption. By substituting the OneTaq® 2X polimerise with DreamTaq PCR Master Mix 2X, a successful PCR reaction was performed. However, this substitution probably does not fully mitigate the effect of surface absorption,

and likely, surfactant and blocking additives are required to achieve reliable PCR on the digital biochip. The reagents used for preparing a PCR mix should also be evaluated, and better methods for studying the surface absorption should be established. Besides the additives, different surfaces or coatings need to be investigated to determine potential compatibility with the PCR reagents.

Sample evaporation presented a significant challenge for performing PCR on the digital biochip. The effect of evaporation is nearly inevitable since close to 50% of the PCR mix content is water, as described in Section 6.4.2. Although the PCR mix droplet is fully submerged in silicone oil, the sample is subjected to sustained temperature over 70 °C and periodically reaching over 90 °C. The conducted experiments showed that a typical PCR cycling on the digital biochip takes on average 1.5 hours and leads to evaporating more than 50% of the starting 10 µL droplet. The evaporation effect not only shrinks the physical footprint of the droplet, but it also changes the concentration of the PCR reagents. The footprint reduction can lead to droplet volume lower than the feasible transport droplet unit size, thus losing actuation capabilities. The evaporation of over 50% also concentrates the PCR mix by a factor of two, which might affect the efficiency of the reaction.

The evaporation problem has been addressed in previous studies, where, for instance, a just-in-time droplet replenishment has been proposed as a solution to the evaporation problem [52]. This approach requires an external actuator dispensing replenishing solution through a port on the bottom plate of the chip. Although feasible, this solution significantly complicates the construction of the droplet actuator and require an external pressure source. Another research suggests reducing the actuation voltage and degassing the silicone oil to reduce the evaporation and consequential bubble formation issues [134]. It is also suggested that the reduced voltage lessens the effect of surface absorption. However, according to our subjective observations reducing the actuation voltage or degassing the silicone oil produced no observable effect on the droplet evaporation and bubbles formation. Another method for reducing the evaporation relies on replacing the filler silicone oil with hexadecane [137] [138] and thus providing better encapsulation of the droplet.

Among the listed issues, the most challenging to address remains the bubbles formed due to the sample evaporation. The severity of the bubble formation problem is shown in Figure 6.23, where the expansion of the bubble due to sample evaporation is presented as video frames over a period of 25 seconds. The experimental setup consisted of a 10 µL PCR mix droplet positioned over the melting temperature region at 92 °C. The first frame already shows the bubbles formed from the previous heating cycle. Over the course of 5 seconds, the two small bubbles on the right side of the sample nearly double their size. The difference between the first and last frames shows that the bubbles have

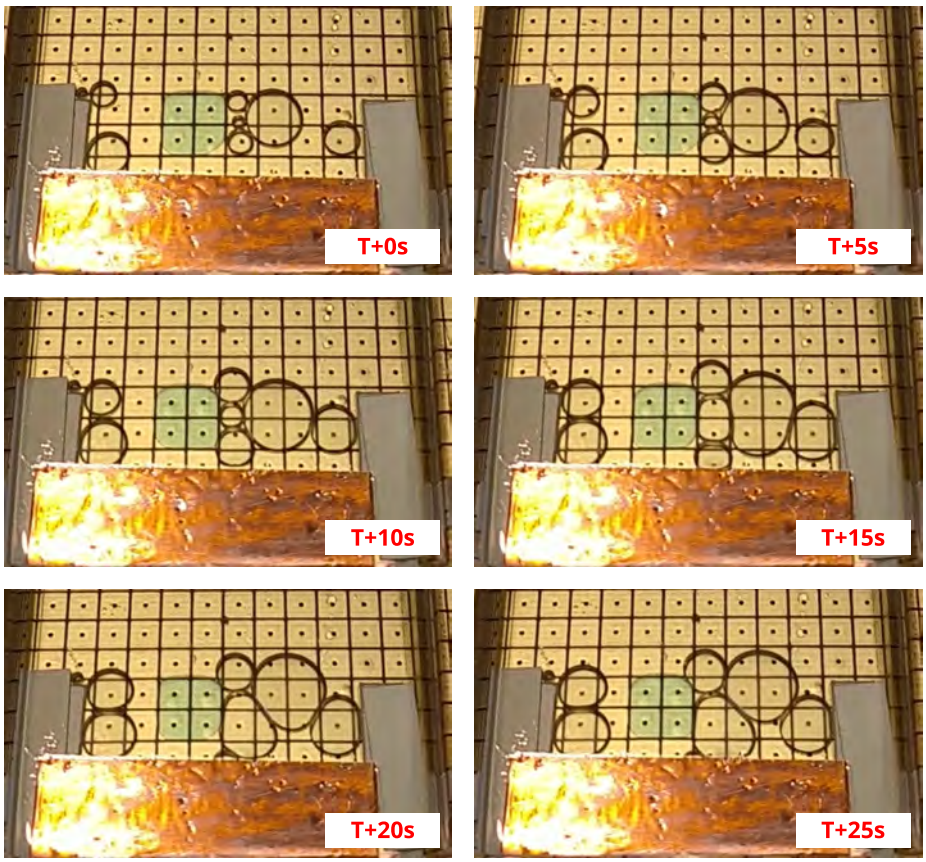

Figure 6.23: Video frames showing bubble formation due to PCR mix evaporation. The PCR mix is placed in the center of the melting temperature zone at 92 °C.

grown in footprint, covering a significant portion of the melting heating zone.

The formation of bubbles in the digital biochip can affect the fidelity or even completely prevent droplet actuation. If a droplet gets surrounded by medium to large bubbles, it can get blocked, thus halting the entire experiment. Moreover, it was observed that when a droplet is in contact with a gas bubble, e.i., there is a liquid-to-gas interface, subjectively, evaporation happens at a higher rate compared to a droplet entirely surrounded by oil. We have also observed that the evaporation rate appeared to be also reduced by using top plate heating. Nevertheless, eliminating the sample evaporation and bubble formation appears to be a nontrivial task. In our experience, the top plate of the system had

to be lifted periodically to allow for the bubbles to escape. Another approach for bubbles discharge is by creating a sloping cavity ending with venting ports on the top plate, as demonstrated in [134]. Potentially, the boiling point of water can be increased by pressurizing the digital biochip and performing the PCR reaction at elevated pressures. However, such an approach will inevitably complicate the experimental setup and make user interaction with the system cumbersome.

Debugging of the biochemical aspects of the PCR experiment proved to be a particularly difficult task due to the lack of the equivalent of probing and measuring tools routinely used in the field of microelectronics and computer programming. Despite the extensive expertise and support from our partners, the PCR debugging process was tedious and involved mainly due to the lack of intermediate monitoring of the process progress. A PCR sample had to be prepared, amplified, and then run on a gel in order to evaluate the result. This process usually took hours and often span over two or more consecutive days. Improvements related to adding intermediate monitoring and establishing a method for analyzing the surface absorption are considered essential next steps.

6.4.11 PCR experiment summary

Achieving DNA amplification through a PCR proved to be more involved than initially anticipated. Nevertheless, after the initial debugging steps, the need for temperature profiling of the TC008 was recognized, which led to developing the temperature sensors interface module previously described in Section 5.4.12. The modularity on all system levels and interfacing models allowed for seamless integration with the fluidic system and the instrumentation platform. Even though the cyber-fluidic platform readily proved capable of matching the functional requirements for performing PCR on the digital biochip, performing a successful reaction took a lengthy debugging process. After examining the effects of temperature, toxicity, and biofouling, a simple substitution of the PCR master mix led to a successful reaction.

Achieving a successful PCR concluded the proof-of-concept phase in the scope of this thesis work. However, it appears that there is yet a long development process ahead until a stable and reliable PCR can be seemingly performed on the digital microfluidics platform. The main difficulty is rooted in the biochemical aspects of the experiment. While understanding and solving the biofouling problems have been lightly addressed in this work, the engineering challenges associated with the cyber-fluidic platform have been mostly overcome, and a range of future platform improvements have been outlined.

6.5 Enzymatic immunoassays

Enzymatic immunoassays are biochemical tests that measure the presence or concentration of proteins, antigens, antibodies, hormones, or peptides in a liquid sample. The measuring mechanism is based on a specific antibody-antigen binding where a detectable signal is generated from an enzyme-linked to a biorecognition molecule, i.e., an antibody. An enzyme acts upon a substrate and produces fluorescence, absorbance, or electrochemical signal used to quantify the outcome of the test. The signal can be either a visible color change, fluorescence, or electrochemical, depending on the enzyme and substrate. The enzyme-linked immunosorbent assay, commonly called ELISA, was discovered in the 1970s and provided an alternative to the, at the time, popular but health-risk posing radioimmunoassay. After its discovery, ELISA has gained popularity for medical diagnostics, toxicology, and in the field of pharmaceutical development, due to its high sensitivity, specificity, and the ability to perform in complex mixtures.

There are four main ELISA formats: direct, indirect, sandwiched, and competitive. The first three types establish the biological detection scheme used further in this work, and therefore their construction is shown in Figure 6.24a. The first two formats, direct and indirect, rely on an antigen immobilized on a surface, and the sandwiched ELISA is based on immobilized capture antibodies. The assays are performed as a repetitive sequence of immobilization, incubation, and washing steps. The sandwich ELISA is the most specific of the three formats due to the indirect immobilization and detection mechanisms. The use of secondary detection antibody conjugate adds a modularity level to the assay, thus avoiding the need for enzyme-linked antibody for every specific antigen. Nonetheless, the enhanced performance comes at the cost of protocol assay complexity in terms of used reagents and an increased number of steps.

The traditional sandwich ELISA is performed on well plates, where the bottom of each well is used as a binding surface for the capture antibodies. An alternative to the traditional well plate ELISA is the magnetic beads-based ELISA, where instead of immobilizing the capture antibodies on a solid surface, they are conjugated to magnetic beads. The use of functionalized magnetic beads on a digital biochip is often referred to as droplet-based magnetic bead immunoassay. The beads are typically made of iron oxide particles bonded together and encapsulated with a stable polymer material. The final diameter of the beads extends from tenths of nanometers to a few micrometers. The magnetic beads are used as functionalized carriers that can be transported together with a droplet on the digital biochip. The main advantage of using beads over the surface functionalization is that magnetic beads ELISA can be performed in a liquid medium compared to the traditional sandwich ELISA, which requires a solid substrate for binding the capture antibody. A magnetic field is used to capture and con-

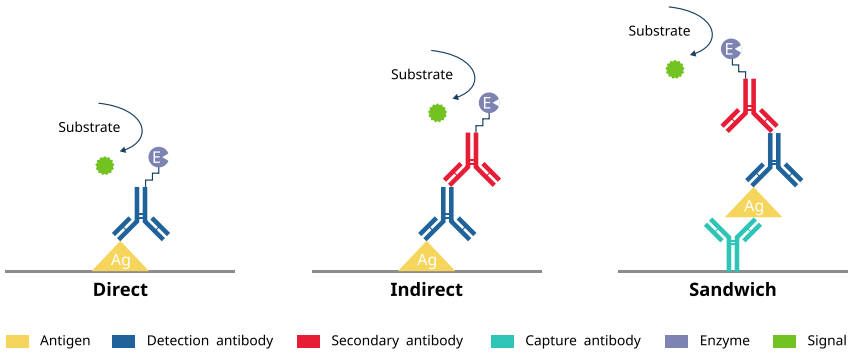

(a) Plate ELISA.

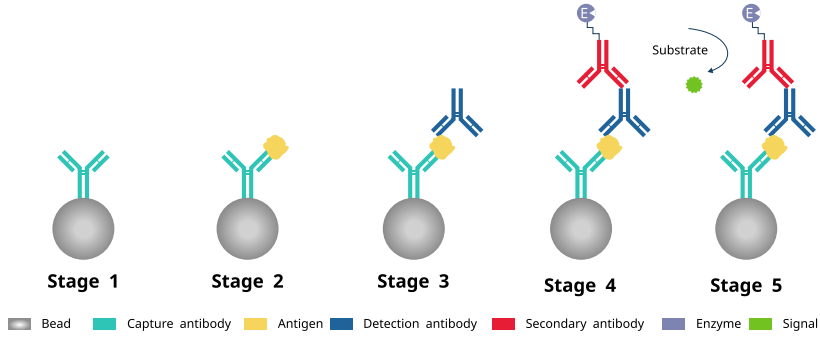

(b) Sandwich beads ELISA.

Figure 6.24: Common ELISA formats.

tain the beads into a designated region on the digital biochip, thus enabling the essential washing steps as a part of the ELISA protocol.

The use of a magnetic bead allows for multiple application-specific functionalizations to be carried out on the digital biochip, thus creating a multiplexed assay, e.g., developing an assay targeting more than one antigen. In contrast, the traditional ELISA generally targets one antigen at a time. Although the multiplexed assays may be a subject of cross-reactivity disturbance, they have the potential to provide unmatched reconfigurability when performed on digital biochips.

Two separate ELISA assays were prepared and tested on the digital biochip as a proof of the capabilities of the microfluidics platform. The assays are described in Section 6.5.1 and Section 6.5.2, and the experiments closely resembled the traditional sandwich ELISA, where the protocol steps are listed below and

illustrated in Figure 6.24b:

1. A droplet containing functionalized magnetic beads is loaded on the digital biochip.
2. A droplet containing the antigen is loaded on the digital biochip, mixed, and incubated with the functionalized magnetic beads. After incubation, the analyte is expected to have bounded to the capture antibodies.
3. A magnetic field is used to immobilizes the magnetic beads.
4. A washing buffer is used to remove the unbound antigen. The washing step is performed as a series of dilutions, where a number of washing buffer droplets are passed through the immobilized beads and discarded to waste.
5. After several washing cycles, the antigen is expected to be bonded to the capture antibody, as illustrated in Figure 6.24b Stage 2. Next, the magnetic field is removed to release the magnetic beads.
6. A droplet containing the detection antibody is loaded on the digital biochip and mixed with the magnetic beads.
7. The magnetic field is applied again to immobilizes the magnetic beads.
8. A washing step performed as described in step 4 to remove the unbound detection antibodies. The outcome of this step is illustrated in Figure 6.24b Stage 3. The magnetic field is removed to release the captured magnetic beads.
9. A droplet containing the secondary enzyme-conjugated antibodies is added, mixed, and incubated with the magnetic beads.
10. The magnetic field is applied again to immobilize the magnetic beads.
11. A washing step performed, as described in step 4, is used to remove the unbound secondary enzyme-conjugated antibodies. The outcome of this step is illustrated in Figure 6.24b Stage 4. The magnetic field is removed to release the captured magnetic beads.
12. A droplet containing the substrate is loaded on the digital biochip and mixed with the magnetic beads. Color development reaction is triggered and used as a readout for the assay, as shown in Figure 6.24b Stage 5.

The protocol above describes the general steps for performing a sandwich magnetic beads-based ELISA on a digital biochip. The two separate assays were designed and prepared by Susan Ibi Preus from DTU Bioengineering to test the

fluidic handling capabilities of the developed cyber-fluidic platform. The selection of materials and methods was solely based on the availability of reagents and processes related to the ongoing research activities at the NaBIS Group at DTU Bioengineering. The two assays are described in detail in Section 6.5.1 and Section 6.5.2, and all experimental work was carried out with the assistance and supervision of Susan Ibi Preus.

The experiments were performed on PTFE foil frames with Teflon or FloroPel1601V-FS coated ITO glass top plate. The spacing between the bottom and the top plate was 325 m. A side-loading technique was used for easy loading and unloading of reagents on the chip. A 1cSt silicone oil was used as a filler fluid. A neodymium magnet was manually handled to deliver a static magnetic field for the immobilization of the magnetic particles.

6.5.1 Detection of MRSA protein

The first assay performed on the digital biochip was based on commercially available antibodies, targeting the detection of a protein on methicillin-resistant Staphylococcus aureus (MRSA). The assay composition reflects the sandwich beads ELISA format shown in Figure 6.24b, where a mouse monoclonal anti PBP2a and rabbit monoclonal anti PBP2a (Antibodies-online GmbH) antibodies were used as capture and detection antibodies, respectively. A goat anti-rabbit IgG HRP conjugation antibody (Abcam PLC) was used as a secondary antibody. A recombinant PBP2a MecA (Antibodies-online GmbH) originating from Staphylococcus aureus was used as an antigen target protein. LodeStars 2.7 Carboxyl superparamagnetic polystyrene particles with 2.7 µ diameter were used as magnetic beads carriers for the capture antibodies. Standard EDC/NHS coupling was used to immobilize the capture antibody on the magnetic beads. One step Ultra TMB ELISA Substrate and STOP Solution (Thermo Fisher Scientific Inc) were used correspondingly to initiate and terminate the enzymatic reaction at the end of the protocol.

Before attempting the full magnetic beads-based ELISA protocol on the digital biochip, the immobilization of the capture antibodies was tested by trial for binding with a labeled secondary antibody. A sample of the magnetic beads was loaded on the digital biochip, followed by the secondary rabbit anti-mouse (HRP) antibody. The two samples were mixed, followed by magnetic immobilization of the magnetic beads. Several washing steps with MiliQ as a buffer were performed, and the progress was monitored by sampling the buffer and testing for the presence of the HRP. The testing was performed by extracting discarded washing droplets and mixing them off the digital biochip with the substrate. The washing procedure was repeated until no significant color development was

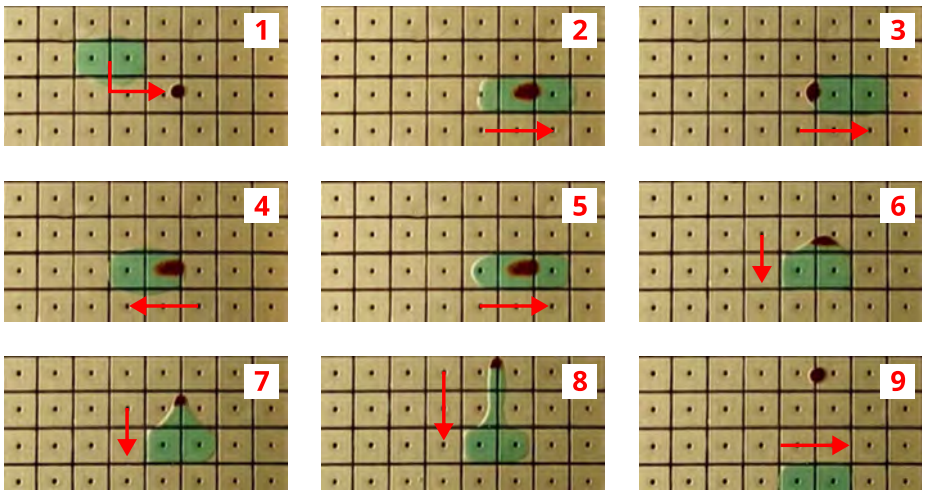

Figure 6.25: Video frames showing a single magnetic beads washing cycle. Blue color dye is added to the washing buffer for clarity. The red arrows are idicating the direction of the droplet actuation.

observed in the sampled used washing buffer. The binding between the capture and the secondary antibodies was tested by loading a substrate droplet on the digital biochip and mixing it with the magnetic beads. The capture antibody immobilization was confirmed by rapid color development.

The non-specific binding between the secondary HRP antibody and the magnetic beads was tested by following the test procedure for the proper capture antibody immobilization. The main difference was using uncoated instead of functionalized magnetic beads. The experiment showed no color development, indicating the lack of non-specific binding between the raw magnetic particles and the secondary HRP antibodies.

After successfully conducting tests for verifying both specific and non-specific binding, a full magnetic beads ELISA was performed on the digital biochip. The experiment consisted of performing all the steps shown in Figure 6.24b on the digital biochip and observing the color development at the end of the reaction. In general, the ELISA protocol consists of multiple representative incubations and thorough washing cycles. A video frame sequence from a single washing procedure is shown in Figure 6.25. The beginning of the washing process is shown in the first two frames where the green dye colored washing buffer is actuated towards and then merged with the magnetic beads. Next, the droplet is mixed with the beads for several cycles by moving the droplet left and right, as shown in frames 2 to 5. The beginning of the magnetic bead extraction is shown

in frame 6, where the buffer is pulled downwards, away from the immobilized magnetic beads. The washing buffer is actuated further away from the magnetic beads, as shown in frames 7 and 8, which leads to the droplet elongation final separation shown in frame 9. Next, the washing buffer droplet gets discarded, and the washing cycle can be restarted. Removing the magnet and allowing the magnetic beads particles to disperse throughout the mixing increases the efficiency of the washing step.

Inevitably, a small amount of fluid residue will remain with the magnetic beads. However, further washing cycles provide additional dilution and extraction of the contaminants. The magnetic beads washing is, to a great extent, a series dilution, where the concentration of contaminants is reduced to a virtually undetectable level. For instance, monitoring the washing efficiency can be automated on the platform by analyzing the discarded washing buffer droplets. However, the efficiency of the washing steps was periodically manually tested by extracting the washing buffer and testing ex-situ in order to ensure proper execution of the protocol.

6.5.2 Detection of SARS-CoV-2 protein

The second assay tested on the digital biochip was based on detecting purified spiked protein of SARS-CoV-2. The detection and capture antibodies, as well as the purified target proteins, were supplied by Prof. MD. Peter Garred and Mikkel-Ole Skjødt from Rigshospitalet in Copenhagen, Denmark. The antibodies were developed as a part of the routine research work at NaBIS group at DTU Bioengineering. The magnetic beads, substrate, and stop solution were identical to the reagents specified in Section 6.5.1.

For the detection of the SARS-CoV-2 spiked protein, an indirect sandwich approach was initially used. The detection antibody (F1_48) was a mouse antibody, and therefore, rabbit anti-mouse IgG (HRP) was used for signal generation. However, the capture antibody (F1_53) was also a mouse antibody, leading to direct binding between capture and signal molecules, thereby producing false-positive results. Hence, to test the assay despite the unfavorable conditions, two parallel experiments were set up and performed on the digital biochip. The first experiment served the purpose of establishing a background reference signal resulting from the binding of secondary antibody to the capture antibody conjugated to the magnetic bead. The second parallel experiment was targeting the actual protein detection by magnetic beads ELISA. Performing the experiments simultaneously on the digital biochip allowed for obtaining the background signal and the SARS-CoV-2 spiked protein assay signal. The intensity difference between the two signals presents the signal of the target

detection.

The background signal experiment consisted of loading a droplet with functionalized magnetic beads on the digital biochip, followed by a droplet containing the antigen. The two droplets were mixed, followed by immobilization of the magnetic beads with a magnet and washing away any unbound antigen. After the washing, it was expected that the sample consists only of a small amount of washing buffer and functionalized magnetic beads matching to Stage 2 of the protocol shown in Figure 6.24b. In this experiment, the antigen is used to bind to the capture antibody, thus preventing binding of the secondary antibody to the beads capture antibody by spatial restrictions or blocking the binding region. Following thorough washing, the secondary antibodies were loaded on the system and mixed with the magnetic beads. After a 5 minutes incubation step, extensive washing was performed to remove any unbound secondary antibodies. Next, the substrate was loaded on the digital biochip and mixed with the magnetic beads. The enzymatic reaction was allowed for 3 minutes. In the meantime, a droplet of the stop solution was loaded on the system and mixed with the magnetic beads exactly at the end of the reaction period. The stop solution terminated the enzymatic reaction providing a snapshot of the color development. The color, color intensity, and rate of development correlate with the concentration of enzymes and, thus, the target analyte concentration.

The magnetic beads ELISA were performed in parallel with the background experiment. The magnetic beads sample and the antigen were loaded on the digital biochip, merged, and followed by mixing and incubation. After washing with MilliQ, a droplet with the detection antibodies was added. The unbound antibodies were removed with a washing procedure, and the secondary HRP antibodies were added and followed by merging, mixing, and thorough washing. The washing process was monitored by periodically extracting from the waste washing buffer and checking for the presence of the enzyme by adding substrate and observing for color development. After washing, a substrate droplet was loaded, merged, and mixed with the magnetic bead. While the color development was taking place, a droplet of the stop buffer was loaded, followed by merging and mixing with the magnetic beads exactly 3 minutes after the initiation of the enzymatic reaction.

The outcome of the background and the detection experiments is Shown in Figure 6.26. The two image frames were cropped from the same photograph and placed side-by-side to display the difference in the color development from the enzymatic reaction. The background experiment made evident the presence of binding between the capture and the secondary antibody. The slight yellow tint on the sample shown in Figure 6.26a shows the presence of the secondary HRP antibody even after the extensive washing. However, the detection sample from the complete magnetic beads ELISA presents a denser yellow color, which

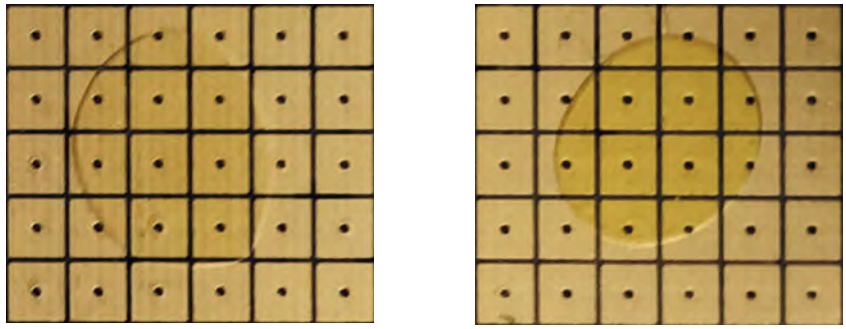

(a) Background signal. (b) Detection signal.

Figure 6.26: Comparison between the background and the detection signal of the SARS-CoV-19 assay.

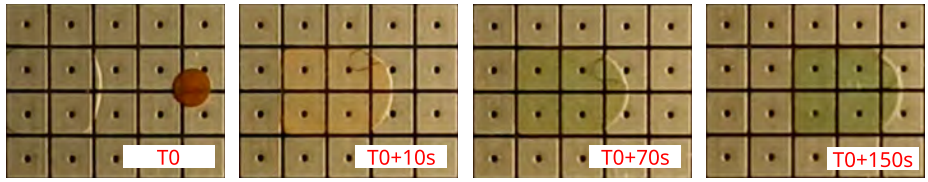

(a) Color development reaction.

(b) Washing series and assay signal

Figure 6.27: Results from the SARS-CoV-2 experiments.

indicates a higher enzymatic activity and, hence a higher concentration of the HRP labeled secondary antibody. The difference between the intensity of the background and the detected signal represents the actual concentration of the SARS-CoV-2 protein.

A different experiment that eliminates the secondary antibody was designed and performed in an attempt to reduce the background signal generation. Besides increasing the specificity of the assay, the major task of the secondary antibody is to serve as a carrier of the HRP enzyme. However, by directly labeling the

detection antibody with HRP, the secondary antibody can be omitted from the assay.

The reduced assay was performed twice, with two different concentrations of the reagents. The first experiment was based on an 5 µL 0.005 mg mL^{-1} spiked antigen, resulting in total of 25 ng, and 5 µL 0.001 mg mL^{-1} HRP labeled detection antibody. After performing the established merging, mixing, incubation, and washing steps, the enzymatic reaction color development process is shown in Figure 6.27a. After mixing the magnetic beads with the substrate, noticeable color development was evident 10 seconds after the start of the reaction. The figure also shows an intermediate step at 70 seconds and a significant color intensity 150 seconds after initiating the reaction. The experiment was considered successful after a test for non-specific binding between the capture and the detection antibody.

The experiment mentioned above was repeated but with lower antigen and higher detection antibodies concentration. This experiment was targeting antigen detection in conditions similar to a low volume and low concentration swab sample. A 5 µL buffer solution was spiked with 0.000 01 mg mL^{-1} antigen, resulting in a total of 50 pg. However, the concentration of the HRP labeled detection antibody was increased to 0.01 mg mL^{-1}. The high concentration of the detection antibody required thorough washing in order to minimize the background signal. The washing progress was monitored by collecting the washing buffer after each washing cycle, and testing for the presence of HRP labeled antibodies. The washing took a total of 24 cycles with 10 µL droplets. The washing progress is shown in Figure 6.27b, where the lighter color indicates a lower presence of HRP bound antibodies. The last labeled sample took approximately 5 minutes to develop the light blue color, and therefore, at this stage, the washing was considered sufficient. Next, the substrate was loaded on the digital biochip, merged, and mixed with the magnetic beads sample. Instant color development was observed, and the last frame in Figure 6.27 shows an image of the sample acquired 5 seconds after initiating the reaction. The fast rate of the reaction proved the presence of antigen-bound HRP detection antibodies and thus indicated successful detection of relatively low antigen concentration. The strength of the reaction can be subjectively assessed by comparing the color of the signal droplet to the color of the last washing step, which, in this case, shows a sharp contrast.

6.5.3 Enzymatic immunoassays discussion and summary

Two separate enzymatic assays targeting the detection of MRSA and SARS-CoV-2 proteins were designed and performed on the cyber-fluidic system. Al-

though the execution of the assays can be challenged from a biological perspective, due to the lack of extensive characterization, detection limits study, consistent blank experimental data, and suboptimal selection of reagents, the execution of the two magnetic beads ELISA protocols were successfully performed from a fluidic handling perspective. Moreover, in the limited experimental trial, the two assays yielded affirmative results and showed excellent potential for automation on the digital biochip.

Several challenges need to be addressed on the path of achieving a fully programable and automated magnetic-beads ELISA on the cyber-fluidics platform. Although direct surface contamination was not confirmed, high concentrations of the two antigens yielded reduced droplet mobility, thus suggesting protein surface absorption. The effect was previously identified in the PCR experiment (see Section 6.4.8), and in general, recognized in the biomedical field. An immiscible filler fluid such as silicone oil reduces the absorption, but it does not eliminate the problem. Optimizing the concentrations of the reagents and additives have been shown to mitigate further the surface absorption of biomolecules [76]. Another viable approach inspired by the programmability of the platform is to schedule and route the droplet paths, such as purposely avoiding or reusing certain clean or contaminated areas of the digital biochip.

Another set of engineering challenges relates to reagents supply, reaction monitoring, and control of the immobilizing magnetic field. All of the three mentioned tasks were manually handled in the current platform instance, but the need for improvement was evident throughout the experiments. The first critical issue relates to the volumes required for performing the washing steps. The last assay required 240 µL washing buffer to reduce the concentration of the HRP labeled antibody. The excessive number of washing steps needed was likely caused by incomplete liquid extraction that compromises the dilution, or a potential unspecific binding of the HRP labeled antibody to the magnetic beads. Nevertheless, the washing buffer volume can roughly be estimated to correspond to nearly 35% of the electrode array area, and such a large area is not practical to be occupied by a planar reservoir. Moreover, considering that there are additional washing cycles, the sheer amount of washing buffer quickly becomes evident. Furthermore, the washing buffer not only needs to be stored and used on the chip, but it also needs to be discarded after use, which will either require a similar-sized reservoir or an external storage approach. While optimizing the reagent concentration has the potential to reduce the required volumes, external reagents storage becomes a necessity in the aspect of a fully automated and programmable cyber-fluidic system. We consider addressing this issue as future work where external reservoirs and piezoelectric fluid pumps will be utilized to implement external fluid storage.

The reaction monitoring and magnet control are instrumentation challenges

that can be addressed with the modular system approach. A camera or dedicated color sensor modules can be developed and integrated with the platform, thus allowing for a programmatic quantification approach of reaction readout or washing efficiency. An alternative to the color detection approach is the chemiluminescence, which can be quantified with a photomultiplier tube (PMT) [9]. The immobilization magnet control needs to be investigated to determine whether a miniature electromagnet can provide a sufficient magnetic field to capture the magnetic beads. Alternatively, a mechanically controlled magnetic stage had been demonstrated as a feasible approach [9].

Although we strived to keep the experimental conditions and reagents concentration within tight tolerances, extensive work needs to be carried out to characterize and derive a systematic method to quantify the outcome of the assay. However, at this exploratory development stage of the cyber-fluidic platform, we consider performing various assays primarily as capabilities demonstrators. Successful reagents handling and recognition for automation potential are considered significant milestones in advancing the cyber-fluidic platform.

6.6 Experimental summary

This chapter presented a snapshot of the ongoing experimental work of this thesis. System integration, testing, and characterization were carried out on a module and platform level in the process of preparing the cyber-fluidics platform for application testing. Following an extensive debugging process, including a PCR temperature evaluation, toxicity tests, and recognizing the effects of surface absorption, a successful PCR was performed on the digital biochip. Although several challenges, including sample evaporation and bubble formation, need to be further addressed, the space domain PCR showed a potential for full automation. Two proof of concept magnetic beads ELISAs for MRSA and SARS-CoV-2 protein detection were designed and successfully performed on the digital biochip. The two assays confirmed materials compatibility and served the purpose of fluidic handling capabilities demonstrators, including magnetic beads immobilization and extensive washing cycles.

Chapter 7

Evaluation and discussion

This chapter begins with an outline of the evolution of the research idea, followed by a discussion on the interdisciplinary research impact of this thesis work. The chapter concludes with a discussion on the notable characteristics of the presented cyber-fluidic platform and ends with an outline for future research directions.

7.1 The road towards the cyber-fluidic processor

The initial goal of this research project was to develop a point-of-care device for measuring the concentration of one or several of the thyroid gland-related hormones TSH, T3, and T4. The vision was to utilize digital microfluidics for sample handling, develop a biosensor for measuring the levels of the thyroid gland hormones, and integrate the sample handling with the sensing into a portable device. The significance of the project was recognized in the fast detection and consequential disease monitoring. The digital biochip and biosensor were intended to be fabricated on a paper substrate using printing techniques and conductive inks, as discussed in Appendix C. The convenience of the point-of-care combined with the envisioned low-cost consumable digital biochip was perceived as "a killer application" due to its potential to improve the quality of life of thyroid patients. Shortly after starting the project, the first prototypes of

a TSH biosensor were prototyped in the NaBIS group at DTU Bioengineering (formerly at DTU Nanotech). Shortly after, it was realized that the predicted need for sample preparation is somewhat limited since, from the user perspective, the diagnostic is more convenient to be carried out on full blood, and the sensing technology appeared capable of meeting the direct sampling. However, while the paper-based digital biochips offer a unique combination of simplicity, low cost, and diagnostic capabilities [123] [10] [23], the potential to scale and perform complex biochemical assays was also acknowledged. At this stage, the project started naturally diverting in two directions; continuing improving the thyroid hormones biosensor and creating the vision of the application-agnostic cyber-fluidic platform.

The TSH biosensor development continued as a part of the research activities carried out in the NaBIS group at DTU Bioengineering. Numerous discussions with doctors, patients, and patient organizations solidified the vision for patient-site monitoring and transformed the project into an endeavor for developing a stand-alone commercial-grade point-of-care device. As of the time of the submission of this dissertation, a collaboration between DTU and InQvation ApS is being established as a spin-out company called THYRA LIFE. The purpose of THYRA LIFE is to develop a thyroid patient tracking app correlating the behavioral and hormonal states of a patient in the quest for a more efficient personalized medication. Although the work on the cyber-fluidic platform and the TSH biosensor development diverged early in the thesis work, the concept for patient site TSH measurement emerged with this research project proposal.

The thesis work continued with establishing in-house fabrication techniques for paper-based digital biochips and biosensors. An inkjet printing method was established for printing the actuation electrode of relatively simple digital biochips, as described in Appendix C. Moreover, a process for mask printing on paper of low-cost carbon-based electrochemical biosensors was developed and refined as a part of this thesis work. The paper-based biosensors were tested for detecting *Pseudomonas aeruginosa*, and they showed a 2.3 fold enhanced performance at a fraction of the cost of similar commercial ceramic-based biosensors [123].

The development of the paper-based digital biochips and biosensors was carried out in parallel with scaling the electrode driver modules to support 2×64 electrodes (see Appendix B). The new electrode drivers were exceeding the single-layer routing capabilities and the printing resolution of the used inkjet printer. Hence, to fully utilize the potential of the upgraded multichannel electrode drives, a two-layer PCB was considered as an alternative fabrication technology for the digital biochips. An array of 8×16 actuation electrodes was designed and fabricated on a two-layer PCB allowing for flexible droplet routing. The larger electrode array made evident the labor-intensive electrode actuation sequence scripting, and the need for a cyber-fluidic software stack became pressing.

The research project was evolving conceptually and technologically driven by the acquired knowledge and expertise. During the timeframe of scaling up the digital biochip and realizing the need for a programming model, the MagicBox project was formed as a collaboration between DTU Compute, DTU Biosustsain, and DTU Bioengineering. The project idea emerged from the Yest Metabolic Engineering group led by Irina Borodina's at DTU Biosustain, as the vision for a MagicBox assisting or fully replacing the routinely performed labor-intensive laboratory tasks related to the cell factories engineering. Hence, the scope of the MacgicBox project covered the development of a reconfigurable, modular, and highly programmable microfluidics platform capable of performing PCR, cloning, and transformation into *E. coli*, as a part of a strain development process. While this thesis work built the vision for the cyber-fluidic processor and the virtual system as an entity (see Section 5.5), Luca Pezzarossa undertook the task of fully conceptualizing and developing the fluidic ISA and an execution model as a part of postdoctoral research at the Embedded Systems Engineering (ESE) section at DTU Compute.

A significant contribution of this dissertation is the holistic approach applied to the process of conceptualization, development, building, and testing the fluidic and instrumentation systems leading to the results presented in Section 5.3 and 5.4. The magnitude of the cyber-fluidic system required system decomposition into fluidic, instrumentation, and virtual subsystems. The core of the fluidic system was the TC008 digital biochip consisting of 640 individually addressable electrodes, 10 reservoirs, and 32 individual heaters that can be configured in up to 8 separate heating zones. The extensive array of electrodes and the reconfigurable heaters reinforced the introduced idea of a cyber-fluidic processor by demonstrating a complexity level becoming difficult to handle without proper automation tools.

The vast discrepancies between running simulations under unrealistic assumptions such as neglecting the droplet volume, assuming absolute droplet actuation fidelity, unconstrained device resources, lack of failure modes, etc., and performing real bioassays on the digital biochip were faced as a part of the system testing process. The encountered issues manifested the need for active feedback, flow control, and a capable runtime environment. The expanding fluidic capabilities, growing system complexity, and the need to handle runtime uncertainty were seen as a strong motivation to investigate the notion of the digital biochip as a cyber-fluidic processor.

7.2 Interdisciplinary research impact

The design of the cyber-fluidic platform was truly an interdisciplinary endeavor that, on the course of three years, was carried out across four departments, namely DTU Compute, the former DTU Nanotech (now DTU Healthtech), DTU Bioengineering, and DTU Biosustain. When a research project spans across several research domains, not only as a formal collaboration between colleagues but also as an active commitment, an engaged dialogue, idea generation, and knowledge transfer inevitably lead to paradigm shifts in each involved party. Established methods and techniques become a subject of harsh questioning, often due to pure curiosity and lack of domain-specific comprehensive understanding. Technological limits get pushed past the accepted margins in the quest for repurposing a given technology. Questions that will never be considered in a given domain get asked, and the answers open new horizons that surprise even the experts. The curiosity in an interdisciplinary context was a main driving force behind the development of the presented cyber-fluidics platform. As a result, this thesis strengthened the collaboration between the research groups and led to new joint research ventures.

Several live demonstration sessions were conducted throughout this thesis project. The portability of the cyber-fluidic platform allowed for effortless demonstration in a casual setting such as exhibition halls, auditoriums, or conference venues. Repetitive actuation sequences and manual droplet actuation control were used to show the fluidic handling capacity of the platform. The platform demonstrated the capabilities of the digital microfluidics technology to a non-scientific audience in a real-life setting. Such a demonstration sends the message that although delicate by nature, the digital microfluidics technology is mature and robust enough to finally start the departure from the research labs and find its way into solving real-world problems.

7.3 Disccussion

Although one might consider the effort of designing, building, and testing an unnecessary task considering the open-source alternatives presented in Chapter 3, we argue that neither of the discussed systems reaches the modularity and standardization level required for the envisioned platform. Moreover, understanding and considering the intrinsic relationships spanning across the system domains is essential for the overall system architecture and performance. The lack of a suitable option, along with the intention for building a cyber-fluidic platform that, due to its scale and complexity, will indeed require the development of a

software stack, motivated the extensive engineering endeavor.

The holistic system engineering approach and experience gained from the predecessor systems helped identify areas where innovation would likely be needed early in the process. The fact that we had full control over the engineering of the system allowed for exploiting certain design aspects and led to at least three innovative methods related to the effective and low-cost digital biochip coating technique, unique heating method, and innovative method for EWOD actuation (Section 1.7 NoI1, NoI2, and NoI3).

The practicality and capability of the cyber-fluidic platform were demonstrated in Section 6.3 in the context of a PCR, and enzymatic assays. Two platform instances were used to meet the instrumentation needs of the PCR and ELISA experiments. Although the PCR and the two ELISA assays showed promising results, there are still engineering challenges to be solved. Biofouling, evaporation, and bubble formation are among the challenging problems yet to be overcome. Nevertheless, the cyber-fluidic platform proved to be capable of carrying out the required fluidic operations, and the reconfigurability was demonstrated with the two system instances.

It was previously stated that preliminary integration tests were carried out with the BioAssmebly ISA and the associated virtual machine (see Section 5.5.3. The test cases include the execution of BioAssembly code with implemented real-time flow control. Data from the heaters controller and an external temperature sensor were monitored, and droplet routing was adjusted based on the sensory input. These simple experiments marked a notable milestone in the roadmap towards materializing the vision for a cyber-fluidic processor.

The capability to attach the instrumentation system to different external controllers was demonstrated by compiling BioScript code [26] with the static open-source compiler [34] that produced electrode actuation sequence specific to the TC008 and the instrumentation platform. The integration was the outcome of collaboration and short research stay with Philip Brisk's group at UC Riverside, CA, USA. The purpose of the integration was to evaluate the BioScrip as a potential high-level programming language for the platform and demonstrate the interfacing benefits of the loosely coupled architecture.

7.4 Future work

As it probably became evident at this point, no doctoral research project is ever finished. Considering the scope and interdisciplinary nature of the cyber-fluidic

system, the list of unfinished work, development ideas, and research directions is relatively extensive. Continuing to work on the platform and addressing technical loose ends is a trivial but essential task for the future development of the platform. Addressing the issues with bubble formation and biofouling is considered of critical importance before continuing the work on implementing biological protocols on the system.

Implementing a droplet position monitoring will provide a fault-tolerant operation and significantly increase the confidence level of unsupervised protocol execution. Position sensing through practice and impedance measurements in conjunction with a computer vision system is considered an essential next step of the development of the cyber-fluidic platform. Absolute actuation fidelity through droplet position feedback is a prerequisite for releasing the full potential of the notion for a cyber-fluidic processor.

The examination of diagnostic applications in the context of digital microfluidics is relevant mainly due to its commercial potential, e.g., optimizing time, cost, and logistics. Hence, sensing technologies and system integration are among the technical issues to be addressed. Moreover, adding sensing capabilities to the digital biochip supports and adds to the materialization of the cyber-fluidic processor.

The future work on the virtual system includes the full conceptualization and development of the microfluidics ISA, virtual machine, and the textual and graphical programming languages. Involving user feedback in the design process of the high-level programming methods is critical for the likelihood of following the integration in routine laboratory research activities.

Chapter 8

Summary and conclusion

The arguments for digital microfluidics overtaking the field of applied microfluidics have been used as opening motivation in countless research publications. Lower reagent volumes, automation potential, shorter hands-on time, miniaturization, scalability, and reduced overall cost are used as common reasons for promoting digital microfluidics. Nevertheless, in addition to the technological challenges, substantial performance, programmability, reliability, and socio-economical roadblocks need to be overcome before the cyber-fluidic systems realize their full potential as a capable fluidic handling technology.

This thesis work was steered based on the comprehensive panorama of the past twenty years of digital microfluidics technological progress, including digital biochips, control systems, and existing and visionary applications. Regardless of the vast amount of reports for novel use of materials, integration techniques, and exciting applications, the lack of a holistic system approach was identified to hinder the technological transfer. From an academic or engineering perspective, developing better microfluidic components broadens the technological perspectives. However, from a user perspective, these advancements are likely to remain unnoticed or considered insufficient to revolutionize the market. For medical diagnostics or even routine biological research, unless the digital microfluidic technology comes as a complete end-to-end solution, the likelihood of successful adoption is virtually nonexistent.

8.1 Summary

The lack of standardization and a common programming model was recognized as a prohibitive factor limiting the transition of digital microfluidics past the applied research stage. To address this, we have proposed a platform-based modular-cyber fluidic architecture capable of adapting and evolving to the needs of a broad range of microfluidic applications. The holistic approach of system engineering was applied in the process of evaluating and deriving the architecture of the cyber fluidic-platform. The platform was split into three loosely coupled parts, namely fluidic, instrumentation, and virtual systems.

The system architecture was unfolded as a physical prototype used to verify the design assumptions. A PCB-based digital biochip with 640 individually addressable actuation electrodes and 32 embedded reconfigurable heaters was prototyped as a demonstrator of the modularity and scalability concepts. Namely, the modular design allows for scaling the electrode size by a factor of two or even four without the need for a significant design effort. The embedded reconfigurable electrodes allow for multiple temperature zones to be formed on the digital biochip, accommodating for DNA amplification applications. A modular foil-frame based approach was demonstrated to provide a low-cost and low-tech equivalent to the traditional fluoropolymer deposition processes.

An extensive part of the instrumentation system was developed and built following the modularity concept. Although the instrumentation system is considered an engineering accomplishment with a limited scientific value, it plays a significant role in the overall cyber-fluidic architecture. The instrumentation system implements the fluidic-to-digital interface and hence allows building the model for a fluidic ISA.

A central contribution of this thesis work is the recognition of the need for the already mentioned fluidic ISA. By drawing parallels with the modern computer architectures and based on the instrumentation system model, a fluidic ISA was conceptualized, and a corresponding software stack consisting of a virtual machine, domain-specific assembly language, compiler, and high-level programming methods was discussed. A graphical flow-based programming language was suggested as an entry point for inexperienced users to cyber-fluidic programming. A domain-specific high-level language and corresponding assembly were considered necessary to support the futuristic use of the cyber-fluidic platform as a truly programmable fluidic processor. The DMF Toolbox application was developed to aid the development of the instrumentation system. The application was architected with scalability as a central design objective in order to serve the purpose of an application shell for the envisioned software stack.

The reconfiguration and fluidic handling capabilities of the instrumentation system were validated with two types of biological assays. A space domain PCR with three separate temperature zones was successfully performed on the digital biochip. The platform capabilities were also demonstrated with magnetic beads ELISA, reporting successful detection of MRSA and SARS-CoV-2 proteins.

8.2 Conclusion

The technological development of digital microfluidics has been showing a steady progress since its establishment in the 2000s. The level of digital biochip complexity and integration has grown to the extent where design automation becomes a limiting factor for future development. We addressed this challenge with the proposed cyber-fluidic architecture, both from a conceptual and practical perspective. The fluidic, instrumentation, and virtual systems discussed in this dissertation not only target the current experimental needs, but they also pave the road towards the envisioned cyber-fluidic processor.

The strength of this dissertation was the holistic cross-disciplinary approach towards cyber-fluidic systems. Regardless of their origin, size, and complexity, problems were always considered in the context of their intrinsic relationships with the rest of the system. As a result, we managed to develop a modular cyber-fluidic platform, which capabilities were demonstrated with PCR and magnetic beads ELISA. Moreover, the ability to programmatically manipulate biological specimens in a cost-effective and portable setting facilitates future expansion towards novel and exciting diagnostics and synthetic biology applications.

Appendix A

Patent landscape

In the early 2000s, the electrowetting on dielectric was identified as a promising droplet propulsion technology that had the potential to revolutionize the microfluidics field [139]. Before this invention, microfluidics were almost exclusively dominated by continuous-flow devices, which offered little flexibility in terms of reconfiguring the fluidic path. This limitation was mainly imposed by the fixed network of microscopic channels, valves, and pumps used to handle the fluidic transport and control. In contrast, the newly invented fluidic handling technique, also known as digital microfluidics, allowed individual droplets to be programmatically moved on an insulated array of electrodes by using an electric field. Hence, small droplets can be moved, merged, dispensed, split, mixed, and incubated without the need for particular topographical features. In effect, digital microfluidics were recognized as an attractive alternative to the continuous flow devices, and a new cross-disciplinary research field was established.

An increasing number of scientific and patent applications followed in the years after the initial invention. The publication timeline provides a good overview of state-of-the-art development and technology adoption, but it does not fully characterize the idea generation and visionary digital microfluidics applications. Therefore, this mini-review focuses on examining the patent landscape with the particular goal of learning more about the technological development and idea generation in chronological order of the early-filled patents. A thorough patent review is not feasible due to the sheer number of patents covering the

full range of topics, from fundamental fluidic operations to various biomedical applications. Furthermore, patents contain comparable, complementary, or even identical claims filled in the race of protecting intellectual property and presumably aiming to demonstrate leadership. Nevertheless, a representative selection based on topic, filling date, and assignee are reviewed in this report in an attempt to capture the development course from different perspectives.

The patent search was primarily conducted using the Google Patents search engine (Google Inc., Mountain View, California, USA). The search was mainly based on using the keyword "electrowetting" since electrowetting on dielectric is the droplet propulsion technology used for digital microfluidics. Nevertheless, the electrowetting effect is also used in different scientific fields such as optics and electronics, which also generates a significant amount of search results that are not related to digital microfluidics. The irrelevant search results were mainly from the optics domain since electrowetting is also used in display technology and optical lenses. Therefore, the search query was modified to exclude results containing the word optical. The search was conducted by restricting the search in portions of five years starting from the year 2000. A search by authors from leading research groups in the field of digital microfluidics was conducted as well. A subjective selection of patents based on interest, innovation, feasibility, application potential, and commercial value was selected for this report.

A.1 Patent landscape

A.2 Early Patents

This section shows some of the early patents on the electrowetting on dielectric as a droplet propulsion technology.

Actuators for microfluidics without moving parts [2000-01-24] This is one of the early patents [140] claiming the use of a series of microactuators for manipulating small amounts of polar liquids without moving parts. The so-called microactuators are the conductive electrodes used for creating the surface energy gradient for achieving the electrowetting effect. The patent discusses a closed digital microfluidics chip with its building components such as the use of two planar and parallel substrates, driving and reference electrodes, insulation and hydrophobic coatings, filler oil, etc. The patent also shows an example of interdigitated electrodes and other electrode configurations for achieving different fluidic operations such as droplet transport ("pumping"), dispensing ("drop

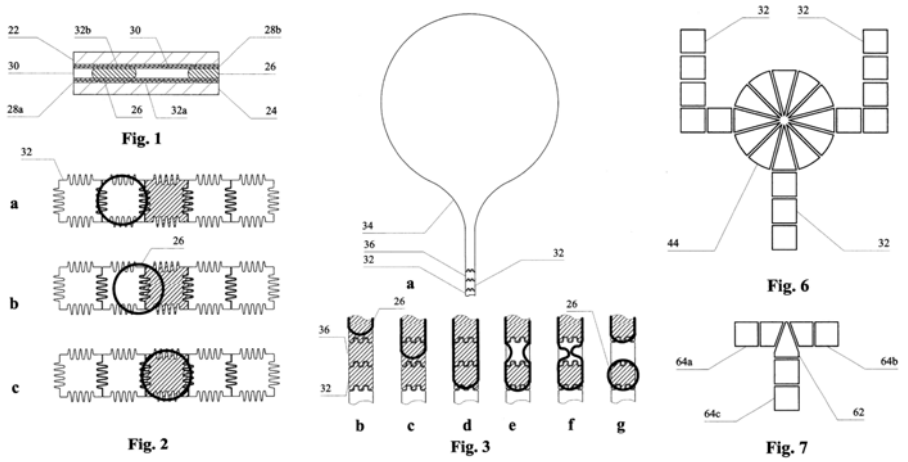

Figure A.1: Drawings from US6565727: *Fig. 1:* Cross-section of a planar electrowetting actuator according to the invention; *Fig. 2:* A linear arrangement of electrodes as a pump; *Fig. 3:* Drop meter and electrode control sequence; *Fig. 6:* Mixer/vortex device used for mixing; *Fig. 7:* Zero-dead-volume valve. Image source [140].

meter"), mixing ("mixer/vortex"), etc. The approach of grouping electrodes together to achieve a particular fluidic function, such as arranging electrodes in a circular pattern for mixing, draws architectural parallels with the continuous flow microfluidics. The patent title also implies this analogy, and it is particularly interesting since it shows the beginning of shifting from the design perspective from application-specific fluidic components to generalized functions on an array of electrodes. The patent has a single inventor, Alexander David Shenderov, and it is assigned to Nanolythics Inc.

Electrostatic actuators for microfluidics and methods for using same [2001-08-30] An interesting electrowetting droplet actuation device is reported in [141], which allows droplets to be moved not only on a two-dimensional array of electrodes by also be lifted vertically. The device has three-layered construction, as shown in Figure A.2, where the bottom plate consists of the two-dimensional droplet manipulation electrode, a distribution middle plate with apertures, and a top plate which has electrodes aligned with the cavities on the middle layer. The main claim of this patent is the construction of the device that allows droplets to be moved in three dimensions - a droplet can be transported vertically in the second top chamber, thus allowing other droplets to pass in the bottom chamber. Furthermore, reaction sides can be added on the top plate aligned with the distribution plate apertures. The reaction sides can

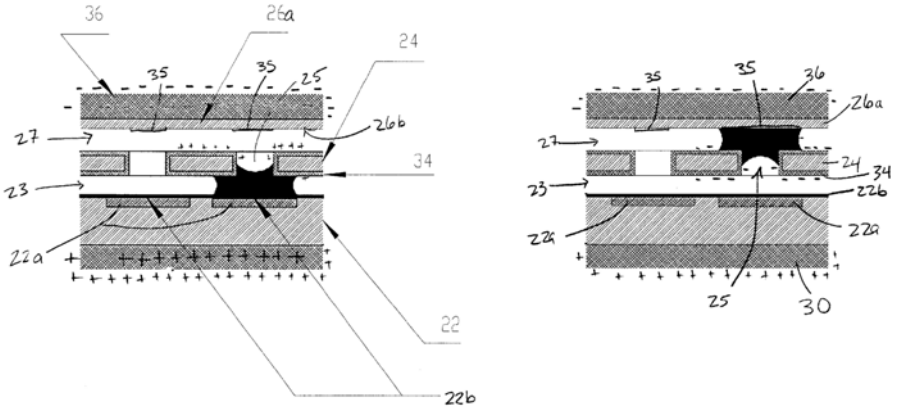

Figure A.2: Electrostatic actuator for microfluidics. *Left:* droplet located in the transportation lower chamber; *Right:* droplet actuated to the top reaction and storage section. Key diagram components; *22:* bottom plate; *22a:* droplet manipulation electrode; *22b:* surface coating; *24: distribution plate 25:* aperture; *34:* distribution plate electrode; *35:* reaction side; *36:* upper electrode. Image source [141].

be covered with different reactive substrates, thus providing selective sensing. Rising a droplet into the top chamber and thus making contact with a reactive substrate allows for multiple reactions to be performed on the device while the bottom chamber is available for droplet transport. This patent seems to discuss a rather theoretical device construction due to the lack of evidence for real prototypes and the somewhat cumbersome and challenging construction.

Method and apparatus for non-contact electrostatic actuation of drop lets [2002-09-24] Another similar device has been reported in [142], where a wire replaces the middle distribution plate from the previously discussed device and serves the purpose of a grounded electrode. This device allows for a droplet to be moved along a bottom plate patterned with electrodes as well as to be transported vertically by applying a positive potential to the top plate. A diagram of this device is shown in Figure A.3. Electrostatic force is used in both patents [142] [141] to move the droplet vertically. The only major difference is that [141] also outlines application cases where the top palate has functionalized spots. It is worth mentioning that [142] was filed before [141] regardless of the use of very similar device construction and operation principles.

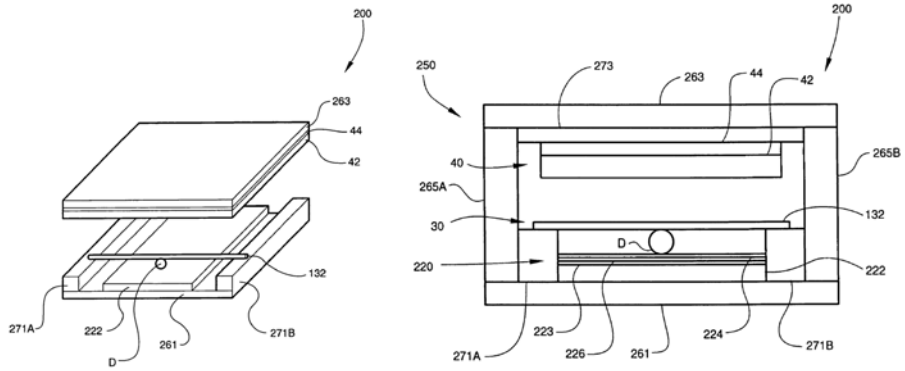

Figure A.3: Device for non-contact electrostatic actuation of droplets: *left:* exploded perspective view; *right:* side elevation view in cross-section. Image source [142].

Apparatus and method for using electrostatic force to cause fluid movement [2002-04-01] A device for manipulating droplets on a planar substrate is reported in [143]. The device claims to operate with electrostatic field force generated from an array of strategically positioned electrodes covered with a hydrophobic isolation layer. The patent claims as an invention the actuation of droplets based on the electrowetting principle as well as merging and mixing droplets on an open digital microfluidic chip. Nevertheless, these claims have already been previously made in [140]. This patent was filed in 2002 from a research group in Palo Alto Research Center after the initial patents for a closed system from Alexander Shenderov [140] [141]

Apparatus for manipulating droplets by electrowetting-based techniques [2002-09-24] This patent [144] claims the construction of a closed digital microfluidic chip and discusses the device components such as substrates, electrodes, coatings, the spacing of the substrates, and the use of a filler fluid. Furthermore, the patent also claims the use of an inlet and outlet ports in order to load and extract fluids from a closed chip. Another notable claim is the use of an electronic controller used to drive the electrodes. It appears that this patent focuses mainly on the device architecture rather than the possible fluidic operations and applications.

Method and apparatus for non-contact electrostatic actuation of drop lets [2002-09-24] This invention claims the independently transporting, merg-

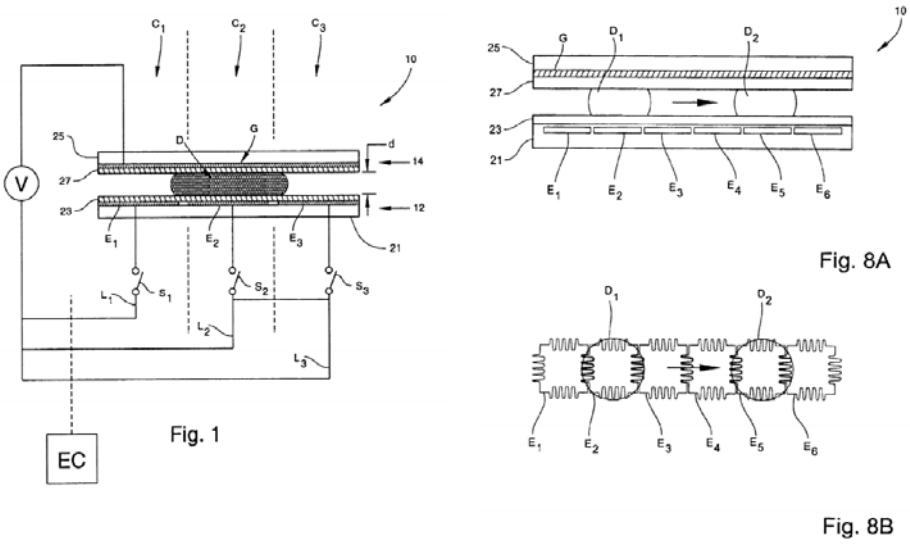

Figure A.4: An apparatus for manipulating droplets. *Fig. 1:* Cross-section view of the an electrowetting actuator. *Fig. 8A and 8B*: illustration of droplet transport by sequentially activating E_1, E_2, E_3, E_4, E_5. Image source [143].

ing, mixing, and processing droplets formed from a continuous flow source [145], and it was filed together with [144]. Furthermore, it appears to be a logical extension of [144], where the focus is mainly on the fluidic handling capabilities of these apparatus. The patent provides detailed actuation electrode designs that define droplet transport, mixing, and splitting procedures. An emphasis is put on mixing and splitting strategies as a part of the process of achieving particular mixing ratios and dilutions. The patent appears to be a follow up of earlier publications [139] [140], which have established the digital microfluidics research.

Methods of using actuators for microfluidics without moving parts [2003-05-06] This patent [146] appears to be on the applications of the first electrowetting actuation device invented by Alexander Shenderov in 2000 [140]. The patent claims as a novelty the use of electrowetting actuation devices for chemical and biochemical reactions in droplets. Nevertheless, this idea has been discussed prior to the patent filing date in scientific publications, such as [147] [148], and this somehow compromises the novelty of the patent. The inventor had been working together with the authors of the mentioned publications.

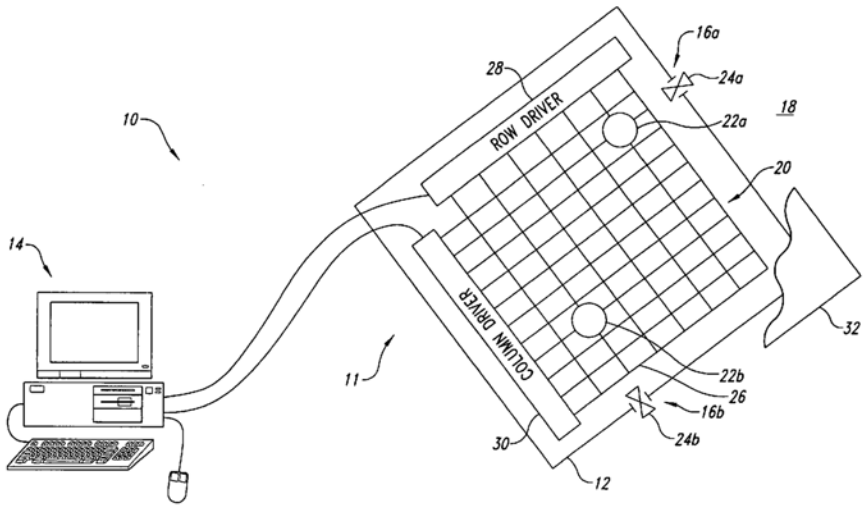

Figure A.5: Schematic diagram of computing controlling system, row and column drivers, and two-dimensional matrix array. *16a* and *16b* are inflow and outflow ports controlled by the corresponding valves *24a* and *24b*. Image source [149]

Method, apparatus and article for microfluidic control via electrowetting, for chemical, biochemical and biological assays and the like [2003-10-16] A microfluidics platform and a two-dimensional open matrix array of control electrodes are shown in Figure A.5. The systems are outlined in a patent [149], where one of the main claims is a method for programmatic control of a microfluidic system based on user interactions with a computing control system or an execution of a preprogrammed actuation sequence. The patent suggests that the fabrication of the presented microfluidic system may take advantage of the well-established process used to fabricate displays. This allows for large arrays of individually addressable electrodes with a relatively high scan update rate and small electrode pitch. The control computing system is thoroughly discussed as well as mechanisms for providing droplets tracking capabilities by using computer vision or capacitive sensing technique.

Method and device for transporting droplet [2004-06-28] Electrowetting actuation typically uses an array of patterned electrodes with uniform pitch and spacing, which allows a droplet to be transported from one electrode to another in a stepwise manner. A different approach for continuous linear actuation was reported in [150] where a pair of comb-like electrodes are placed symmetrically along an actuation axis as shown in Figure A.6. The angle between the

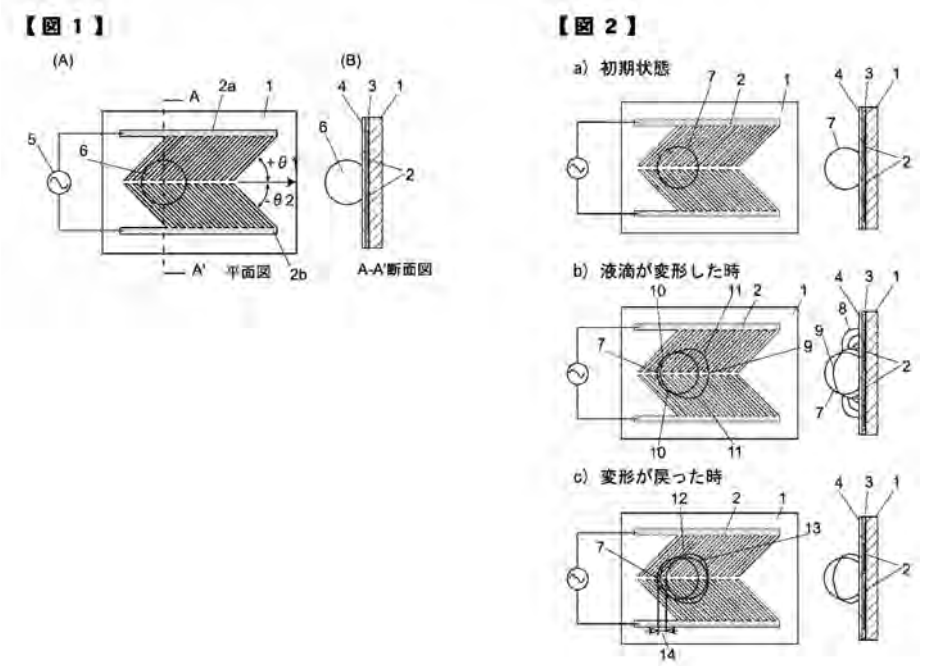

Figure A.6: Electrowetting actuation on a comb-like electrodes: *Left:* device construction; *Right:* droplet actuation steps - *a)* initial state with electrodes off, *b)* control voltage applied to the electrodes, and *c)* control voltage removed and droplet transported to a new location. Image source [150].

electrodes can be in the range from 10 degrees to 80 degrees with respect to the droplet traveling direction. By controlling the actuation voltage and frequency, the speed of the droplet can be varied to the point of the system resonances. When voltage is applied to the electrodes, the droplet naturally gets stretched to cover more surface area towards the narrower angle formed by the electrodes. After disconnecting the voltage source, the droplets return to its equilibrium in a position offset from the initial one due to the already moved center of mass, as it is shown in Figure A.6.

Single-sided apparatus for manipulating Droplets be electrowetting on dielectric technique [2005-10-18] Conceptually electrowetting devices can be split on single-sided (open) and two-sided (closed) where the top side is a single conductive grounded electrode. The standard technique used to produce a wetting gradient for single-sided devices is to selectively bias a pair of neigh-

bouring electrodes. An alternative approach is presented where an addition of a grounding electrode embedded in the isolation layer is used to provide constant reference ground area [151]. The suggested device construction is shown in Figure A.7. One of the main novelty claims of this patent is the layered construction of the device - the actuation electrodes are coated with two dielectric films with a reference ground electrode deposited between them. The device is built on the surface of a standard 4-inch silicon wafer using traditional lithographic processes: first, an array of control electrodes, followed by a layer of the dielectric film, ground electrode is formed, another dielectric film, and the electrowetting-compatible surface. This exact device structure is claimed as part of the invention.

A.3 Patents from Advanced Liquid Logic Inc.

Advanced Liquid Logic Inc. was a spin-off from Duke University, and their work pioneered the field of digital microfluidics. More than 130 patents were issued on a broad range of technology and applications. A small representative subset has been selected and discussed here.

The first patents on the technology and methods for droplet actuation [140] [141] were filed with an assignee Nanolitics Inc, but it appears that later they were transferred to Advanced Liquid Logic. Another patent covering the basics of a droplet splitting operation on an electrowetting device is covered in [152], which is similar to previously filed [144] and [142].

Method and device for conducting biochemical or chemical reactions at multiple temperatures [2006-05-10] A device for and methods for conducting reactions under controlled temperature conditions is claimed in [153]. The device consists of an electrowetting array and at least two reaction zones which maintain stable preset temperatures by using any type of heating (resistive, infrared, or induction heating) or cooling. The patent also describes a method for moving a reaction droplet between temperature-controlled reaction zones in order to follow a predetermined temperature profile. An interesting design characteristic is that the device has defined physical paths constructed out of driving electrodes rather than a large array of individually addressable electrodes. In the outlined design, the paths are used to connect the temperature zones and can also provide a loop-back path for the sample to its initial position. The device can also incorporate detection zones that are built either on the bottom of the top substrate for optical detection. Fluorescent or radioactive labels can be used as signals for detection. One of the possible applications of the

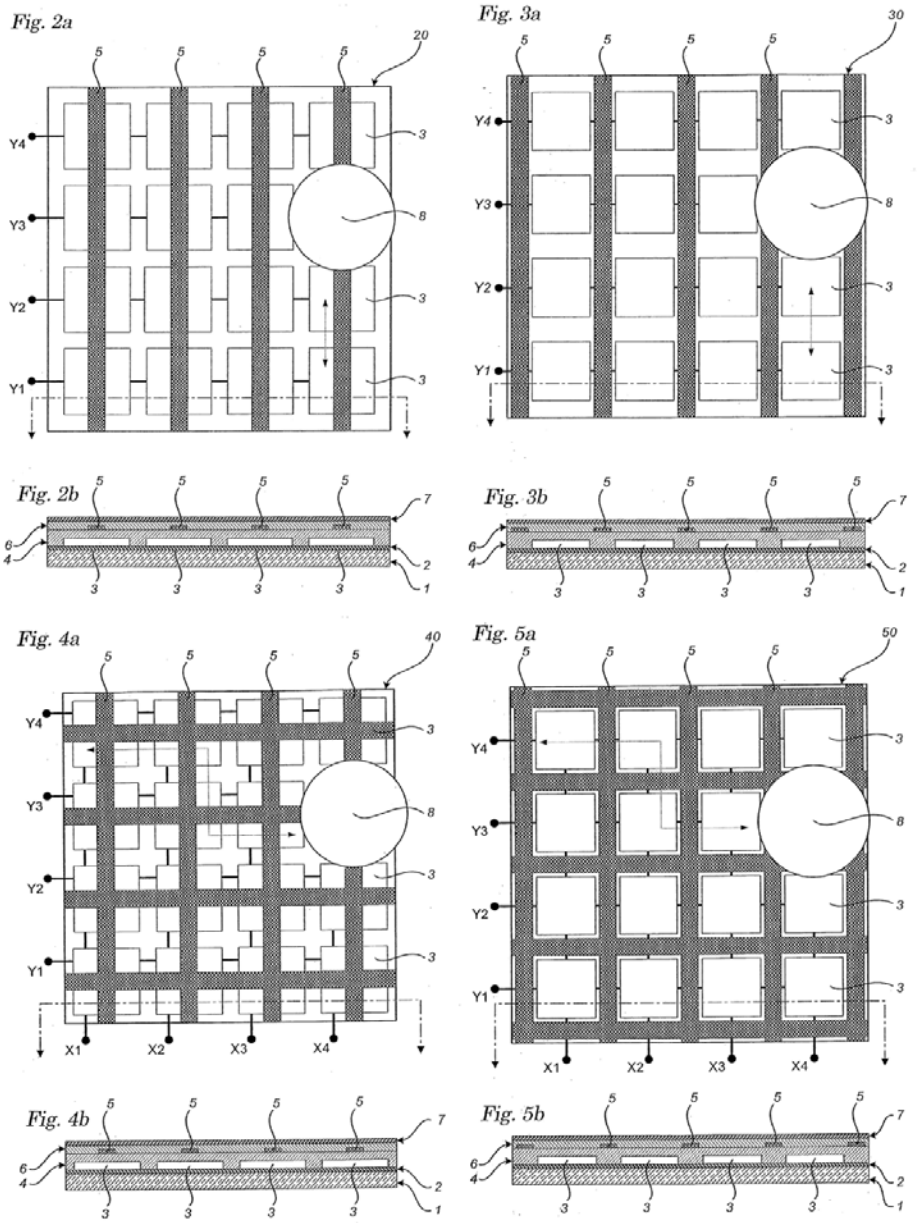

Figure A.7: Single-sided apparatus for manipulating droplets with integrated ground electrode. *Fig. 2*, *Fig. 3*, *Fig. 4*, *Fig. 5* show: *a* top plan view and *b* cross-section of different ground electrode configurations. Ground electrodes are denoted by *5* and driving electrodes are denoted by *3*. Image source [151].

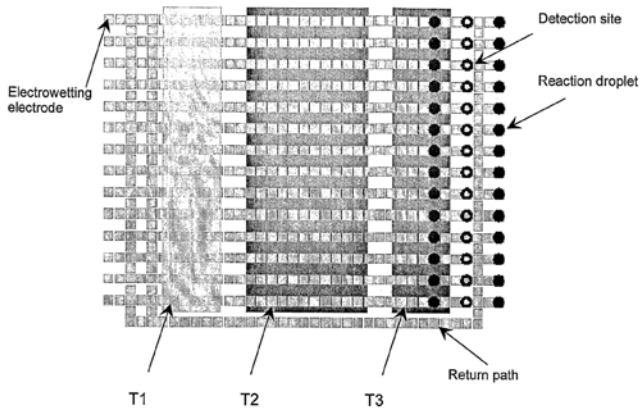

Figure A.8: An example layout of a PCR electrowetting device. *T1*, *T2*, and *T3* are three individual temperature zones. Image source [153].

device claimed in the patent is conducting nucleic acid amplification reactions that require temperature cycling such as polymerase chain reactions (PCR), quantitative PCR, or possibly isothermal amplification. This patent is particularly interesting since nucleic acid manipulations (including amplification) are especially interesting and relevant to digital microfluidics.

Mitigation of biomolecular adsorption with hydrophilic polymer additives [2006-05-18] This patent [154] discusses methods for mitigating molecular absorption on the hydrophobic surface by the use of hydrophilic polymers. Test data from the use of non-ionic surfactants and polymers show a significant reduction of molecular absorption, which enables microfluidic devices to handle samples with high concentrations of biomolecules. The patent reports several tested additives such as pluronic surfactants, polyethylene glycol, methoxypolyethylene glycol, poly-sorbate (polyoxyethylene sorbitan monooleates or Twe en(R), polyoxyethylene octyl phenyl ether (Triton X-100R), polyvinyl pyrollidone, etc. The weight by volume concentration varies in the range of 0.01% to 25%. The patent outlines experimential results from using Horse Radish-Peroxidase (HRP), which is widely used in diagnostics, but it also has a high tendency towards bio-fouling, which makes it impossible to move by electrowetting. One experiment reported that a solution of HPR and PBS (phosphate-buffered saline) was impossible to transport droplets until 0.01% w/v polyethylene glycol (PEG) was added. Further experimental data is provided for Bovine Serum Albumin (BSA) as a fouling agent and PEG as a non-fouling substance. In general, the patent claims the use of surfactants and hydrophilic polymers as a means to allow samples containing biomolecules to be actuated on an electrowetting

device.

Filler fluids for droplet operations [2006-12-15] This patent [155] claims as an invention the use of any filler fluid or gas that allows for the electrowetting actuation to function, such as silicon oil, fluorosilicone oils, different alkanes, parafin oils, argon, carbon dioxide, variety of inert gasses, etc. The use of immiscible oils as a filler fluid that can improve droplet actuation by providing a thin film between the device surface, which serves as a lubrication layer as well as it reduces biofouling. Another function of the filler fluid is to decrease evaporation by encapsulating the sample when reactions are performed at elevated temperatures. Additionally, the patent claims the use of surfactants and their ratios to the filler fluid. Magnetically responsive beads functionalized with antibodies, together with the use of washing droplets, are reported as a part of the invention. Nevertheless, the use of filler fluids, surfactant washing techniques have been reported in a scientific publication prior to the filing date of this patent, which somehow puts in question the purpose of the patent.

Droplet-based nucleic acid amplification device, systems, and methods [2006-12-15] The method of conducting reactions under controlled temperature is claimed in [153], and this patent [156] appears to be an application extension on the previously discussed heating and cooling techniques. The patent claims the use of thin-film heaters, thermoelectric coolers, and Peltier devices as a means to implement temperature-controlled regions under actuation electrodes. Notably, the temperature regions should provide sufficient temperatures for annealing, denaturalization, and extension for performing PCR protocols. The patent also covers the inclusion of a measurement step in the PCR protocol, which is used to measure the concentration of the amplified target nucleic acid and branch the execution of the protocol based on the measured concentration. A corresponding control system capable of driving the electrodes and controlling the temperature zones is claimed as a part of the invention. The droplet microactuator, an illustration of a portable hand-held device, and an illustration of the instrument user interface are shown in Figure A.9. This patent also covers the use of a magnetic field for immobilization of magnetically responsive beads, which is particularity useful for sandwiched affinity-based assays. The magnetic field can be generated from an electromagnet or mechanically actuating a magnet.

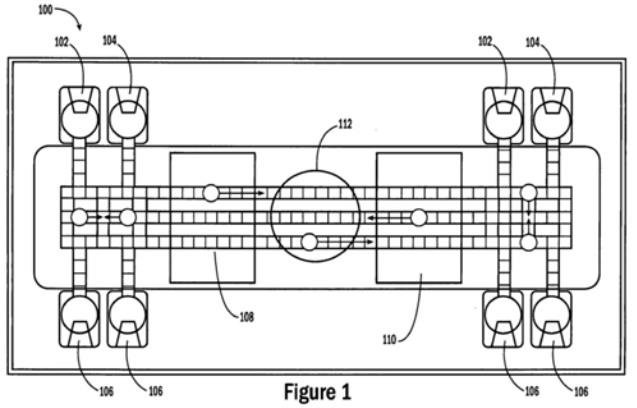

Figure 1

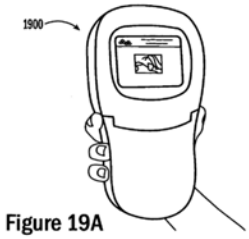

Figure 19A

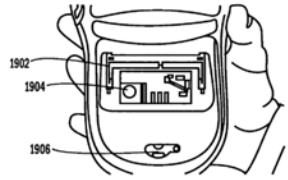

Figure 19B

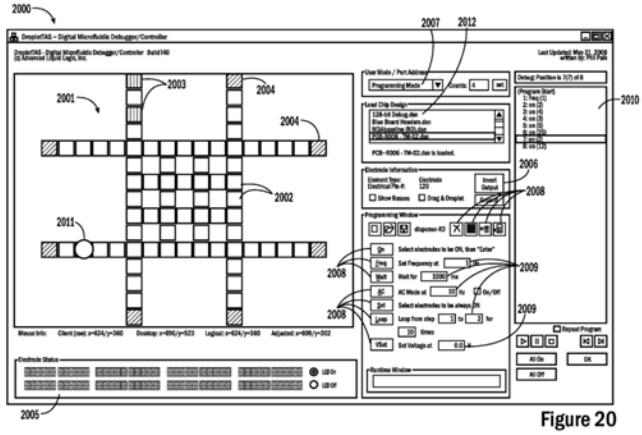

Figure 20

Figure A.9: Droplet-based nucleic acid amplification device. *Figure 1:* Top plan view of the droplet actuator. Reservoirs denoted with *102, 104,* and *106. 108,* and *110* are the device temperature zones. *Figure 19A* and *Figure 19B*are illustrations of a portable hand-held device. *Figure 20* is an illustration of a droplet control system. Images source [156].

A.4 Patents from Wheeler Microfluidics Laboratory

Wheeler's group is one of the leading groups doing research in the field of digital microfluidics. Probably one of their most notable contributions is the development and the release of an open-source digital microfluidics platform called DropBot [29]. The platform dates back to 2013, and it has gained wide popularity among researchers. Naturally, the group has been working on innovative digital microfluidic applications, which resulted in a number of publications and patents. Next, we will review some of these innovative applications.

Droplet-based on-chip sample preparation for mass spectrometry [2005-06-06] One of the earliest patents [157] from the group claims a method for sample preparation for mass spectrometry on a digital microfluidic device. An interesting concept of controlled droplet evaporation for concentration adjustment and solid deposition has been discussed as well. Droplets can also absorb already dried substances. Deposition by evaporation and dissolving of already deposited solids effectively allows for dried solids to be transported on the device using droplets as containers.

Exchangeable sheets pre-loaded with reagent depots for digital microfluidics [2008-10-01] Digital microfluidics chips require a hydrophobic isolation layer to be deposited on the array of control electrodes. Traditionally this layer is deposited on the surface (thus permanently bonded) using processes such as spin coating or vapor deposition. If there is a risk of contamination, the whole device needs to be replaced after use. However, this is not a cost-effective solution since only the top layer of the coating can be contaminated, and the rest of the device is not affected. An innovative solution for a replaceable foil-based top layer is presented in [158] and the device construction is shown in Figure A.10. Furthermore, reagents can be introduced as dried spots on the top foil or peeled off together with the top foil and sent for further analysis or processing. The patent also discusses different materials, fabrication techniques, and important challenges. The stated tested materials for the removable sheet were plastic food-wrap, electrical adhesive tape, and stretched sheets of wax.

Digital microfluidic devices with integrated electrochemical sensors [2015-10-21] This patent [159] covers the use of electrochemical sensors within digital microfluidic devices. The authors describe in detail different electroceramic sensor electrodes configurations and geometries. Two and three-electrode

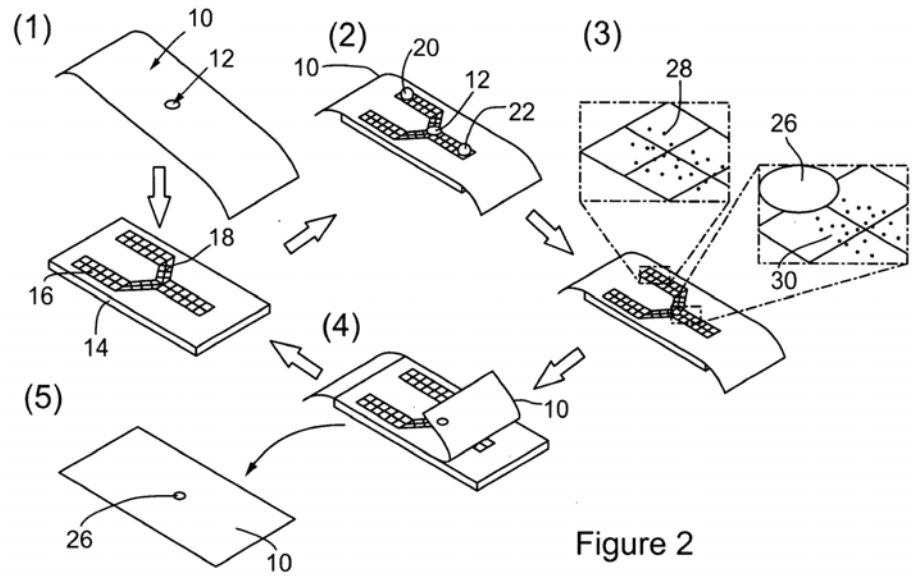

Figure A.10: Removable preloaded sheet strategy. The application and operation procedure is as follows: *(1)* plastic sheet, *12* with dried reagent is applied on the chip; *(2)* device operation where reagents *21* and *22*are moved on the chip; *(3)* residue *30* is left on the chip; *(4)* plastic foil *10* is piled off from the device; *(5)* reaction product *26* can be further analysed. Image source [158].

sensor configurations are discussed. The patent also discloses procedures for fabricating the electrodes on the top and bottom plate of a digital microfluidic device. A generalized idea of including detection zones on digital microfluidic devices was previously discussed in [153], and it has been demonstrated in scientific publications. Nevertheless, it seems that this patent focuses mainly on electrode configuration, sizing, and ratios.

Printed digital microfluidic devices methods of use and manufacture thereof [2017-03-13] Printing the conductive electrodes on a digital microfluidic device holds the potential to drastically reduce the fabrication per-unit cost and thus allow extensive commercialization of single-use devices. This patent [160] claims methods for printing actuation electrodes with conductive ink on porous, glass, or polymer substrate. Different printing technologies, such as ink-jet printing, screen printing, and micro-contact printing, are included in the claimed methods. A detailed discussion about ink types, composition, and printing techniques is included as well. Surface modification such as surface plasma treatment has been used to adjust the surface energy of the substrate in order to optimize the printing process.

A.5 Reflections

A patent is a form of a legal document describing intellectual property, potentially providing the inventor with exclusive rights to take advantage of the claimed novelty. Even though patents usually discuss technical matters, they are structured and written in formal "patent jargon," which is significantly different from the style used for traditional scientific papers. Usually, the goal of a scientific paper is to clearly and concisely convey results from a conducted research where patents are trying to be somehow inclusive and broad in their claims. Patents can also claim an idea and vision without the need for scientific proof that it is even feasible. The amount of information varies significantly, and a patent can easily be a few pages of illustrations claiming an instrument enclosure design [161] or packed with information and approaching hundred of pages [155].

Nevertheless, most of the reviewed patents cover technical details in great length and depth. Information is presented inclusively, often with references or pointers to more sources. Patents are also a great indication of how visionary and exciting ideas were generated and thus set directions in the research field.

In general, the filed of digital microfluidics appears to be heavily patented in

both technological and application domains. Nevertheless, it is hard to tell whether these patents will hold in case of a patent dispute since there are a lot of overpainting ideas and claims among the limited number of patents outlined here. Moreover, claims in patents were published even though they were already explored in scientific papers before the patent filing date, which somehow discredits the novelty of the reported invention. Plausibly some of these patents were filed with the sole purpose of enhancing a patent portfolio rather than aiming for protecting competitive technological advantage.

Appendix B

Platform-based cyber-fluidic platform concept validation

This chapter presents an incremental step of the agile development of the cyber-fluidic platform. A small scale platform prototype was developed to serve as a proof of concept, technology evaluation setup, and a pilot system for the cyber-fluidic platform subject of this thesis work.

The prototype was based on the modular design concepts and implemented the cyber-fluidic architecture outlined in Chapter 5. The prototype is shown in Figure B.1, and its implementation was intentionally kept minimalistic in all aspects. The limited implementation was justified with the fact that the prototype was meant to be used only to test the different system components such as the new microcontroller, communication, modules, bus interface isolators, power subsystem, high-voltage power supply design, and the scalability of the new electrode drivers concept.

The selected Cortex M7 (STM32F767ZIT6) processor with its associated toolchain proved to be a more capable alternative to the previously used Cortex M4. Moreover, the toolchain provided by the manufacturer of the microcontroller provided a range of configuration tools and software modules, which accelerated the prototyping process.

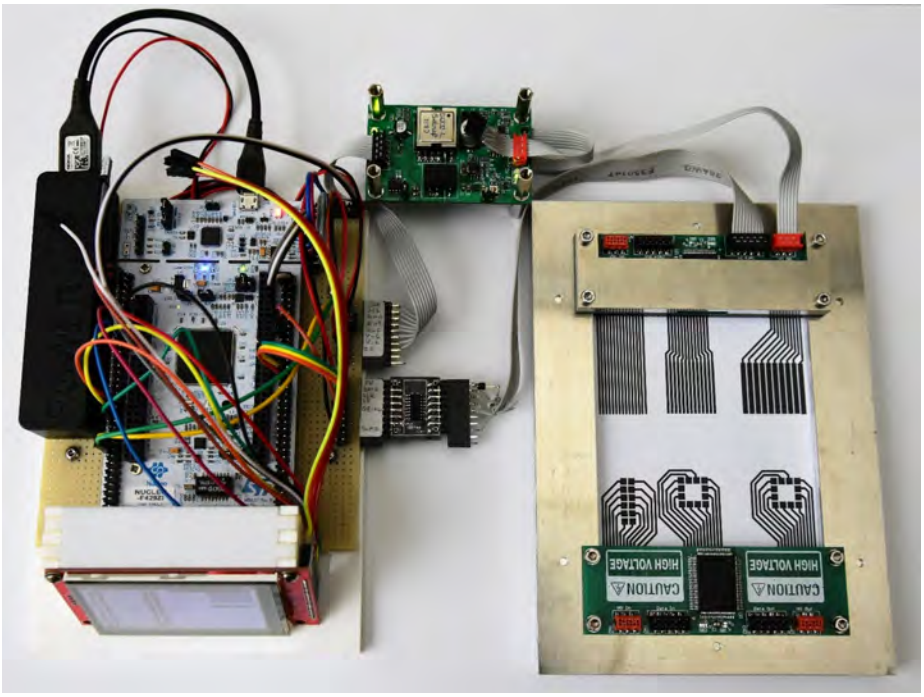

(a) The platform prototype with a mounted paper-based digital biochip.

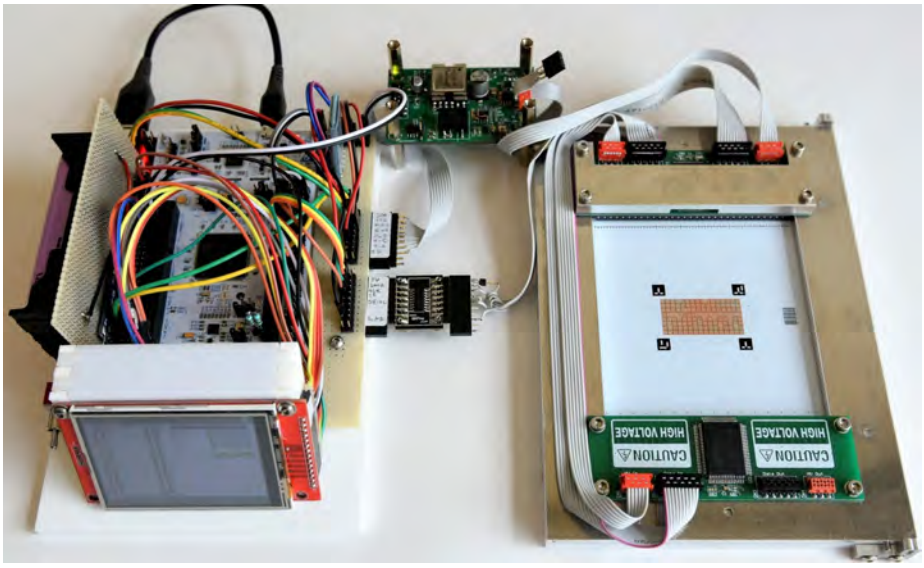

(b) The platform prototype with a mounted PCB-based digital biochip.

Figure B.1: Platform-based cyber-fluidic system concept validation prototype.

The high voltage power supply prototype showed precision and reliability, and the module was later employed in the next, scaled-up version of the cyber-fluidics system. Although the initial redesign intension to fit into the modular concept, the high voltage power supply module remained unchanged, and it was added to the top of a prototyping module (see Section 5.4.7) to comply with the modular design.

A hinged digital biochip holder was developed to evaluate the developed fluidic system approach. The holder was designed to accommodate two electrode driver boards, each capable of controlling 64 individual electrodes. A multipin spring-loaded connector was used to establish a connection between the driver boards and the removable digital biochip. The holder was designed to interface with a device with up to 128 actuation electrodes and dimensions of 10 cm×15 cm. This prototype played an instrumental role in the development of the paper-based digital biochip outlined in Appendix C. Figure B.1a shows the system with a mounted paper-based device. Moreover, the high number of electrode control channels and the removable digital biochip promoted migrating to the PCB fabrication technology. The prototype system with mounted PCB digital biochip implementing an array of 8×16 actuation electrodes is shown in Figure B.1b.

The platform prototype successfully served the purpose of testing the envisioned system architecture. Moreover, it was used for technology evaluation and as a testbed in the initial development steps of the digital biochips.

Appendix C

Paper-based digital biochips

This chapter presents experimental results regarding the fabrication of paper-based digital biochip and shadow masks-printable electrochemical biosensors.

C.1 Inkjet printable digital biochips

Inkjet printing was used as an additive method to deposit conductive electrodes on three different types of paper (two batches of HP Advanced Photo paper) and special printing media (NB-RC-3GR120, Mitsubishi Paper Mills Limited). A desktop inkjet printer Brother DCP-J562DW, empty refillable cartridges LC-221, and Silver Nano Particle Ink NBSIJ-MU01 (Mitsubishi Paper Mills Limited, Japan) were used to prepare the printing setup. Custom-formulated carbon nanotubes aqueous inkjet inks have been demonstrated as well [10] [23] However, commercially available inks were considered due to the expected reliability and proven qualities [55] [162] [163].

The NBSIJ-MU01 conductive ink sinters at room temperature without any extra processing steps. A test series of 50 mm long tracks with width in the range of 0.05 mm to 2 mm was printed on the three types of paper and the special printing media. The test was targeting to evaluate the compatibility of the

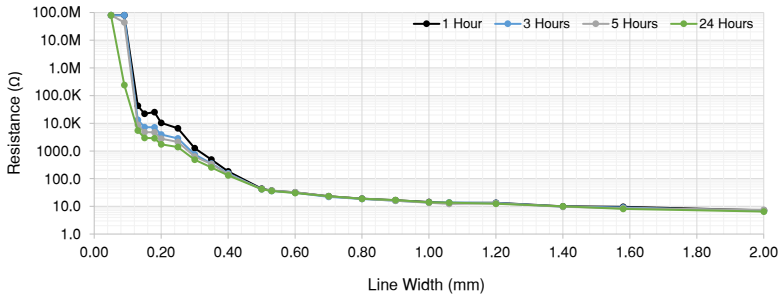

(a) NB-RC-3GR120

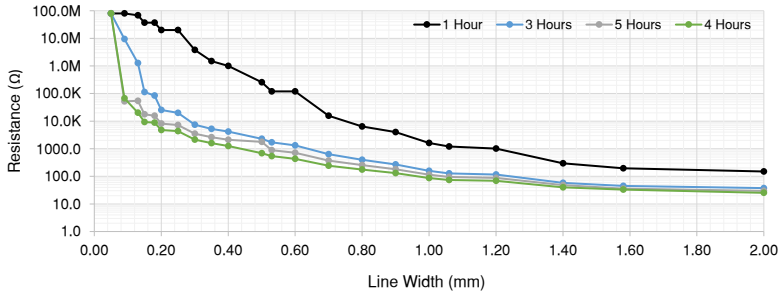

(b) HP Advanced Photo paper - Bach 1

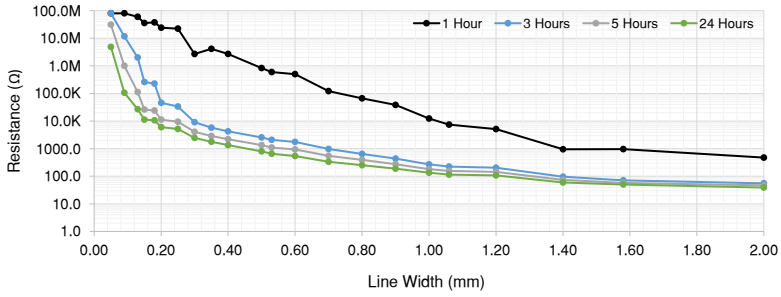

(c) HP Advanced Photo paper - Bach 2

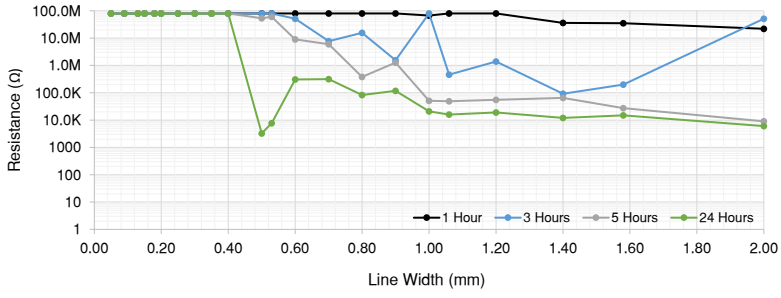

(d) Dualsided inkjet printing paper

Figure C.1: The resistance of a printed track as a function of track width and sintering time.

printing substrate with the conductive ink, determine the correlation between resistance and track width, and study the effect of sintering time at ambient conditions.

After printing, the four samples were let sinter at room temperature, and resistance measurements of each printed track were taken at 1, 3, 5, and 24 hours after the printing. The test results are shown in Figure C.1, and naturally, the special printing medial (NB-RC-3GR120) exhibits the shortest and the most consistent sintering time. Moreover, this substrate resulted in the lowest overall track resistance.

As anticipated, the two batches of HP Advanced Photo paper showed similar sintering time and overall performance, which is a good indicator of the paper production process. The high track resistance and the variable data points showed that dual-sided inkjet paper is not suitable for printing conductive electrodes. This also showed the importance of the microporous structure of the printing media since only the dual-sided inkjet paper did not have that structure and failed to deliver low resistance tracks.

The experiment data shows that the usable conductive track width on the NB-RC-3GR120 media starts from 125-150 µm, and on the commercial photo paper, although with higher resistance, it starts from 200 µm. Sintering time of 3 hours was, in general, sufficient under the tested conditions. A notable fact is that the resistance of the wider tracks is less dependant on the sintering time.

The horizontal and vertical printing resolution was tested by printing a rectangular pattern with increasing gaps between the electrodes. The same pattern was printed in a horizontal and vertical direction, hence testing the spatial resolution of the printer. The resulted prints are shown in Figure C.2, where Figure C.2a shows the results when the gap is oriented horizontally, i.e., the gap is lateral to the linear movement of the printing heads, and Figure C.2b shows the printing patter, when the gap is oriented perpendicularly to the moving direction of the heads assembly. A resistive measurement was used to determine what is the smallest printable gap that provides electrical isolation in each printing direction. It was found that with the current printing setup 75 µm and 150 µm were correspondingly the minimum horizontal and vertical spacing.

Two paper-based digital biochips were fabricated using the established inkjet printing setup. The first device consisted of test electrode patterns, as shown in Figure C.3a. The second device consisted of more elaborate electrode paper, as shown in Figure C.3b. The outline dimensions of the two devices were 10×15cm.

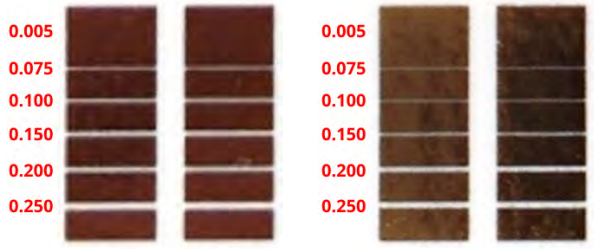

(a) Horizontal gap alignment.

(b) Vertical gap alignment.

Figure C.2: Horizontal and vertical printing resolution. The labeled distance between the electrodes in µm.

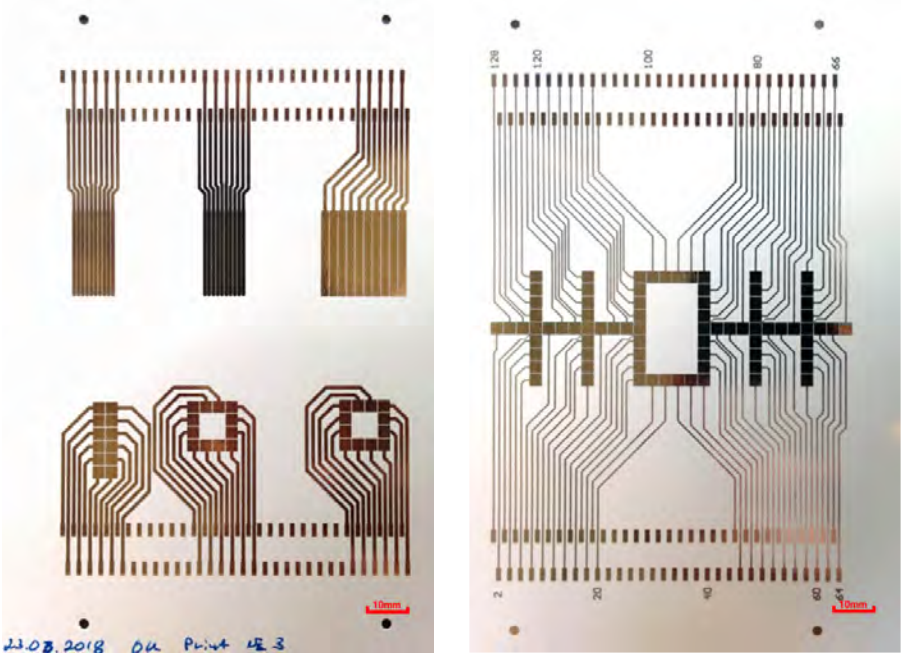

(a) Test electrode geometries.

(b) An example of an actuation electrode pattern.

Figure C.3: Inkjet printed digital biochips. Device dimensions 10 cm×15 cm.

C.2 Printable paper-based biosensors

On the quest for a fully integrated digital biochip, a method for shadow printing of electrochemical biosensors was developed as a part of this thesis work [123]. The fabrication process and used materials are described in the referenced article.

The objective was to fabricate inkjet printable actuation electrodes and mask or screen printed conducting structure forming biosensor. In the timeframe of this thesis work, both of these methods were developed, such actuation and sensing electrodes can be fabricated on the same substrate. However, due to a change in research focus, the integration was deemed as future work. For illustration purposes, a batch of electrochemical biosensors fabricated on a commercial photo paper is shown in Figure C.4.

Figure C.4: A batch of paper-based electrochemical biosensors.

Bibliography

[1] A. Murry, "Heat sensitive printing element and method," U.S. Patent 2 556 500, Jun. 12, 1951.

[2] A. Manz, N. Graber, and H. M. Widmer, "Miniaturized Total Chemical Analysis Systems : a Novel Concept for Chemical Sensing," *Sensors and Actuators B: Chemical*, vol. Volume 1, no. Issues 1–6, pp. 244–248, 1990.

[3] M. A. Unger, H. P. Chou, T. Thorsen, A. Scherer, and S. R. Quake, "Monolithic microfabricated valves and pumps by multilayer soft lithography," *Science*, vol. 288, no. 5463, pp. 113–116, 2000.

[4] H. P. Chou, M. A. Unger, and S. R. Quake, "A microfabricated rotary pump," *Biomedical Microdevices*, vol. 3, no. 4, pp. 323–330, 2001.

[5] F. K. Balagaddé, L. You, C. L. Hansen, F. H. Arnold, and S. R. Quake, "Microbiology: Long-term monitoring of bacteria undergoing programmed population control in a microchemostat," *Science*, vol. 309, no. 5731, pp. 137–140, jul 2005.

[6] K. Choi, A. H. Ng, R. Fobel, and A. R. Wheeler, "Digital Microfluidics," *Annual Review of Analytical Chemistry*, vol. 5, no. 1, pp. 413–440, 2012.

[7] V. Srinivasan, V. K. Pamula, and R. B. Fair, "Droplet-based microfluidic lab-on-a-chip for glucose detection," *Analytica Chimica Acta*, vol. 507, no. 1, pp. 145–150, 2004.

[8] E. Samiei, G. S. Luka, H. Najjaran, and M. Hoorfar, "Integration of biosensors into digital microfluidics: Impact of hydrophilic surface of biosensors on droplet manipulation," *Biosensors and Bioelectronics*, vol. 81, pp. 480–486, 2016.

[9] N. A.H.C., F. R., F. C., L. J., R. D.G., S. A., D. C., D. M.D.M., L. C., H. M., M. N.S., L. V., A. M.A.M., S. E.A., C. M.D., J. R., O. M., S. H.M., K. A., R. P.A., M. N., C. P.M., N. M., N. R., K. N., K. J., K. M., B. J.W., B. P., and L. E., "A digital microfluidic system for serological immunoassays in remote settings," *Science Translational Medicine*, vol. 10, no. 438, p. eaar6076, 2018.

[10] N. Ruecha, J. Lee, H. Chae, H. Cheong, V. Soum, P. Preechakasedkit, O. Chailapakul, G. Tanev, J. Madsen, N. Rodthongkum, O.-S. Kwon, and K. Shin, "Paper-Based Digital Microfluidic Chip for Multiple Electrochemical Assay Operated by a Wireless Portable Control System," *Advanced Materials Technologies*, vol. 201600267, p. 1600267, 2017.

[11] E. Wulff-Burchfield, W. A. Schell, A. E. Eckhardt, M. G. Pollack, Z. Hua, J. L. Rouse, V. K. Pamula, V. Srinivasan, J. L. Benton, B. D. Alexander, D. A. Wilfret, M. Kraft, C. B. Cairns, J. R. Perfect, and T. G. Mitchell, "Microfluidic platform versus conventional real-time polymerase chain reaction for the detection of Mycoplasma pneumoniae in respiratory specimens," *Diagnostic Microbiology and Infectious Disease*, vol. 67, no. 1, pp. 22–29, 2010.

[12] T. B. Yehezkel, A. Rival, O. Raz, R. Cohen, Z. Marx, M. Camara, J.-F. Dubern, B. Koch, S. Heeb, N. Krasnogor, C. Delattre, and E. Shapiro, "Synthesis and cell-free cloning of DNA libraries using programmable microfluidics," *Nucleic Acids Research*, vol. 44, no. 4, pp. e35–e35, feb 2016.

[13] J. Zhou, L. Lu, K. Byrapogu, D. M. Wootton, P. I. Lelkes, and R. Fair, "Electrowetting-based multi-microfluidics array printing of high resolution tissue construct with embedded cells and growth factors," in *Virtual and Physical Prototyping*, vol. 2, no. 4, 2007, pp. 217–223.

[14] A. H. Ng, B. B. Li, M. D. Chamberlain, and A. R. Wheeler, "Digital Microfluidic Cell Culture," *Annual Review of Biomedical Engineering*, vol. 17, no. 1, pp. 91–112, 2015.

[15] T. B. Yehezkel, A. Rival, O. Raz, R. Cohen, Z. Marx, M. Camara, J.-F. Dubern, B. Koch, S. Heeb, N. Krasnogor, C. Delattre, and E. Shapiro, "Synthesis and cell-free cloning of DNA libraries using programmable microfluidics," *Nucleic Acids Research*, vol. 44, no. 4, pp. e35–e35, feb 2016.

[16] H. Baig, "Methods and Tools for the Analysis , Verification and Synthesis of Genetic Logic Circuits Hasan Baig," 2017.

[17] V. Singh, "Recent advances and opportunities in synthetic logic gates engineering in living cells," *Systems and Synthetic Biology*, vol. 8, no. 4, pp. 271–282, 2014.

[18] "Baebies," www.baebies.com, accessed: 2020-10-30.

[19] "Genmarkdx," www.genmarkdx.com, accessed: 2020-10-30.

[20] "Oxford nanopore - voltrax," www.nanoporetech.com/products/voltrax, accessed: 2020-10-30.

[21] M. G. Pollack, V. K. Pamula, V. Srinivasan, and A. E. Eckhardt, "Applications of electrowetting-based digital microfluidics in clinical diagnostics," pp. 393–407, 2011.

[22] C. Dixon, A. H. C. Ng, R. Fobel, M. B. Miltenburg, and A. R. Wheeler, "An inkjet printed, roll-coated digital microfluidic device for inexpensive, miniaturized diagnostic assays," *Lab Chip*, vol. 16, pp. 4560–4568, 2016.

[23] V. Soum, Y. Kim, S. Park, M. Chuong, S. R. Ryu, S. H. Lee, G. Tanev, J. Madsen, O. S. Kwon, and K. Shin, "Affordable fabrication of conductive electrodes and dielectric films for a paper-based digital microfluidic chip," *Micromachines*, vol. 10, no. 2, 2019.

[24] B. Hadwen, G. R. Broder, D. Morganti, A. Jacobs, C. Brown, J. R. Hector, Y. Kubota, and H. Morgan, "Programmable large area digital microfluidic array with integrated droplet sensing for bioassays," *Lab on a Chip*, vol. 12, no. 18, pp. 3305–3313, 2012.

[25] P. M. Levine, P. Gong, R. Levicky, and K. L. Shepard, "Active CMOS sensor array for electrochemical biomolecular detection," *IEEE Journal of Solid-State Circuits*, vol. 43, no. 8, pp. 1859–1871, 2008.

[26] J. Ott, T. Loveless, C. Curtis, M. Lesani, and P. Brisk, "BioScript: programming safe chemistry on laboratories-on-a-chip," *Proceedings of the ACM on Programming Languages*, vol. 2, no. OOPSLA, pp. 1–31, oct 2018.

[27] G. M. Whitesides, "The origins and the future of microfluidics," *Nature*, vol. 442, no. 7101, pp. 368–373, 2006.

[28] G. Whitesides, "The lab finally comes to the chip!" *Lab on a Chip*, vol. 14, no. 17, p. 3125, jul 2014.

[29] R. Fobel, C. Fobel, and A. R. Wheeler, "DropBot: An open-source digital microfluidic control system with precise control of electrostatic driving force and instantaneous drop velocity measurement," *Applied Physics Letters*, vol. 102, no. 19, 2013.

[30] A. Mirela and U. Gaudenz, "OpenDrop: An Integrated Do-It-Yourself Platform for Personal Use of Biochips," *Bioengineering*, vol. 4, no. 4, p. 45, may 2017.

[31] Anon, "A Full-Stack Microfluidics Platform with Multi-Level Feedback Control," *ASPLOS-sbm*, 2019.

[32] V. Ananthanarayanan and W. Thies, "BioCoder: A programming language for standardizing and automating biology protocols," *Journal of Biological Engineering*, vol. 4, no. 1, p. 13, 2010.

[33] C. Curtis, D. Grissom, and P. Brisk, "A compiler for cyber-physical digital microfluidic biochips," *Proceedings of the 2018 International Symposium on Code Generation and Optimization - CGO 2018*, pp. 365–377, 2018.

[34] D. Grissom, C. Curtis, S. Windh, C. Phung, N. Kumar, Z. Zimmerman, K. O'Neal, J. McDaniel, N. Liao, and P. Brisk, "An open-source compiler and PCB synthesis tool for digital microfluidic biochips," *Integration, the VLSI Journal*, vol. 51, pp. 169–193, 2015.

[35] P. Pop, M. Alistar, E. Stuart, and J. Madsen, *Fault-Tolerant Digital Microfluidic Biochips*. Cham: Springer International Publishing, 2016.

[36] N. Blow, "Microfluidics: In search of a killer application," *Nature Methods*, vol. 4, no. 8, pp. 665–670, 2007.

[37] F. Mugele and J.-C. Baret, "Electrowetting: from basics to applications," *Journal of Physics: Condensed Matter*, vol. 17, no. 28, pp. R705–R774, 2005.

[38] J. T. Stock, "Gabriel Lippmann and the capillary electrometer." *Bull. Hist. Chem*, vol. 29, no. 1, pp. 16–20, 2004.

[39] D. C. Grahame, "The Electrical Double Layer and the Theory of Electrocapillarity." *Chemical Reviews*, vol. 41, no. 3, pp. 441–501, 1947.

[40] B. Berge, "Surface and Interface Physics," 1993.

[41] C. Quilliet and B. Berge, "Electrowetting: A recent outbreak," *Current Opinion in Colloid and Interface Science*, vol. 6, no. 1, pp. 34–39, 2001.

[42] M. Vallet, B. Berge, and L. Vovelle, "Electrowetting of water and aqueous solutions on poly(ethylene terephthalate) insulating films," *Polymer*, vol. 37, no. 12, pp. 2465–2470, 1996.

[43] H. J. Verheijen and M. W. Prins, "Reversible electrowetting and trapping of charge: Model and experiments," *Langmuir*, vol. 15, no. 20, pp. 6616–6620, 1999.

[44] M. K. Chaudhury and G. M. Whitesides, "How to Make Water Run Uphill," *American Association for the Advancement of Science*, vol. 256, no. 5063, pp. 1539–1541, 1992.

[45] Y. Li, R. Chen, and R. J. Baker, "A fast fabricating electro-wetting platform to implement large droplet manipulation," in *2014 IEEE 57th International Midwest Symposium on Circuits and Systems (MWSCAS)*. IEEE, aug 2014, pp. 326–329.

[46] M. Washizu, "Electrostatic actuation of liquid droplets for microreactor applications," *IEEE Transactions on Industry Applications*, vol. 34, no. 4, pp. 732–737, 1998.

[47] M. G. Pollack, R. B. Fair, and A. D. Shenderov, "Electrowetting-based actuation of liquid droplets for microfluidic applications," *Applied Physics Letters*, vol. 77, no. 11, pp. 1725–1726, 2000.

[48] V. Srinivasan, V. K. Pamula, and R. B. Fair, "An integrated digital microfluidic lab-on-a-chip for clinical diagnostics on human physiological fluids," *Lab on a Chip*, vol. 4, no. 4, p. 310, 2004.

[49] ——, "An integrated digital microfluidic lab-on-a-chip for clinical diagnostics on human physiological fluids," *Lab on a Chip*, vol. 4, no. 4, p. 310, 2004.

[50] M. G. Pollack, A. D. Shenderov, and R. B. Fair, "Electrowetting-based actuation of droplets for integrated microfluidics," *Lab on a Chip*, vol. 2, no. 2, p. 96, 2002.

[51] M. Abdelgawad and A. R. Wheeler, "Rapid prototyping in copper substrates for digital microfluidics," *Advanced Materials*, vol. 19, no. 1, pp. 133–137, 2007.

[52] M. J. Jebrail, R. F. Renzi, A. Sinha, J. Van De Vreugde, C. Gondhalekar, C. Ambriz, R. J. Meagher, and S. S. Branda, "A solvent replenishment solution for managing evaporation of biochemical reactions in air-matrix digital microfluidics devices," *Lab Chip*, vol. 15, no. 1, pp. 151–158, 2015.

[53] R. Fobel, A. E. Kirby, A. H. Ng, R. R. Farnood, and A. R. Wheeler, "Paper microfluidics goes digital," *Advanced Materials*, vol. 26, no. 18, pp. 2838–2843, 2014.

[54] H. Ko, J. Lee, Y. Kim, B. Lee, C. H. Jung, J. H. Choi, O. S. Kwon, and K. Shin, "Active digital microfluidic paper chips with inkjet-printed patterned electrodes," *Advanced Materials*, vol. 26, no. 15, pp. 2335–2340, 2014.

[55] Y. Kawahara, S. Hodges, B. S. Cook, and G. D. Abowd, "Source Thermoplastic polyurethane tpu resin / tpu pallet on m.alibaba.com," *UbiComp'13*, pp. 363–372, 2017.

[56] "Agc chemical company - cytop," www.agc-chemicals.com/jp/en/fluorine/products/detail/index.html?pCode=JP-EN-F019, accessed: 2020-10-30.

[57] "Cytonix products," www.cytonix.com/Articles.asp?ID=252, accessed: 2020-10-30.

[58] S. H. Au, P. Kumar, and A. R. Wheeler, "A new angle on Pluronic additives: Advancing droplets and understanding in digital microfluidics," *Langmuir*, vol. 27, no. 13, pp. 8586–8594, 2011.

[59] P. Q. Vo, M. C. Husser, F. Ahmadi, H. Sinha, and S. C. Shih, "Image-based feedback and analysis system for digital microfluidics," *Lab on a Chip*, vol. 17, no. 20, pp. 3437–3446, 2017.

[60] H. Ren, R. B. Fair, and M. G. Pollack, "Automated on-chip droplet dispensing with volume control by electro-wetting actuation and capacitance metering," *Sensors and Actuators, B: Chemical*, vol. 98, no. 2-3, pp. 319–327, 2004.

[61] R. A. Strumer, V. Srinivasan, and A. Sudarsan, "Microfluidic feedback using impedance detection," U.S. Patent US9 492 822, Nov. 15, 2016.

[62] R. Fobel, A. Kirby, and A. R. Wheeler, "Multiplexed droplet actuation and sensing in digital microfluidics," Canada Patent US2019/0 201 902, Feb. 13, 2019.

[63] S. Cho, H. Moon, and C.-J. Kim, "Creating, Transporting, Cutting, and Merging Liquid Droplets by Electrowetting-Based Actuation for Digital Microfluidic Circuits," *Journal of Microelectromechanical Systems*, vol. 12, no. 1, pp. 70–80, 2003.

[64] J. Gong and C. J. C. Kim, "Characterization and design of digitizing processes for uniform and controllable droplet volume in ewod digital microfluidics," *Technical Digest - Solid-State Sensors, Actuators, and Microsystems Workshop*, vol. I, pp. 159–162, 2006.

[65] J. Gong and C.-J. C. J. Kim, "All-electronic droplet generation on-chip with real-time feedback control for EWOD digital microfluidics." *Lab on a chip*, vol. 8, no. 6, pp. 898–906, 2008.

[66] P. Paik, V. K. Pamula, and R. B. Fair, "Rapid droplet mixers for digital microfluidic systems," *Lab on a Chip*, vol. 3, no. 4, pp. 253–259, 2003.

[67] L. Wan, T. Chen, J. Gao, C. Dong, A. H. H. Wong, Y. Jia, P. I. Mak, C. X. Deng, and R. P. Martins, "A digital microfluidic system for loop-mediated isothermal amplification and sequence specific pathogen detection," *Scientific Reports*, vol. 7, no. 1, pp. 1–11, 2017.

[68] B. J. Coelho, B. Veigas, H. Águas, E. Fortunato, R. Martins, P. V. Baptista, and R. Igreja, "A digital microfluidics platform for loop-mediated isothermal amplification detection," *Sensors (Switzerland)*, vol. 17, no. 11, 2017.

[69] S. C. C. Shih, G. Goyal, P. W. Kim, N. Koutsoubelis, J. D. Keasling, P. D. Adams, N. J. Hillson, and A. K. Singh, "A Versatile Microfluidic Device for Automating Synthetic Biology," *ACS Synthetic Biology*, vol. 4, no. 10, pp. 1151–1164, 2015.

[70] A. Farzbod and H. Moon, "Integration of reconfigurable potentiometric electrochemical sensors into a digital microfluidic platform," *Biosensors and Bioelectronics*, vol. 106, no. November 2017, pp. 37–42, 2018.

[71] D. S. M. W. A. b. c. Dryden M.D.M.a Rackus, "Integrated digital microfluidic platform for voltammetric analysis," *Analytical Chemistry*, vol. 85, no. 18, pp. 8809–8816, 2013.

[72] V. Srinivasan, V. Pamula, M. Pollack, and R. Fair, "A digital microfluidic biosensor for multianalyte detection," in *The Sixteenth Annual International Conference on Micro Electro Mechanical Systems, 2003. MEMS-03 Kyoto. IEEE*, vol. 111, no. 479. IEEE, 2003, pp. 327–330.

[73] M. H. Shamsi, K. Choi, A. H. Ng, M. Dean Chamberlain, and A. R. Wheeler, "Electrochemiluminescence on digital microfluidics for microRNA analysis," *Biosensors and Bioelectronics*, vol. 77, pp. 845–852, 2016.

[74] M. J. Jebrail and A. R. Wheeler, "Let's get digital: Digitizing chemical biology with microfluidics," *Current Opinion in Chemical Biology*, vol. 14, no. 5, pp. 574–581, 2010.

[75] V. Srinivasan, V. K. Pamula, and R. B. Fair, "An integrated digital microfluidic lab-on-a-chip for clinical diagnostics on human physiological fluids," *Lab on a Chip*, vol. 4, no. 4, pp. 310–315, 2004.

[76] V. N. Luk, G. C. Mo, and A. R. Wheeler, "Pluronic additives: A solution to sticky problems in digital microfluidics," *Langmuir*, vol. 24, no. 12, pp. 6382–6389, 2008.

[77] A. T. Jafry, H. Lee, A. P. Tenggara, H. Lim, Y. Moon, S. H. Kim, Y. Lee, S. M. Kim, S. Park, D. Byun, and J. Lee, "Double-sided electrohydrodynamic jet printing of two-dimensional electrode array in paper-based digital microfluidics," *Sensors and Actuators, B: Chemical*, vol. 282, no. November 2018, pp. 831–837, 2019.

[78] A. Amin, M. Thottethodi, T. Vijaykumar, S. Wereley, and S. C. Jacobson, "Aquacore: a programmable architecture for microfluidics," *Proceedings of the 34th annual international symposium on Computer architecture*, pp. 254–265, 2007.

[79] R. Fobel, C. Fobel, and A. R. Wheeler, "DropBot: An open-source digital microfluidic control system with precise control of electrostatic driving force and instantaneous drop velocity measurement," *Applied Physics Letters*, vol. 102, no. 19, pp. 1129–1132, 2013.

[80] M.-C. Liu, J.-G. Wu, M.-F. Tsai, W.-S. Yu, P.-C. Lin, I.-C. Chiu, H.-A. Chin, I.-C. Cheng, Y.-C. Tung, and J.-Z. Chen, "Two dimensional thermoelectric platforms for thermocapillary droplet actuation," *RSC Adv.*, vol. 2, no. 4, pp. 1639–1642, 2012.

[81] N. Bjelobrk, H.-L. Girard, S. Bengaluru Subramanyam, H.-M. Kwon, D. Quéré, and K. K. Varanasi, "Thermocapillary motion on lubricant-impregnated surfaces," *Physical Review Fluids*, vol. 1, no. 6, p. 063902, oct 2016.

[82] U. Lehmann, S. Hadjidj, V. K. Parashar, A. Rida, and M. A. Gijs, "Two dimensional magnetic manipulation of microdroplets on a chip," in *Digest of Technical Papers - International Conference on Solid State Sensors and Actuators and Microsystems, TRANSDUCERS '05*, vol. 1, no. figure 1, 2005, pp. 77–80.

[83] P. Y. Chiou, H. Moon, H. Toshiyoshi, C. J. Kim, and M. C. Wu, "Light actuation of liquid by optoelectrowetting," *Sensors and Actuators, A: Physical*, vol. 104, no. 3, pp. 222–228, 2003.

[84] S.-Y. Park, M. a. Teitell, and E. P. Y. Chiou, "Single-sided continuous optoelectrowetting (SCOEW) for droplet manipulation with light patterns." *Lab on a chip*, vol. 10, no. 13, pp. 1655–61, 2010.

[85] J. S. Batchelder, "Dielectrophoretic manipulator," *Review of Scientific Instruments*, vol. 54, no. 3, pp. 300–302, 1983.

[86] P. R. Gascoyne, J. V. Vykoukal, J. A. Schwartz, T. J. Anderson, D. M. Vykoukal, K. W. Current, C. McConaghy, F. F. Becker, and C. Andrews, "Dielectrophoresis-based programmable fluidic processors," *Lab on a Chip*, vol. 4, no. 4, pp. 299–309, 2004.

[87] M. D. Dryden, R. Fobel, C. Fobel, and A. R. Wheeler, "Upon the Shoulders of Giants: Open-Source Hardware and Software in Analytical Chemistry," *Analytical Chemistry*, vol. 89, no. 8, pp. 4330–4338, 2017.

[88] M. G. Pollack, A. D. Shenderov, and R. B. Fair, "Electrowetting-based actuation of droplets for integrated microfluidicsElectronic supplementary information (ESI) available: six videos showing droplet flow, droplet dispensing and electrowetting. See http://www.rsc.org/suppdata/lc/b1/b110474h/," *Lab on a Chip*, vol. 2, no. 2, p. 96, 2002.

[89] H. Ren and R. B. Fair, "Micro/nano liter droplet formation and dispensing by capacitance metering and electrowetting actuation," *Proceedings of the IEEE Conference on Nanotechnology*, vol. 2002-Janua, pp. 369–372, 2002.

[90] Shih-Kang Fan, C. Hashi, and Chang-Jin Kim, "Manipulation of multiple droplets on NxM grid by cross-reference EWOD driving scheme and pressure-contact packaging," in *The Sixteenth Annual International Conference on Micro Electro Mechanical Systems, 2003. MEMS-03 Kyoto. IEEE*, vol. 2. IEEE, 2003, pp. 694–697.

[91] I. Swyer, R. Fobel, and A. R. Wheeler, "Velocity Saturation in Digital Microfluidics," *Langmuir*, vol. 35, no. 15, pp. 5342–5352, 2019.

[92] "Sci-bots," www.sci-bots.com/, accessed: 2020-10-30.

[93] "Opendrop v4," www.gaudi.ch/OpenDrop/?p=544, accessed: 2020-10-30.

[94] "Gaudilabs," www.gaudi.ch/GaudiLabs/, accessed: 2020-10-30.

[95] "Advanced liquid logic," www.ece.duke.edu/about/news/entrepreneurs/advanced-liquid-logic, accessed: 2020-10-30.

[96] "Illumina neoprep," www.emea.support.illumina.com/sequencing/sequencing_instruments/neoprep-library-system.html, accessed: 2020-10-30.

[97] J. Li and C. J. Kim, "Current commercialization status of electrowetting-on-dielectric (EWOD) digital microfluidics," *Lab on a Chip*, vol. 20, no. 10, pp. 1705–1712, 2020.

[98] "Genmarkdx and advanced liquid logic," www.biospace.com/article/releases/genmark-diagnostics-and-advanced-liquid-logic-enter-into-/agreement-to-develop-an-all-electronic-fully-integrated-diagnostic-/platform-/, accessed: 2020-10-30.

[99] N. E. Babady, M. R. England, K. L. Jurcic Smith, T. He, D. S. Wijetunge, Y.-W. Tang, R. R. Chamberland, M. Menegus, E. M. Swierkosz, R. C. Jerris, and W. Greene, "Multicenter Evaluation of the ePlex Respiratory Pathogen Panel for the Detection of Viral and Bacterial Respiratory Tract Pathogens in Nasopharyngeal Swabs," *Journal of Clinical Microbiology*, vol. 56, no. 2, pp. 1–11, dec 2017.

[100] T.-D. Huang, E. Melnik, P. Bogaerts, S. Evrard, and Y. Glupczynski, "Evaluation of the ePlex Blood Culture Identification Panels for Detection of Pathogens in Bloodstream Infections," *Journal of Clinical Microbiology*, vol. 57, no. 2, pp. 1–11, nov 2018.

[101] "Oxford nanopore - minion," www.nanoporetech.com/products/minion, accessed: 2020-10-30.

[102] "First dna sequencing in space a game changer," www.nasa.gov/mission_pages/station/research/news/dna_sequencing, accessed: 2020-10-30.

[103] "Digi.bio," www.digi.bio/, accessed: 2020-10-30.

[104] "Miroculus," www.miroculus.com/, accessed: 2020-10-30.

[105] K. J. Schlager, "Systenas Engineering-Key to Modern Development," *Ire Transactions on Engineering Management*, pp. 1953–1955, 1953.

[106] M. D. Watson, "Systems Engineering Principles and Hypotheses," *INSIGHT*, vol. 22, no. 1, pp. 18–28, may 2019.

[107] "Nasa system engineering handbook," www.nasa.gov/seh/3-3-project-pre-phase-a-concept-studies, accessed: 2020-10-30.

[108] G. Tanev and J. Madsen, "A Correct-by-Construction Design and Programming Approach for Open Paper-Based Digital Microfluidics," 2017.

[109] "Biological interface group at sogang uuniversity," www.sites.google.com/view/biologicalinterfaceslab/home, accessed: 2020-10-30.

[110] "lab311 at sogang university," www.sites.google.com/view/lab311, accessed: 2020-10-30.

[111] "Second predecessor system on national korean broadcasting," www.youtube.com/watch?v=JOCa-LwV9us&feature=emb_logo, accessed: 2020-10-30.

[112] A. Sangiovanni-Vincentelli and G. Martin, "Platform-based design and software design methodology for embedded systems," *IEEE Design & Test of Computers*, vol. 18, no. 6, pp. 23–33, 2001.

[113] G. Tanev, W. Svendsen, and J. Madsen, "A modular reconfigurable digital microfluidics platform," in *2018 Symposium on Design, Test, Integration & Packaging of MEMS and MOEMS (DTIP)*. IEEE, may 2018, pp. 1–6.

[114] G. D. Micheli, *Embedded, Cyber-Physical, and IoT Systems*, S. S. Bhattacharyya, M. Potkonjak, and S. Velipasalar, Eds. Cham: Springer International Publishing, 2020.

[115] J. Gong and C. J. Kim, "Direct-referencing two-dimensional-array digital microfluidics using multilayer printed circuit board," *Journal of Microelectromechanical Systems*, vol. 17, no. 2, pp. 257–264, 2008.

[116] "Samtec's 1.00 mm ultra-low profile compression interposer connector," www.samtec.com/products/za1, accessed: 2020-10-30.

[117] T. Chen, Y. Jia, C. Dong, J. Gao, P. I. Mak, and R. P. Martins, "Sub-7-second genotyping of single-nucleotide polymorphism by high-resolution melting curve analysis on a thermal digital microfluidic device," *Lab on a Chip*, vol. 16, no. 4, pp. 743–752, 2016.

[118] L. Malic, D. Brassard, T. Veres, and M. Tabrizian, "Integration and detection of biochemical assays in digital microfluidic LOC devices," pp. 418–431, 2010.

[119] C. Zhang and D. Xing, "Miniaturized PCR chips for nucleic acid amplification and analysis: Latest advances and future trends," *Nucleic Acids Research*, vol. 35, no. 13, pp. 4223–4237, 2007.

[120] B. Janocha, H. Bauser, C. Oehr, H. Brunner, and W. Göpel, "Competitive electrowetting of polymer surfaces by water and decane," *Langmuir*, vol. 16, no. 7, pp. 3349–3354, 2000.

[121] M. Abdelgawad and A. R. Wheeler, "Low-cost, rapid-prototyping of digital microfluidics devices," *Microfluidics and Nanofluidics*, vol. 4, no. 4, pp. 349–355, apr 2008.

[122] M. Yafia, S. Shukla, and H. Najjaran, "Fabrication of digital microfluidic devices on flexible paper-based and rigid substrates via screen printing," *Journal of Micromechanics and Microengineering*, vol. 25, no. 5, 2015.

[123] F. A. Z. a. Alatraktchi, J. S. Noori, G. P. Tanev, J. Mortensen, M. Dimaki, H. K. Johansen, J. Madsen, S. Molin, and W. E. Svendsen, "Paper-based sensors for rapid detection of virulence factor produced by Pseudomonas aeruginosa," *PLoS ONE*, vol. 13, no. 3, pp. 1–9, 2018.

[124] Y. Y. Lin, R. D. Evans, E. Welch, B. N. Hsu, A. C. Madison, and R. B. Fair, "Low voltage electrowetting-on-dielectric platform using multi-layer insulators," *Sensors and Actuators, B: Chemical*, vol. 150, no. 1, pp. 465–470, 2010.

[125] "High voltage, low noise, dc/dc converters," www.analog.com/media/en/technical-documentation/application-notes/AN118fb.pdf, accessed: 2020-10-30.

[126] "64-channel serial-to-parallel converter with high-voltage push-pull outputs," www.microchip.com/wwwproducts/en/HV507, accessed: 2020-10-30.

[127] "Autoprotocol," www.autoprotocol.org, accessed: 2020-10-30.

[128] "Scratch programming language," www.scratch.mit.edu, accessed: 2020-10-30.

[129] "Python," www.python.org, accessed: 2020-10-30.

[130] "C documentaion," www.csharp.net, accessed: 2020-10-30.

[131] "Prism mvvm pattern," www.prismlibrary.com/docs/wpf/legacy/Implementing-MVVM.html, accessed: 2020-10-30.

[132] "Prism framework," www.prismlibrary.com/index.html, accessed: 2020-10-30.

[133] "Imagej," www.imagej.nih.gov/ij/index.html, accessed: 2020-10-30.

[134] Y. Khilko, P. D. Weyman, J. I. Glass, M. D. Adams, M. A. McNeil, and P. B. Griffin, "DNA assembly with error correction on a droplet digital microfluidics platform," *BMC Biotechnology*, vol. 18, no. 1, p. 37, dec 2018.

[135] R. Kodzius, K. Xiao, J. Wu, X. Yi, X. Gong, I. G. Foulds, and W. Wen, "Inhibitory effect of common microfluidic materials on PCR outcome," *Sensors and Actuators, B: Chemical*, vol. 161, no. 1, pp. 349–358, 2012.

[136] A. R. Prakash, M. Amrein, and K. V. I. S. Kaler, "Characteristics and impact of Taq enzyme adsorption on surfaces in microfluidic devices," *Microfluidics and Nanofluidics*, vol. 4, no. 4, pp. 295–305, apr 2008.

[137] R. Sista, Z. Hua, P. Thwar, A. Sudarsan, V. Srinivasan, A. Eckhardt, M. Pollack, and V. Pamula, "Development of a digital microfluidic platform for point of care testing," *Lab on a Chip*, vol. 8, no. 12, p. 2091, 2008.

[138] B. Coelho, B. Veigas, E. Fortunato, R. Martins, H. Águas, R. Igreja, and P. V. Baptista, "Digital microfluidics for nucleic acid amplification," 2017.

[139] M. G. Pollack, R. B. Fair, and A. D. Shenderov, "Electrowetting-based actuation of liquid droplets for microfluidic applications," *Applied Physics Letters*, vol. 77, no. 82, pp. 1725–1726, 2000.

[140] A. D. Shenderov, "Actuators for microfluidics without moving parts," U.S. Patent 6 565 727, May 20, 2003.

[141] Alexander David Shenderov, "Electrostatic actuators for microfluidics and methods for using same," U.S. Patent 6 773 566, Sep., 1997.

[142] P. Kolar and R. B. Fair, "Method and apparatus for non-contact electrostatic actuation of droplets," U.S. Patent 6 989 234, Jan. 24, 2006.

[143] S. A. Elrod, E. Peeters, F. E. Torres, D. K. Biegelsen, J. L. Dunec, and A. G. Bell, "Apparatus and method for using electrostatic force to cause fluid movement," U.S. Patent 7 147 763, Dec. 12, 2006.

[144] V. K. Pamula, M. G. Pollack, P. Y. Paik, H. Ren, and R. B. Fair, "Apparatus for manipulating droplets by electrowetting-based techniques," U.S. Patent 6 911 132, Jun. 28, 2005.

[145] Vamsee K. Pamula and Michael G. Pollack and Phillip Y. Paik and Hong Ren and Richard B. Fair, "Method and apparatus for non-contact electrostatic actuation of droplets," U.S. Patent 20 040 058 450, Mar. 25, 2004.

[146] A. D. Shenderov, "Methods of using actuators for microfluidics without moving parts," U.S. Patent 7 255 780, Aug. 14, 2007.

[147] J. Ding, K. Chakrabarty, and R. B. Fair, "Scheduling of microfluidic operations for reconfigurable two-dimensional electrowetting arrays," *IEEE Transactions on Computer-Aided Design of Integrated Circuits and Systems*, vol. 20, no. 12, pp. 1463–1468, 2001.

[148] V. Pamula, P. Paik, J. Venkatraman, M. Pollack, and R. Fair, "Microfluidic electrowetting-based droplet mixing," in *2001 Microelectromechanical Systems Conference (Cat. No. 01EX521)*. IEEE, 2002, pp. 8–10.

[149] J. D. Sterling, C.-Y. Chen, and A. Nadim, "Method, apparatus and article for microfluidic control via electrowetting, for chemical, biochemical and biological assays and the like," U.S. Patent 20 040 231 987, Nov. 25, 2004.

[150] M. Gunji, H. Nakanishi, and M. Washizu, "Method and device for transporting droplet," Japan Patent 2 006 007 120A, Jan. 13, 2010.

[151] R. N.McRuer, M. Island, and M. L. Stolowitz, "Single-sided apparatus for manipulating droplets be electrowetting on dielectric technique," U.S. Patent 20 080 169 197, Jul. 17, 2008.

[152] V. K. Pamula, M. G. Pollack, P. Y. Paik, H. Ren, and R. B. Fair, "Methods for manipulating droplets by electrowetting-based techniques," U.S. Patent 7 569 129, Aug. 4, 2009.

[153] A. D. Shenderov and M. G. Pollack, "Method and device for conducting biochemical or chemical reactions at multiple temperatures," U.S. Patent 9 517 469, Dec. 14, 2016.

[154] U. B. Yi, P.-P. D. Gusman, and W. P.-W. Liu, "Mitigation of biomolecular adsorption with hydrophilic polymer additives," U.S. Patent 8 481 125, Jul. 9, 2013.

[155] V. Srinivasan, M. G. Pollack, P. Y. Paik, V. K. Pamula, and R. B. Fair, "Filler fluids for droplet operations," U.S. Patent 8 980 198, Mar. 17, 2015.

[156] M. G. Pollack, P. Y. Paik, and V. K. Pamula, "Droplet -based nucleic acid amplification device, systems, and methods," U.S. Patent 20 080 038 810, Feb. 14, 2008.

[157] A. Wheeler, R. Gabrella, C. jin Kim, and H. Moon, "Droplet-based on-chip sample preparation for mass spectrometry," U.S. Patent WO2 007 136 386A2, Nov. 29, 2007.

[158] A. R. Wheeler, I. Bardulovic-Nad, H. Yang, and M. Abdelgawad, "Exchangeable sheets pre-loaded with reagent depots for digital microfluidics," U.S. Patent 20 100 081 578A1, Apr. 01, 2010.

[159] A. R. Wheeler, Y. Tu, and M. Shamsi, "Digital microfluidic devices with integrated electrochemical sensors," U.S. Patent 20 170 315 090A1, Nov. 2, 2017.

[160] R. Fobel, A. Kirby, and A. R. Wheeler, "Printed digital microfluidic devices methods of use and manufacture thereof," U.S. Patent 20 170 184 546A1, Jun. 29, 2017.

[161] D. S. Chapin and D. M. Stipe, "Benchtop intrument housing," U.S. Patent USD599 832, Sep. 8, 2009.

[162] Y. Kawahara, S. Hodges, N. W. Gong, S. Olberding, and J. Steimle, "Building functional prototypes using conductive inkjet printing," *IEEE Pervasive Computing*, vol. 13, no. 3, pp. 30–38, 2014.

[163] G. Cummins and M. P. Desmulliez, "Inkjet printing of conductive materials: a review," *Circuit World*, vol. 38, no. 4, pp. 193–213, 2012.